UNIVERSITY OF SOUTHAMPTON

Electroluminescence and Ageing of Polyethylene

by

David H. Mills

A thesis submitted for the degree of Doctor of Philosophy

in the

Faculty of Physical and Applied Sciences

Department of Electronics and Computer Science

April 2012

UNIVERSITY OF SOUTHAMPTON

ABSTRACT

FACULTY OF PHYSICAL AND APPLIED SCIENCES
Department of Electronics and Computer Science

Doctor of Philosophy

Electroluminescence and Ageing of Polyethylene

by David H. Mills

Electrical insulation is known to age when under electrical stress. One cause of this is thought to relate to the movement and build up of charge within the insulation. The emission of a low level of light from polymeric materials when under electrical stressing is shown to occur before the onset of currently detectable material degradation. This light is termed electroluminescence (EL) and under an ac electric field is thought to relate to the interaction of charge in close proximity to the electrode-polymer interface. Understanding the cause of this light emission gives a very high resolution way of monitoring charge interaction and its influence on material ageing. This report presents the improvement to a system to measure changes in EL emission during the cycle of the applied field (point on wave measurements) under various electric fields.

To investigate the relationship between EL and ageing, 100 μm, low-density polyethylene (LDPE) films were ultraviolet (UV) aged in 3 and 7 day intervals up to 17 days. The samples were aged in both air and nitrogen environments to separate the affect of photo-oxidation from photo-irradiation reactions on charge movement. Changes as a result of ageing were characterised in terms of optical, chemical and electrical properties. These were investigated using ultraviolet and visible (UV-Vis) and Fourier transform infrared (FTIR) spectroscopy, ac ramp breakdown measurements and dielectric spectroscopy. The accumulation of space charge (SC) was then investigated using the pulsed electro acoustic (PEA) technique.

This collection of results were used to explain changes in EL in terms of intensity and phase difference. A model using the bipolar charge recombination theory was then developed using trends shown in the characterising measurements to explain changes in EL. Results support the use of EL as a tool to investigate changes in charge movement very near the electrode-polymer interface.

Contents

List of Figures

List of Tables

Declaration of Authorship

I, David Mills, declare that this thesis entitled:

'Electroluminescence and Ageing of Polyethylene'

and the work presented in the thesis are both my own, and have been generated by me as a result of my own original research. I confirm that:

- this work was done wholly or mainly while in candidature for a research degree at this University;
- where any part of this thesis has previously been submitted for a degree or any other qualification at this University or any other institution, this has been clearly stated;
- where I have consulted the published work of others, this is always clearly attributed;
- where I have quoted from the work of others, the source is always given. With the exception of such quotations, this thesis is entirely my own work;
- I have acknowledged all main source of help;
- where the thesis is based on work done by myself jointly with others, I have made clear exactly what was done by others and what I have contributed myself;
- parts of this work have been published as:

    1. F. Baudoin, D. H. Mills, P. L. Lewin, S. Le Roy, G. Teyssedre, and C. Laurent, 'Modeling electroluminescence in insulating polymers under ac stress: effect of excitation waveform', *Journal of Physics D: Applied Physics*, vol. 44(16), (2011)

2. F. Baudoin, D. H. Mills, P. L. Lewin, S. Le Roy, G. Teyssedre, and C. Laurent, 'Modelling electroluminescence in insulating polymers under sinusoidal stress: Effect of applied voltage, frequency and offset', *IEEE international conference on electrical insulation and dielectric phenomena*, pp. 820-823, (2011)
3. D. H. Mills, P. L. Lewin, and G. Chen, 'Ageing of high voltage cable insulation', *IEEE international conference on electrical insulation*, pp. 438-442, (2011)
4. A. S. Alghamdi, D. H. Mills, and P. L. Lewin, 'Influence of ageing on space charge and electroluminescence of epoxy resin', *IEEE intenational conference on solid dielectrics*, pp. 88-91, (2010)
5. F. Baudoin, D. H. Mills, P. L. Lewin, S. Le Roy, G. Teyssedre, and C. Laurent, 'Contribution to the modelling of electroluminescence in high voltage polymeric material', *IEEE international conference on electrical insulation and dielectric phenomena*, pp. 353-356, (2010)
6. D. H. Mills, P. L. Lewin, G. Chen, and A. Mohd Ariffin, 'Electroluminescence of ultraviolet and thermally aged low density polyethylene', *IEEE international conference on solid dielectrics*, pp. 68-71, (2010)
7. D. H. Mills, P. L. Lewin, G. Chen, 'Comparison between the electroluminescence and space charge of ultraviolet and thermally aged low density polyethylene', *IEEE international conference on electrical insulation and dielectric phenomena*, pp. 129-132, (2010)

Signed: .....

Date: .....

Acknowledgements

Firstly, I would like to thank my supervisors, Professor Paul Lewin and Dr. George Chen for their continued support and critical discussion throughout my PhD and for their faith in me to get to this point.

I would also like to acknowledge Dr Abdulsalam S. Alghamdi and Dr Fulbert Baudoin for their assistance in collecting some of the results included within this report. I am also grateful to Dr Christian Laurent and Dr Gilbert Teyssedre at the Laborataire Plasma et Conversion D'Energie, Toulouse, for their invitation and financial support to collect comparative measurements with their experiment.

I would like to further my gratitude to many members of the Tony Davies High Voltage Laboratory who provided advice, interesting discussion and humour during my research. In particular the help of Dr Ian Hosier, Dr Marting Reading, Dr James Pilgrim, Mr Jack Hunter, Ms Alex Holt, Ms Nicky Freebody and Ms Celia Yeung; their help was greatly appreciated. Thanks also goes to the technical support of the lab, without whom the experiment would not have been possible.

I would also like to thank many members of the Southampton University Mountain Bike Club for providing a great distraction from the pressures of research. Particular thanks goes to Mr Patrick McSweeney, Mr Sam Woodcock, Mr Tom Rand and Mr Callum Corbin.

Finally thanks goes out to my family and friends for their ongoing support and understanding throughout all of my studies. However, most of all I would like to thank Ms Holly Dolan for her continued and unconditional support throughout the inevitable highs and lows of a PhD. She has kept me focussed and grounded when I have needed it most.

To you all I will be forever grateful!

Symbols

k	Boltzmann constant (8.617×10^{-5} eV K^{-1})
ρ_{hm}	Charge density of mobile holes
ρ_{ht}	Charge density of trapped holes
ρ_{em}	Charge density of mobile electrons
ρ_{et}	Charge density of trapped electrons
μ	Charge mobility
$R_{em,ht}$	Recombination of a mobile electron with a trapped hole
$R_{hm,et}$	Recombination of a mobile hole with a trapped electron
χ_c	Crystallinity
$\tan\delta$	Dielectric loss tangent
E_0	Electric field at the injecting electrode
I_1	Electroluminescence from ring electrode
I_2	Electroluminescence from plane electrode
e	Elementary charge (1.602×10^{-19} C)
ΔH_{f100}	Enthalpy of fusion of a 100% crystalline polymer
ΔH_f	Enthalpy of fusion
ϵ''	Imaginary relative permittivity
h	Plank's constant
A	Absorption due gold coating and optical arrangement
B	Absorption due to polymer bulk
ϵ'	Real relative permittivity
$M_{em,ht}$	Recombination coefficient for a mobile electron with a trapped hole
$M_{eh,et}$	Recombination coefficient for a mobile hole with a trapped electron
ϵ^*	Complex relative permittivity
X	Space charge region
T_c	Crystallisation temperature
T_g	Glass transition temperature
T_m	Melting temperature
Δt_{EL}	Time increment for simulating electroluminescence

$\Delta t_{_R}$	Time increment for Runge-Kutta method
Q	Total charge
$I_{_{total}}$	Total electroluminescence
$\epsilon_{_0}$	Permittivity in a vacuum (8.854×10^{12} F m^{-1})

Abbreviations

BASE^{TM}	Bias active stabilization engine
N_2	Nitrogen
SF_6	Sulphur hexafluoride
ac	Alternating current
ATR	Attenuated total reflectance
CCD	Charge coupled device
CIC	Clock induced charge
dc	Direct current
DSC	Differential scanning calorimetry
DVM	Digital volt meter
EL	Electroluminescence
EM	Electron multiplication
EMCCD	Electron multiplying charge coupled device
V_{off}	Applied field off
V_{on}	Applied field on
FTIR	Fourier transform infrared
HN	Havriliak-Negami
HDPE	High-density polyethylene
HV	High voltage
ICCD	Intensified charge coupled device
IR	Infrared
LAPLACE	Laboratory on Plasma and Conversion of Energy, Toulouse
LDPE	Low-density polyethylene
LED	Light emitting diode
LIMM	Laser induced modulation method
LIPP	Laser induced pressure pulse
PD	Partial discharge
PE	Polyethylene
PEA	Pulsed electro acoustic

PEN	Polyethylene napthalate
PEO	Polyethylene oxide
PET	Polyethylene terephthalate
PIC	Peripheral interface controller
PL	Photoluminescence
PMT	Photomultiplier tube
POW	Point on wave
PP	Polypropylene
PVC	Polyvinyl chloride
PVDF	Polyvinylidene fluoride
rms	Root mean square
ROI	Region of interest
SC	Space charge
TDHVL	Tony Davies High Voltage Laboratory, Southampton
TPM	Thermal pulse method
TSC	Thermally stimulated current
TSM	Thermal step method
TTi	Thurlby Thandar Instruments Ltd.
UV	Ultraviolet
UV-Vis	Ultraviolet and visible
XLPE	Cross-linked polyethylene

Chapter 1

Introduction

Due to the continued world wide growth in electricity demand there is an ongoing requirement for new or increased energy capacity. Two options exist for the transmission of energy over long distances as either overhead power lines or underground cable systems. Traditionally overhead power lines are used due to the typical installation cost being approximately 10 times cheaper than the equivalent underground system [1]. However, in recent years there has been an increased demand in the use of underground systems due to a range of influencing factors. Due to the cost and availability of land in densely populated areas, overhead pylons are rarely seen. Therefore the cost difference between overhead lines and underground cables is significantly reduced, increasing their use. There is also a growing awareness amongst the general public of aesthetic and environmental factors. Although the use of underground cables is not necessarily environmentally friendly due to their comparatively limited recyclability, their use removes the aesthetic impact enough to reduce the environmental worry. There is currently a growth in research to identify insulation for underground cables with improved recycling potential. Another situation for the use of underground cables relates to their use in situations where overhead lines are impractical or impossible. Such examples are their use near airports or across large expanses of water.

The use of underground cables also offers some advantages due to their enclosed nature. The conductor is protected from environmental factors that can burden overhead power lines, such as, wind, ice, lightning strikes and airborne pollution to name a few. This same enclosed nature and underground use also brings with it some operational disadvantages. The heat dissipation is a major concern as excessive heating may lead to melting of polymeric insulation or premature ageing, this being the limiting factor on the power carrying capability of a cable system.

Another big concern is the usable service life of the system and the ability to identify and locate faults. The significant initial investment installing the cable underground means any reliability issues can be very costly. Firstly, identifying and fixing electrical faults in a system are particularly problematic, expensive and time consuming. Secondly, replacing the cable at the end of its usable life is another expensive investment that needs to be included at the initial decision. The latter of these problems is the reason understanding the ageing process is of particular interest and an important area of research [2–6].

Improvements in understanding the ageing process can benefit cable lifetime in two areas. Initially being able to accurately understand the ageing process, along with its operating conditions, would allow improved lifetime estimation. Secondly the ability to accurately monitor the remaining lifetime whilst in service would require knowledge of the affect the service conditions have on the ageing processes. The ideal situation being the lifetime estimation and monitoring to such an accuracy that cable replacement occurs when loss of service is imminent.

1.1 Cable Construction

Originally underground cables consisted of oil-impregnated paper as an insulating medium but as advances in the production of polymers developed polymeric insulation began to be used instead [1]. Polymeric materials offer a high electrical strength (up to 10^3 kV mm^{-1}), low dielectric loss ($\tan\delta$ of less than 10^{-3}), high dc resistivity (greater than 10^{16} Ω m) and good mechanical strength, all at a relatively low cost [2]. The polymeric material widely used in new cable systems for the bulk of the insulation system is cross-linked polyethylene (XLPE). Though as further developments in the understanding of polymeric systems develop there is a lot of research being undertaken into the use of other insulation systems. Examples include the use of recyclable insulation and the inclusion of micro- and nano-fillers to custom design particular insulation properties [7, 8].

An example of the typical construction of a polymeric cable is shown in figure 1.1. The main components consist of a bundle of conductors usually constructed from copper or aluminium for low electrical resistivity and cost. The bulk of the electrical insulation is provided by the polymeric insulation, typically XLPE. The conductors around the edge of the insulator act as an earth or neutral conductor and provide some mechanical protection to the cable. Between the conductor-insulator and insulator-earth conductor exists a semiconducting layer to ensure the electric field is uniform and avoid localised enhanced electrical stressing

points. A final outer layer (typically polyvinyl chloride) is used to keep the cable as a complete system and protect it from the environment (e.g., water or dirt penetration).

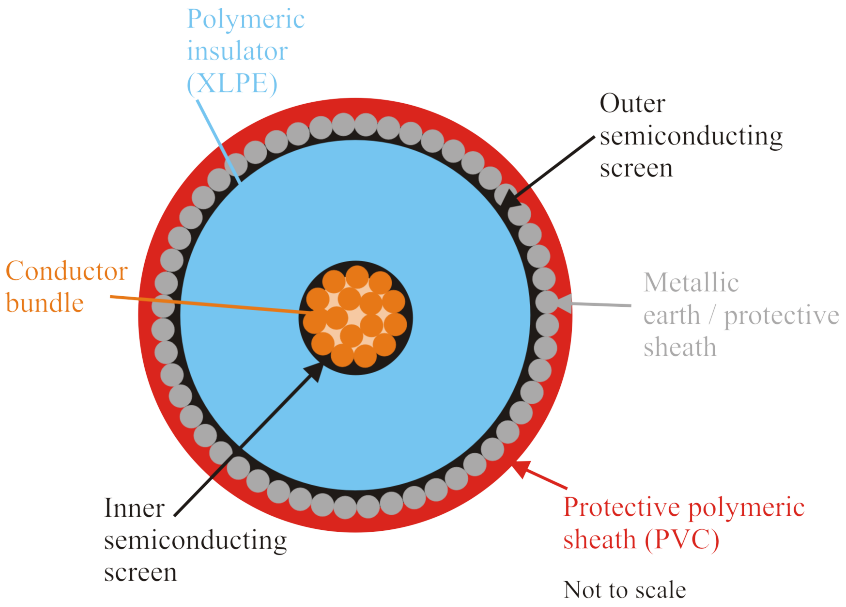

FIGURE 1.1: Schematic of a polymeric cable construction

1.2 Ageing

During the 40 to 60 year design life of an underground cable it will experience a range of stresses such as, electrical, thermal, chemical and environmental. These will all act to cause chemical changes to the polymer, eventually resulting in the degradation and catastrophic failure of the system [2]. The process by which this ageing mechanism occurs is therefore of particular interest in improving lifetime prediction and condition monitoring techniques. Traditionally this was thought to relate to the presence of impurities, protrusions and voids within the polymer resulting in locally enhanced electrical stresses [9]. These enhanced electrical stresses can lead to the initiation of partial discharge (PD) or growth of electrical trees within the insulation.

As manufacturing quality has improved the focus has moved away from these macroscopic impurities to a more molecular level to understand the accumulation of space charge [10]. Space charge is detectable in polymeric materials and can occur in two forms. The injection of charge from the electrodes forming regions of homocharge or the ionisation of particles within the insulation resulting in the formation of hetrocharge. Homocharge being of the same polarity as the field at the injecting electrode and acts to reduce the local electric field. Hetrocharge being of

the opposite polarity and therefore enhances the local electric field. The enhanced stresses created by this charge accumulation is therefore thought to contribute to the ageing of the polymeric material. Zhang *et al.* [11] have shown the formation of space charge (SC) in XLPE under a direct current (dc) field to locally enhance the applied field by as much as eight times.

This is high enough for the formation of electrical trees and the start of the degradation process. Understanding the mechanisms behind this SC formation is therefore of particular importance in understanding polymeric material ageing [11, 12].

There are many ageing sources, including electrical, mechanical, ultraviolet (UV), chemical, thermal and water stresses [9]. Each source may cause different ageing mechanisms and this will affect the electrical insulation in different ways. These could all have an influence on the formation of SC within the polymer. This formation of SC does not exclusively lead to a problem in all polymeric systems. If space charge is uniformly distributed across the polymer then it effectively reduces the localised electrical stress. A problem arises in uniformly distributing charge in what is a heavily disordered system. This can be achieved to a degree by raising its conductivity, but this limits its use as an electrical insulator. If the movement of space charge and how it varies with material ageing can be fully understood then there is the possibility of designing materials that have specific properties to inhibit any ageing process.

1.3 Space Charge and Electroluminescence

Space charge is detectable through a range of systems, those of most interest being the non destructive methods that measure the formation of space charge within the polymer. Various methods have been developed over the years including; the thermal pulse method (TPM), the thermal step method (TSM), the laser induced modulation method (LIMM), the laser induced pressure pulse (LIPP) and the pulsed electro acoustic (PEA) techniques [13–16]. Another mechanism thought to investigate the charge interaction within a polymer non destructively is the emission of electroluminescence (EL) [17–20]. This is a very low level of light emission in the visible spectrum when a polymer is subjected to an electric field. The light emission occurring before the onset of any detectable degradation mechanism, such as; electrical trees or partial discharge [21]. Under a dc field, correlation with SC measurements have suggested the EL to originate due to the recombination of opposite polarity charge within the bulk of the polymer [20].

Under ac fields the charge is not thought to be able to migrate far enough into the polymer to recombine with charge injected from the opposite polarity electrode [19, 22, 23]. Instead it is suggested that charge is injected and remains in close proximity to the injecting electrode during one half cycle to then recombine with opposite polarity charge during the following half cycle. This gives the potential for EL to investigate changes in the interaction of charge in a very small region near the electrode-polymer interface.

An investigation by Montanari and Fabiani [24] showed the inversion of an applied field to lead to enhanced degradation. This is thought to be due to the formation of homocharge near the electrodes becoming hetrocharge on field reversal and causing local electric field enhancements. However, it is not just the accumulation of SC that is of interest but the molecular changes that create charge trapping sites. Zhou *et al.* [25] has suggested that understanding the formation and density of trapping sites may act as ageing markers. The presence of higher energy sites likely to have the most adverse effect on the lifetime of electrical insulation [12].

1.4 Research Aims and Objectives

A full understanding into the mechanisms of EL emission is still unknown but the development of models and comparison with other space charge measurement techniques is supporting current theories. This work aims to provide further results and analysis to strengthen or contradict with current theories, furthering discussion of the charge interaction that results in EL.

To investigate the processes resulting in EL, the changes in emission from polyethylene (PE) as a result of ageing were investigated. The material will be aged using UV radiation in oxygen containing and oxygen free environments. Both of these environments are expected to have a significant affect on the SC formation due to changes in the chemical structure within the polymeric material. Changes in EL as a result of ageing may then explain changes in charge movement near the electrode-polymer interface. Understanding the chemical changes as a result of ageing and using them to interpret changes in the EL emission will provide support for its potential use as a condition monitoring tool.

Due to the complex nature and experimental difficulties associated with investigating complete cable systems this work looks at films of polymer. In particular the work focusses on low-density polyethylene (LDPE) due to its use in electrical insulation systems (XLPE) but in a less chemically complex form. Thus removing

the added complexity of understanding the influence cross-linking additives have on ageing and EL phenomena.

1.5 Contribution of this Work

This work has contributed to the field of dielectric insulation in a few areas. Initially a development to an existing EL experiment setup is presented, reducing data collection time and improving on the sensitivity and accuracy of the system. LDPE films have been UV aged and characterised by a range of different methods to identify changes in the optical, chemical and electrical properties. This is compared with SC and EL data to identify changes in the charge movement and its relationship with this ageing mechanism. The changes in EL develop an understanding of the pheonemena and its potential use as a condition monitoring tool. Finally a model that simulated the EL of virgin materials has been further developed, simulating changes as a result of ageing. Interpreting the simulation provides possible explanations for the changes in charge movement at the electrode-polymer interface.

1.6 Thesis Outline

This thesis is divided into 6 separate chapters. The background to polyethylene structures, chemical changes as a result of ageing and the current theories on mechanisms leading to EL will be detailed in chapter 2. A detailed description of the chemical structure of a polymer is used to explain the disordered nature and therefore complex energy structure. A detailed explanation of possible chemical changes as a result of photo-irradiation and the potential changes in localised energy states is given. A summary of previous SC and EL investigations confirms current theories that correlate with experimental results.

To investigate the changes as a result of UV ageing a range of experiments are required, the theory and procedures for these experiments are presented in chapter 3. These experiments consist of Fourier transform infrared (FTIR) spectroscopy to understand changes in the chemical structure, dielectric strength measurements to identify changes in electrical properties and dielectric spectroscopy to measure changes in the molecular charge properties of the material. The principles and use of the pulsed electro acoustic (PEA) technique is given to measure changes in the bulk dc SC accumulation along with a detailed description of the design, procedure and validation of EL measurements.

Chapter 4 presents the results of changes in the optical, chemical and electrical properties before a detailed investigation of changes in SC accumulation and EL emission. Changes in EL are presented in terms of intensity and its phase relationship with the applied field. These results are compared and discussed in chapter 5. A bipolar charge recombination model is presented and used to simulate changes as a result of ageing. Results of this simulation allow the changes in EL as a result of ageing to contribute towards understanding the EL phenomena.

Finally Chapter 6 details the conclusions that have been drawn for this research and outlines potential areas of further work.

Chapter 2

Background Theory

Polymeric insulation used for high voltage cables commonly takes the form of XLPE due to the excellent electrical properties of PE (high breakdown strength, low dielectric loss and high dc resistivity [26]) as well as the improved thermal and mechanical properties created by the process of cross-linking [27]. This work investigates the original, non-crosslinked form, LDPE, due to its chemically simpler nature and extensive use in EL measurements [28, 29]. To understand changes in charge movement as a result of ageing this chapter describes the chemical structure of PE along with the possible changes as a result of ageing. A review of the current theories regarding charge movement in polymeric systems and the EL phenomena is also presented.

2.1 Polyethylene

polyethylene is formed from the polymerisation of a monomer molecule (ethylene) consisting of 2 carbon and 4 hydrogen atoms covalently bonded as depicted in figure 2.1(a) [27]. The polymerisation causes the ethylene molecules to bond together, forming long chains as represented in figure 2.1(b). The original polymerisation method, developed in the 1930s, involved completing reactions at high temperatures (100 - 200 ^{o}C) and pressures (500 - 3000 atmospheres) [30]. Developments to this method in 1956 allowed the use of much lower pressures (approximately 35 atmospheres) resulting in the formation of high-density polyethylene (HDPE) and the former becoming known as low-density polyethylene (LDPE). These two PE differ in their structure due to the formation of side branches from the polymer backbone [2]. Side branching restricts the ability for regular molecular arrangements and therefore a reduced density, approximately 0.92 typical for LDPE [26].

HDPE consists of fewer side branches and therefore tighter packing, creating a mechanically superior but more difficult to mould polymer.

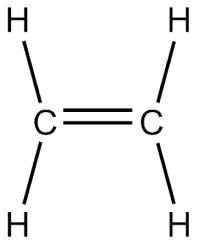

(a) Ethylene

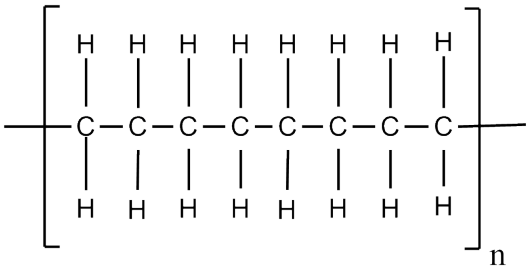

(b) Polyethylene

FIGURE 2.1: Polymerisation of ethylene

2.1.1 Physical and Chemical Structure

In an ideal polymer, polymerisation would consist of long chains formed from repeating molecular units joined by strong covalent bonds [27]. These repeating units are joined to form a continuous chain as shown in figure 2.1(b), becoming tightly folded to produce a crystalline structure. In reality this does not occur due to the formation of side branches and inclusion of other molecules, halting the chain growth. The degree of side branching affects the density of crystallisation in the polymer with LDPE having a typical amorphous-crystallinity ratio of 50% [2, 26, 27, 31, 32].

The formation of crystalline regions in a polymer occurs during cooling from its liquid state, the molecules become more closely packed and generate crystalline regions. These crystalline regions consist of lamellae which grow from a single nucleus to form spherulites (depicted in figure 2.2). Lamellae are thought to consist of tight chain folds next to each other to form an ordered region [27]. Some defects are commonly present, for example a chain leaving a lamellae region

to enter at another point or into another lamella, crossing the amorphous region. Typical dimensions of lamella in PE are thought to be 0.1 - 1 μm in the growth plane, with a thickness of 10 nm, the chains perpendicular to the growth plane of the lamella [33]. These continue to grow from the nuclei until either they meet other spherulite regions, impurities that inhibit further growth or the temperature becomes too cold for successful molecular realignment [32]. These spherulites behave like a collection of lamellae crystallites with amorphous regions in between rather than a single crystal. The result being a semi-crystaline polymer with the ratio between crystalline and amorphous regions affecting both the mechanical and electrical properties [34].

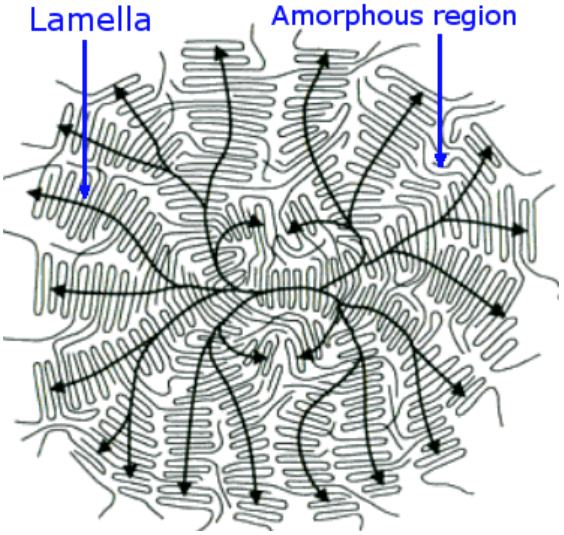

FIGURE 2.2: Formation of lamella and spherulites during crystallisation. Black arrows representing direction of growth [35]

During the production of polymers cross-linking may take place, common in LDPE used for high voltage cable insulation to form XLPE. The process of cross-linking results in the formation of bonds across the amorphous region to link different points of the polymer chains and side branches. These cross-links reduce the capability of molecular chain movement and rearrangement and so the resultant polymer is viewed as one giant molecule. On heating it is therefore more difficult to melt, a desirable feature in cable insulation allowing the range of operating loads to be increased. Cross-linking reactions are possible through irradiation or the use of a catalyst, a peroxide catalyst most economical in high voltage cable systems [1]. This does not react during polymer extrusion but rather when the cable is subsequently treated at high temperatures and pressures. Due to the complex initial structure the resultant polymer consists of cross-linked parts, non cross-linked parts, remaining catalyst and byproducts as well as the other impurities commonly seen in polymer production. These byproducts typically

consist of acetophenone, cumyl alcohol and α-methylstyrene resulting from the decomposition of the peroxide [36]. All of these byproducts are thought to contribute to the formation of space charge [37]. This creates an added complexity in understanding the EL phenomena, therefore work here focusses on the simpler non-crosslinked form of LDPE.

2.1.2 Energy State Structure

The traditional energy band model for covalently-bonded crystals has a solid valence and conduction band with a clear energy gap [33]. In polymers, particularly PE, this energy band model is not appropriate due to the presence of both amorphous and crystalline regions. The formation of spherulites creating a highly disordered structure and therefore not supporting the continuous crystal structure required for valence and conduction bands [27]. To explain the presence of space charge and low levels of conduction an alternative theory is needed. Due to the disordered nature, a current theory relates to the presence of localised energy differences creating a range of energy levels [2, 38, 39]. This theory suggests that since a continuous band is not possible a collection of discrete energy sites exists, as depicted in figure 2.3. The greatest density of charge acceptor (hole) or donor (electron) sites occuring at the locations were traditionally a valance or conduction band would be seen in a semi-conductor model. In the middle of the energy gap there becomes a lower probability of an energy state being present, but possible. The movement of charge can then occur between these states through charge hopping or tunnelling mechanisms (section 2.1.3).

These localised energy states are often described as either physical or chemical depending on the possible cause of the site [38, 40, 41]. Physical traps relate to the structure of the polymer; chain folds, chain ends, chain branches, amorphous regions, crystalline boundaries, etc. Chemical traps relate to additives or impurities that differ from the theoretical polymer system (carbon and hydrogen in the case of PE), such as; antioxidants, cross-linking by-products and oxidation products [15]. It is not currently possible to determine exactly the cause of specific trapping sites and their associated energy levels [42]. Investigations into the movement of charge after altering physical and chemical properties does suggest typical energy levels. Physical defects are commonly thought to require less energy, 10ths of eV, and are termed shallow trapping sites. Chemical impurities requiring a few eV are then termed deep trapping sites [31, 40, 43, 44]. Some recent attempts at molecular modelling has estimated physical traps relating to conformational disorder in the amorphous regions to have depths 0.15 eV to 0.3 eV [45]. Chemical traps relate

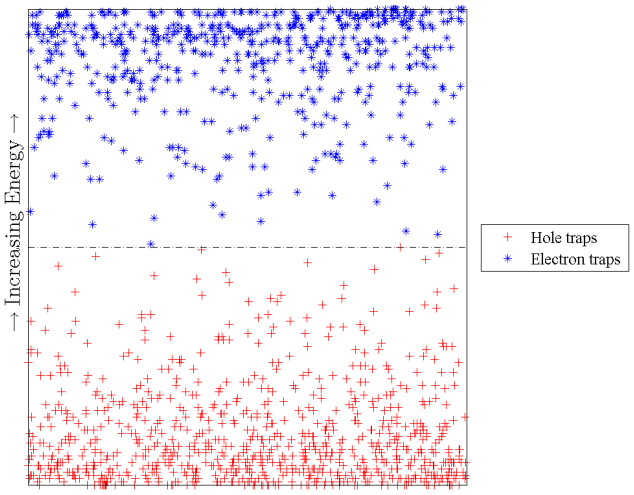

FIGURE 2.3: Pictorial representation of a theory for the energy structure in a disordered polymer

to typical impurities found in polymer systems have depths approaching 1.5 eV. It is also suggested that the conformational disorder that may result from the inclusion of chemical impurities, such as oxidation products, produces both deep and shallow trapping sites [46].

2.1.3 Electrode-Polymer Interface

The previous section discussed the origin of different charge trapping sites within a polymeric system. In order for charge to be injected into the polymer it must cross the electrode-polymer interface.

Contact between two different materials requires an equilibrium in energy differences to be reached such that a continuous Fermi energy level exists. In two dissimilar metals this would be achieved by the flow of electrons from one electrode to the other until the Fermi energy level becomes continuous across both [27]. However, in the case of a polymer free of any impurities, charge would not be able to flow between the two materials to achieve an equilibrium in energy differences. To explain this it is assumed that there is a large amount of disorder near the polymer surface creating a large quantity of localised energy states. Charge is able to move between these states to form an equilibrium in energy differences (figure 2.4) [38]. The height of the energy barrier (ϕ_0) an electron must overcome to be injected from the valence band in the metal to an acceptor state in the polymer can be calculated using.

$$\phi_e = \phi_m + \chi_P \tag{2.1}$$

Where ϕ_m is the work function of the metal and χ_P is the electron affinity of the polymer (approximately -1 eV in PE). In reality it is not that simple due to the presence of various physical and chemical defects near the polymer's surface and the quality of the electrode-polymer contact will all influence the local barrier height [47].

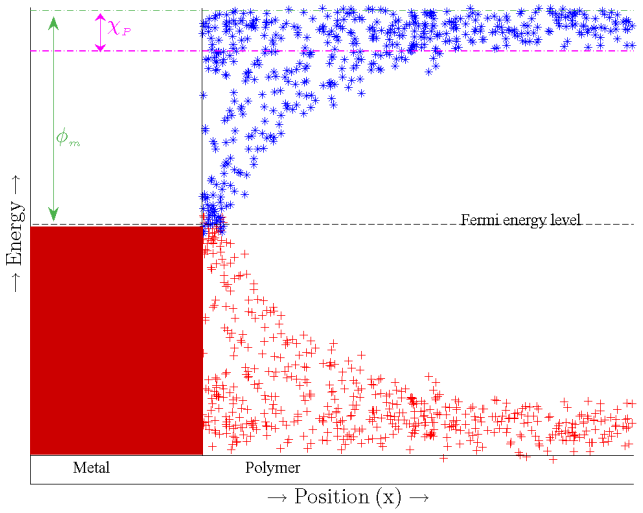

FIGURE 2.4: Pictorial representation of local electric states at the electrode-polymer interface

In the process of reaching Fermi equilibrium the electrons that leave the electrode creates a vacant positive charge, commonly termed a hole. Electrons now in the polymer will experience an electrostatic attraction towards the positively charged hole. The force (F_{image}) between the charge and its image charge can be calculated using Coulomb's law [48], i.e.,

$$F_{image}(x) = \frac{e^2}{4\pi\epsilon_0\epsilon'(2x)^2} = \frac{e^2}{16\pi\epsilon_0\epsilon' x^2} \tag{2.2}$$

Where e is elementary charge (1.602×10^{-19}), x is the separation distance between the electron and the interface and therefore $2x$ between both charges, ϵ_0 and ϵ' are the vacuum (8.85×10^{-12} Fm^{-1}) and relative permittivities respectively. Integrating this with respect to x gives the potential energy (ϕ_{image}) to move the injected electron from x to infinity, such that;

$$\phi_{image}(x) = \int_x^\infty F_{image}(x)dx = -\frac{e^2}{16\pi\epsilon_0\epsilon' x} \tag{2.3}$$

If there is a constant electric field (E) applied across the interface then the electron will experience a force (F_{field}) proportional to its electric field.

$$F_{field} = -eE \qquad \phi_{field}(x) = \int_x^\infty F_{field} = -eEx \tag{2.4}$$

This will alter the potential energy of the electron by (ϕ_{field}) and the energy barrier adjusted, as described by;

$$\phi(x) = \phi_{image}(x) + \phi_{field}(x) = -\frac{e^2}{16\pi\epsilon_0\epsilon' x} - eEx \tag{2.5}$$

The actual height of the potential barrier (ϕ_{res}) can be determined by differentiating equation 2.5 in terms of x and equating to 0.

$$\frac{d\phi}{dx} = \frac{e^2}{16\pi\epsilon_0\epsilon' x^2} - eE = 0 \tag{2.6}$$

Solving for x allows the position of a local maximum (x_{max}) to be determined.

$$x_{max} = \sqrt{\frac{e}{16\pi\epsilon_0\epsilon' E}} \tag{2.7}$$

Substituting x_{max} back into equation 2.5 shows the reduction in the energy barrier due to the application of the electric field.

$$\Delta\phi = -\frac{e}{2}\left(\frac{eE}{\pi\epsilon_0\epsilon'}\right)^{\frac{1}{2}} \tag{2.8}$$

The resultant energy barrier that an electron must overcome can then be determined.

$$\phi_{res} = \phi_e + \Delta\phi = \phi_e - \frac{e}{2}\left(\frac{eE}{\pi\epsilon_0\epsilon'}\right)^{1/2} \tag{2.9}$$

Depending on the level of the applied field two processes are commonly used to determine the resultant current density [2]. At lower fields (less than 10^2 kV mm^{-1} [13]), Richardson-Schottky thermionic emission is thought to dominate and at higher fields (greater than 10^3 kV mm^{-1} [2]) Fowler-Nordheim injection takes over (figure 2.5). Richardson-Schottky thermionic emission accounts for the thermal excitation of the electrons. Those with enough thermal energy will be able to hop over the energy barrier, will form an injection current such that;

$$j = AT^2 \exp\left(-\frac{\phi_{res}}{k_B T}\right) \tag{2.10}$$

Where j is the current density at the electrode-polymer interface, A is the Richardson-Dushman constant (1.20×10^6 A m^{-2} K^{-2}), T is the absolute temperature and k_B is the Boltzmann constant (8.617×10^{-5} eV K^{-1}).

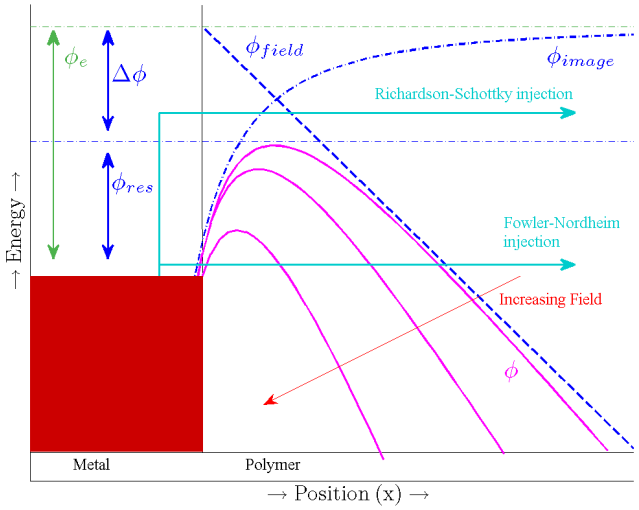

FIGURE 2.5: Diagram representing Richardson-Schottky and Fowler-Nordheim charge injection

In the case of very large electric fields the energy barrier becomes sufficiently narrow that the electron is able to tunnel directly through the barrier (Fowler-Nordheim injection) [2]. This tunnelling possible due to the wave-particle duality nature of an electron. This mechanism is no longer temperature dependent and the resultant equation for current density is.

$$j = \frac{e^3 E^2}{8\pi h \phi_{res}} \exp\left(-\frac{4}{3}\left(\frac{2m}{\hbar^2}\right)^{\frac{1}{2}} \frac{\phi_{res}^{\frac{3}{2}}}{eE}\right) \tag{2.11}$$

Where h is Plank's constant (4.14×10^{-15} eV s), $\hbar$ is $\frac{h}{2\pi}$ and m is the effective mass of an electron (9.11×10^{-31} kg).

2.2 Ageing of polymeric materials

Polymeric materials age during their life time until eventually failure occurs. These ageing processes can be enhanced by mechanical, electrical, thermal and chemical stresses. The ability to understand, control and identify these changes would allow for improved material design and life-time prediction. A common mechanism in the ageing of polymeric insulation involves enough energy to separate chemical bonds allowing for the rearrangement of the chemical structure. In the presence of reactive gases, such as oxygen, this can result in the inclusion of oxidation products in the polymer structure [49]. In the absence of oxygen other processes may take place such as changes in the crystallinity of the polymer, cross-linking or shortening of polymer chains. All of these processes or products alter the original chemical structure of the polymer and therefore the original insulation properties associated with electrical systems. Any of these changes may have an influence on the movement of charge in the polymeric system potentially leading to enhanced electrical stresses, further ageing and premature failure.

This section will provide a brief overview of the different ageing mechanisms and processes thought to occur in electrical insulation followed by a summary of accelerated ageing tests reported in the literature. This work particularly focusses on photo-irradiation based ageing processes, both oxidative and non-oxidative, which will be described in detail.

2.2.1 Ageing Mechanisms

The prolonged use of electrical insulation in high voltage systems subjects the polymeric material to a number of different stresses. In the case of cables, the polymer is subjected to electrical stresses due to the applied field, thermal stresses due to heat from the current in the conductor and mechanical stresses created during the installation or subsequent heating [9].

In the case of electrical stresses the accumulation of charge in the polymer can lead to enhanced electric fields. Charge accumulation under a dc electric field has suggested localised electric stresses to be up to eight times that of the applied field [11]. This high electrical stress is capable of leading to the start of material degradation through the growth of electrical trees. Typically electrical trees are

thought to grow from high electrical stress locations due to the accumulation of charge at impurities or protrusions formed from mechanical stresses during installation [4, 38].

At elevated temperatures, but below its melting point, PE is relatively stable in the absence of oxygen [50]. However, in the presence of oxygen PE readily oxidises, creating significant changes in both its physical and chemical structure. Typical changes result in a reduction in electrical strength and an increases in the electrical losses of the polymer [4, 30]. Cable insulation is manufactured in a low oxygen environment along with the inclusion of antioxidant additives to delay the formation of oxidation products. However, measurements of cables removed from service life still show the formation of oxidation products (carbonyl and hydroxyl groups) [51].

As the quality of cable manufacturing improves the presence of impurities and protrusions in the cable reduce and therefore the research focus of the ageing process has moved further towards the accumulation of charge and the enhanced electrical stress it may cause [52]. Understanding this movement of charge and the changes in behaviour as a result of ageing are therefore of particular interest.

2.2.2 Accelerated Ageing

Various mechanisms exist for the accelerated ageing of polymeric systems in terms of both single- and multi- factor ageing [9, 53]. Multi-factor ageing aiming to replicate the stresses experienced by in-service insulation to provide estimates of service life; typically consisting of combined electrical, thermal and environmental stressing [54–56]. Single-factor ageing looks to investigate the affect of particular changes commonly seen in service life on the electrical properties. Those of particular interest are; oxidation products, cross-linking, chain scission and changes in crystallinity [57, 58]. One way of achieving this is through the irradiation of the polymer under UV or gamma radiation sources in various environments [59–61].

This work aims to look at single-factor ageing to investigate the influence changes near the surface of the polymer may have on the charge movement affecting EL emission. Due to the lack of a complete understanding in the EL phenomena, single-factor ageing allows the chemical changes to be controlled to the greatest degree and therefore limits the possible causes affecting the EL. In this work it was chosen to focus on photo-irradiation in both an oxygen and oxygen free environment the full details of which are described in the next section.

2.3 Photo-Irradiation of Polyethylene

In theory an ideal LDPE structure contains only covalently bonded carbon and hydrogen atoms (figure 2.1). It is therefore not expected to absorb in the electromagnetic spectrum at wavelengths greater than 190 nm [50]. In practice this is not the case, LDPE is seen to be highly susceptible to wavelengths up to 300 nm [59, 62]. This indicates the presence of other absorbing species within the polymer system, such as; carbonyls, chromophores, additives and impurities that are known to absorb at wavelengths in the range 200 to 300 nm [50, 59].

The exposure of PE films to UV radiation leads to the the generation of new chemical products and changes in the chemical structure [50, 59, 63–65]. Typical products that are seen involve the formation of carbonyl, hydroxyl and vinyl groups along with the evolution of acetone, water and carbon oxides. Changes in the chemical structure that produce these products can also result in an increase in material brittleness and the production of cross-links [66]. All these potential changes as a result of photo-irradiation influence charge movement and energy levels within the polymer and therefore the movement of charge leading to EL [67].

Commercial polymers often have photo-stabilisers added in an effort to reduce the affect from photo-irradiation and photo-oxidation processes [50]. Though they do reduce it significantly they are not normally able to fully stop the process and are eventually consumed as well as influencing the original electrical and mechanical properties [30, 59].

2.3.1 Photo-Irradiation Reactions

In order for chemical changes in a polymer to occur due to UV radiation there is an initiation step resulting from the absorption of energy causing bond dissociation and the production of free radicals [50]. In the case of pure PE this will form from carbon and hydrogen, i.e.

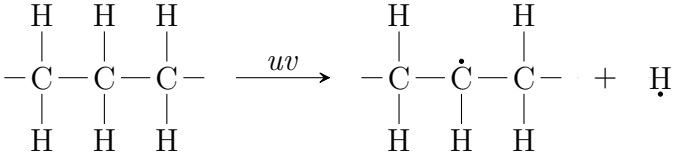

(2.12)

In all the chemical equations given here, the open bonds (C−) represent the continuation of the normal polymer chain and • represents a free radical.

In (2.12) The hydrogen is separated from the polymer chain leaving a hydrogen radical (H•) and polymer chain radical (C•). It is also possible for the C — C bonds to be broken but due to the energy required it is less likely to occur [68], i.e.

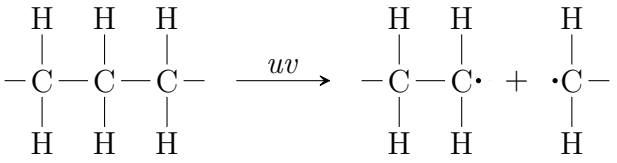

(2.13)

After the formation of these radicals the dominant next steps depends on the atmosphere of irradiation. There is a contest between oxygen based reactions and oxygen free reactions. The typical difference being the resultant stable reaction forming oxidation products or cross-links [50].

Oxygen based reactions

If the photo-irradiation takes place and oxygen is available then photo-oxidation reactions are able to continue as shown in (2.14) and (2.15). The highly reactive polymer radical (C•) is able to react with oxygen resulting in the formation of a peroxy polymer radical (COO•). Two of the hydrogen radicals (H•) are able to react together resulting in the release of hydrogen gas (H_2). The rate of formation of these peroxy radicals is controlled by the propogation of oxygen into the polymer. If no oxygen is available then reactions will continue as per the oxygen free environment shown in the following section.

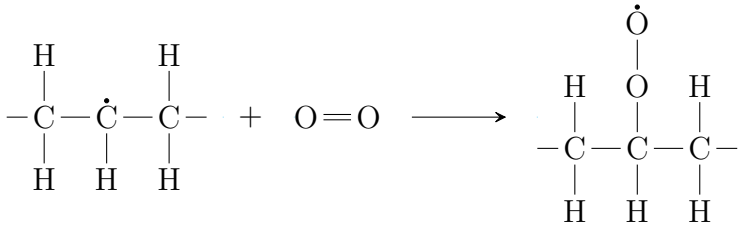

(2.14)

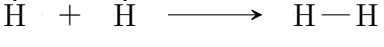

(2.15)

The newly formed peroxy radical (COO•) is able to extract hydrogen from the polymer chain to form hydroperoxide and another polymer radical (C•).

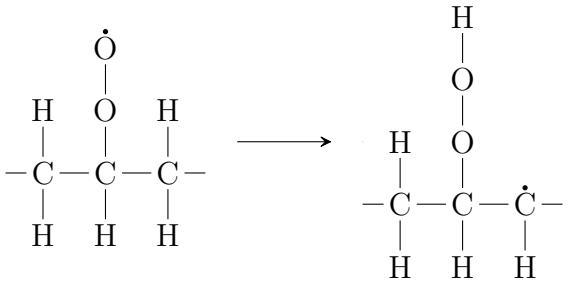

(2.16)

The hydrogen atom is most likely to be extracted from a tertiary bonded hydrogen atom or a hydrogen radical ($H^{\bullet}$) remaining from the initial reaction (2.12) [50]. These hydroperoxides are unstable and so will decompose to form further radicals from the continued UV radiation [59]. White and Turnbull [54] suggests a range of possible decomposition processes, these are;

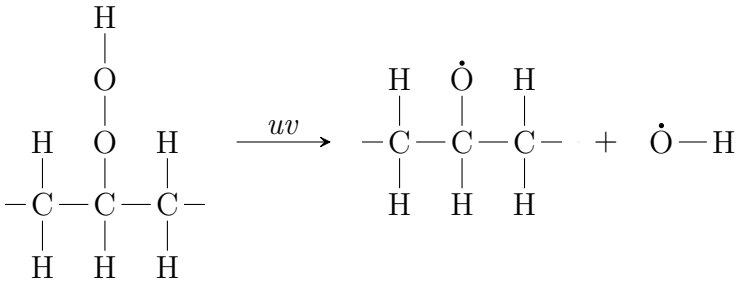

(2.17)

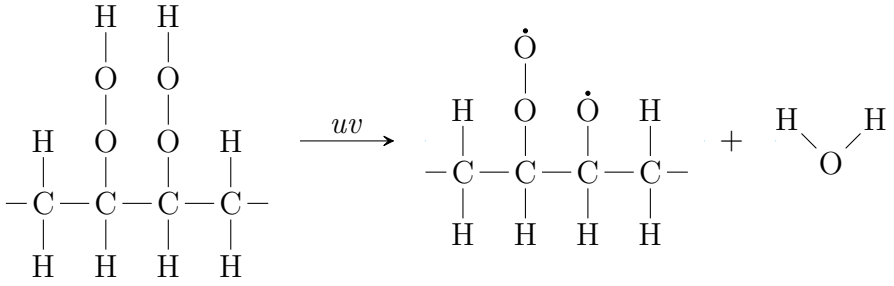

(2.18)

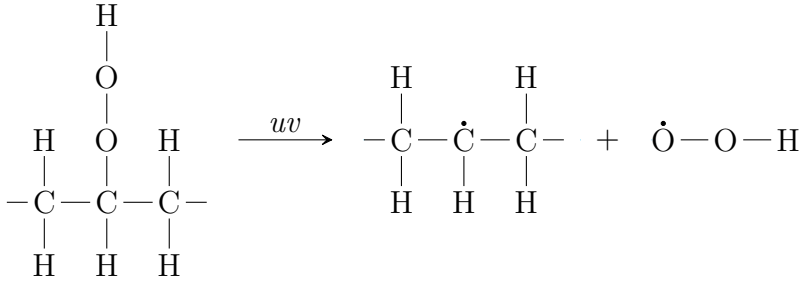

(2.19)

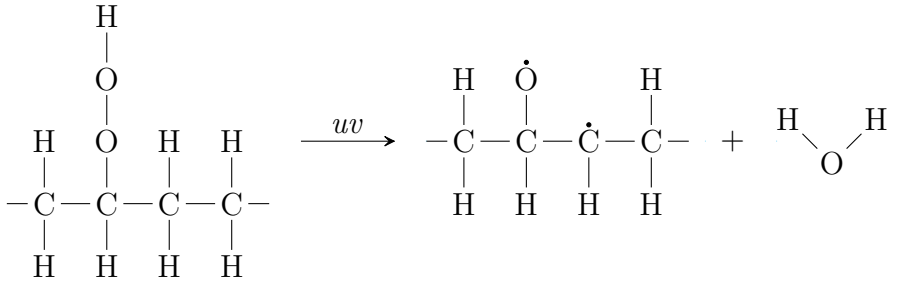

(2.20)

Some of these decomposed hydroperoxide products are reactive free radicals that will then go on to form other more stable products. The alkoxy polymer radicals (CO•) can react with the polymer chain to form hydroxyl groups (-OH) (equation 2.21). These hydroxyl groups form along the polymer chain, along side branches or at the end groups, though the later are rather rare [50]. There presence is typically shown by an increase in the infrared (IR) spectroscopy absorption band from 3500 to 3000 cm^{-1} [56].

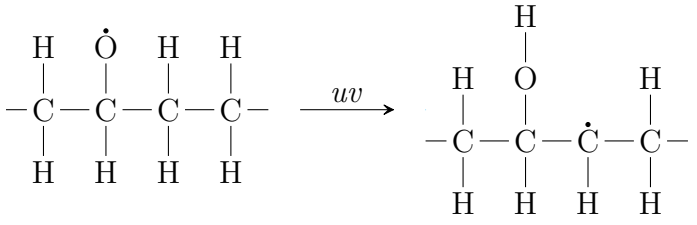

(2.21)

Another product commonly associated with oxidation is the production of carbonyl groups (C=O), the formation of which can result in a range of new molecules. The formation of carbonyl groups is also thought to play a key role in the chain scission of the polymer back bone [50]. The formation of a simple ketone group which is measurable by IR spectroscopy with an absorption at 1722 cm^{-1} [69] is common, i.e.

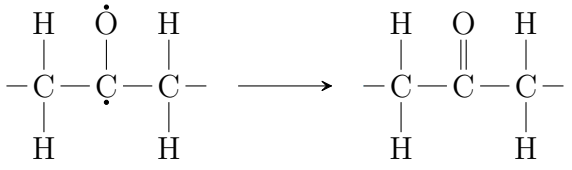

(2.22)

Another common carbonyl group seen in photo-oxidised LDPE is aldehyde, measurable by IR spectroscopy with an increased absorption at 1730 cm^{-1} [69]. The formation is thought to typically result in the scission of the polymer chain [68], i.e.

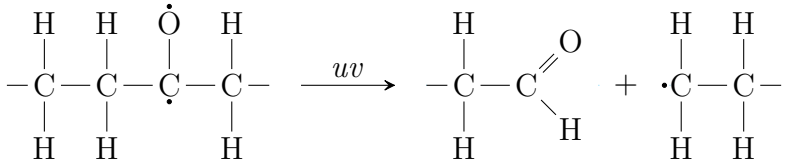

(2.23)

A further reaction with oxygen to the aldehyde can result in the addition of a hydroperoxide that decomposes to form a hydroxyl group, resulting in carbonxylic acid. This is measurable by IR spectroscopy absorption at 1710 cm^{-1} and an increase in the associated hydroxyl band (3500 to 3000 cm^{-1}) [69]. The reaction is;

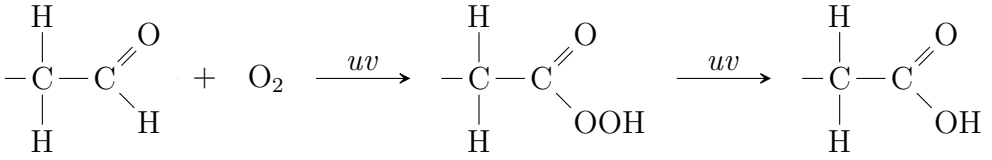

(2.24)

Of these three common carbonyl groups resulting from photo-oxidation, ketones are typically seen as the most dominant product LDPE exposed to UV radiation at 253.7 nm [70].

Depending on the physical location of the initial peroxy polymer radicals (COO$\cdot$) along the polymer chain, it is possible for them to form oxygen containing crosslinks. If they occupy neighbouring positions in the polymer structure then the formation of peroxides or epoxides may continue as shown below [50].

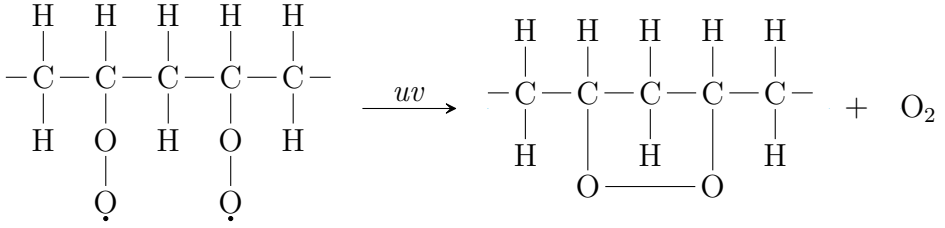

(2.25)

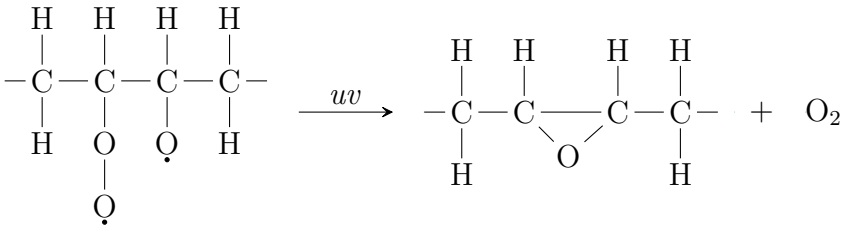

(2.26)

Two peroxy polymer radical containing chains located physically near to each other may also form cross-links.

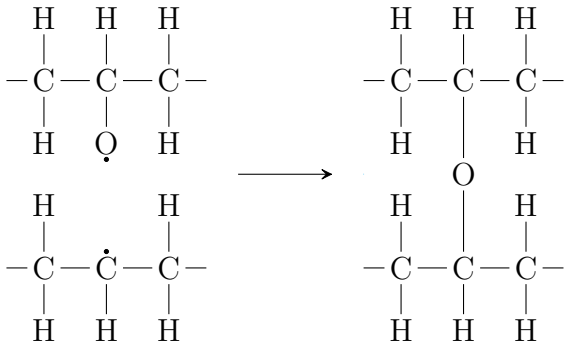

(2.27)

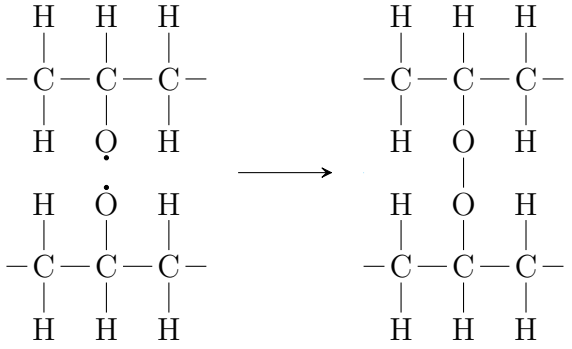

(2.28)

The various oxygen containing cross-links can increase the polymer rigidity as well as providing the chemical trapping sites associated with oxygen groups (section 2.1).

There are various other products and cross-links that can form as a result of photo-oxidation of PE but are not regularly measured in large enough quantities to be described here [50, 68]. Some of the products resulting from oxidation reactions are also thought to act as absorbing centres over the region 200 to 300 nm [54]. This can result in further reactions known as Norrish type 1 and Norrish type 2. Norrish type 1 reactions result in the formation of further reactive polymer radicals, i.e.

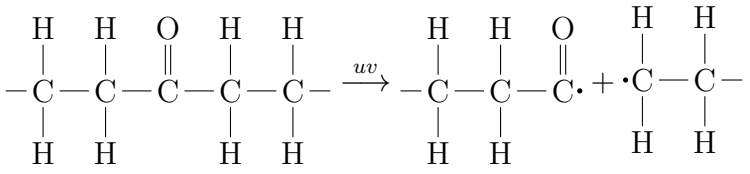

(2.29)

and Norrish type 2 reactions cause stable scission of the polymer chains [59, 68], i.e.

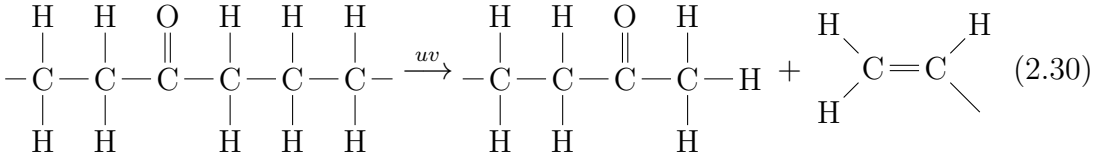

(2.30)

Oxygen free reactions

In the case when PE is photo irradiated and oxygen is unavailable, due to the ageing atmosphere (e.g. nitrogen) or the diffusion rate of the oxygen, the peroxy polymer radicals (COO•) cannot be formed. After the initial formation of polymer and hydrogen radicals (equation 2.12) other reactions are able to take place. Typically these result in the formation of cross-links, such as;

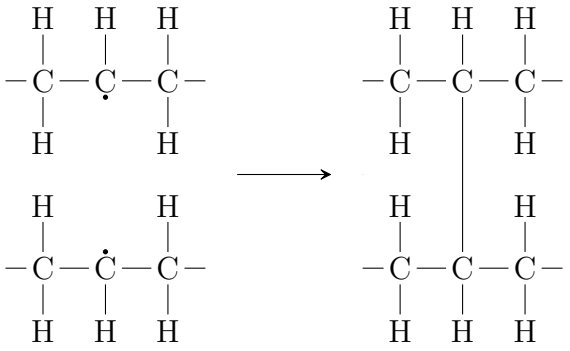

(2.31)

or the process of chain scission, resulting in vinyl groups on the polymer chain [68].

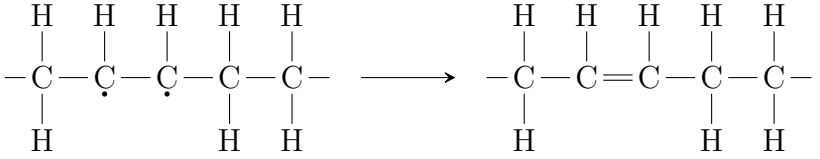

(2.32)

During photo-irradiation there is competition between reactions that form cross-links and those that form oxidation products (hydroxyl and carbonyl groups). Samples aged in an oxygen free environment therefore show a higher quantity of cross-linking [71].

2.3.2 Investigations into the Photo-Irradiation of Polyethylene

The distinction between photo-irradiation processes in an oxygen environment and oxygen free environment are only applicable in the case of pure PE. In reality, for an antioxidant free polymer, some oxidation will take place during processing and manufacture such that oxidation products will be present [72]. Some of the oxidation reactions will then continue when subjected to UV radiation, such as Norrish type 1 or 2 reactions, but assuming a completely oxygen free environment the oxidation products will not increase in concentration.

During photo-irradiation it is thought that the majority of changes will occur within the amorphous and crystalline edge regions of the polymer due to the limited ability for chain movement in the crystalline part of the polymer, leaving the crystalline region relatively unaffected [58, 73, 74]. Confirmation of this can be seen with a greater increase in oxidation products for LDPE than HDPE when subjected to the same photo-irradiation conditions [50, 71]. Investigating molecular relaxations with dielectric spectroscopy has also shown a greater change in β-peaks than α-peaks [55, 74]. The β-peaks are thought to relate to chain movements in the amorphous part of the polymer. The majority of cross-linking is also expected to form in the amorphous region due to the easier chain rearrangement but not excluded from the crystalline regions as the polymer radical ($C^{\bullet}$) may be able to move along the polymer backbone [68]. LDPE crystallinity is seen to decrease as a result of photo-irradiation, expected to be due to chain scission processes within the crystalline regions of the polymer. The measurement of decreases in crystallinity of the polymer as cross-linking increases support this [50].

The rate at which oxidation processes can occur is dependent on many influencing factors such as: the free volume within the polymer matrix, the energy of the incident radiation, the absorbance spectra of the specific material and the temperature at which photo-irradiation occurs [48, 65]. Work by Peacock [68] showed the rate of photo-oxidation to be significantly enhanced at temperatures above 100 ^{o}C. There is also a control over the depth of oxidation product formation relating to the diffusion of oxygen into the bulk of the polymer versus the quantity of photons absorbed by the polymer matrix. An oxygen-diffusion limited affect is often seen for LDPE with the oxygen being consumed near the surface through photo-oxidation reactions and therefore mainly the formation of cross-links within the bulk of the polymer [71]. Investigations into the depth of carbonyl group formation versus the generation of cross-links shows the carbonyl groups preferential

to the polymer surface [56, 66, 75, 76]. Gulmine *et al.* [56] suggesting an exponential decay of carbonyl group concentration from the polymer surface, reducing by more than 70% within the first 10 μm and has been supported by others [77]. Cross-linking of PE due to irradiation by γ-radiation has shown a reduced permeability to oxygen [30]. Therefore oxidation products may form closer to the surface as UV ageing duration increases.

Irrelevant of the location of photo-oxidation reactions, different rates of carbonyl group formation are often shown. Some researchers show an approximately linear increase in carbonyl groups with oxidation time (thermal, UV- or γ-irradiation) [56, 69, 70]. Others have suggested a time squared relationship between carbonyl groups and ageing duration [78–80]. The latter group particularly focuses on continued UV ageing at 253.7 nm rather than intermittent exposure or longer wavelength radiation. The explanations given for a time squared increase relate either to the presence of anti-oxidants in the polymer system which initially are consumed or auto-acceleration due to increased absorption at the excitation wavelength (200 - 300 nm) [50, 77].

The scission of chains and increased stresses as a result of photo-irradiation are also expected to produce rougher surfaces due to the formation of cracks [54, 73]. Though this is expected only to be significant at very late stages of ageing, correlating with an increase in the brittleness of the polymer films [56]. The chain scission process is also expected to account for the reduction in molecular weight of LDPE as a result of the shortening in average chain lengths [66].

2.4 Space Charge in Polyethylene

Under electrical stress, charge accumulates in PE and has been investigated by a variety of methods that will be discussed later (section 3.5). At a metal-polymer interface, on application of an electric field, charge is able to inject into a polymer according to the injection mechanisms discussed previously (section 2.1.3). This charge becomes trapped near the electrode-polymer interface and is of the same polarity as the electrode, termed homocharge [47, 81]. This homocharge accumulation reduces the local electric field near the interface and in some cases is thought to cause a SC limited charge injection situation [41, 81]. Alternatively the application of a large enough electric field can cause ionisation of impurities within the polymer bulk [82]. These ionised impurities will then migrate under the electric field to the opposite polarity electrode, causing the formation of heterocharge at

the electrode-polymer interface. This heterocharge accumulation will then enhance the local-electric field in this region.

Homocharge formation is thought to be dominant at low field levels and heterocharge at higher fields, though the exact levels being material and impurities dependent [82]. Investigations into different PE based materials showed measurable charge accumulation in the bulk to occur at fields as low as approximately 10 $kV_{dc}\,mm^{-1}$ in LDPE and XLPE but approximately 15 $kV_{dc}\,mm^{-1}$ in HDPE [41]. During charge decay a large quantity of homocharge near the electrode is seen to decay slowly in HDPE, suggesting the difference to be due to the early accumulation of homocharge very near the electrodes, creating a SC limited charge injection condition. The slow charge decay suggesting an increased quantity of deep (higher energy) trapping sites in the HDPE [25].

Other work investigating changes in SC accumulation due to different material properties has suggested a relationship between the charge movement in crystalline and amorphous regions. Investigating LDPE with a range of crystallinity ratios has shown less SC accumulation within the bulk of the polymer as the crystallinity ratio increased [83]. This suggests the trapping of the majority of injected charge occurs within the amorphous regions, where the most likely concentration of impurities and chain defects are to occur [36, 64].

2.4.1 Space Charge in Alternating Fields

Under a symmetrical alternating current (ac) field it could be expected that there should be no net accumulation of SC since any injected charge during one half cycle should be extracted or recombined during the following half cycle. Experimentation though has shown that with a high enough field and continued ac stressing there is a significant build up in one polarity of charge over the other [12]. This is expected to be due to unsymmetryical charge trapping energies causing an enhancement of one polarity charge trapping. Typically in LDPE the build up of SC under an ac field is negative [12].

2.4.2 The Affect of Ageing on Charge Movement

As polymeric insulation ages there is expected to be rearrangements of the chemical structure along with the addition of some new chemical groups and impurities (section 2.2). Differences in the chemical structure or chemical make up can significantly affect the accumulation of charge within the polymer [64]. The

biggest changes as a result of photo-irradiation relate to the formation of oxidation products and the generation of cross-links within the polymer structure. If the simple carbonyl and hydroxyl oxidation products are considered in terms of their Lewis structure [84], then an increase in charge trapping can be expected, i.e.

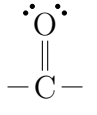

(2.33)

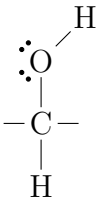

(2.34)

The presence of oxidation products on the polymer chains create unbonded valence electrons. The formation of cross-links and chain scission also disturbs the movement of charge along the polymer chains and alters charge trapping properties.

Investigations into the effect of oxidation products have shown increases in charge trapping as a result of oxidation products [85]. Typically an increase in the negative homocharge injected from the electrode is seen [16, 86]. The formation of oxidation products are expected to generate high energy trapping sites and some early thermally stimulated current (TSC) spectroscopy results have supported this [87, 88]. As the oxidised samples are warmed a peak is seen that is thought to relate to the relaxation of charge trapped by carbonyl group dipoles and is suggested to release at an energy of approximately 1.4 eV.

Increases in oxidation products have also shown an increase in conduction under a dc field [76, 85]. If carbonyl groups are expected to generate deep trapping sites then these would not easily explain an increase in conduction without a very high electric field. To explain this, it is suggested that carbonyl groups may generate two energy levels of charge trap, one being a deep trap and the other one shallow [46, 85, 89]. Huzayyin *et al.* [46] has completed some quantum simulations that suggest the presence of a carbonyl group produces a deep trap at approximately 2 eV and a shallow trap at approximately 0.4 eV. Though the trap levels are not yet accurately measurable experimentally, the concept of two different trap levels makes the explanation of an increase in trapped charge along with increased dc conduction possible. Alternatively, it is thought the increase in polar groups near the electrode-polymer interface (such as carbonyl groups from photo-oxidation) may ionise and therefore enhance the local electric field causing a greater injection of charge into the polymer [90].

2.5 Electroluminescence in Polyethylene

EL is the emission of a low level of light when a polymeric material is subjected to an electric field. Measurements have been reported under both dc [91–93] and ac [94–96] fields. EL measurements under dc are thought to originate from the bulk of the polymer and have been correlated with dc space charge measurements and simulations [91, 92]. The results showed an initial EL emission at field turn-on and then a continuous emission starting approximately 10 minutes later. The initial emission is thought to relate to dipole rearrangements from the initial field application and the continuous emission due to the recombination of charge in the polymer bulk [20]. Under an ac field the charge does not have time to recombine within the polymer bulk. Instead the emission is thought to originate from very near the electrode-polymer interface. Due to the potential of investigating charge movement in a very small region, ac EL is currently of great interest [19, 97, 98].

2.5.1 Source of Light Emission

In order for the polymer to release a photon of light, an electron needs to be excited to a higher energy state and the various excitation mechanisms are discussed later (section 2.5.2). During a subsequent relaxation it may release the energy radiatively as a photon of light or non-radiatively as thermal energy [21]. These radiative and non-radiative relaxations can occur along either physical or chemical pathways [99]. Decay along a physical pathway allows the associated molecule to excite and relax along a purely reversible process, a chemical pathway is an irreversible process due to the associated changes in chemical structure. The various radiative and non-radiative relaxations are detailed in the Perrin-Jablonski diagram (figure 2.6).

The molecule is excited due to the recombination of opposite polarity charge and excited into a higher energy state. From this higher energy state various energy conversions take place to allow the excited electron to decay back to its ground state (S_0). Initially vibrational relaxation and inter system crossing (both non-radiative) will bring the excited electron to the bottom of the lowest excited singlet state (S_1). From this point the energy can be lost through further vibrational relaxations or the radiative emission of a photon, known as fluorescence. Due to the energy lost before the radiative emission of light the fluorescence does not relate to the excitation energy from charge recombination. Alternatively, if inter-system crossing takes place the excited electron will lose energy to reach the lowest possible

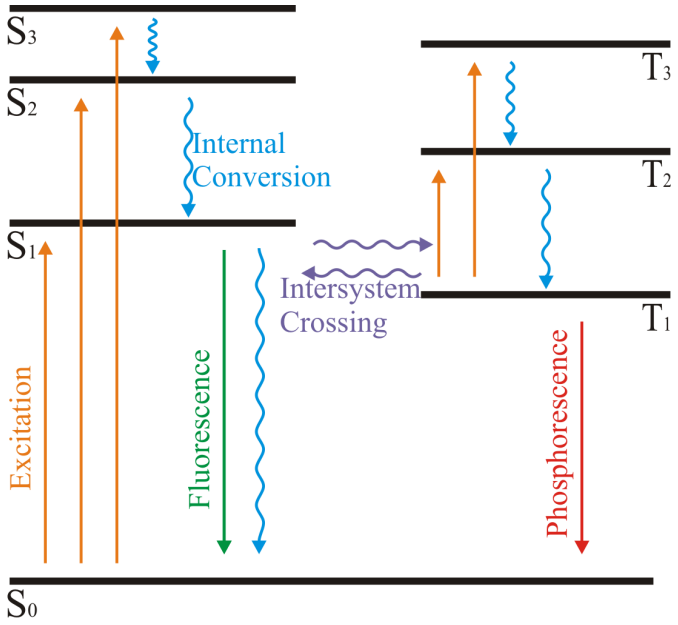

FIGURE 2.6: Perrin-Jacblonski diagram of energy conversion within a polymer

excited triplet state (T_1). This would result in greater non-radiative energy loss and therefore the emission has a longer wavelength (lower energy), this time known as phosphorescence [50].

In theory the excitation energy can be calculated using the Planck-Einstein equation,

$$E = \frac{hc}{\lambda} \tag{2.35}$$

Where E is the energy (in units of eV), h is Plank's constant (4.136×10^{-15} eV s), c is the speed of light in a vacuum (approximately 3×10^8 m s^{-1}) and λ is the wavelength of the emitted light (in units of m).

Using (2.35) over the typical range of wavelengths related to EL (400 to 800 nm [100]), the relaxation energy is between 4.15 and 1.60 eV. As explained, these energies do not directly relate to the excitation energy due to the other possible mechanisms of energy loss (i.e. internal conversion) before the release of a photon [50]. Therefore it is not possible to ascertain the exact chemical groups related to the trapping and recombination centres. Teyssedre *et al.* [101] suggest that the relaxation must occur from a triplet excited state due to the close relationship between phosphorescence and EL spectra (section 2.5.3). This may be possible due to the relatively efficient inter system crossing from the excited singlet to the excited triplet state in LDPE.

Other possible sources of light emission relating to electrical fields could be mistaken for EL, though they have very different excitation mechanisms. Examples of these light emissions are those caused by PD or the growth of electrical trees [102]. It is easy to identify the differences between these sources of emission from EL by the inception field, level of signal, typical wavelengths of the emission and spatial distribution. PD is seen to occur with a strong emission at fields as low as 1.6 $kV_{rms}\,mm^{-1}$ and produce a strong emission in the UV region [102, 103]. The emission from electrical trees occurs only at the ends of the branches in the form of spots [102, 104]. EL has no measurable emission in the UV region and is typically only detectable above approximately 10 $kV_{pk}\,mm^{-1}$ with a uniform emission from the entire electrode area [99, 105].

2.5.2 Excitation Mechanisms

Three different mechanisms are commonly discussed by which an electron can be excited to a higher energy level; direct field excitation, hot electron injection and bipolar charge recombination [19, 21, 106]. Direct field excitation involves the excitation of a low energy electron directly into a higher energy state across the forbidden region. Hot electron injection is the injection of a very high energy electron that collides with the polymer matrix to directly excite lower energy electrons. The bipolar charge recombination theory involves the injection of charge carriers into the polymer that become trapped in localised energy states and then recombine with opposite polarity charge carriers.

Direct field excitation is highly unlikely in the case of PE based materials due to the large energy gap of the polymer. The field required at room temperature is greater than the typical breakdown strength of the polymer (approximately 160 $kV\,mm^{-1}$) [18, 39, 107]. EL measurements have also been completed at both ambient and liquid nitrogen temperatures showing an increase in EL emission at cooler temperatures [108]. The opposite would be expected as a result of the direct field excitation due to the thermal excitation of some charge.

The hot electron theory involves the collision of injected or de-trapped electrons with the molecules of the polymer lattice. The kinetic energy present from this collision results in an increase in the kinetic energy of the molecule and either dissociation of the molecule or excitation to a higher energy state [109]. Further collisions and reactions may then occur from the free radicals of the high energy state molecules produced. The relaxation from these high energy states results in the release of a photon and is a purely chemical process. Some recent work has

compared the light emission of a polymer bombarded with high energy electrons to that of EL showing a correlation in the spectra of emission [110]. It is often argued that the viability of the hot electron theory requires a significant free volume within the polymer to exist for injected electrons to gain very high kinetic energies [21, 106].

The bipolar charge recombination theory involves the injection, trapping and recombination of charge carriers with each half cycle and is currently the most supported theory [111–113]. The diagram shown in figure 2.7 gives a simplified example of how bipolar charge recombination may take place. Charge is injected during 1 half cycle and on removal of the field, some charge remains trapped in the localised energy states discussed earlier (section 2.1.2). During the following half cycle, the opposite polarity charge carriers are injected and able to recombine with the previously trapped charge, causing excitation to a higher energy state. The subsequent relaxation from this results in the emission of a photon in the visible part of the spectrum. Not all the charge injected during each half cycle recombines and some remains trapped, ready to recombine during the following half-cycle. This EL should therefore occur in the first and third quadrants of the applied field, as has regularly been shown [47, 94, 97].

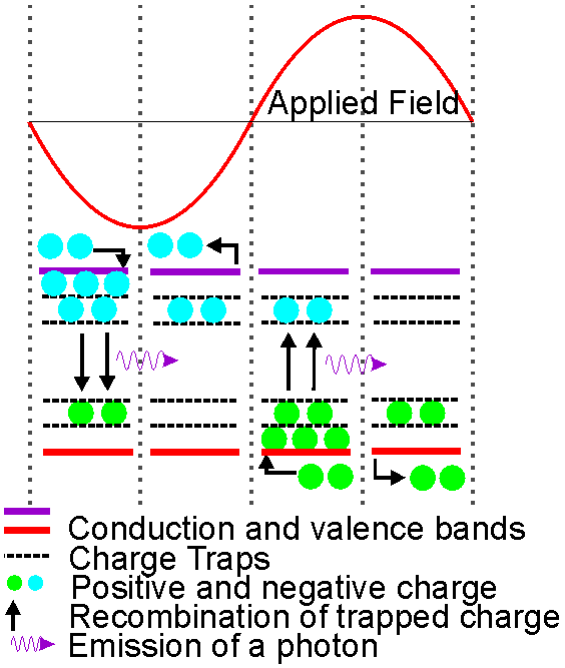

FIGURE 2.7: Representation of electroluminescence due to bipolar charge recombination theory

Recent work has reinforced the idea of bipolar charge injection as the dominant mechanism for the generation of EL in LDPE [19, 22, 93, 98, 112]. Modelling

has shown a good correlation between the bipolar charge recombination theory and various experimental conditions (under a range of frequencies, fields and waveforms) [22, 98].

2.5.3 Previous Electroluminescence Investigations

A lot of research has been completed investigating EL characteristics of various polymeric materials with a selection of differing experiment set-ups. Initial detection systems used a photomultiplier tube (PMT) to measure light emission but the lack of spatial information to confirm the source of the emission created uncertainty in results [108, 114]. Further developments included the use of cooled charge coupled device (CCD) cameras to confirm the source and uniformity of EL [29, 108]. Some investigators showed bright spots in their images of EL under uniform electrode arrangements [93, 115]. This is thought to be due to locally enhanced electric fields and further work showed the enhancement to relate to poor sample manufacture and the presence of impurities such as dust particles under the gold coating [47, 116].

There is a lot of discussion in literature about the threshold level of EL and the possibility of it showing the field at which electrical ageing begins [93]. Measurements under dc fields have suggested this is possible, the accumulation of SC corresponding to the onset of EL (PEA sensitivity of approximately 0.1 $\mathrm{C\,m^{-3}}$) [20]. Under ac fields PEA measurements for XLPE have shown space charge accumulation great enough to affect the local electric field at 12 $\mathrm{kV\,mm^{-1}}$ [117]. EL however is seen at approximately 10 $\mathrm{kV\,mm^{-1}}$ [105]. The actual presence of a threshold for ac EL is not currently identifiable due to the sensitivity limits of measurement systems.

Effect of Polymeric Material

The choice of material and environment can play a key role in EL. Investigations have been reported for a range of materials including; HDPE [94], XLPE [94], polyethylene terephthalate (PET) [17, 28, 29, 118], polyethylene napthalate (PEN) [17, 28, 29] as well as LDPE [28, 29, 94]. Comparison between LDPE and both HDPE and XLPE showed greater EL from LDPE [94]. This is thought to be due to the greater availability of charge trapping due to physical differences (such as short chains and amorphous regions) that do not appear in HDPE. XLPE would however be expected to have various by-products from the cross-linking reactions

which could be expected to enhance the charge trapping properties but the energy of the site may not be suitable.

More thorough testing has compared the EL of PET and PEN materials with that of LDPE due to the greatly different chemical structures [28, 29]. All results show PET and PEN to have a stronger intensity, explained due to the presence of aromatic rings on the polymer chain, phenyl in PET and naphthalene in PEN. These systems are thought to act as charge trapping and luminescent centres therefore enhancing the emission [21]. The spectral emission of the materials is similar. PET has a greater intensity around 450 nm, suggesting a stronger emission towards the UV part of the spectrum than PEN or LDPE [29].

The temperature dependence of EL has also been investigated. Cooling samples to -140 ^{o}C in a nitrogen (N_2) environment resulted in EL being nearly 3 times stronger than measurements taken at room temperature (20 ^{o}C) [72]. This suggested that EL may relate to the relaxation of triplet excited states, being more dominant in LDPE photoluminescence measurements at low temperatures [101].

The effect of different environments on EL have also been investigated, testing both under high vacuum (better than 10^{-4} Pa) and under different gasses. No change is seen between investigations under high vacuum and those complete in a nitrogen environment [100]. The presence of a glow discharge at pressures above 1 Pa mean either high vacuum or an inert gas environment are required [119]. Comparison of different gases showed nitrogen to be favourable, with oxygen and sulphur hexafluoride (SF_6) atmospheres quenching the emission [120].

Typical Spectral Characteristics

Fully resolving the spectrum relating to EL would allow the excited chemical states causing the emission to be better understood and therefore the process of excitation and relaxation mechanisms. However, the internal energy transfer processes within polymers are thought to be very efficient and therefore the luminescence spectrum does not confidently relate to the initial excited state [99]. A lot of work has been undertaken to investigate the spectrum of EL in various materials showing it to occur in predominately the visible part of the electromagnetic spectrum (400 - 800 nm) [28, 29, 108, 110, 119]. Due to the very low intensity of the emission only a broad spectrum has been possible by most researchers (approximately 50 nm bands). Peaks in the EL spectrum were seen in the 500 - 600 nm range and the 700 - 800 nm range. A more detailed spectrum has shown the peak EL for LDPE at 570 ± 4.5 nm [100]. The red (700 - 800 nm)

range is thought to relate to surface roughness of the gold coating creating surface plasmons and therefore is not a phenomena of EL emission. This is supported by the lack of red emission from dc excited EL, assuming both ac and dc EL to occur predominately from bipolar charge recombination [100].

The relationship between EL and ageing as either a cause or symptom of polymer degradation is often discussed in literature [21, 103, 108, 117]. Jonsson *et al.* [108] suggests that if any of the EL emission originates within the UV region there may be enough energy to cause chemical degradation. However since spectral measurements have only shown very weak emission in the UV region then this degradation mechanism would only be able to occur due to absorption of UV radiation and subsequent emission at a longer wavelength (fluorescence or phosphorescence). A comparison of various luminescence techniques (photo-induced fluorescence, chemiluminescence, recombination-induced luminescence) shows little correlation with EL [21]. Due to the UV absorption properties of LDPE, for the EL to generate enough light to cause significant changes there would still be a significant quantity available for detection [100]. A more detailed interpretation of the spectrum from polymers under various excitation mechanisms has led Laurent *et al.* [21] to conclude that EL originates from triplet excited states due to its strong correlation with low temperature phosphorescence emission. The decay of triplet excited states is thought to be a strong identifier of relaxation through chemical pathways and therefore suggests that EL may have the potential to cause and monitor material ageing [99]. The limit to fully understanding the degradation mechanisms relates to the very low level light emission and the limited sensitivity of high resolution EL spectroscopy systems.

Point on Wave Measurements

Improvements in detection system sensitivity and data acquisition speed have also made it possible to investigate changes in the EL during the cycle of the applied field, termed point on wave (POW) measurements [19, 94, 116, 121]. Typical results under 50 Hz sinusoidal fields have shown two peaks in the emission, one in the first quadrant and another in the third. These support the bipolar charge recombination theory (section 2.5.2), due to the release of photons from charge carrier recombination in both half cycles of the applied field.

Comparisons between the peaks in EL and the peaks of a sinusoidal applied field show that EL occurs first [91, 96]. As the field increases this phase difference between the peaks also increases, most noticeably in PET and PEN [18, 47]. This is thought to be caused by the accumulation of charge very near the electrode-

polymer interface, causing the local electric field to lead the applied field. The EL in PET and PEN is stronger than LDPE and increases at a greater rate, due to the aromatic rings present on the polymer backbone. This suggests greater injection of charge and more local trapping sites available compared to LDPE and therefore PET and PEN have a greater influence on the local electric field near the electrode-polymer interface.

Unsymmetrical phase differences are often seen in POW EL data and initial assumptions have suggested a bias towards the injection of one polarity charge carrier over the other. Recent work has suggested this is more likely to relate to differences in the quality of the electrode-polymer contact. The presence of bright spots in EL images correlating with an enhancement to the emission during one half cycle, this is thought to be due to a local field enhancement [47, 119]. Differences in surface roughness due to the manufacturing process of epoxy samples also showed a difference in polymer peaks, the dominant peak depending on which surface faced the detection system [122].

2.5.4 Changes in Electroluminescence with Ageing

Some investigations into correlations between EL and ageing have been completed in terms of electrical stressing [99], thermally ageing [113] and UV ageing [123, 124].

Investigations into the thermal ageing of polymeric materials have shown a range of behaviours. Yang *et al.* [67] has shown EL and SC measurements for thermally oxidised (at 90 ^{o}C) LDPE, below its melting point, for 0 to 600 hours. The results showed a stronger EL intensity at lower field strengths as the ageing time increased. As the field increased this reversed such that the aged samples produced a weaker emission. Alternatively, Laurent *et al.* [113] showed a reduction in EL at all field levels. The reduced EL put down to the increase in the carbonyl group concentration resulting from the ageing process.

Investigations into the changes in dc EL as a result of UV ageing of PEN have shown a reduction in the intensity at all field levels along with a reduction in the current [124]. This is suggested to be due to the greater trapping of charge near the electrode, reducing the local electric field and restricting the charge injection into the bulk and therefore less charge is available for recombination. Changes in the spectra of the emission were also reported, showing an increase in the emission at 600 nm and a reduction in the emission at 500 nm. Investigations into the ac EL intensity after UV ageing of polypropylene (PP) also showed a reduction in

intensity as ageing duration increased [123]. This was suggested to be due to the increase in carbonyl groups acting to quench the light emission.

Investigating changes in EL of cables after electrical stressing and combined thermal and electrical stressing showed a reduction in intensity [99]. The reduction in intensity was suggested to be due to the consumption of chromophores that were originally acting as recombination centres. Similarly long term dc electrical stressing over 12 days showed the EL to decrease along with the injection current [125]. The changes in the EL spectrum were also presented, showing a relative shift in the emission to longer wavelengths.

2.6 Summary

This chapter has discussed the physical and chemical structure of LDPE. Due to its complex disordered structure a theory for the charge movement is not trivial. To explain the presence of charge within the material, various localised energy levels are suggested, allowing for trapping and movement of charge between them. A method of investigating this charge movement is the phenomena of a low level light emission, EL, from electrically stressed polymers. Investigation into EL in various conditions has suggested light is emitted due to the injection, trapping and recombination of charge carriers, the bipolar charge recombination theory.

Ageing of LDPE films through photo-irradiation results in various chemical changes, including the production of oxidation products and cross-linking. These chemical changes are thought to influence the movement of charge through the polymer due to the generation of new trapping sites. Some initial investigations into the effect of ageing on EL have typically shown a reduction in intensity but with no consistent explanation. Since EL is thought to relate to the injection, trapping and recombination of charge, any changes in the charge trapping sites are expected to influence it. EL under an ac field will be investigated here due to its potential to probe changes in charge movement very near the electrode-polymer interface.

Chapter 3

Experiment Methodology

The previous chapter described the chemical structure of PE and its possible changes as a result of photo-irradiation. The main constituents of oxidation products and cross-linking that result from this are expected to generate charge trapping sites and influence the movement of charge in the polymer. As discussed, the measurement of EL phenomena is thought to investigate the charge movement very near the electrode-polymer interface and therefore show changes that result from ageing.

This chapter describes some of the experiments that identify changes in the chemical structure of the UV aged LDPE and electrical properties. A detailed description of the EL experiment and its development is also included.

3.1 Ageing Setup

To artificially age LDPE a UV lamp with a peak emission of 253.7 nm is used. The relative spectrum of emission intensities was confirmed by using a Princeton Instruments SP2500 spectrograph (figure 3.1). This shorter UV wavelength was chosen due to its common use in literature [126–128], higher energy and its stronger absorption by LDPE than longer wavelengths. Since 100 μm LDPE is not fully absorbent at this wavelength, photo-irradiation is therefore not restricted to the sample surface [60].

Samples consisted of 100 ± 5 μm additive-free LDPE supplied in rolled films by Goodfellows Ltd. [129]. To minimise ageing to the virgin material, samples were stored in a dark box at a constant temperature until needed. Ageing took place in 3 and 7 day intervals up to 21 days, after which the samples were too fragile to

reliably complete any measurements. An elevated temperature of 40 ^{o}C ensured a constant temperature throughout the ageing process, removing its affect as an influence on the rate of oxidation [59, 77, 130]. At temperatures this low it has been shown to cause no measurable change in oxidation products, carbonyl and hydroxyl groups only being detected after 28 days of ageing at greater than 70 ^{o}C [2, 131, 132].

Samples were cut into strips (60×300 mm) and 4 were located around the UV source at approximately equal distances (figure 3.2). The samples were mounted far enough away from the UV source for the surface temperature to be maintained at the 40 ^{o}C of the oven. The surface temperature of the sample was confirmed over a 6 hour ageing duration to change by less than 2 ^{o}C. The samples were mounted 220 mm from the UV source. The irradiation power at the surface of the samples is 4.1 mW cm^{-2}, not accounting for the reflection of any light, this is within the range used by other researchers [66, 126, 128].

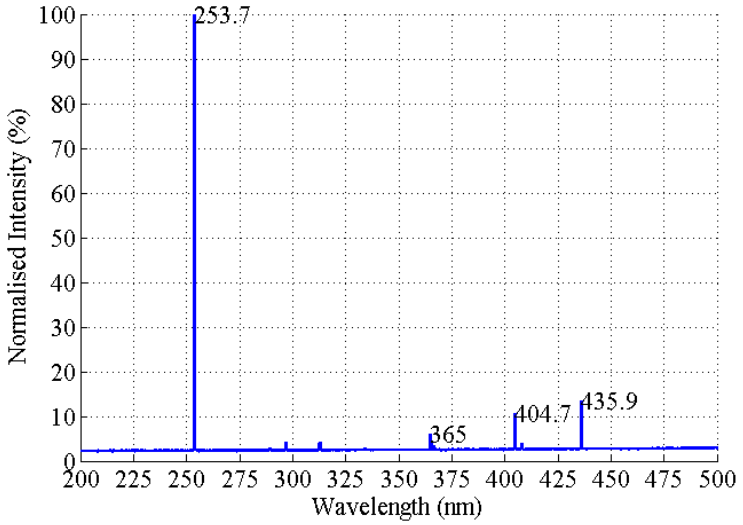

FIGURE 3.1: Spectra of ultraviolet ageing tube

3.1.1 Nitrogen Ageing

To confirm the effect of oxidation products rather than other photo-irradiation changes, some samples were also UV aged in an oxygen free environment. To achieve this, samples were placed in a quartz vessel (figure 3.3) with a UV transparency of approximately 90 % [133]. The vessel was evacuated for 10 minutes before backfilling with dry nitrogen. The nitrogen gas was filled to a pressure of approximately 10^4 Pa below atmosphere so any gas leaks during ageing could be identified at the end. The sample was mounted the same 220 mm away from the UV source (figure 3.2).

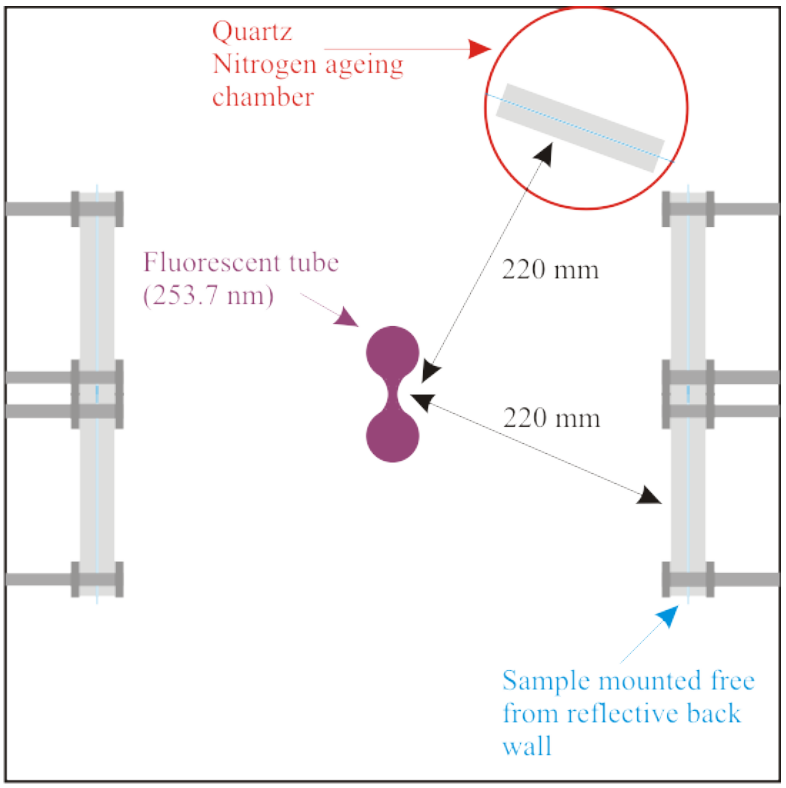

FIGURE 3.2: Diagram of UV ageing arrangement

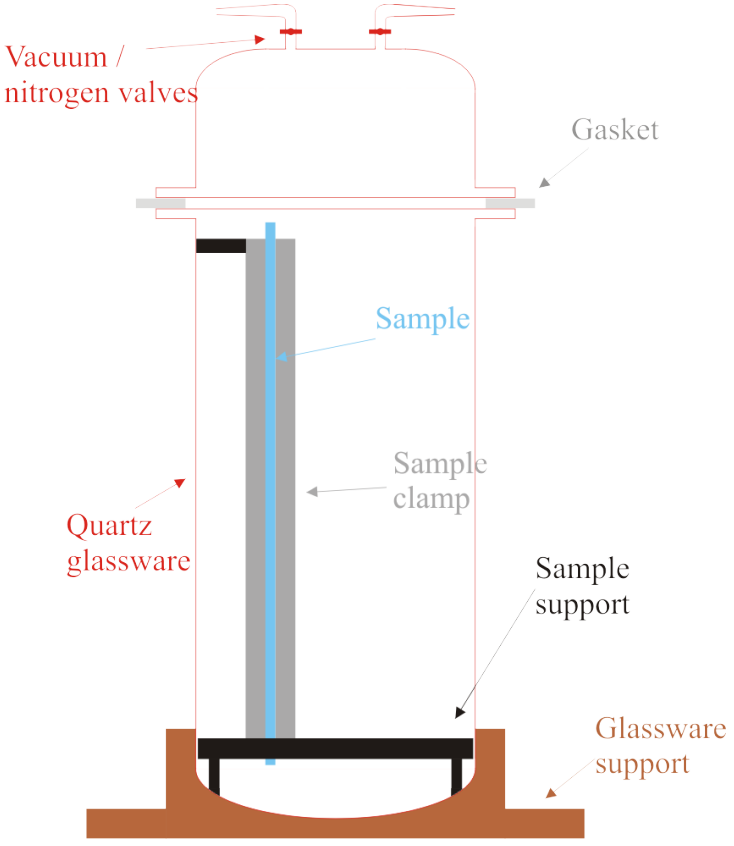

FIGURE 3.3: Diagram of nitrogen ageing vessel

3.2 Fourier transform infra-red spectroscopy

infrared (IR) spectroscopy makes use of the infrared region of the electromagnetic spectrum to investigate the molecular structure of samples. Using a combination of near (14000 - 4000 cm^{-1}), mid (4000 - 400 cm^{-1}) and far (400 - 10 cm^{-1}) IR the rotation or vibration of molecules can be determined. At certain wavelengths the bonds of particular molecules will absorb the IR radiation and alter the dipole moment of the bonds [134]. The vibrational movements of these bonds for simple molecules, such as a CH_2 groups, are often classified as; symmetrical stretching, anti-symmetrical stretching, scissoring, rocking, wagging and twisting (figure 3.4). Measuring the percentage of IR absorbed by the material allows its chemical composition to be identified.

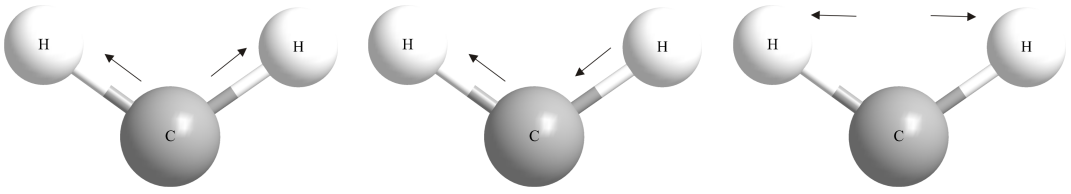

(a) Symmetrical Stretching
Moving towards and away from the carbon atom

(b) Antisymmetrical Stretching
Moving towards and away from the carbon atom

(c) Scissoring
Moving perpendicular to the carbon atom

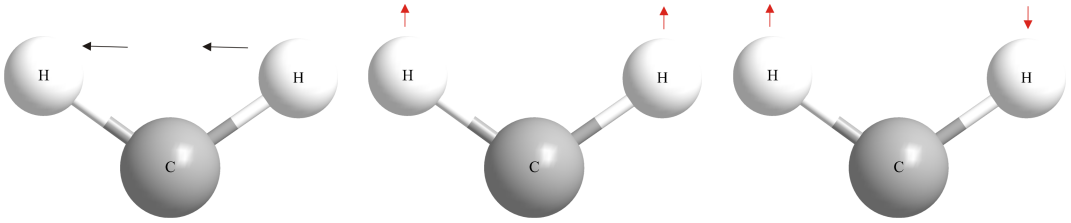

(d) Rocking
Moving perpendicular to the carbon atom

(e) Wagging
Moving into and out of the page

(f) Twisting
Moving into and out of the page

FIGURE 3.4: Pictorial representation of vibrational modes detected using FTIR spectroscopy

Results for IR spectroscopy are usually quoted in wavenumbers rather than wavelength, the conversion is made using [134].

$$\bar{v} = \frac{1}{\lambda} \tag{3.1}$$

Where $\bar{v}$ is the wavenumber (with units cm^{-1}) and λ is the wavelength (with units cm). The use of wavenumbers offers the advantage of increasing linearly with energy.

Use of the Beer-Lambert law along with IR absorption allows the actual concentration of a specific chemical group to be determined [50, 134].

$$\ln \frac{I}{I_0} = -alc' \tag{3.2}$$

Where I is the transmitted light, I_0 is the incident light, a is the absorption coefficient (with units $\mathrm{cm}^2\,\mathrm{g}^{-1}$), l thickness of the sample (with units cm), c' is the concentration (with units $\mathrm{g\,cm}^{-3}$). The law relates the intensity of radiation transmitted through a material with the absorbing centres within the material. In order to establish a value for a, a calibration measurement must be taken for a sample with a known concentration. This has not been completed in this work since only changes in concentration are desirable which can be interpreted by comparisons in absorption spectra between the virgin and aged samples.

In this work IR spectroscopy was undertaken using the FTIR method. This is a faster method of determining the IR spectrum by measuring a range of wavelengths transmitted through the material at any one time. Post processing using a Fourier transform allows the absorption at specific wavelengths to be determined [134]. Measurements in this work are completed using a Perkin Elmer, FT-IR spectrum GX system with MIRTGS sensor, covering the range 4000 to 500 cm^{-1}, with a resolution of 1 cm^{-1}. To avoid the measurements being affected by different gas environments the system has a continuous nitrogen purge through the sample chamber. The sample chamber is opened for the minimum amount of time and left for 30 minutes before any measurements are taken to ensure a stable atmosphere. A background spectrum is initially taken to account for absorption of the measurement system and gas environment in the sample data.

The greatest change in IR absorption is expected as a result of photo-irradiation in air and therefore an increase in oxidation products [50, 63]. Typical wavenumbers were shown in the previous chapter (section 2.3) relating to the formation of carbonyl groups ($\mathrm{C{=}O}$) consisting of ketones, aldehydes and carboxylic acid with absorption in the range 1800-1700 cm^{-1}. The absorption relating to hydroxyl ($-\mathrm{OH}$) groups produced a much broader spectrum over the 3500 to 3000 cm^{-1} range.

3.3 Dielectric Strength

As materials age their ability to withstand electrical stressing is expected to reduce [27]. The electrical strength is determined by linearly increasing a field until the sample can no longer withstand it as per the ASTM D149-97a standard [135]. The eventual failure of the polymeric insulator is due to a high current between the two electrodes resulting in the melting of the polymer. The processes leading to this eventual failure are not fully understood, but often categorised into 3 areas, purely electronic, purely thermal and electromechanical failure [27, 38]. Electronic breakdown relates to the injection or acceleration of electrons within the polymer able to ionise the polymer matrix, producing further charge carriers and associated increase in current until irreversible damage occurs [2]. A purely thermal failure relates to the energy lost through conduction and polarisation currents which if large enough will thermally heat the polymer at a greater rate than the energy can be dissipated. Electromechanical failure occurs due to the electrostatic attraction of the electrodes, the applied force will decrease the thickness of the insulation and result in an increased electric field.

Due to the various failure mechanisms, differences in material properties and other external influences the failure strength covers a large range and so a simple average calculation is rarely appropriate [2]. Instead a 2 parameter Weibull distribution is commonly used which allows the typical breakdown strength and range in data to be easily presented and interpreted [136–139]. This originates from the 3 parameter Weibull distribution allowing the probability of failure to be calculated using.

$$F(x) = 1 - \exp\left(-\left(\frac{x - x_{t_0}}{\alpha}\right)\right)^{\beta} \tag{3.3}$$

Where $F(x)$ is the cumulative probability of failure at time x, x_{t_0} is the threshold before which a failure cannot occur, α is location parameter and β is the shape parameter. In this case since the voltage increases linearly with time, the field at which failure occurs is used for x and 0 kV is used for x_{t_0} resulting in a 2 parameter distribution. α is often used to give an approximation of the breakdown strength and β determines the spread in the data such that a large value of α and large β are desirable features of an electrical insulator. A thorough statistical analysis of the Weibull distribution has been presented by Green [140].

Measurements were completed by increasing a 50 Hz, sinusoidal field, at a rate of 50 Vs^{-1} until the sample failed. The experiment set-up has been discussed in detail in literature and is represented by the diagram in figure 3.5 [137, 138, 140, 141].

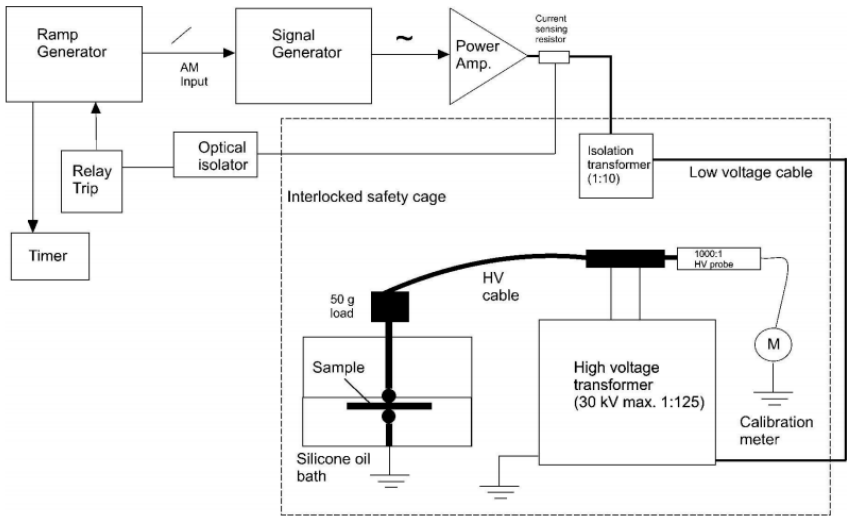

FIGURE 3.5: Diagram of ac ramp breakdown experiment from [142]

The experiment consists of two 6.3 mm stainless steel ball bearings as electrodes, changed every 10 breakdowns to avoid enhanced stresses due to electrode pitting affecting the results [141]. Samples are mounted between the ball bearings and to avoid surface flash overs are submerged in a tank containing silicone oil (Dow Corning® 200/20 CS). A function generator supplies a 50 Hz sinusoidal voltage and the use of an amplifier ramps the high voltage across the sample at a rate of 50 $V\,s^{-1}$. A digital volt meter (DVM) measures the voltage across the sample through a 1000:1 transformer and on failure records the maximum voltage reached. Samples consist of approximately 25×25 mm squares with 10 individual breakdown sites located per sample. The thickness of each site is measured and accounted for in calculating the electric field at the point of failure. The dielectric strength of a polymer is known to be significantly affected by temperature [38]. All measurements were completed at room temperature and the temperature recorded. Due to the time required for measurement collection not all results could be completed within one day. To minimise the affect of daily and seasonal temperature drifts, a virgin sample and either all air or nitrogen ages were tested during each session. The parameters and confidence limits of the 2 parameter Weibull distribution were determined using the commercially available software, Reliasoft Weibull++® 7.

3.4 Dielectric Spectroscopy

To investigate changes in the dielectric properties of the material, dielectric spectroscopy measurements were completed. This investigates the relationship between complex relative permittivity (ϵ^*) and frequency [74]. Maxima in the ϵ^* relative to changes in frequency can be associated with particular molecular movements in the dielectric, termed dielectric relaxations [143]. Placing a dielectric material between two oppositely charged plates will cause any negative charge to be drawn towards the positive electrode and vice versa for positive charge. This results in the orientation of dipoles in the polymer with the electric field, as such it becomes polarised. The rate at which the dipole organsisation occurs is controlled by the molecular structure within the polymer. Changes in the movement or frequency allows changes in the molecular structure to be interpreted, some movements however will also require the supportive movement of nearby chains [144].

This can be explained further by considering the affect an electric field (E) has on the dipoles within the polymer,

$$E = E_0 \cos \omega t \tag{3.4}$$

Due to restrictions on molecular movement the polarisation of dipoles within the polymer will lag behind that of the electric field [27]. This can be represented by.

$$\begin{aligned} D &= D_0 \cos(\omega t - \delta) \\ &= D_0 \cos\delta \cos\omega t + D_0 \sin\delta \sin\omega t \\ &= D_1 \cos\omega t + D_2 \sin\omega t \end{aligned} \tag{3.5}$$

Where E is the electric field, E_0 is the amplitude, D and D_0 are the associated displacements, ω is the angular frequency and δ is the phase lag. From this real relative permittivity ($\epsilon^{'}$) and imaginary relative permittivity ($\epsilon^{''}$) can be defined as,

$$\epsilon^{'} = \frac{D_1}{\epsilon_0 E_0} \qquad \epsilon^{''} = \frac{D_2}{\epsilon_0 E_0} \tag{3.6}$$

The complex relative permittivity (ϵ^*) can then be shown to be [27],

$$\epsilon^* = \epsilon^{'} - i\epsilon^{''} \tag{3.7}$$

The real meanings of these relative permittivities can be understood by considering a dielectric in an electric field to be a capacitor (C_0). When a voltage (V) is applied across the capacitor there will be a complex current produced (I^*). The real part of the complex current being 0 in an ideal capacitor. This complex current can be calculated,

$$I^* = \omega C_0 \left(\epsilon^{''} + i\epsilon^{'}\right) V \tag{3.8}$$

Allowing for the current relating to the capacitive (I_C) and resistive (I_R) components to be calculated.

$$I_C = i\omega C_0 \epsilon^{'} V \tag{3.9a}$$
$$I_R = \omega C_0 \epsilon^{''} V \tag{3.9b}$$

For consistency, the same 100 μm thick samples were used for dielectric spectroscopy. It is known that a thicker sample is often desired to reduce the surface effects and aid in measuring the true dielectric response from the bulk of the material [136]. However, due to the high electric fields required for EL measurements and the capabilities of the high voltage amplifier thinner 100 μm samples had to be used for consistency between experiments. The samples were sputter coated on both sides with gold (approximately 34 mm diameter and approximately 40 nm thick per side) to provide uniform electrodes.

Samples were mounted in a custom built cell, depicted in figure 3.6. This custom built cell shields the sample from most electrical noise and allowed measurements over the range 10^{-2} to 10^{6} Hz. Due to its use in an operating high voltage laboratory measurements can become quite noisy at greater than 10^{4} Hz in low loss samples. Measurements at frequencies below 10^{-1} Hz take a very long time and so was the lower measurement limit of this work. After testing a sample the electrodes can be fixed in place and the sample removed. This allows a background measurement to be taken, accounting for other capacitances in the system (connections, cabling, internal capacitances, etc.).

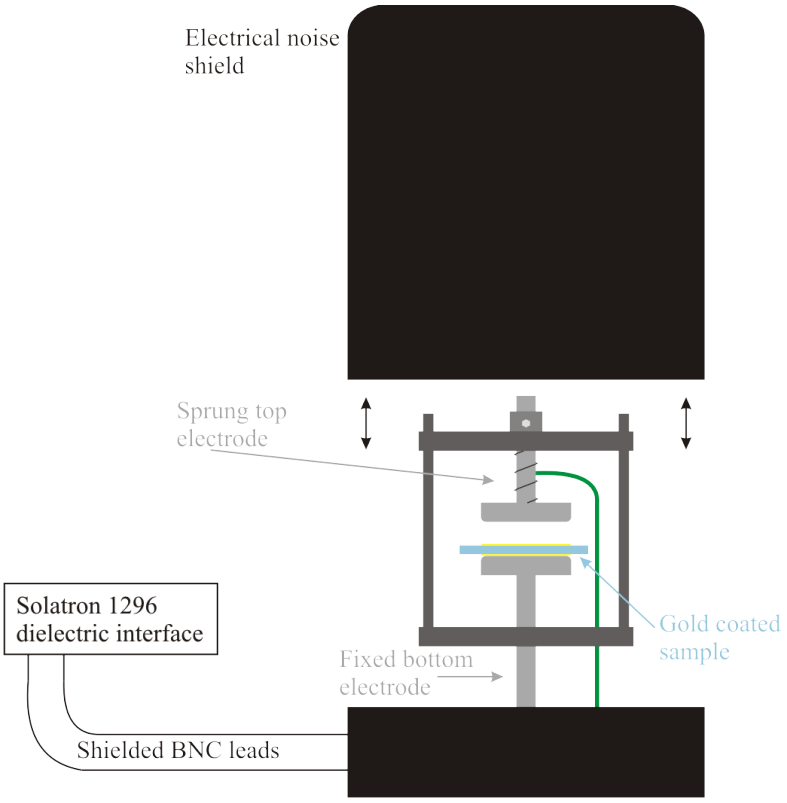

FIGURE 3.6: Dielectric spectroscopy custom chamber and experiment arrangement

Measurements were collected using a Solatron system consisting of a 1296 dielectric interface, SI1260 impedance/gain-phase analyzer and a computer controller. The system was set to integrate over 20 cycles at 1 V, producing a good signal to noise ratio. Measurements were completed from 10^{-1} to 10^{6} Hz with 20 per decade. The system records the capacitance and phase angle between the voltage and current such that dielectric loss tangent ($\tan\delta$), $\epsilon^{'}$, $\epsilon^{''}$ can be calculated using;

$$\tan\delta = \tan(\delta_{sample} - \delta_{background}) \tag{3.10}$$

$$\epsilon^{'} = \frac{C_{sample}}{C_{background}} \tag{3.11}$$

$$\epsilon^{''} = \epsilon^{'}\tan\delta \tag{3.12}$$

Where δ_{sample} and $\delta_{background}$ are the phase angles between the voltage and current for the sample and background measurement respectively and $C_{sample/background}$ the associated capacitance.

3.5 Space Charge Accumulation

There are various techniques to measure the formation of SC within polymeric materials (section 2.4) and are regularly described in literature [2, 14, 16]. The method chosen for this work is the pulsed electro acoustic (PEA) technique, a full description of which has been regularly presented in literature [16, 27, 67, 145]. The system measures charge by applying a short duration voltage pulse (V_p), this creates an electrostatic force (F_e) on any charge within the polymer (figure 3.7). The displacement (D) of the charge as a result of the force creates an acoustic pressure wave which propagates through the material. A piezoelectric based sensor converts this into electrical signals (V_s) and passes it through 2 stages of amplification before being recorded by an oscilloscope. Synchronisation between the measured signal and the pulse system allows the signal to be time resolved. The amplitude of the signal then determines the quantity of charge and the delay indicates the position within the polymer. Since the oscillations of negative and positive charge will be in opposite directions, the PEA system will only present the net accumulation of charge at any position.

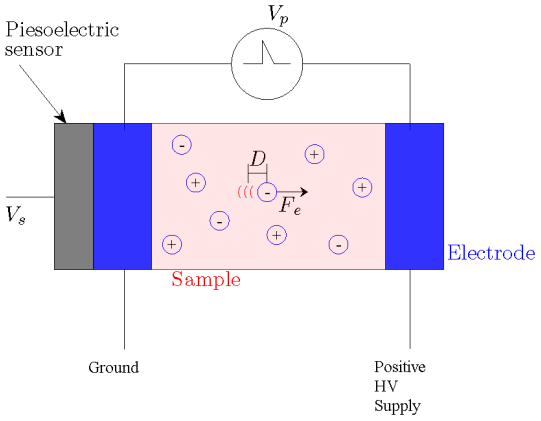

FIGURE 3.7: Schematic for the theory behind the pulsed electroacoustic system

The PEA system used is the Pulsed Electroacoustic Nondestructive Test System (PEANUTS) from Five Labs. The experiment (figure 3.8) consists of two electrodes and an enclosed polyvinylidene fluoride (PVDF) piezoelectric sensor and amplifier system.

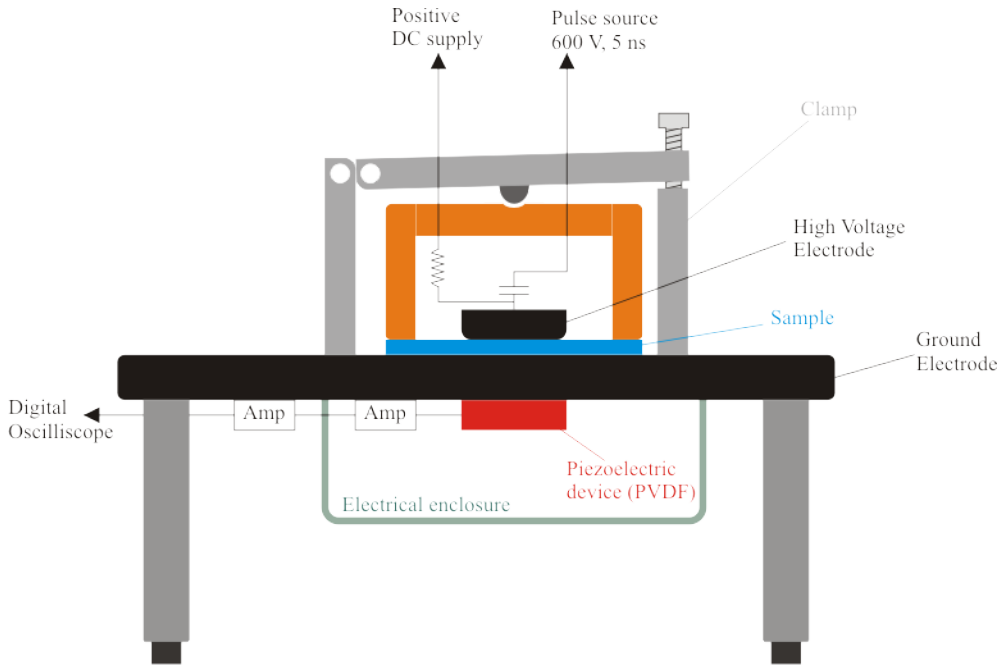

(a) Diagram of experiment

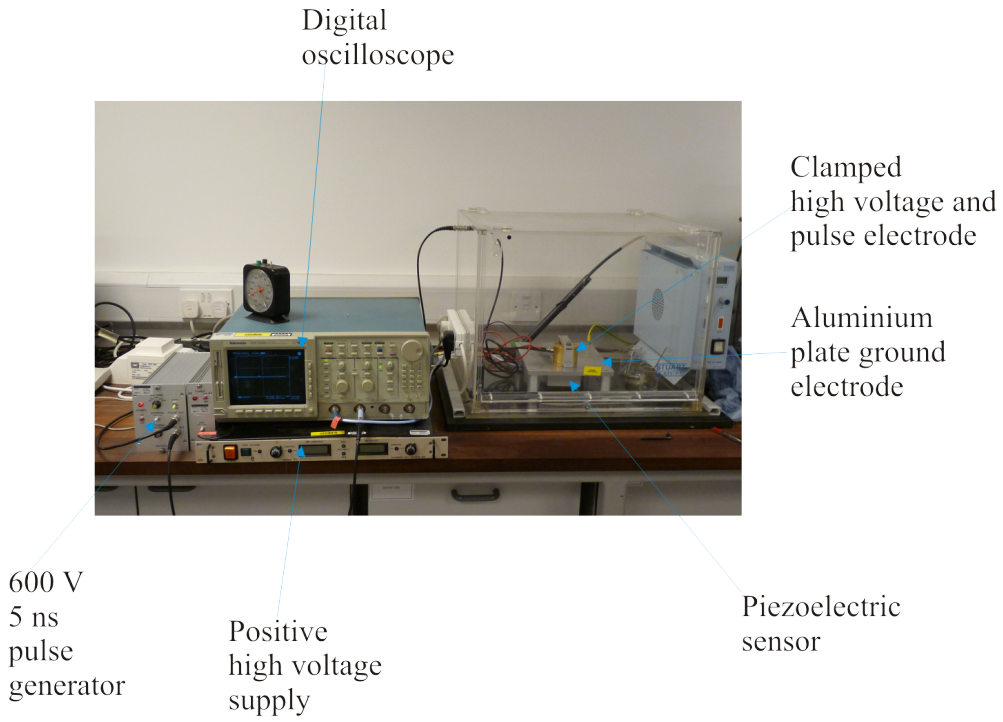

(b) Photo of experiment

FIGURE 3.8: Experiment arrangement for measuring space charge using the PEA technique

The bottom (ground) electrode is made from a thick aluminium block to provide a time delay in the signal and therefore reduce interference as a result of vibrations from the pulse voltage. The top (high voltage) electrode is made from XLPE loaded with carbon black (semicon) for acoustic matching with the PE based polymer [146]. The top electrode is 5 mm in radius and so samples were cut into 40×40 mm squares to avoid surface flashover. Ideally, for close comparison with EL measurements, samples would be coated with gold electrodes but this has been shown to inject significantly less charge and reduce the resolution of the PEA measurement [145, 147]. A very thin layer of silicone oil (Dow Corning® 200/20 CS) is placed on either side of the sample to help with transfer of the acoustic signal. In this work a 5 ns, 600 V pulse is used and the pulse generator also triggers the oscilloscope.

In order to convert the electrical output signal from the oscilloscope (mV) into a space charge density ($\mathrm{C\,cm^{-3}}$) the acoustic impedance of the system needs to be determined [13, 146]. To achieve this a measurement is taken before the accumulation of any charge in the sample. The signal can then be assumed to only relate to surface charge created at the electrode-polymer interface and using this the acoustic impedance determined. Ideally this would be collected purely based on the pulse system without the application of any dc field to reduce the possibility of charge accumulation during calibration [148]. Due to the operation of the system in a working high voltage laboratory the signal to noise ratio is not good enough. Instead a small dc field ($10\ \mathrm{kV_{dc}\,mm^{-1}}$) was applied for less than 10 seconds, minimising the possibility of SC forming [149].

The output signal from the oscilloscope will also contain signals due to the non-ideal system response. The desired data can be deconvoluted from the output signal with the use of a transfer function. The full theory and technique for this has regularly been detailed in literature [13, 150]. The transfer function is calculated by the software to convert the calibration signal to the expected profile for a measurement with only surface charge. This same transfer function can then be processed on the sample after electrical stressing to analyse the accumulated SC.

There is a strong temperature dependence for charge injection and trapping in polymers [151, 152]. To avoid variations in results both SC and EL measurements were completed in a temperature controlled environment at approximately 20 ^oC. Space charge measurements can be collected with the applied field on (V_{on}) and off (V_{off}). applied field on (V_{on}) measures the SC within the bulk as well as

any charge at the electrodes. Charge at the electrodes is due to the presence of charge within the polymer and that created by the applied field. applied field off (V_{off}) measurements only show charge accumulated within the polymer. An image charge will also be seen at the electrodes.

3.6 Development of Electroluminescence Experiment

As discussed in literature (section 2.5.3) a range of different arrangements exist for detecting the EL. The systems operate in different ways each having its various advantages and disadvantages. This section will give a thorough description of the system developed and used in this work.

The experiment (figure 3.9) consists of a sample holder mounted on a 3 dimensional moveable stage (x and y for positioning and z for focussing). The holder is mounted within a vacuum / pressure chamber. Either end of the chamber has a steel plate, one end with a high voltage bushing and the other a fused quartz window through which the EL is measured. The entire arrangement is on an optical stage within a Faraday cage to block out unwanted light, electrical noise and vibration. The emission is focussed onto the detector using a fixed focal length lens (focal length = 59.8 mm, diameter = 50.8 mm) with an anti reflective coating (350 - 700 nm). The lens is chosen due to its high quantum efficiency and low effective aperture (maximum light collection) [153]. A function generator and high voltage amplifier allow various waveforms to be applied and a custom built trigger synchronises the camera and applied field.

3.6.1 Detection System

To detect EL, two different techniques exist, a cooled PMT measuring the total light intensity from the sample [108, 114] or a cooled CCD allowing imaging of the sample and obtaining the intensity from the quantified data [28]. A PMT system offers greater sensitivity but it is difficult to collect spatial information about the light. A CCD allows the intensity and spatial information to be collected simultaneously, but requires larger electric fields. The ability to confirm the source and uniformity of the emission is important in identify samples containing non characteristic bright spots. Therefore, the experiment at the Tony Davies High Voltage Laboratory, Southampton (TDHVL) was designed with a Peltier cooled electron multiplying charge coupled device (EMCCD) camera (Princeton Instru-

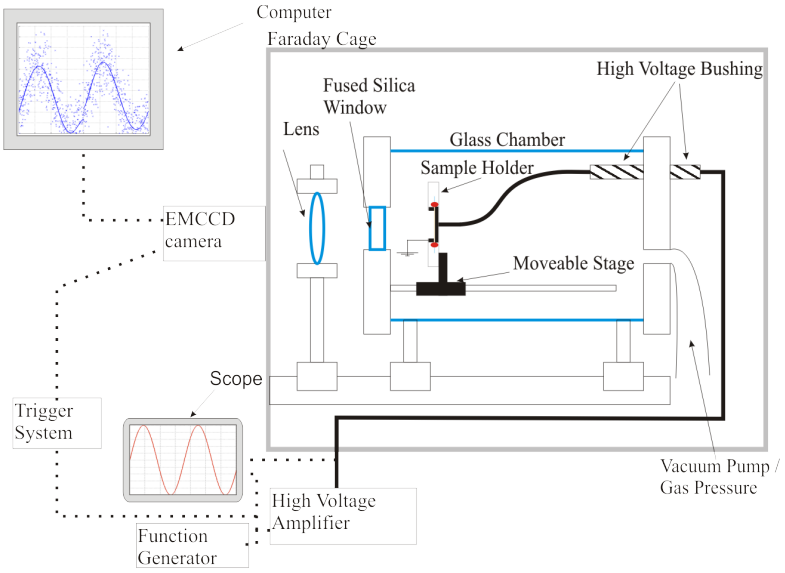

(a) Schematic of electroluminescence experiment

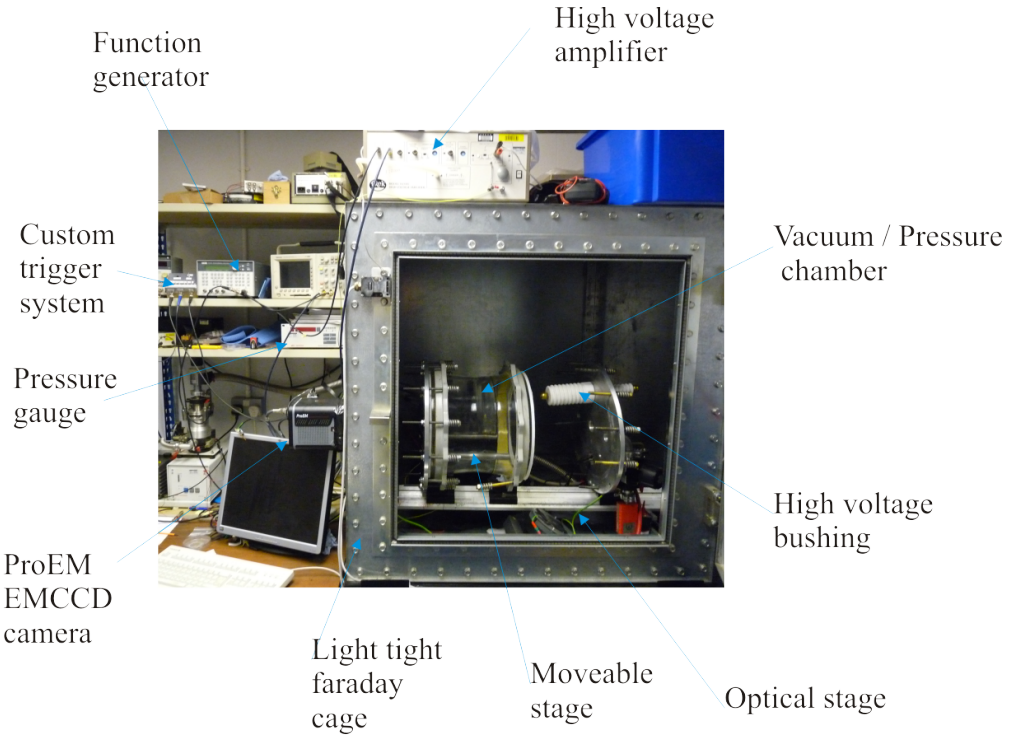

(b) Photo of electroluminescence experiement

FIGURE 3.9: Electroluminescence experiment

ments ProEM:512B [154]). This offers very high quantum efficiency (appendix A) over the desired detection range of (400 - 800 nm) [93, 155]. It also has the benefit of being able to take long, low noise, images as well as very high speed quantified measurements. This is achieved through two distinct modes of operation, the traditional slow, low noise readout of a CCD or the use of the electron multiplication (EM) circuit for high speed operation.

There are two types of noise associated with traditional CCD arrays, dark current and readout noise [47, 156]. Dark current is the thermally induced build up of charge on the CCD. Since the build up of charge is both time and temperature dependent it can significantly reduce the sensitivity of the detection system when taking long duration exposures. The ProEM system uses a Peltier element capable of cooling the CCD to -90 ^{o}C when circulated with 15 ^{o}C coolant. At this temperature the typical dark current is less than 0.005 e^{-} pixel^{-1} s^{-1} [154], significantly reducing its effect on long term image acquisition. The readout noise of the system is generated from electrical noise during conversion of the charge on the CCD to a digital voltage level for output, the greater the digitisation speed the higher the readout noise [156]. The ProEM offers a very low readout noise of approximately 3 e^{-}_{rms} using the slowest digitisation rate of 100 kHz [154]. However, this slow digitisation rate is not suitable when collecting the much higher speed measurements required for accurate POW data.

To allow higher speed measurements the EM amplifier can be used, allowing the signal to be amplified before digitisation. The EM amplifier output differs from the traditional low noise mode by transferring the charge through an additional serial register before digitising the charge. This EM register contains higher voltage clock pulses (greater than 40 V) causing the electrons to be multiplied through the process of impact ionisation as they are transferred (figure 3.10) [156, 157]. The probability of impact ionisation in each step is actually very low but the use of a large number of steps makes very high gains achievable. In this mode the ProEM is capable of a digitisation rate of 10 MHz which has an associated readout noise of approximately 50 e^{-}_{rms}. Since the EM process occurs before the output amplifier the readout noise is effectively less than 1 e^{-}_{rms} [154].

The process of EM does however generate other electrical noise in the output data. These are due to variations in the baseline level and clock induced charge (CIC). CCD arrays produce a stable (offset) baseline level irrelevant of any light exposure, this level is recorded and subtracted from any real data. The complex electronics used for EM readout systems cause this baseline level to vary between frames,

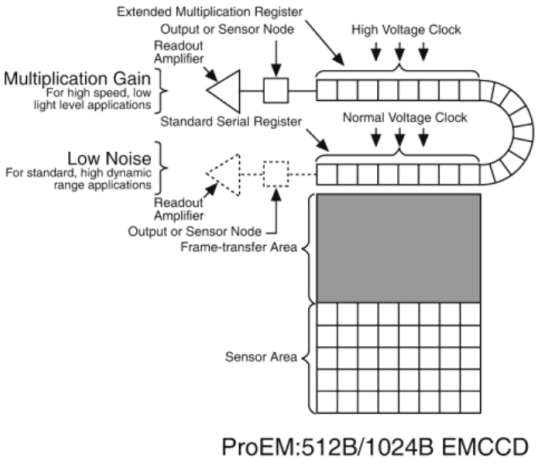

(a) Low noise and electron multiplication amplifiers

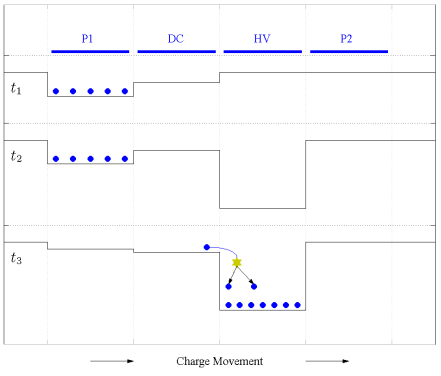

(b) Electron multiplication register. t_x represents various time steps, P1,P2 are arbitrary states, DC is a constant level and HV is the increased voltage to cause impact ionisation as the charge is moved.

FIGURE 3.10: Electron multiplication

causing perceived changes in intensity level. The ProEM camera has a built-in system to minimise this affect, named bias active stabilization engine (BASE^{TM}). This makes use of pixels permanently masked from the emission to actively correct the bias level during readout [158]. clock induced charge (CIC) is noise generated due to the clocking cycles required to move charge across the CCD. It is present in both the low noise and EM readout modes but the higher clocking voltages and subsequent amplification make it a larger problem in the latter. The presence of these noise levels cannot be accounted for through background measurements and can therefore produce an error if accurate photon estimation is completed [157, 158].

3.6.2 Sample holder and focussing

The sample holder (figure 3.11) consists of an insulating holder with a 30 mm diameter stainless steel plane electrode and a ring electrode (30 mm external and 25 mm internal diameter). The ring electrode allowing light to be detected by the CCD. The plane electrode is connected to the high voltage supply and the ring electrode to the laboratory high voltage earth, along with the Faraday cage. The sample is secured in position between the two electrodes, the ring electrode sprung to ensure a uniform force across the sample surface and allow for different thickness samples. A mask with a square window (8×8 mm^2) is placed over the

sample holder to produce a square image of EL from the centre of the sample. This excludes measurements due to any enhanced field at the electrode edges.

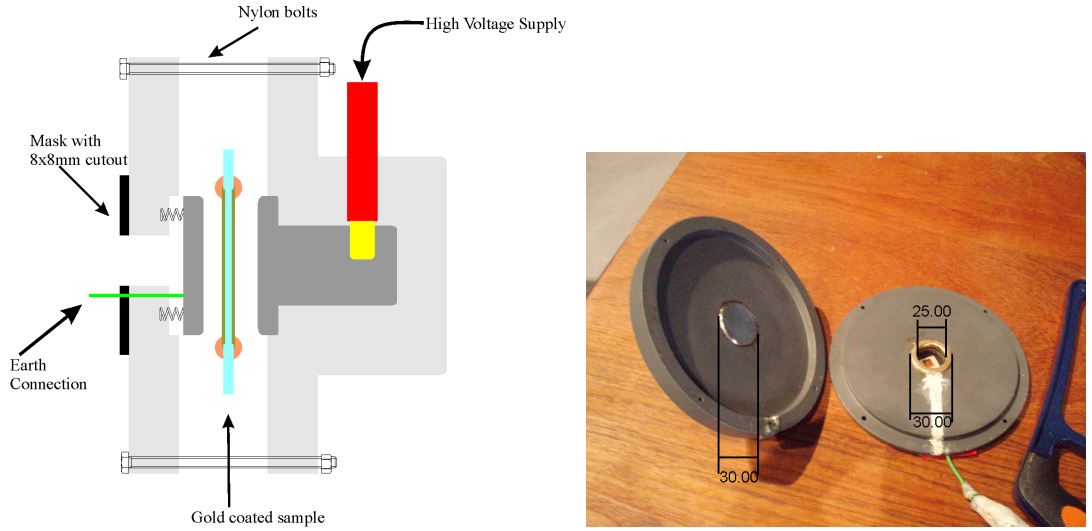

(a) Diagram of sample holder

(b) Picture of sample holder (dimensions in mm)

FIGURE 3.11: Sample holder for electroluminescence measurements

EL emission is very weak and therefore highly sensitive to any movement in the optical system. Also in order to quantify and accurately compare different samples the region of interest (ROI) needs to remain constant. To achieve this a system for repeatable focussing of the CCD was developed. A printed grid of text backlit by an LED was installed in the exact location of the sample. This could then be installed in the optical system and the lens moved to adjust the size and focus of the image on the CCD. A typical example is shown in figure 3.12. Once focussed all moveable optics were locked in place and samples could then be repeatedly installed in the same location with the same ROI for analysis.

The vacuum system used at the TDHVL is not capable of the high vacuum (better than 10^{-4} Pa) levels used by some researchers but comparison with measurements in a nitrogen environment has shown no difference in results (section 2.5.3). After installing the sample holder the chamber is then sealed and air evacuated to a pressure of better than 10^{-1} Pa, removing moisture and the affects of oxygen on EL emission [90, 120]. The chamber is then backfilled with dry nitrogen to avoid light emission from other electrical discharges. The chamber is maintained at a pressure of approximately 10^{5} Pa above atmosphere to ensure gas can only leak out of the chamber.

FIGURE 3.12: Focussing electroluminescence optical arrangement

3.6.3 High Voltage System

The high voltage is applied to the sample using a digital function generator (Thurlby Thandar Instruments Ltd. TG1304) and high voltage amplifier (Trek 10/10B). The high voltage amplifier delivers a 2000:1 gain and is capable of a 10 kV peak voltage and 10 mA peak current. This set-up allows various high voltage waveforms to be applied. A scope linked to the output of the high voltage amplifier is used to confirm the applied field shape and an example of the various applied voltages capable of being investigated are shown in figure 3.13. Due to the inrush current when applying a square waveform the maximum rise time had to be controlled at a rate of 10 $\mathrm{kV\,ms^{-1}}$.

3.6.4 Sample Preparation for Electroluminescence

To account for the ring electrode and electrode roughness samples are coated with a gold layer to achieve a good electrical contact and uniform field arrangement. Samples were gold coated using a EMTech k550X Sputter Coater [159] which minimises any sample heating during deposition. A circular mask of 34 mm diameter is placed on both sides of the sample, producing a circular gold electrode slightly larger than the electrodes of the EL experiment. This allows a ring of silicone rubber to be placed around the edge to avoid surface flashovers along with securing the samples in place. Before gold coating samples are blown with compressed air to remove any larger dust particles, thought to be a possible cause of bright spots [47]. An example of a prepared sample is shown in figure 3.14.

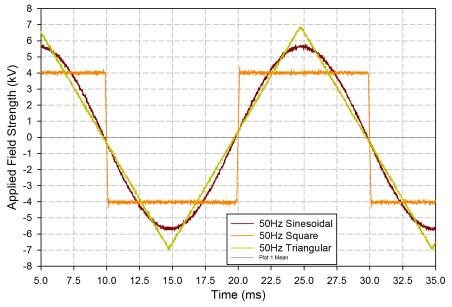

(a) Varying waveform at 50 Hz 4 kV_{rms}

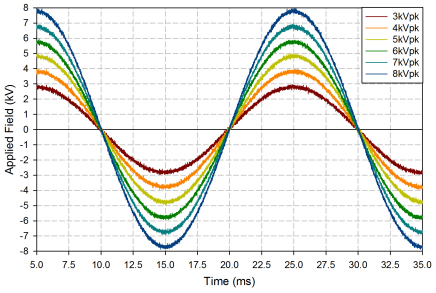

(b) Varying field of sinusoidal waveform at 50 Hz

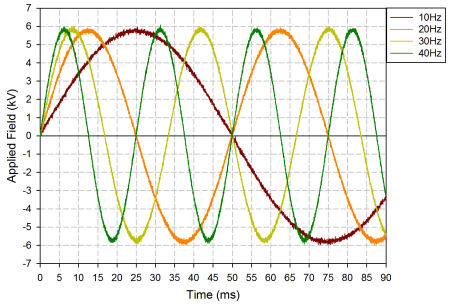

(c) Varying frequency of sinusoidal waveform at 6 kV_{pk} (10-40 Hz)

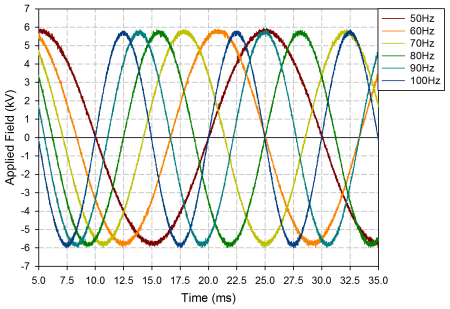

(d) Varying frequency of sinusoidal waveform at 6 kV_{pk} (50-100 Hz)

FIGURE 3.13: Waveform of applied fields from high voltage amplifier

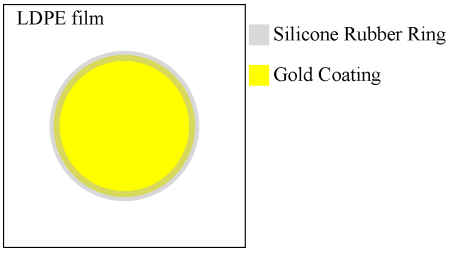

(a) Diagram of gold coated sample

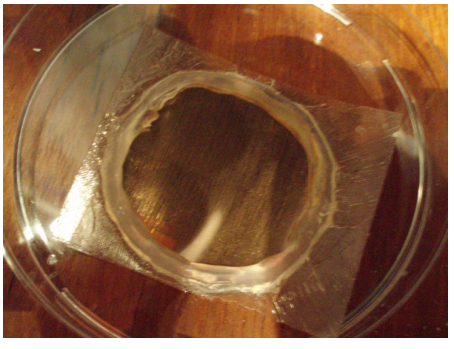

(b) Picture of gold coated sample

FIGURE 3.14: Prepared electroluminescence sample

Due to the optical nature of the EL experiment gold coating the samples results in a trade off between the increased conductivity and reduced optical transparency. A series of tests was conducted to determine the most appropriate gold thickness. The optimum is a coating time of 2 minutes at 25 mA on each side (approximately 25 nm according to the manufacturers data sheet [159]). Due to the very thin gold layer, results were very sensitive to the operation of the gold coater. Since the purpose of the gold coat is to ensure a good electrode contact there is no way to measure the gold thickness or resistance on each sample without risking damage to the gold. Instead the optical transmission of the sample was monitored using ultraviolet and visible (UV-Vis) spectroscopy. An accepted range of transmission was determined based on EL results of virgin samples. The UV-Vis results are shown in figure 3.15 after 1 side has been gold coated. Samples not within the acceptable range of transmission were not used in this work. This measurement technique does not provide any accurate determination of the gold thickness due to differences in light scattering and reflection from the gold layer. It does though provide a means to investigate the gold layer quickly, with minimum risk of surface damage.

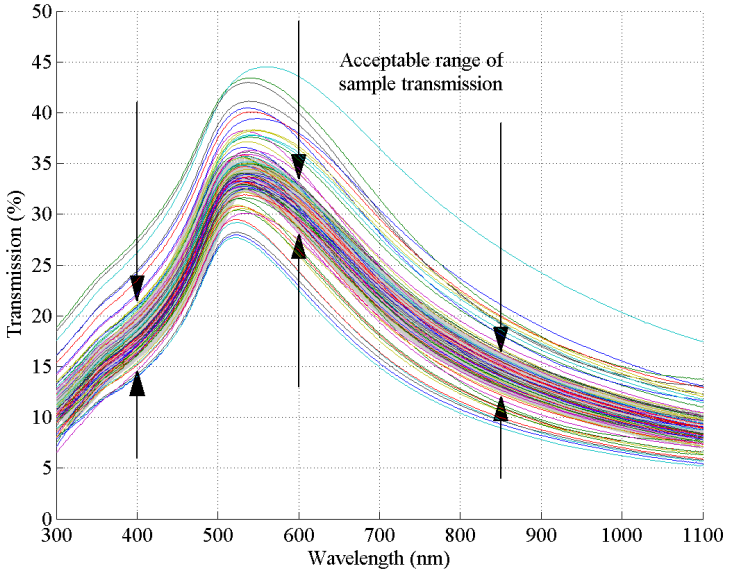

FIGURE 3.15: Ultraviolet-visible spectroscopy of gold coated samples

3.6.5 Imaging and Intensity of Electroluminescence

A selection of different experiments has been presented in the literature (section 2.5) but those that allow the most investigation into the EL phenomena involve measuring the spectra, intensity and phase difference of the EL. Before any

quantified data can be collected the source and uniformity of the EL need to be confirmed. An image of the emission quickly allows this to be done. The low noise (100 kHz) readout mode is used for imaging and intensity measurements, minimising the noise level. Although the EM mode would allow quicker exposures it did not produce as clear an image of the emission. Images were taken using a 10 minute on chip accumulation for the entire CCD array.

To measure the intensity a region of interest (ROI) is used to only look at part of the CCD array. It is set to cover the full CCD chip vertically (512 rows) and just inside the edges of the emission horizontally (200 columns), as shown in figure 3.16(a). To ensure an accurate value for the intensity at each field level 20×5 second exposures are recorded. At the end of each exposure the CCD array is vertically summed (binned) on the CCD, increasing the signal before the addition of readout noise (figure 3.16(b)). The single row is then readout and averaged to produce a single value for each exposure. The average intensity and error is then calculated from all 20 exposures.

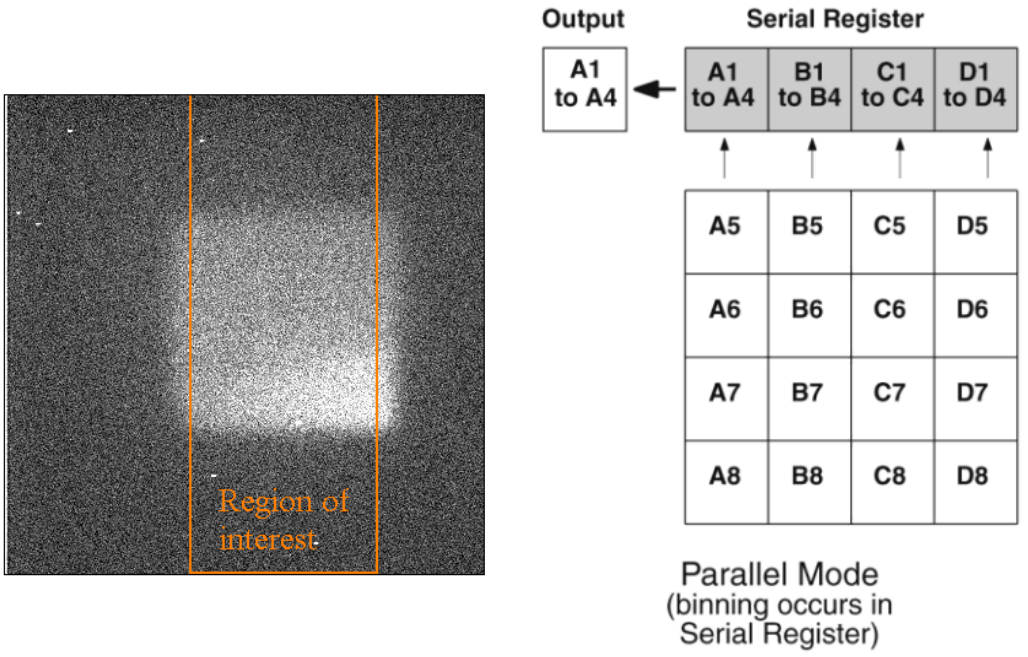

(a) Region of interest

(b) Binning process

FIGURE 3.16: Region of interest and binning process for point on wave measurements

To investigate the spectrum of the emission the EL system was coupled to a Princeton Instruments SP2500 spectrograph using an optical coupling and optical fibre. The spectrograph uses a PIMAX3 intensified charge coupled device (ICCD)

detector to measure the light emission. Due to the relatively high dark charge levels and readout noise, long exposures were not possible [160]. This prevented the wavelength of the EL for LDPE being detected due to its weak emission.

3.6.6 Point on Wave Measurements

point on wave (POW) measurements allow the relationship between EL and the phase of the applied field to be investigated. Due to the low signal strength this is achieved by measuring the emission relating to sections of the applied field over many cycles. This is possible due to the stable nature of EL under electrical stressing [47]. Long term stressing has shown EL to reduce, but remains constant for the first 60 minutes [161]. The continued stressing following the procedure for POW measurement described below lasts for less than 10 minutes.

To synchronise the camera with the applied field a custom built trigger is used. The trigger receives inputs from the function generator and the ProEM camera. The input from the function generator identifies the zero crossing point of the applied field, going from negative to positive. The input from the ProEM determines when the camera is ready to start its next exposure. Using these inputs the trigger system can directly control the start of each exposure following the process shown in figure 3.17.

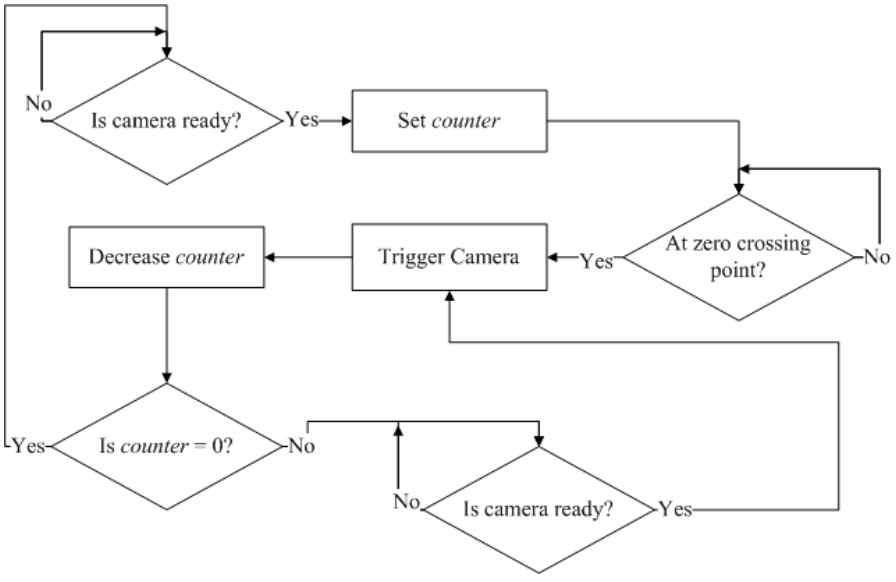

FIGURE 3.17: Process flowchart for ProEM trigger system

The trigger system is controlled by a peripheral interface controller (PIC) (PIC16F628A [162]), the code and circuit arrangement for which can be found in appendix B.1. Initially the trigger waits until the camera is ready, it then

waits until the zero crossing point signal is given by the function generator. The PIC then triggers the first exposure and each subsequent exposure as soon as the camera is ready, decrementing a counter with each exposure. The value of this counter is controlled by a selection of switches, determining the number of measurements before the system resynchronises with the applied field. Testing showed the minimum time taken between 2 subsequent exposures to be 2.168 ms without any negative affects on CCD temperature. The ideal number of exposures is the point at which the entire field has been covered and the exposure time stamps begin to repeat. After 300 exposures the average difference between any 2 points is 0.067 ms. Increasing the number of exposures further slightly improves this error but significantly increases the electrical stressing duration for data collection, data quantity and associated processing time. At 50 Hz, 300 exposures equates to an error of approximately 1.2^o between any 2 data points, better than typical errors in published data [47]. To build up results representing the emission during a complete ac cycle, 500 sets of 300 exposures are collected using the custom built trigger system. Trial measurements showed 500 sets to be the optimum compromise between data collection time and quantity with an appropriate signal to noise ratio.

In order to maximise the signal to noise ratio the same ROI is used as that of intensity measurements. In this case, after vertically binning the 512 pixel rows the charge is passed through the EM register with maximum gain (arbitrary value of 1000). The single row is then passed through the output amplifier (10 MHz digitisation) and post processing by the computer calculates the mean value for each exposure.

To confirm and calibrate the triggering system and post processing, a circuit was made to artificially generate a known light output at a specific point on an applied waveform, the results and analysis are shown in appendix B.2. An unpredictable delay (timing jitter) can occur depending on the location in the clock cycle that the ProEM receives the trigger. The maximum jitter is less than 150 ns [163] and therefore not significant compared with measurement error.

Post processing of the raw data requires each exposure to be associated with a point on the applied field, the middle of the exposure has been used for all these results. Due to possible delays of up to 1 ac cycle between the camera being ready and the zero crossing point trigger the first measurement from each set of exposures is ignored. The remaining data then represent a single cycle of the

applied field. All 500 sets are averaged to produce the EL during 1 cycle of the applied field.

Due to the low signal strength the resulting POW measurement can be noisy. In order to extract phase angle information a reliable fit to the noisy data is required. A low pass filter is used to remove the high frequency noise, suitable since EL only occurs at twice the applied field frequency [116, 117, 121]. A filter was designed and optimised using the MATLAB® filter design and analysis package. The low pass filter designed to remove any signal with a frequency greater than 4 times the frequency of the applied waveform, an example for a 50 Hz field is shown in figure 3.18(a). Filtering the data could generate an artificial shift in the phase of the data. To minimise this the filter is run twice as per figure 3.18 effectively removing any phase shift.

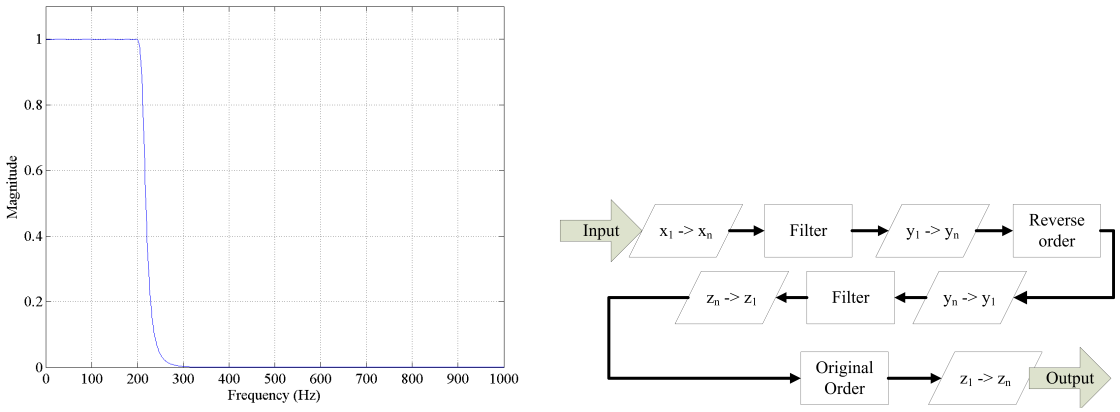

(a) Low pass filter

(b) Filtering procedure

FIGURE 3.18: Low pass filter to produce fit for raw data

Figure 3.19 compares a raw data set of a virgin LDPE sample under a 50 Hz 60 $kV_{pk}\,mm^{-1}$ sinusoidal field with the filtered data superimposed. A good fit between the raw and filtered data can be seen.

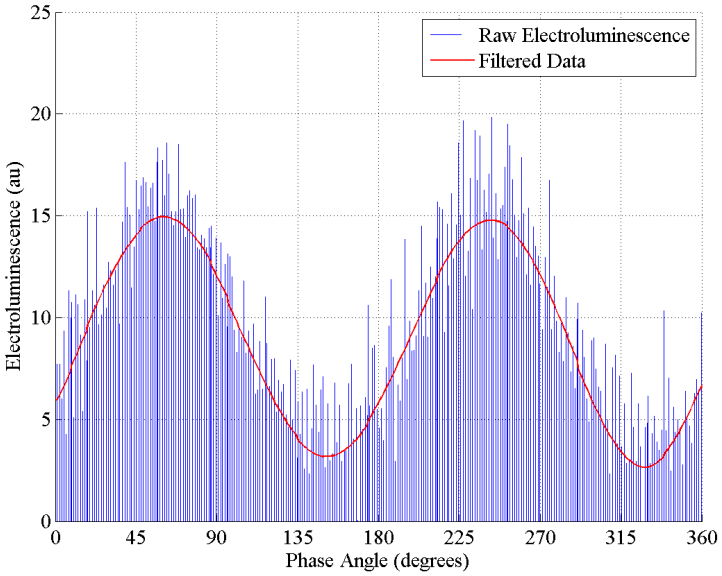

FIGURE 3.19: Raw and filtered electroluminescence data of 100 μm LDPE under a 50 Hz sinusoidal 60 $kV_{pk}\,mm^{-1}$ field

3.7 Confirmation of Electroluminescence Experiment

The previous section presented developments and modifications to the EL experiment. To confirm these developments this section compares EL from virgin LDPE with those in literature. This is also important to establish repeatable testing methods for comparing the emission during different stages of UV ageing presented in the following chapter.

To confirm the source and uniformity of EL, images were taken under a sinusoidal 40 $kV_{rms}\,mm^{-1}$ field before any quantified measurements were collected. Any samples which did not produce a roughly uniform emission but contained bright spots were not tested further (example shown in figure 3.20). These bright spots are thought to originate due to the imperfections or trapped impurities created during sample preparation [47].

3.7.1 Electroluminescence intensity

To measure the intensity of the EL emission, measurements were taken using the EMCCD camera in low noise mode (100 kHz digitisation) and accumulated on the CCD over a 5 second duration. After 5 seconds the desired ROI was summed (binned) vertically and then averaged horizontally, producing a single value for

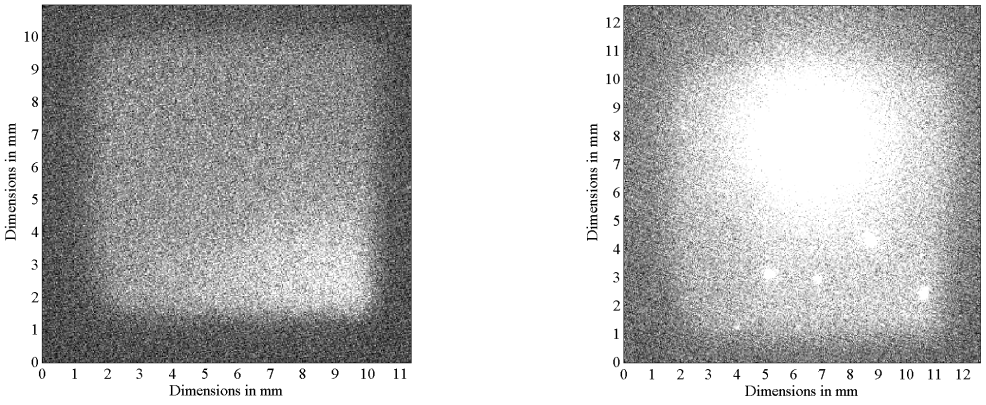

(a) Uniform electroluminescence

(b) Non uniform electroluminescence

FIGURE 3.20: Typical image of electroluminescence. LDPE films stressed under sinusoidal fields at 50 Hz with fields 40 kV_{rms} mm^{-1}

each 5 second exposure (section 3.6.5). These readings were repeated 20 times whilst continually stressing the sample to collect an average EL intensity for each field level.

To compare changes in the intensity of EL a collection of measurements were completed on virgin LDPE samples to understand the typical emission and range in results. 4 samples were tested under a 50 Hz, sinusoidal field with electrical stress increasing from 0 to 60 $kV_{rms}\,mm^{-1}$ in 10 $kV\,mm^{-1}$ steps. Figure 3.21 shows the mean result with error bars representing the data range in the collected results. The results clearly show a growing increase in EL for a linear increase in electrical stress. A similar trend has been shown for other work on virgin LDPE [28, 105, 164] and other materials [94, 123].

Since EL is thought to relate to the injection, trapping and recombination of charge carriers, any previous charging of the sample should have an influence. Space charge measurements under ac fields have shown the accumulation of charge in the bulk as a result of prolonged electrical stressing [12]. Some of this charge will be trapped in deep trapping sites and will remain for a long time after field removal. This remaining charge is likely to affect the electric field at the electrode and therefore the subsequent charge injection that leads to EL.

To investigate the effect accumulated charge has on EL a virgin LDPE sample had the same intensity measurements as above repeated 4 times. After test 1 was completed both electrodes were grounded for 10 minutes before repeating the measurements (test 2). Between test 2 and test 3 the sample was left grounded

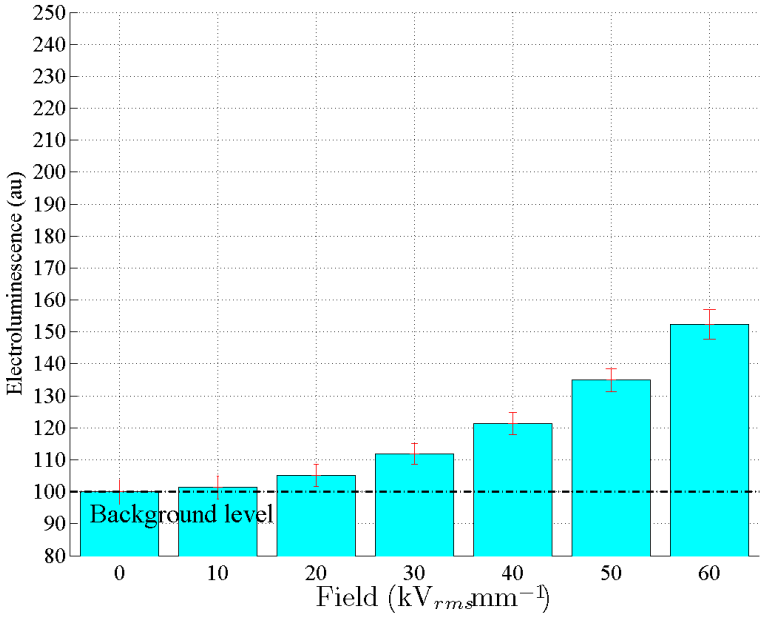

FIGURE 3.21: Total electroluminescence during a 5 second exposure at increasing field strengths

for 72 hours. The sample was then grounded for a further 10 minutes after test 3 before collecting test 4.

The results from these 4 tests are shown in figure 3.22. Clearly the process of collecting measurements influences future results. This is most likely due to the influence of charge left over from previous measurements. Leaving the sample longer allowed the trapped charge to relax further resulting in the EL intensity becoming closer to that of the initial measurement. To ensure measurements can be compared between different samples a testing procedure was established. In all virgin and aged samples a single image is taken first to confirm the source and uniformity of the light emission. The intensity measurements as described above are then taken. Finally any POW measurements are completed using the same stressing conditions and durations between samples.

3.7.2 Point on wave electroluminescence measurements

POW EL measurements allow the phase relationship between the EL intensity and the applied field to be determined. This section presents a confirmation of the developments to the experiment setup by comparing measurements of the same material at another research laboratory.

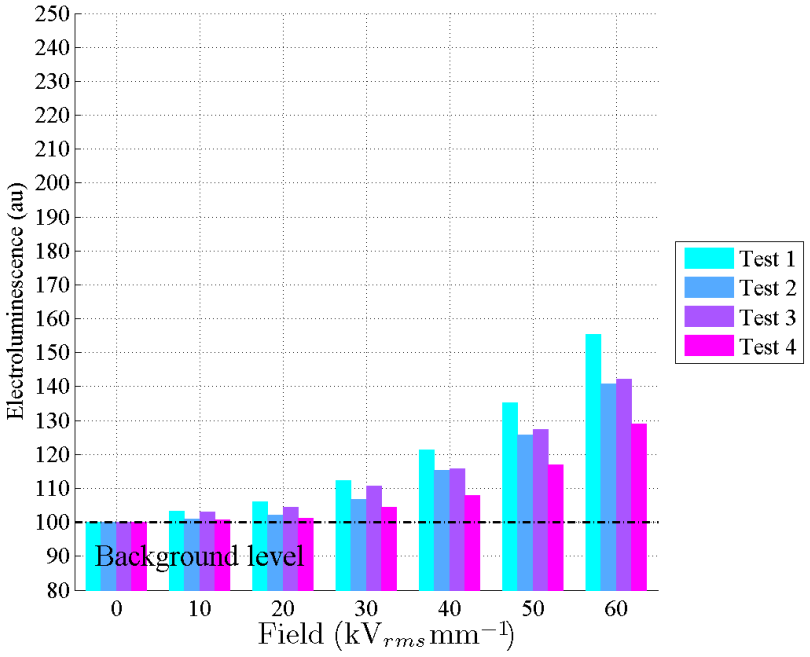

FIGURE 3.22: The affect of repeated electroluminescence measurements

In order to confirm the accuracy of the system at the TDHVL, 100 μm thick virgin LDPE samples from the same batch were also tested at the Laboratory on Plasma and Conversion of Energy, Toulouse (LAPLACE). The exact same samples could not be tested due to the previously discussed affect one measurement may have on the other (figure 3.22) as well as differences in electrode size. The measurement system at the LAPLACE operates in a very different way to that at the TDHVL. The LAPLACE makes use of a PMT based detection system, as opposed to the CCD system at the TDHVL. The measurement process at the TDHVL was extensively described previously (section 3.6.6) and the LAPLACE system will be summarised here, full details can be found in the literature [17, 97].

The experimental arrangement at the LAPLACE also uses a uniform electrode arrangement by using gold coated samples between a ring and plane electrode. A PMT was used to measure the EL intensity, this does not allow any imaging to confirm the source of the emission and therefore a uniform emission had to be assumed. Measurements were completed under high vacuum (better than 10^{-1} Pa) with a 50 Hz, sinusodial electric field. POW EL measurements were completed using a 100 μs dwell time repeated 200 times to cover the 20 ms cycle of the applied field. Readings were integrated over 10,000 ac cycles to increase the signal above the noise level. Each cycle of 200 readings was triggered by the peak of the positive half cycle of the applied field. The different trigger points (zero crossing point at

the TDHVL) are accounted for in the results and the appropriate background levels subtracted.

The results shown in figure 3.23 compare the POW results as the field increases from 50 to 80 $kV_{pk}\,mm^{-1}$ under a 50 Hz, sinusoidal waveform. Due to the different values generated by different measurement systems the results have been normalised with respect to the peak intensity of the 80 $kV_{pk}\,mm^{-1}$ result. The results clearly show 2 peaks in the EL, appearing in the first and third quadrants of the applied field. This supports the theory of bipolar charge recombination and is in agreement with other published results [94, 115].

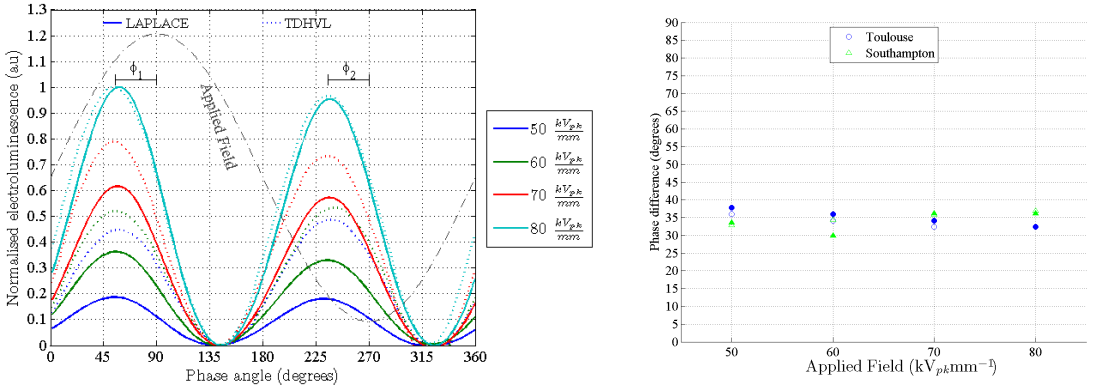

(a) Point on Wave emission

(b) Phase difference. Unfilled for ϕ_1, filled for ϕ_2

FIGURE 3.23: Comparison of point on wave electroluminescence data from Southampton and Toulouse

Comparing the intensity of the two results shows the emission from the TDHVL to cover a smaller change than those from LAPLACE. These differences may be due to the differences in data collection. The LAPLACE system integrates the measured emission and therefore any signal above the noise level significantly increases. The TDHVL system averages the signal and therefore these results show that at 50 $kV_{pk}\,mm^{-1}$ the signal is already well above the noise level.

Comparing the angle between the peak of the applied field and the peak of the EL shows the EL to lead the field by a phase difference of approximately 35^o, in agreement with some results seen in literature [94, 117]. This phase difference is thought to be due to the build up of charge near the electrode-polymer interface, resulting in the local electric field leading the applied field. As the field increases this phase difference shifts slightly due to changes in the affect of charge accumulation on the local electric field. This affect is more noticeable

in other materials, particularly in PET and PEN due to their aromatic backbones enhancing charge trapping and EL [28, 29].

Investigating the LAPLACE and the TDHVL measurements in terms of phase difference shows them approximately the same. However, as the applied field increases the LAPLACE measurement reduces in phase difference whereas the TDHVL increases. Literature has always shown the phase difference to increase, albeit marginally for LDPE. One item to consider is the resolution of the two systems in terms of phase angle. The LAPLACE system integrates over a 100 μs exposure giving a phase accuracy of 1.8^o, not accounting for any trigger system jitter. The TDHVL system integrates over a 2.168 ms exposure but only synchronising with the applied field every 300 exposures. Therefore, the phase angle at 50 Hz between two measurements is approximately 1.2^o, giving a marginally greater accuracy to changes in the phase angle.

3.7.3 Discussion of Virgin Electroluminescence Results

This section has presented a selection of EL results for virgin LDPE. The POW measurements for increasing field strength show an approximately 35^o phase difference between the peak of the applied field and EL. This phase difference is thought to be due to the charge trapped near the electrode-polymer interface causing the local electric field to lead the applied field.

The phase difference of EL for LDPE covers a range of values in the literature of approximately 10^o [96], approximately 40^o [94, 117] and approximately 50^o [95]. An explanation of this range shown by different researchers may relate to differences in material composition and experiment setup. A material may offer a greater quantity of charge trapping sites due to the different chemical structures, perhaps due to the addition of additives or impurities during manufacture. These different chemical structures could be expected to alter the charge movement and therefore EL phase difference. Another possibility is the range of different methods for collecting the POW data which require various post processing techniques to smooth the raw data into a presentable from. The samples tested here were supplied by the same manufacture (Goodfellows Ltd.) as those tested by Ariffin *et al.* [96], yet the phase differences differ greatly. However, the same samples tested at LAPLACE using a different technique showed the same results. Therefore, differences seen in the literature may be due to phase shifts generated in the processing of raw data.

3.8 Summary

This chapter has described the experiment for ageing the LDPE films in air and nitrogen environments. Changes as a result of UV ageing can then be characterised in terms of electrical and chemical properties to explain changes in charge movement leading to EL. Changes in the chemical bonds within the polymer using FTIR spectroscopy allow increases in oxidation products (typically carbonyl and hydroxyl groups) to be identified. The UV ageing of the material is also expected to alter its electrical strength which can be determined by ac ramp breakdown measurements. These may be analysed using a Weibull 2-parameter distribution. Dielectric spectroscopy will show changes in $\epsilon^{'}$ and $\epsilon^{''}$ as a result of ageing which may identify changes in the polarisation and bond rearrangements within the polymer.

To determine changes in the formation and movement of SC the PEA method will be used. This can indicate changes in the quantity and energy level of charge trapping sites within the bulk of the polymer. EL will be measured using the TDHVL developed EMCCD based detection system allowing the images, intensity and POW measurements to be completed. EL relates to the charge injection, trapping and recombination very near the electrode polymer interface and so changes in charge trapping sites within this region should heavily influence it. Changes are best investigated in terms of intensity relating to the quantity of charge recombination and the phase angle relationship between the applied field and EL due to changes in the local electric field.

A series of EL measurements were presented on virgin LDPE to confirm the various developments made to the TDHVL measurement system with the use of an EMCCD camera. A good agreement between these results and those published in literature was shown. A comparison using the same material with different detection systems (PMT and CCD) showed the post processing technique to be suitable.

Investigations into EL from virgin LDPE also identified the importance of testing order. To avoid misinterpreting the affect of residual charge from one measurement on subsequent measurements a procedure was established for testing different samples. Initially an image is taken to confirm the uniformity and source of the emission followed by intensity measurement as the field is increased. Finally any POW measurements are taken, in the case of comparing virgin and aged sam-

ples, tests compare increasing field strength. This ensures repeatability between different samples and allows measurements to be reliably compared.

Chapter 4

Results after Ageing

This chapter investigates the effects that the photo-irradiation of LDPE has on its EL emission. To interpret these changes the samples are characterised in terms of optical and chemical changes as well as dielectric properties. Changes in bulk charge properties are also investigated using the PEA technique to measure SC. Correlating these results with changes in EL allows the consideration of this form of measurement as a condition monitoring tool.

4.1 Ultraviolet and visible spectroscopy

Due to the optical nature of EL experiments it is very important to identify any changes in the transparency of the samples as a result of ageing. UV-Vis spectroscopy investigates the absorption of the material in the UV and visible parts of the electromagnetic spectrum. A Perkin Elmer, Lambda 35, ultraviolet and visible spectrometer was used with quartz cells, covering the range 190 - 1100 nm in 0.5 nm steps [165].

When light travels into a material it can be reflected (I_r), scattered (I_s) or absorbed (I_a) [50], such that;

$$I_{out} = I_{in} - (I_r + I_s + I_a) \tag{4.1}$$

Where I_{out} is the measured light and I_{in} is the incident light. To minimise reflection and scattering, samples are immersed in a solution of similar refractive index (n). Three available solutions were investigated to identify the most suitable over the wavelengths of interest (200 - 800 nm). Figure 4.1 presents results for silicone oil

(n of approximately 1.51 [166]), distilled water (n of approximately 1.35 [167]) and pentadecane (n of approximately 1.43 [168]) as possible immersion fluids for investigating LDPE (approximately 1.51 [33]). Although silicone oil would give the closest refractive index it absorbs at wavelengths below 250 nm, an area of particular interest due to the UV ageing. The results show that only distilled water gives a large optical transparency right into the UV range of interest and was therefore chosen as the medium for measurements.

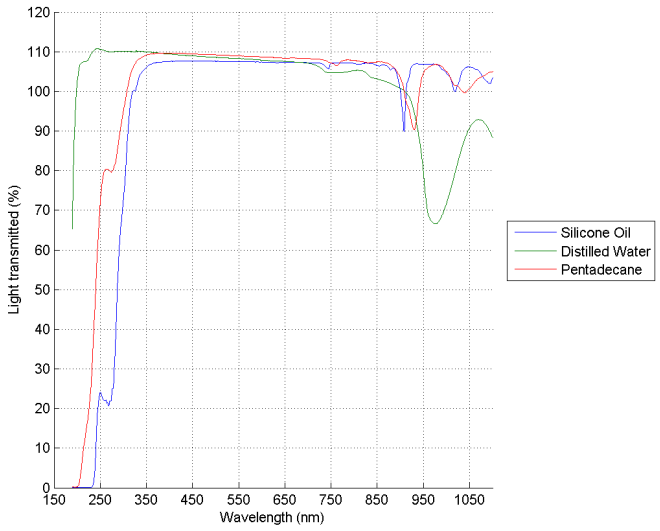

FIGURE 4.1: Different immersion fluids

There are two regions of particular interest relating to UV-Vis measurements, the visible spectrum relevant to EL (400 - 800 nm) and the 200 - 300 nm UV region. Figure 4.2(a) shows results for the LDPE samples aged in air and nitrogen environments, the EL region is marked for reference [47]. It can clearly be seen that there is very little change in the absorption over the EL region after ageing in either environment. Therefore any significant change in intensity may be related directly to changes in charge interactions rather than absorption by the sample.

Over the UV region samples aged in air show an increased absorption at approximately 250 nm. This is thought to be due to the chemical products resulting from photo-oxidation reactions, thought to absorb over the range 230-330 nm and lead to Norrish type 1 and type 2 reactions [50]. The samples aged in a nitrogen atmosphere showed only a small increase in absorption at approximately 250 nm. No increase in oxidation products are expected due to the nitrogen environment but some oxygen may have remained in the sample after degassing.

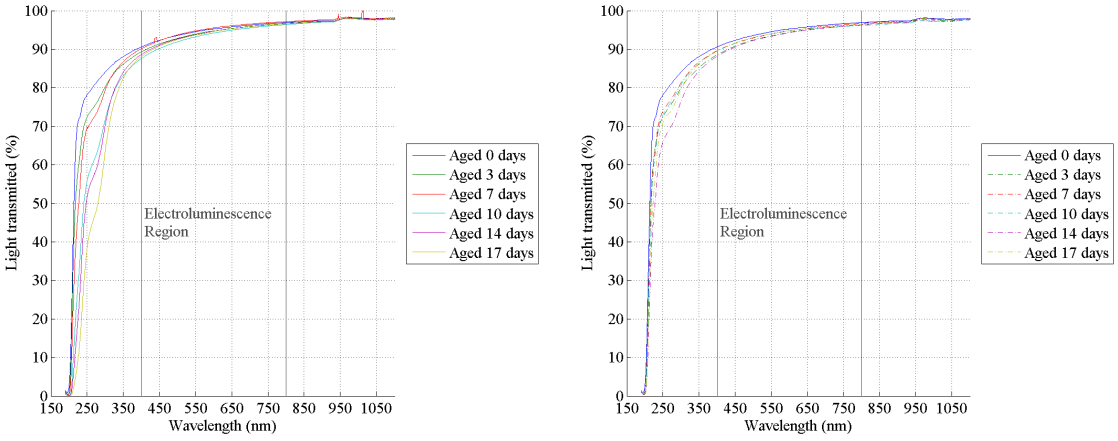

(a) Samples aged in air

(b) Samples aged in nitrogen

FIGURE 4.2: Ultraviolet-visible spectroscopy measurements of aged samples

4.2 Fourier transform infrared spectroscopy

Fourier transform infrared (FTIR) spectroscopy was used to identify changes in the chemical bonds as a result of ageing. Measurements were taken over the range 4000 - 500 cm^{-1} using the Perkin Elmer, FT-IR Spectrum GX system with MIRTGS sensor at a resolution of 1 cm^{-1}. The areas known to be of most interest relevant to photo-oxidation processes are 3500 - 3000 cm^{-1}, relating to hydroxyl groups (-OH) and 1800 - 1600 cm^{-1}, relating to carbonyl (C=O) groups [64, 73]. 32 measurements were taken with the background spectra subtracted and then averaged to ensure a good signal to noise ratio.

As shown previously (figure 3.2) there are a selection of ageing positions. To confirm oxidation processes occur equally across all sample locations, figure 4.3 presents spectra from 4 different samples, aged 7 days, in the 4 different locations. Comparison between the virgin and aged sample shows a significant change due to the increase in oxidation products but very small difference with ageing location. Therefore comparisons can be made between samples aged in different locations, though the position was still recorded for subsequent analysis.

The results presented in figure 4.4 shows the FTIR spectra as ageing time increases for samples aged in air. The results are an average of measurements from samples aged in different positions. There is clearly an increase in both hydroxyl and carbonyl groups due to photo-oxidation. These chemical groups are thought to act as charge trapping sites due to their unbonded valence electrons [44].

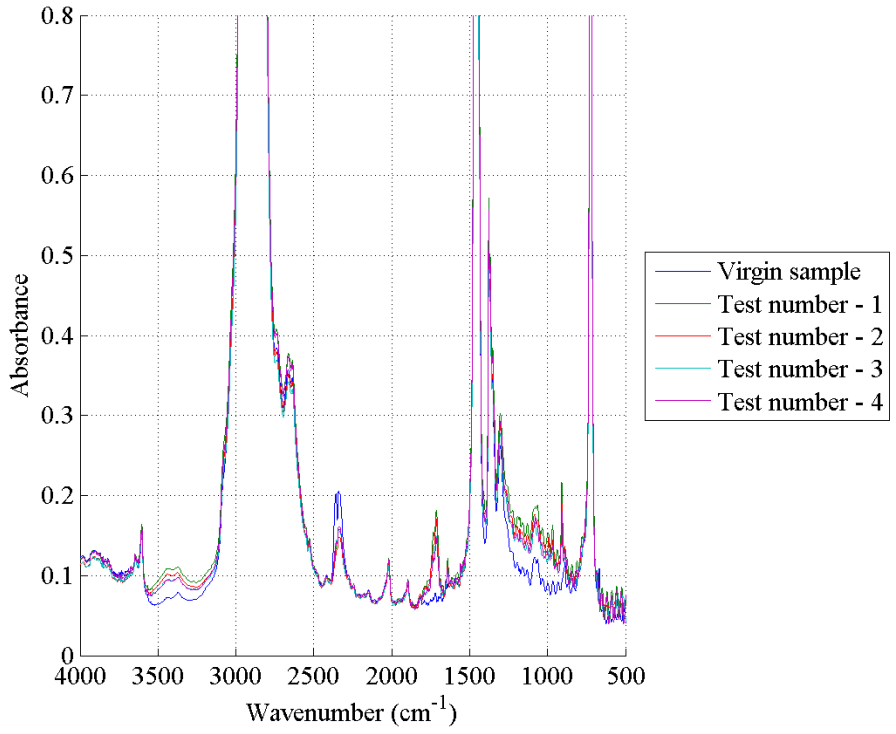

FIGURE 4.3: FTIR transmission spectra of 7 days UV aged LDPE from various ageing positions

To confirm the influence of oxidation products on charge movement some samples were aged in a nitrogen atmosphere, using the experiment setup described previously (section 3.1.1). This minimises the generation of oxidation products, allowing the analysis of the affect of other ageing processes on charge movement. The results presented in figure 4.5 shows the FTIR results for samples aged in a nitrogen environment, the samples aged 10 days in air included for reference. There is clearly a significantly smaller concentration of oxidation products as a result of ageing. The slight increase most likely due to oxygen remaining in the bulk of the polymer after degassing.

The absorption in IR spectra responsible for carbonyl groups results from a range of overlapping chemical stretching movements. The biggest absorption being due to increased quantities of aldehydes, ketones and carboxylic acids with absorption over the range 1730 - 1710 cm^{-1} [69, 128]. These are expected to grow in roughly equal quantities as a result of photo-oxidation [169]. Typical hydroxyl groups relate to alcohols and carboxylic acids along with some remaining hydroperoxides from the initial reactions (section 2.3) [58, 69]. All of these are expected to influence the charge movement due to their trapping properties and polar nature [42, 76]. It has also been suggested that due to the permeability of polyethylene to oxygen and

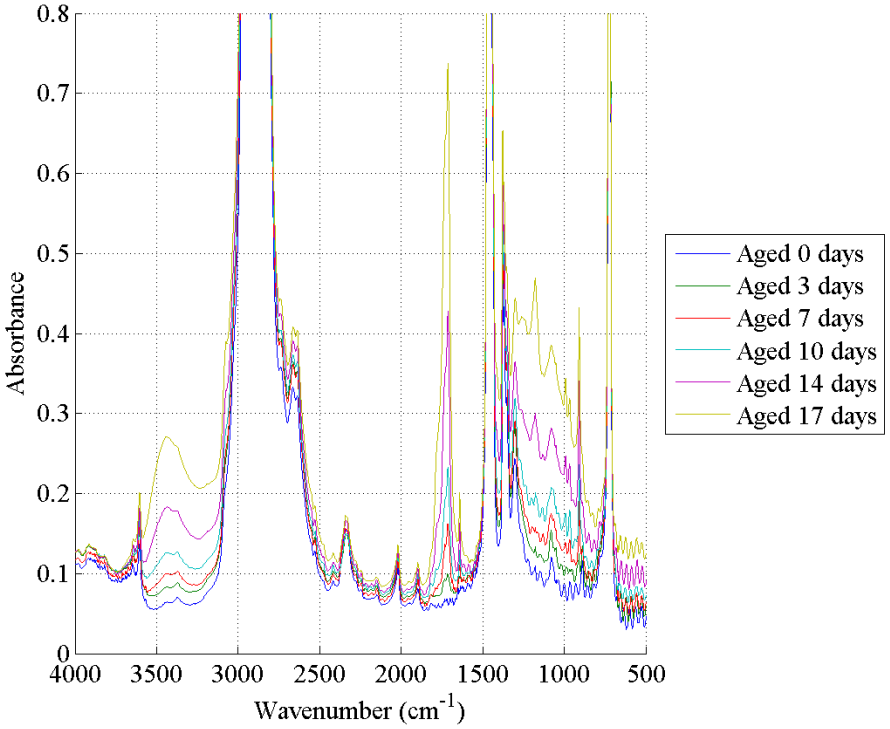

FIGURE 4.4: FTIR transmission spectroscopy of LDPE samples UV aged in air

relative easiness of chain movement, oxidation products are most likely to form in the amorphous regions and crystalline boundaries [58, 74].

The changes seen in the 1500 - 700 cm^{-1} region are often termed the finger-print region [169]. Changes in this region are thought to relate to bonding arrangement of the polymer chain. Increases in this region are associated with increased chain scission resulting in new chain end groups, double carbon bonds (C=C) and increased side branching [63, 170]. As a result of these the broad increase at 1300 cm^{-1} is commonly associated with changes in the amorphous phase of the polymer [82]. This suggests there is a greater change for samples UV aged in air, most likely due to the influence of the oxidation products on the polymer structure. These oxidation products are expected to occur mainly in the amorphous regions of the polymer due to the limited ability of oxygen to penetrate the crystalline regions.

4.2.1 Photo-irradiation products

To investigate changes in oxidation products with ageing the absorption of particular groups are monitored. Changes in carbonyl groups at 1714 cm^{-1} relating to ketones are shown in figure 4.6(a) and hydroxyl groups at 3440 cm^{-1} in figure

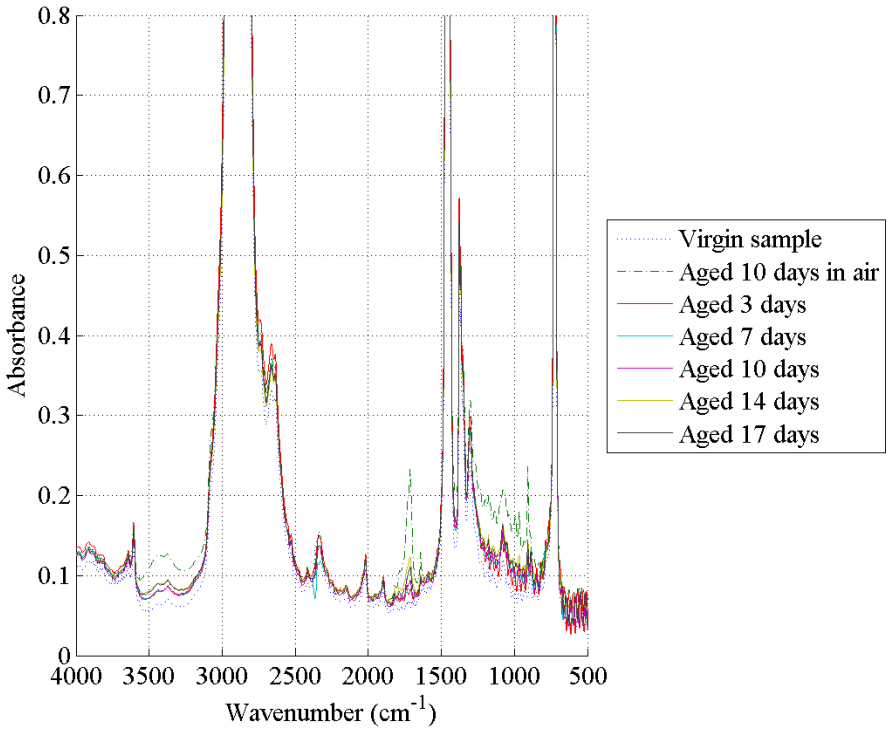

FIGURE 4.5: FTIR transmission spectroscopy of LDPE samples UV aged in nitrogen

4.6(b). The results for samples aged in air show a significant increase over those aged in nitrogen. A best fit line is included for the samples aged in air using equations 4.2 and 4.3. Other published work supports these, suggesting that carbonyl groups increase with a time squared relationship and hydroxyl groups linearly with ageing time [50]. The parameters for the equations are shown in table 4.1.

$$\text{Carbonyl Concentration}(t) = m.t^2 \ + \ c \tag{4.2}$$

$$\text{Hydroxyl Concentration}(t) = m.t \ + \ c \tag{4.3}$$

TABLE 4.1: Paremeters used for FTIR best fit curves

Parameters	**Carbonyl**	**Hydroxyl**
m	0.0017	0.009
c	0.067418	0.06399

The samples aged in a nitrogen environment are not expected to increase in carbonyl or hydroxyl group concentration due to the lack of oxygen. To show this the constant level for a virgin sample is shown. It can be seen that with a long ageing duration there is still a slight increase in the oxidation products. This

is likely to be due to a small quantity of oxygen remaining in the bulk of the polymer after degassing.

Explanations for the time squared increase in carbonyl groups relates to either the initial consumption of antioxidant or increased UV absorption [50, 77]. Products from the photo-oxidation reactions act as absorbing centres for UV light and cause the auto-acceleration of photo-irradiation reactions [50, 73].

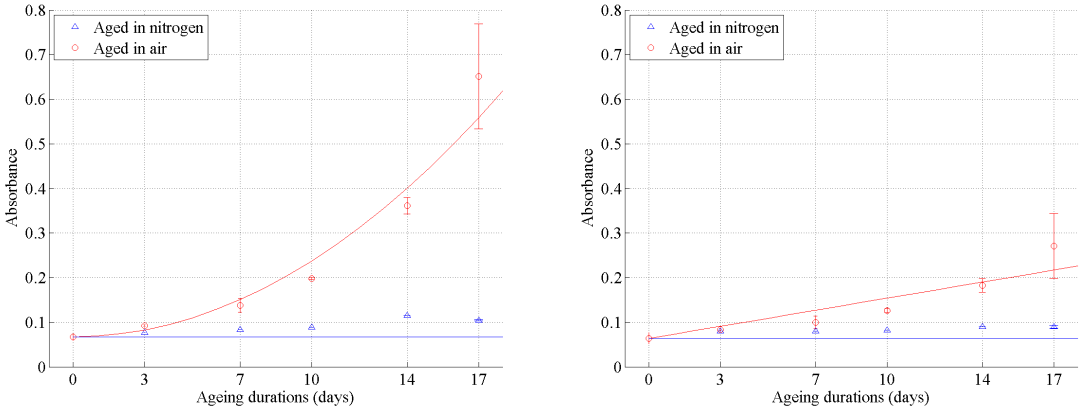

(a) Carbonyl absorbtion at 1714 cm^{-1}

(b) Hydroxyl absorption at 3440 cm^{-1}

FIGURE 4.6: Increase in oxidation products as ageing time increases

4.2.2 Relaxation of oxidation products

Due to the extensive time taken for sample preparation and testing involved in EL measurements, it is important to determine any relaxation of oxidation products after removal from the ageing system. Once aged, samples were stored in air at atmospheric pressure within a dark box to avoid any uncontrolled UV exposure. To ensure there is no change in oxidation products after removal from the ageing system the carbonyl concentration was monitored through IR absorption (at 1714 cm^{-1}). As before, measurements of a selection of samples were taken from different areas within the ageing experiment and they showed no significant change in carbonyl level over a 45 day duration. No samples were left as long as this between ageing and testing.

4.2.3 Elevated temperature used for ageing

As discussed in section 3.1, samples were aged at an elevated temperature of 40 ^{o}C to ensure no seasonal or daily fluctuations in temperature affected the rate

of photo-oxidation [77, 130]. It was not expected that the elevated temperatures would cause the generation of oxidation products [131]. In order to confirm this, a selection of samples were installed masked from the UV source. The FTIR results shown in figure 4.7 shows no measurable change in oxidation products between the masked samples and the virgin results.

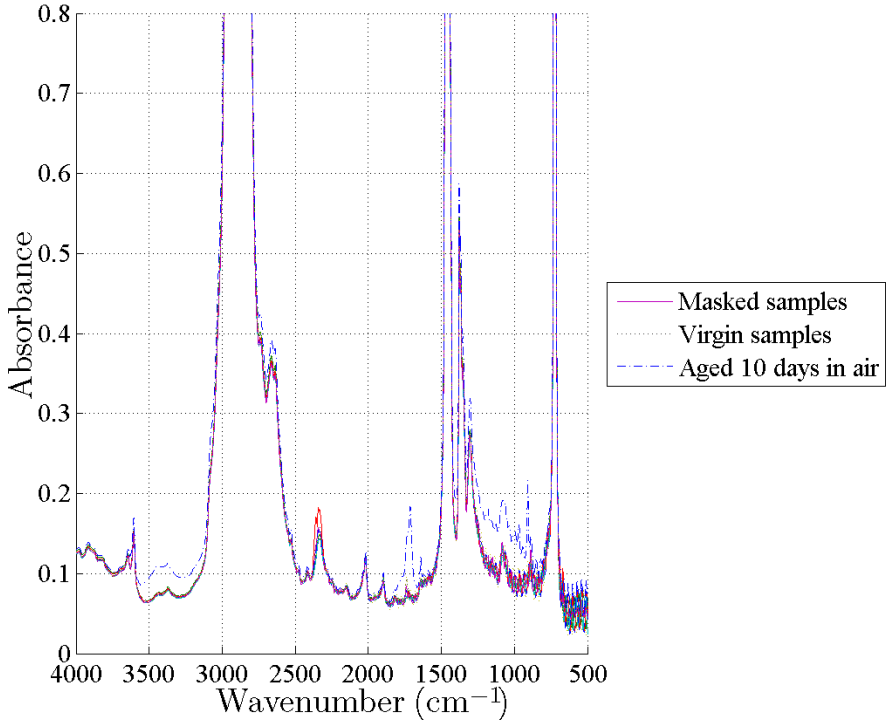

FIGURE 4.7: Effect of elevated temperature on formation of oxidation products

4.2.4 Photoluminescence spectroscopy

photoluminescence (PL) spectroscopy measures the light emission from a material as a result of excitation by a light source (typically in the UV range). The wavelength and intensity of the emission is heavily dependent on the particular absorbing properties of the molecular bonds within the polymer. Changes in the bonds due to photo-irradiation, such as the formation of oxidation groups, can be expected to alter the emission.

The emission of a photon occurs due to the excitation of a molecule to a higher energy state ($S_{1,2,3,...}$) due to the absorption of a photon of light. As discussed previously (section 2.5) and depicted by the Jablonski-diagram (figure 2.6), the subsequent relaxation back to a ground state (S_0) can occur through a mixture of both radiative and non-radiative processes. The radiative pathways resulting

in the emission of fluorescence or phosphorescence. Fluorescence occurs due to relaxation from a singlet excited state ($S_{1,2,3,...}$) whilst phosphorescence requires inter-system crossing to a triplet state ($T_{1,2,3,...}$) before relaxation. Due to the energy lost by internal-vibration or inter-system crossing the emitted photon is at a longer wavelength (lower energy) than the excitation photon. The distinction between emission type can be made by the wavelength, (phosphorescence being longer than fluorescence) and lifetime, fluorescence occurring in 10^{-9} to 10^{-6} s and phosphorescence, 10^{-3} to 10^{0} s after excitation [50]. In LDPE, phosphorescence emission is only seen from liquid nitrogen cooled samples, a capability not possible with the experiment arrangement in the TDHVL [171].

The same uncoated strips of aged polymer as used in FTIR spectroscopy were used for PL spectroscopy. The measurements were collected using the Perkin Elmer LS 45 Fluorescence Spectrometer. Excitation wavelengths were used in 5 nm intervals from 200 to 300 nm, with the emission measured over the 200 to 1100 nm range. The spectrograph was set to scan at 500 $\mathrm{nm\,min^{-1}}$. This particular system is unable to account for the second-order affects of the spectrograph and UV source so measurements at these wavelengths are removed for clarity.

The measurements of most interest are from excitations at 225 and 250 nm. The results for samples aged in air are presented in figure 4.8. The virgin material shows a peak fluorescence emission at 340 and 580 nm when excited by 225 nm light. Under a 250 nm excitation only a single emission peak at 355 nm is seen. The emission from an excitation at 225 nm is stronger than that from 250 nm. A similar shape and wavelength fluorescence emissions have been shown in literature [72, 172]. Similarly their emission was also seen to shift to longer wavelengths as the excitation energy was reduced.

Comparing the fluorescence from the virgin sample with that from samples aged in air shows significant changes after very short ageing durations. The results from excitation at 225 nm shows the fluorescence emission reduces, the shoulder at 300 nm almost disappearing while the peaks at 340 and 580 nm significantly reduce. The fluorescence intensity reduces with increasing ageing duration, with the exception of the 17 days aged sample, appearing out of sequence but still weaker than the virgin sample. Investigating the fluorescence emission from the 250 nm excitation shows a shift in the wavelength of the emission to longer wavelengths for all ageing durations. After just 3 days of ageing the peak of the emission has shifted from 340 to 360 nm and shifts slightly further with continued ageing.

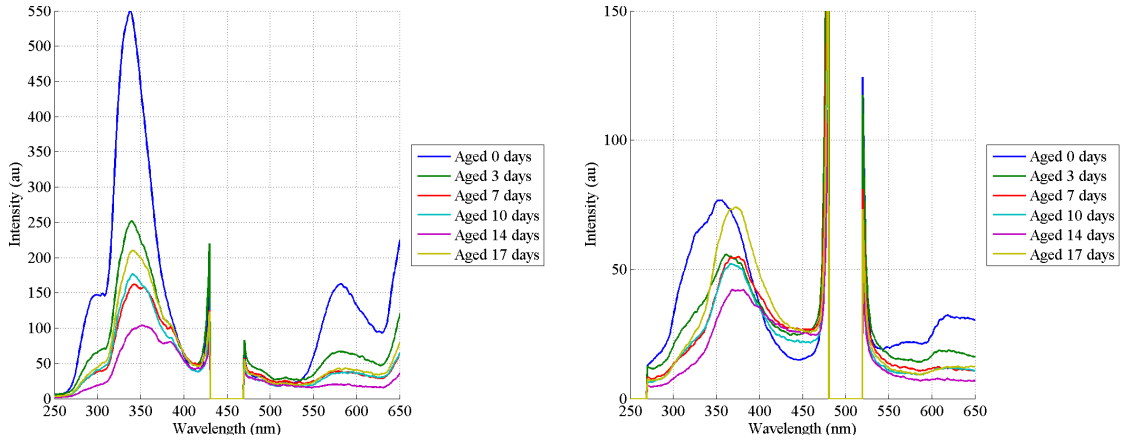

(a) 225 nm excitation

(b) 250 nm excitation

FIGURE 4.8: Fluorescence emission for samples UV aged in air

The samples aged in a nitrogen atmosphere showed different trends in the fluorescence spectra (figure 4.9). The fluorescence emission from excitation at 225 nm also reduces in intensity but not to the same extent as those aged in air. The fluorescence spectra from a 250 nm excitation showed a similar shift to longer wavelengths, the peak shifting to approximately 370 nm. In this case though the intensity of the fluorescence has increased rather than reduced after just 3 days of ageing. As the ageing time increases the fluorescence intensity does reduce but not as low as the samples aged in air.

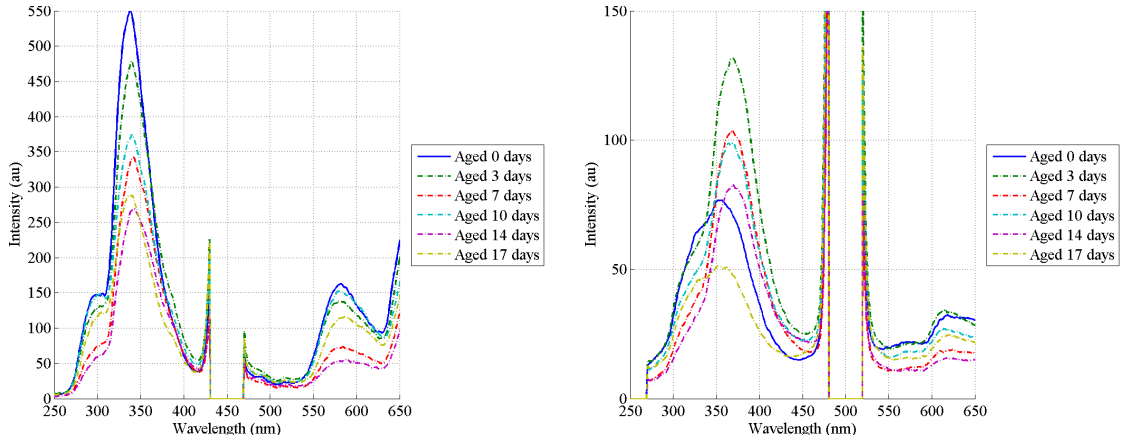

(a) 225 nm excitation

(b) 250 nm excitation

FIGURE 4.9: Fluorescence emission for samples UV aged in nitrogen

This reduction in intensity of the fluorescence emission is thought to be due to the increased concentration of oxidation products. Similar trends have been

reported elsewhere [173, 174]. Investigations at the longer excitation wavelength (approximately 250 nm) have suggested cross-linking links to the stronger and shifted fluorescence [172]. Cross-linking is expected to occur as a result of photo-irradiation and measurements to investigate this are detailed in the following section. The amount of cross-linking is greatest in the oxygen free samples as a result of ageing in nitrogen. This suggests the fluorescence shift in wavelength seen for the 250 nm excitation is due to cross-linking. The reduction in intensity as ageing duration increases is then explained by the increasing concentration of oxidation products, being greatest in the air aged samples.

4.3 Cross-Linking

The process of photo-irradiation causes the breaking of bonds and subsequent generation of free radicals. These free radicals are able to react with oxygen, creating carbonyl and hydroxyl groups. If there are no other molecules available then the free radicals may react together forming cross-links between various chains within the polymer. LDPE is very prone to cross-linking due to its tertiary bonded carbon atoms, large quantities of side branches and amorphous regions allowing for chain movement [175]. It is also possible for the cross-links to form with the inclusion of other molecules (such as oxygen).

To investigate the level of cross-linking and its relationship with UV ageing, samples were dissolved in boiling xylene (at approximately 140 ^{o}C) as per the ASTM standard D2765-01 [176]. Due to the limited quantity of aged material, approximately 0.1 g of sample was used for each measurement rather than the 0.3 g set out in the standard. Samples were placed in stainless steel mesh pouches (120 mesh, 0.149 mm aperture) and suspended in the xylene for 6 hours [177–179]. Samples were then removed and placed in a preheated (100 ^{o}C) vacuum oven to be dried until a stable weight was reached (approximately 4 hours) [180]. The sample remaining represents the cross-linked part of the original and so the percentage of the cross-linked material can be calculated using [176];

$$\text{Percentage cross-linked (gel content)} = \frac{(W_4 - W_3)}{(W_2 - W_1)} \times 100 \tag{4.4}$$

Where W_1 is the weight of the open pouch, W_2 is the weight of the sample and open pouch, W_3 is the weight of the closed pouch including the sample before dissolving and W_4 is the weight of the pouch and remaining sample after drying. A total of 3 samples were measured for each ageing condition and the mean results are shown in

figure 4.10, where error bars show the range in measured values and account for the accuracy of the scales. The samples aged in air show nearly 43 % of the material cross-linked after only 3 days of UV ageing. With further ageing this continues gradually until reaching a peak of 47 % after 10 days. Continued exposure to UV radiation causes the cross-linking to reduce, (approximately 29 % after 17 days). This gradual increase to a peak is thought to be due to the excessive cross-links creating a very rigid structure stopping the molecular rearrangement required for further cross-linking [126]. This does not explain however the reduction in cross-linking evident from further ageing when a plateau would be expected. This may be explained due to the increase in oxidation products. The continued bombardement of UV energy allowing the cross-links to be broken and the free radicals to join with oxygen, supporting the reduction in cross-links at the same time as an increase in oxidation products. A similar trend for LDPE has been reported by others [179, 181], although the irradiation energy and times are not comparible.

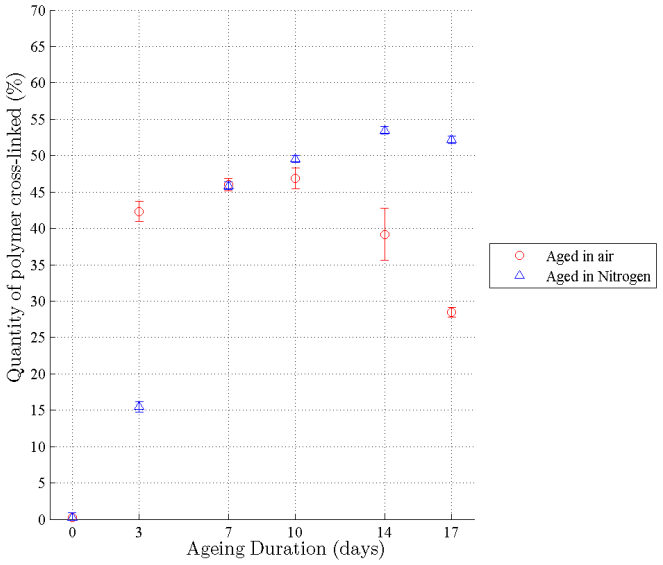

FIGURE 4.10: Percentage cross-linking for all ageing conditions

The samples aged in a nitrogen environment had no oxygen available and so cross-linking was expected to be the dominant reaction for the free radicals. The results shown in figure 4.10 show an initially slower increase in cross-linked content but the continued increase until 14 days of ageing. After 14 days of ageing the cross-linking content reaches a constant level. The samples aged in nitrogen reach a maximum of approximately 55 %, 8 % more than that of the samples aged in air. The constant level is thought to be due to the restriction in molecular rearrangement created by

the cross-links. The cross-linking is likely to occur in the amorphous regions and therefore the limited reorientation due to cross-links prevents further cross-linking [182]. Similar measurements for the maximum cross-link concentration of LDPE have also been reported by other researchers [183–185]. It appears that between 14 and 17 days of ageing the cross-link concentration begins to reduce. Without investigating longer ageing durations this cannot be confirmed. It could also be due to breaking of cross-links that are then able to form with some of the oxygen remaining within the bulk of the polymer.

The samples aged in a nitrogen environment show a lower cross-link level after 3 days than that of samples aged in air. This is likely to be due to the UV transparency of the quartz vessel. At the UV excitation wavelength (253.7 nm) the vessel is approximately 90% transparent and therefore fewer reactions are expected to take place, resulting in a slower rate of photo-irradiation reactions [133]. The eventual high level reached is due to the reduced competion between oxidation products forming and cross-linking reactions compared with samples aged in air.

4.3.1 Differential Scanning Calorimetry

Most changes in the chemical structure are expected to occur in the amorphous regions. Still the breaking of bonds along with the production of radicals, oxidation groups and cross-links can still disturb the crystallinity of the polymer. One method to investigate this is the use of differential scanning calorimetry (DSC). DSC measures the heat flow into a polymer as the temperature is increased linearly with time, a full description of the principles have been shown in the literature [136, 186]. As the temperature rises the polymer will experience thermal transitions at specific temperatures, known as: glass transition temperature (T_g), crystallisation temperature (T_c) and melting temperature (T_m). These transitions are identifiable due to significant changes in the energy required to raise the temperature of the polymer past these temperatures. These transitions have been measured to be approximately -118^{o}C, 96^{o}C and 108^{o}C for the T_g, T_c and T_m of LDPE respectively.

The DSC measurements were completed using a Perkin-Elmer DSC 7, controlled by the Perkin-Elmer, Pyris analysis software. A chiller was used to maintain a stable background temperature (20 ^{o}C) at the DSC head. Samples were cut into pieces and approximately 10 mg ($\pm$ 0.5 mg) were placed in DSC cans with a lid then attached and sealed. To ensure accurate measurements the DSC was

calibrated before use using a sample with a known T_m. In this work indium is used with a melting point of 156.6 ^{o}C [136]. The calibration measurement is completed with the same scan rate (10 ^{o}C min^{-1}) as desired for measurements, but over a more appropriate range (140 to 170 ^{o}C).

Measurements were taken from 50 to 150 ^{o}C and then cooled rapidly back to 50 ^{o}C. Three samples were tested per ageing condition and a typical DSC curve is presented in figure 4.11 for samples aged in air and nitrogen environments. Traditionally a DSC measurement is run twice and the second measurement used for analysis [136], ensuring all samples have undergone the same thermal history to allow for comparison. As the temperature rises from 50 to 150 ^{o}C there is a clear peak in the heat flow. This indicates the transition from a semi-crystalline structure to a fully molten state as it crosses its T_m. Comparison of the curves shows no significant change as a result of ageing in either air or nitrogen environments. The onset of the rise in heat flow appears to occur slightly sooner but the peak heat flow and temperature show little change.

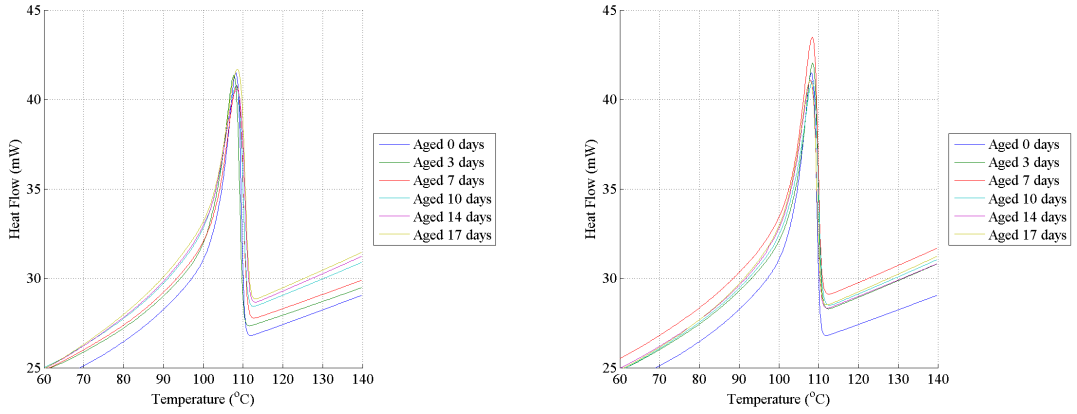

(a) Samples aged in air

(b) Samples aged in nitrogen

FIGURE 4.11: Differential scanning calorimetry of UV aged LDPE

A lot of information can be extracted from the DSC curves but in this case changes in T_m and crystallinity (χ_c) are of most interest. The value of T_m is obtained using the analysis software as the onset of the melting peak, i.e. the point at which the heat flow increase signifies the melting of the polymer. The peak of the curve marks the point at which all the polymer has melted which is clear from the results shown in figure 4.11 to have changed very little.

The χ_c of the sample can be approximated by the ratio of energy required to melt it with the energy required to melt a sample that has 100 % crystalline form [2],

$$\chi_c = \frac{\Delta H_f}{\Delta H_{f_{100}}} \times 100 \tag{4.5}$$

Where ΔH_f is the enthalpy of fusion required to melt the sample and $\Delta H_{f_{100}}$ is the enthalpy of fusion for a 100% crystalline form ($\Delta H_{f_{100}} = 293.1$ J g^{-1} for PE [187]). ΔH_f is calculated by integrating the area under curve covering the melting point and dividing by the mass of the sample.

Figure 4.12 presents the changes in T_m and χ_c as ageing duration increases. It is clear that the chemical changes resulting from photo-irradiation in both air and nitrogen environments reduces the T_m of the polymer. In both air and nitrogen aged samples T_m reduces constantly over the first 10 days of ageing. The nitrogen aged samples continues to reduce slightly with further ageing but the air aged samples seem to reach a plateau. This reduction in T_m is thought to relate to the increased cross-link concentration and similar trends have been seen in LDPE cross-linked by irradiation or peroxide methods [175, 182, 188]. The nitrogen samples showed the greatest and continued increase in cross-link concentration for the 14 days of photo-irradiation.

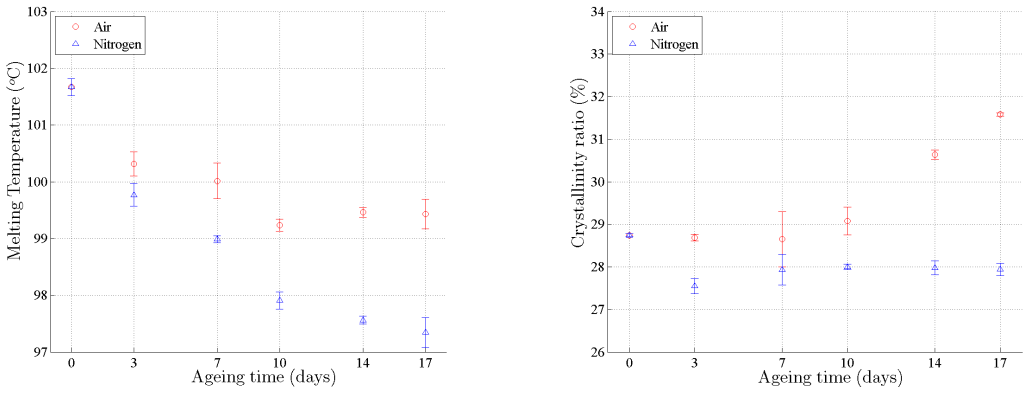

(a) Melting Temperature

(b) Crystallinity ratio

FIGURE 4.12: Crystallinity ratio and melting temperature for UV aged LDPE

The χ_c also changes as a result of the ageing process, in this case the trend differing between air and nitrogen aged samples. The sample aged in air shows an increase in χ_c as the ageing duration increases. The nitrogen samples initially show a reduction in χ_c and then remain approximately constant. The cross-linking of samples has been associated with a reduction in crystallinity for the second run DSC measurements [175]. This is thought to be due to cross-links between different

amorphous regions restricting the movement in the molten state and therefore ability to form large crystalline regions. The increase in crystallinity as a result of photo-irradiation in an air environment is thought to be due to the production of oxidation products. A similar trend has been seen as a result of thermal and plasma induced oxidation [132, 189]. The photo-oxidation causing the scission of links between different amorphous regions and therefore increasing the possibility of chains to rearrange in the molten state and from crystalline regions.

4.4 Dielectric Strength

As materials age there is a reduction in their associated dielectric strength [27]. To investigate the reduction in breakdown strength with ageing, samples were stressed under an increasing ac field until failure. Results were collected as set out in section 3.3 and analysed using the 2 parameter Weibull distribution method [137, 138, 140]. Figure 4.13 shows the breakdown results comparing virgin samples with 7 and 17 days UV aged samples. More than 25 measurements where completed for each sample to ensure confidence in the calculated Weibull parameters. Preliminary investigations showed the same trend for 3, 10 and 14 days aged samples and so are not included for clarity.

The results show a reduction in the breakdown strength as ageing time increases and an increasing spread in data. The values for α and β (table 4.2) are a way of representing the changes in breakdown strength and spread of data. A higher β value suggests a small spread of breakdown values in a data set and a higher α value shows a higher breakdown strength.

TABLE 4.2: Changes in α and β of 2-parameter Weibull distribution with ageing duration

Ageing Condition	**Beta**	**Alpha (kV mm^{-1})**
Virgin	43	160.1 ± 1.2
Aged 7 days	19.9	154.4 ± 2.5
Aged 17 days	17.7	151.1 ± 2.7

The values for β suggest a significant increase in the spread of the data with ageing. Analysis of the breakdown system showed it to be operating at its limit for some of the virgin sample failures. Every breakdown site was checked to confirm failure had occurred rather than another event causing the system to trip (such as a flashover). As the amplifier approached its upper limit the applied sinusoidal waveform becomes distorted, thus enhancing the probability of failure. This suggests that the α value may actually be higher for virgin LDPE and that

the β value is therefore artificially high. For the aged samples β reduced as sample ageing time increases, suggesting a reduction in the uniformity of the sample. This suggests there maybe a change in the dominant breakdown mechanisms as ageing time increases, resulting in a reduction in the dielectric strength (α).

Measurements were also attempted on nitrogen aged samples but the failure voltage increased. The typical voltage was now above the stable operating range of the test system. This increase in breakdown strength can only be explained due to the formation of cross-links, creating a more rigid structure. An increase in dielectric strength due to cross-linking is regularly seen [190, 191]. This suggests the reduction in breakdown strength seen for samples aged in air relates to the increase in oxidation products with the tested samples.

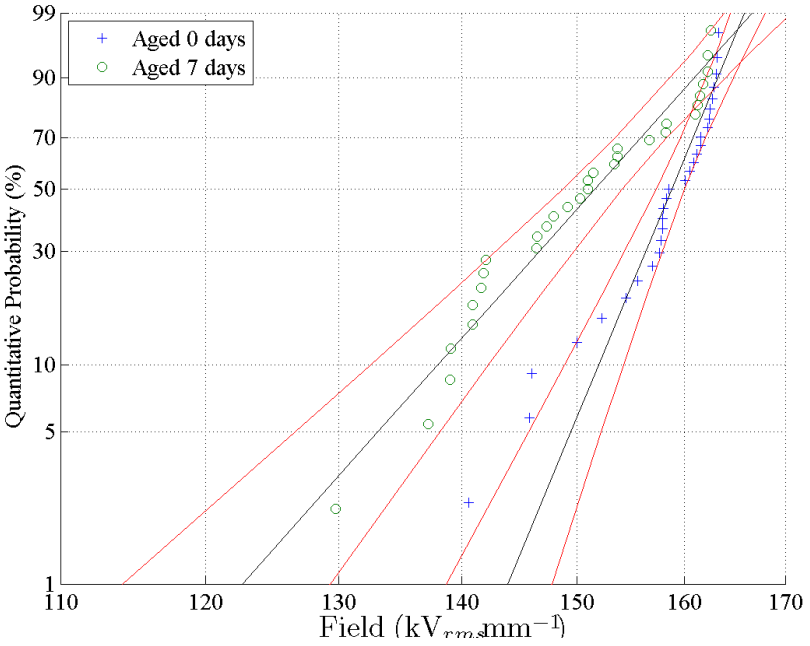

(a) UV aged 7 days

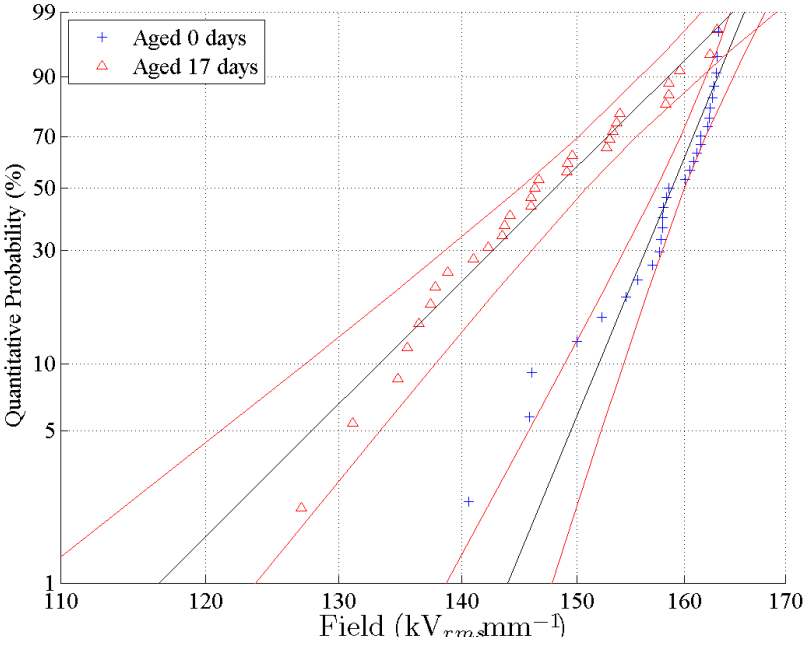

(b) UV aged 17 days

FIGURE 4.13: Two parameter Weibull plots of AC ramp breakdown results for 100 μm LDPE UV aged in air

4.5 Dielectric Spectroscopy

The previous sections have described changes in the chemical structure as a result of UV ageing. Results showed increases in oxidation products and cross-link concentration. The following sections investigate the affect ageing has on the interaction of charge with the polymer.

This section investigates changes in the dielectric properties of the polymer in terms of real relative permittivity ($\epsilon^{'}$) and $\tan\delta$ over a range of frequencies as a result of ageing. Measuring changes in $\epsilon^{'}$ relates to the polarisability of the polymer, changes in $\tan\delta$ give an interpretation of energy losses during polarisation [27].

The dielectric response of 100 μm LDPE films was investigated, however, ideally thicker samples should be used to reduce the influence of surface effects [136]. This would remove direct comparability with SC and EL measurements along with altering the ageing characteristics. Typically $\epsilon^{'}$ and $\tan\delta$ measurements are expected to give smooth changes with frequency, in practice electrical noise interferes with the low signal strength [27]. This is particularly a problem with the very low imaginary relative permittivity ($\epsilon^{''}$) of LDPE and therefore noisy $\tan\delta$ measurements, particularly at higher frequencies. To aid in presenting a comparison of $\epsilon^{'}$ and $\tan\delta$ measurements of aged samples the results were smoothed over the range 10^{-1} to 10^{3} Hz. Above this frequency the signal became too noisy to accurately smooth or compare.

Figure 4.14 shows the changes in $\epsilon^{'}$ and $\tan\delta$ over the frequency range 10^{-1} to 10^{3} Hz with 20 points per decade. The $\epsilon^{'}$ for virgin samples shows a constant level (approximately 2.3) across the frequency range, typical of LDPE at a constant temperature [192]. As the ageing duration increases so does $\epsilon^{'}$, but also develops a slight frequency dependence above 10^{2} Hz. The samples aged in air show a greater increase in $\epsilon^{'}$ than the samples aged in nitrogen. The $\tan\delta$ of the virgin results show a frequency dependence above 10^{2} Hz. As the material is aged there is clearly an increase in $\tan\delta$, the greatest increases are for samples aged in air.

An increase in $\epsilon^{'}$ suggests an increase in the dipole movement leading to an increase in the polarisability and is most likely associated with increases in polar groups, such as oxidation products [26, 27]. A smaller increase in oxidation products occurred in nitrogen aged samples and supports this with a smaller increase in $\epsilon^{'}$. The restriction in the molecular movements as a result of cross-linking can also be expected to influence the permittivity of the polymer but more likely to

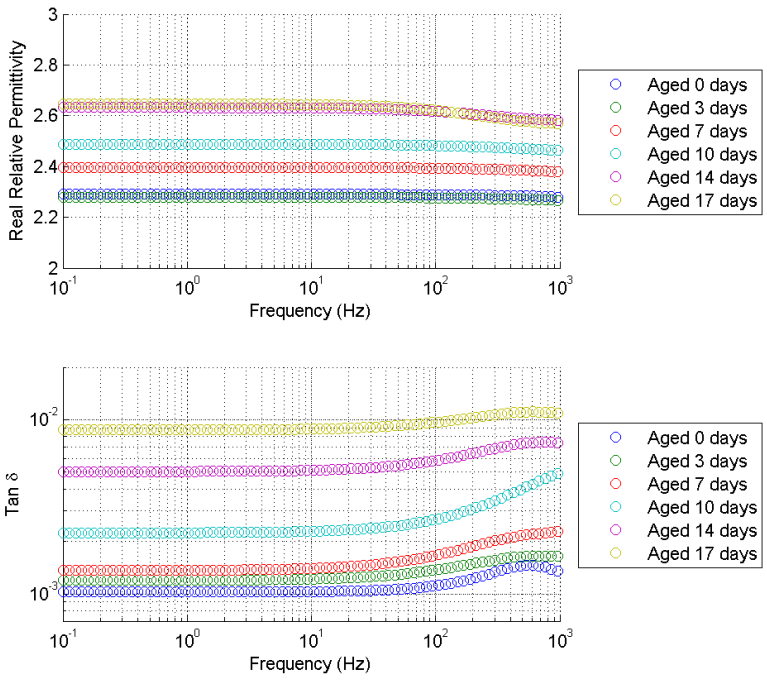

(a) Aged in air

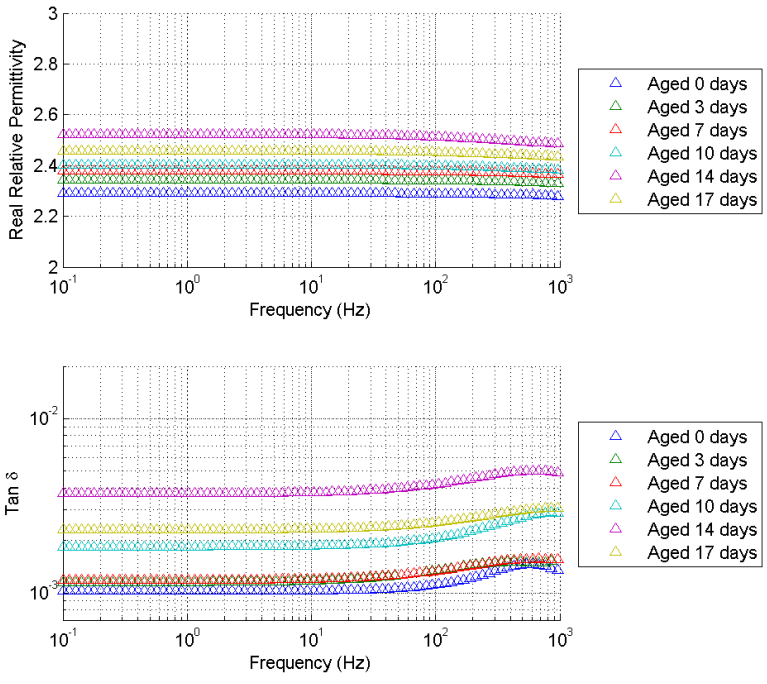

(b) Aged in nitrogen

FIGURE 4.14: Dielectric response comparing virgin and UV aged LDPE samples

be detectable at higher temperatures [74]. The nitrogen aged samples were more dominant in cross-linking but show a smaller increase in $\epsilon^{'}$ suggesting the oxidative products to have the biggest influence. Increases in $\tan\delta$ are also commonly associated with ageing of polymers and often associated with oxidation products [193]. An increase in $\tan\delta$ relates to a bigger loss of energy during each cycle of the applied field.

To further analyse the affect ageing has on $\epsilon^{'}$ and $\tan\delta$, values extracted at 50 Hz are shown in figure 4.15. 50 Hz is chosen due to its relevance to the EL measurements detailed in section 4.7. The results shown in figure 4.15 are the mean values, with error bars showing the measurement range from at least 3 samples.

The results show that at 50 Hz the $\epsilon^{'}$ for samples aged in air increases almost linearly with ageing. For the samples aged in nitrogen $\epsilon^{'}$ initially increases and then remains roughly constant with further ageing. The 50 Hz $\tan\delta$ measurement for samples aged in air and nitrogen increase at a similar rate for the first 7 days of ageing. Further ageing of samples in air and the $\tan\delta$ loss increases significantly. The samples aged in nitrogen increase slowly with further ageing thought to be due to the smaller concentration of oxidation products. A similar behaviour has been seen for long term weathering of LDPE with and without antioxidant [55].

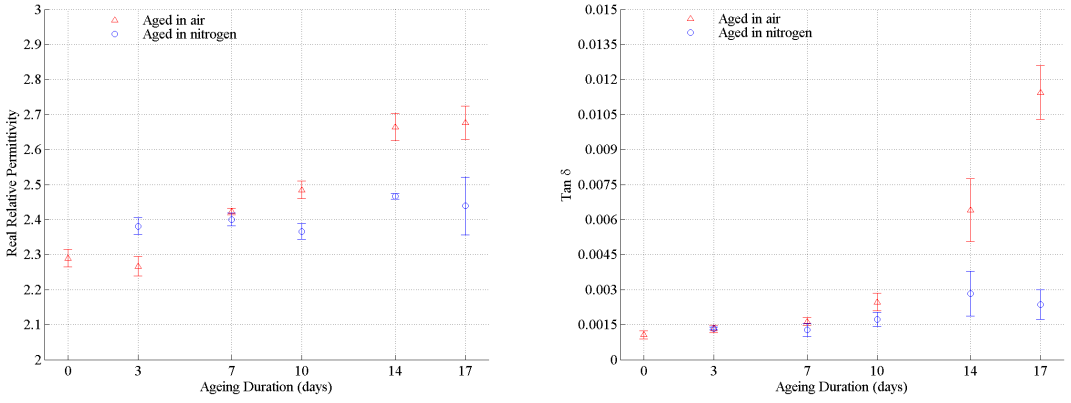

(a) Real relative permittivity ($\epsilon^{'}$)

(b) Dielectric loss tangent ($\tan\delta$)

FIGURE 4.15: Real relative permittivity and dielectric loss tangent at 50 Hz

4.5.1 Imaginary permittivity and the Havriliak-Negami model

Changes in full ϵ'' with frequency can show particular relaxation peaks. These relaxation peaks relate to the losses due to polarisation of dipoles within the polymer [27, 74]. The level of these relaxations is expected to be unmeasurable in an ideal, non-polar polymer but due to impurities present within LDPE measurements are possible. Changes resulting from photo-irradiation can therefore be expected to alter the ϵ'' relaxation curves [74].

At very low frequencies increases in ϵ'' as frequency decreases relate to dielectric loss mechanisms [144]. If ϵ' also increases as frequency reduces the losses may be considered to relate to polarisation or electrode affects [194]. However, in this case ϵ' has been shown to be frequency independent over the measurement range, irrelevant of the ageing condition. Therefore the loss mechanisms can be considered to relate to the conduction of charge [60]. At frequencies above these, increases in ϵ'' relate to relaxation peaks. These relaxations are caused by dipole movements and controlled by the localised bonding arrangements. Typically in LDPE, two relaxation peaks are seen over this frequency range [195].

These conduction and relaxation processes cannot be assumed to be frequency independent of each other. To enable further analysis of the ϵ'' data a fit can be produced using the Havriliak-Negami (HN) model 4.6 [195–197], that is;

$$\epsilon''(\omega) = \frac{a\sigma}{\epsilon_0 \omega^s} - \sum_i \mathrm{im}\left[\frac{\Delta\epsilon_i}{(1+(j\omega\tau_i)^{\alpha_i})^{\gamma_i}}\right] \tag{4.6}$$

Where σ is the dc conductivity, a is a constant, s is the parameter relating to interfacial polarisation with restriction $0 < s < 1$, i is the number of peaks (2 in this case), $\Delta\epsilon$ is the dielectric strength of the material, τ is the relaxation time, α and γ are the asymmetric and broadening parameters respectively with constraints $0 < \alpha$ and $\alpha\gamma < 1$.

The HN model is an empirical model based on the original Debye relaxation but accounting for the asymmetry and broadening of dielectric relaxation curves [198]. The model represents ϵ'' measurements by summing the individual relaxation spectra across the frequency range. Figure 4.16 shows the raw ϵ'' measurements from 10^{-2} to 10^6 Hz along with the HN model result for virgin LDPE. The results show the contribution from dc conduction (green line), the first relaxation peak

(blue line) and the start of the second relaxation peak (magenta line). The HN model (red line) shows the sum of this data to produce a good fit with the measured data. The optimised values for σ, a, s, $\Delta\epsilon_1$, τ_1, α_1, γ_1, $\Delta\epsilon_2$, τ_2, α_2 and γ_2 are all shown in tables 4.3 and 4.4.

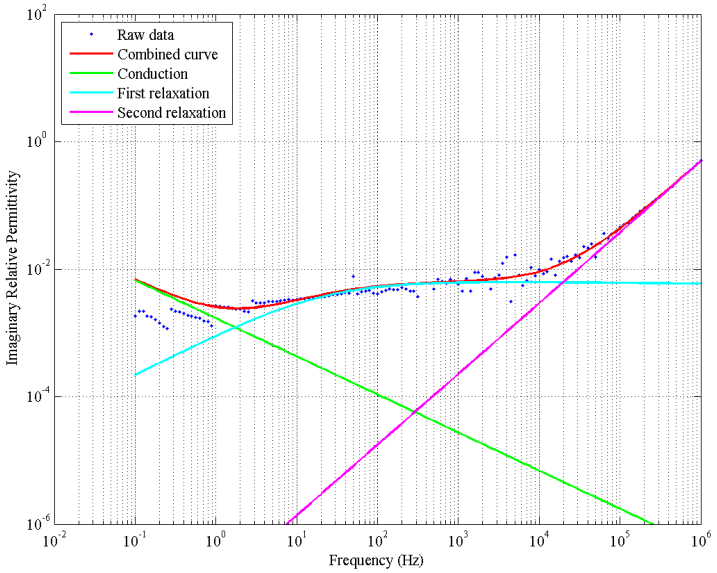

FIGURE 4.16: Imaginary relative permittivity of virgin LDPE

Figures 4.17 to 4.21 show the ϵ'' data and HN model for samples UV aged in air. The optimised parameters are also shown in table 4.3. The results show a broadening of the first relaxation peak (blue line) as ageing time increases, with the exception of the 10 days aged sample. As a result of this the start of the second relaxation peak (magenta line) either increases to higher frequencies or reduces in effect due to the higher ϵ'' values.

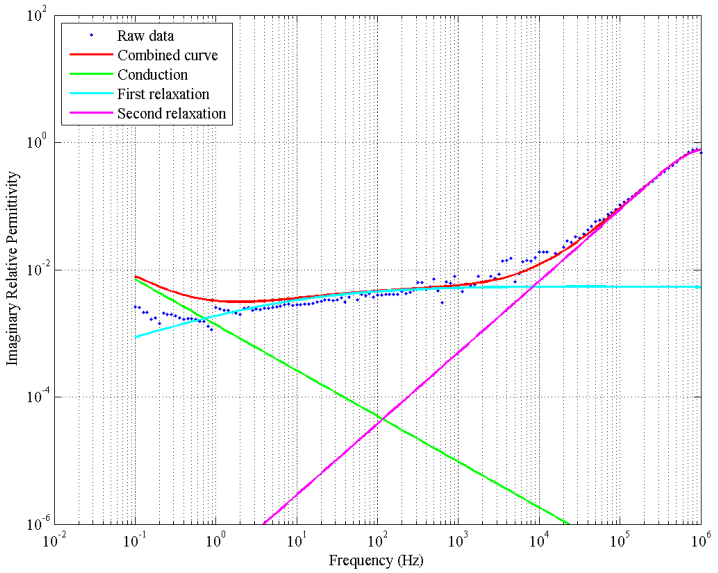

FIGURE 4.17: Imaginary relative permittivity of LDPE UV aged 3 days in air

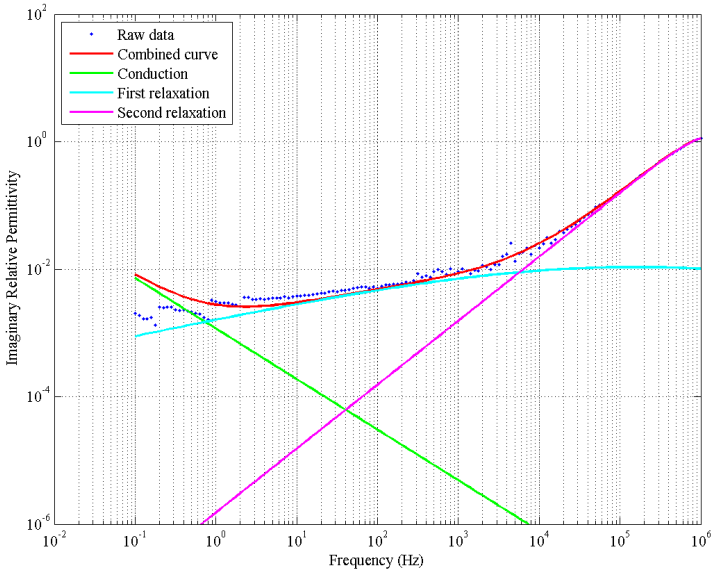

FIGURE 4.18: Imaginary relative permittivity of LDPE UV aged 7 days in air

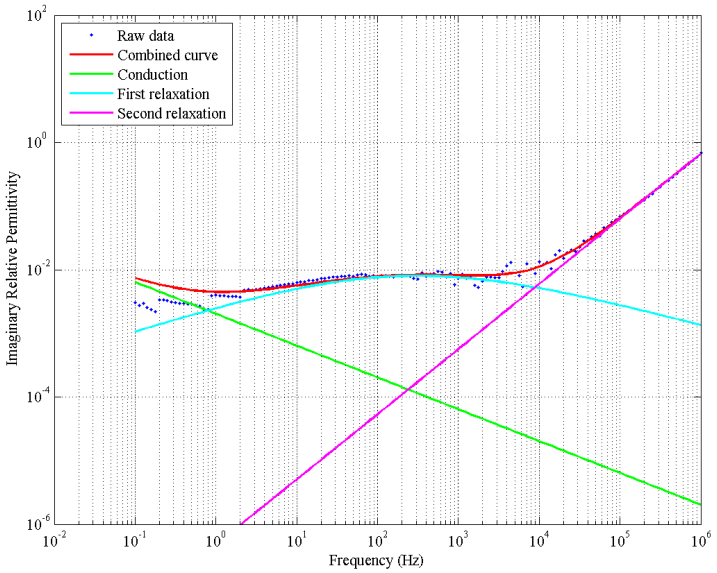

FIGURE 4.19: Imaginary relative permittivity of LDPE UV aged 10 days in air

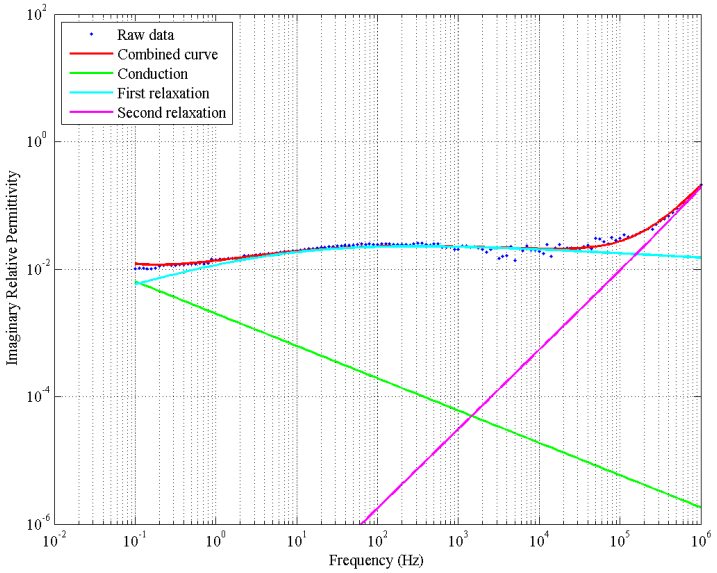

FIGURE 4.20: Imaginary relative permittivity of LDPE UV aged 14 days in air

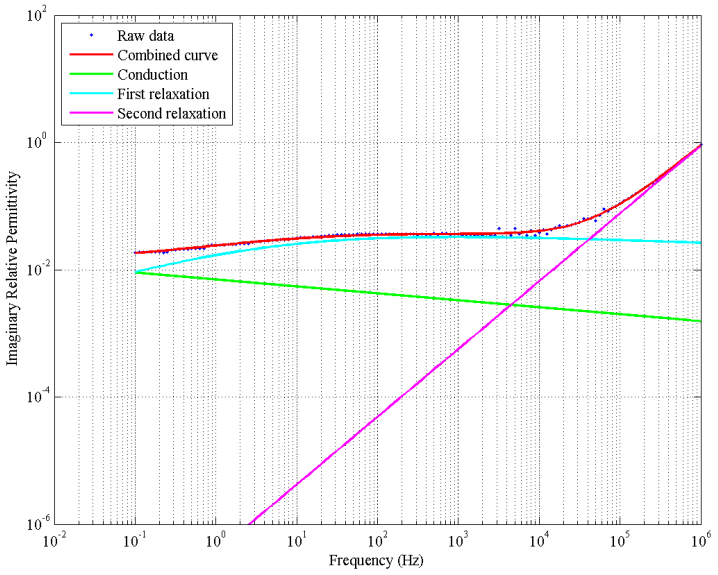

FIGURE 4.21: Imaginary relative permittivity of LDPE UV aged 17 days in air

Figures 4.22 to 4.26 show the ϵ'' and HN model for nitrogen aged samples. The optimised parameters are shown in table 4.4. These results show initially a broadening of the first relaxation peak (blue line) after 3, 7 and 10 days of ageing. After 14 and 17 days the first relaxation peak has narrowed and the second relaxation peak occurs at much lower frequencies.

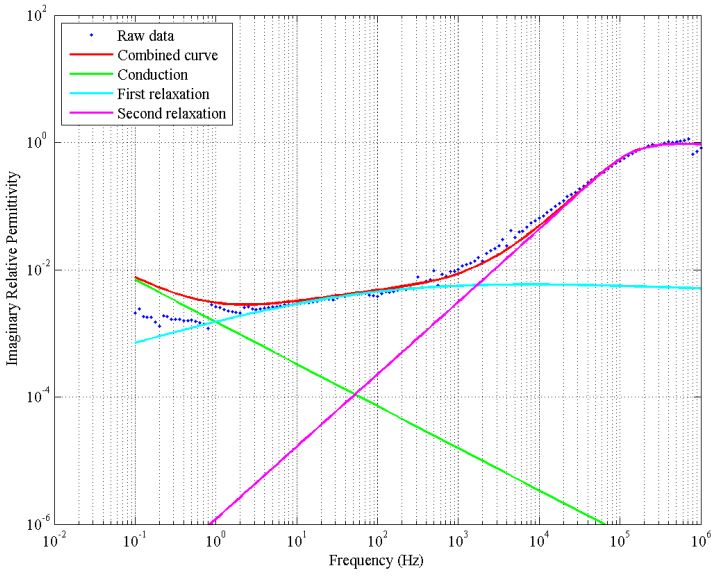

FIGURE 4.22: Imaginary relative permittivity of LDPE UV aged 3 days in nitrogen

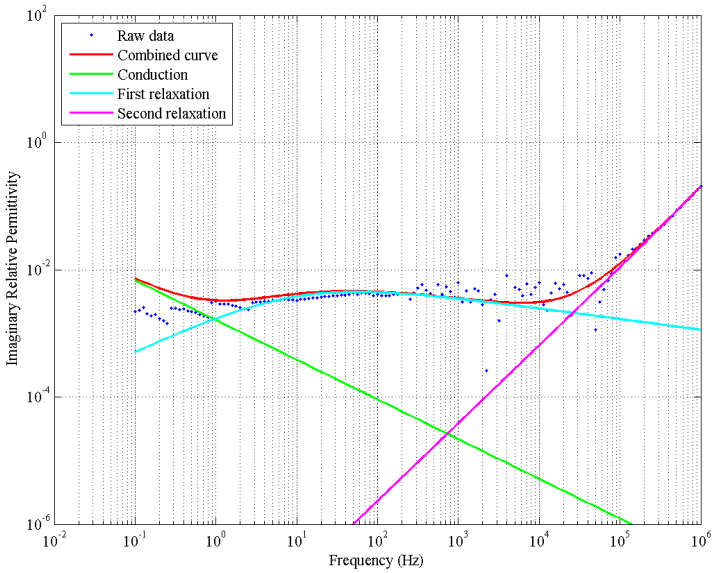

FIGURE 4.23: Imaginary relative permittivity of LDPE UV aged 7 days in nitrogen

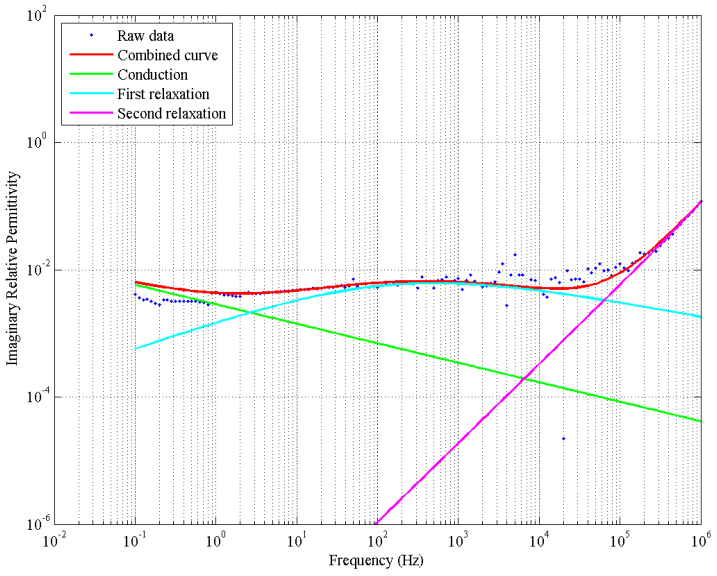

FIGURE 4.24: Imaginary relative permittivity of LDPE UV aged 10 days in nitrogen

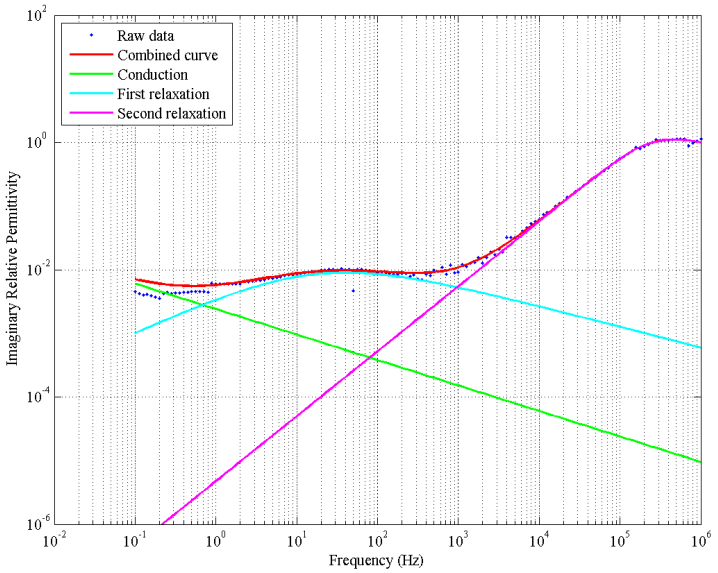

FIGURE 4.25: Imaginary relative permittivity of LDPE UV aged 14 days in nitrogen

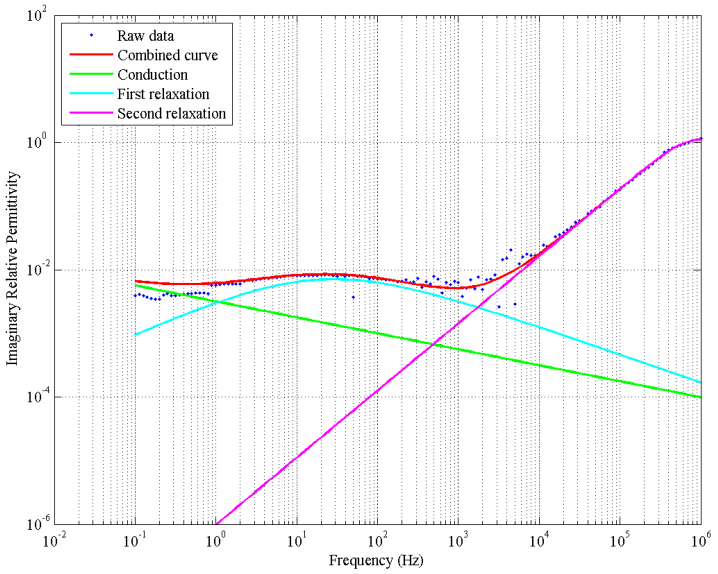

FIGURE 4.26: Imaginary relative permittivity of LDPE UV aged 17 days in nitrogen

The results clearly show significant changes in the ϵ'' data as a result of photo-irradiation in both air and nitrogen environments. Increases in the losses as a result of increased oxidation products make observing the dc contribution more challenging. Broadening of the middle peak is thought to be due to an increase in the quantity of oxidation products and free radicals that result from the photo-irradiation reactions [60]. A similar broadening is seen initially in the nitrogen aged results suggesting some broadening of the peak may be due to cross-linking of the polymer [195, 199].

TABLE 4.3: Parameters used for Havriliak-Negami model for air aged samples

Ageing Duration	σ	a	s
0	2.22E-14	2	5.97E-01
3	2.22E-14	2	7.17E-01
7	2.22E-14	2	7.93E-01
10	2.22E-14	2	5.00E-01
14	2.22E-14	2	5.06E-01
17	3.80E-14	2	1.10E-01

Ageing Duration	$\Delta\epsilon_1$	τ_1	α_1	γ_1
0	3.13E-01	1.00E-02	6.42E-01	2.19E-02
3	4.04E-01	2.80E-02	4.25E-01	2.23E-02
7	1.06E-01	1.95E-06	2.70E-01	8.41E-01
10	5.10E-02	7.68E-04	4.09E-01	8.43E-01
14	3.25E-01	3.11E-02	4.10E-01	1.78E-01
17	6.44E-01	3.86E-02	3.70E-01	1.29E-01

Ageing Duration	$\Delta\epsilon_2$	τ_2	α_2	γ_2	**Error**
0	3.17E+00	3.72E-08	1.11E+00	7.71E-01	7.46E-04
3	2.31E+00	2.01E-07	1.12E+00	3.84E-01	1.78E-02
7	2.76E+00	1.14E-05	1.00E+00	8.02E-01	1.15E-03
10	6.24E+00	2.55E-08	1.02E+00	6.94E-01	1.24E-03
14	6.21E-01	7.05E-08	1.24E+00	7.87E-01	7.78E-04
17	3.98E+00	4.82E-08	1.06E+00	7.93E-01	1.68E-03

TABLE 4.4: Parameters used for Havriliak-Negami model for nitrogen aged samples

Ageing Duration	σ	a	s
0	2.22E-14	2	5.97E-01
3	2.23E-14	2	6.61E-01
7	2.22E-14	2	6.24E-01
10	2.22E-14	2	3.06E-01
14	2.22E-14	2	4.00E-01
17	2.22E-14	2	2.51E-01

Ageing Duration	$\Delta\epsilon_1$	τ_1	α_1	γ_1
0	3.13E-01	9.85E-03	6.42E-01	2.19E-02
3	1.03E-01	2.89E-03	3.80E-01	1.48E-01
7	3.17E-02	2.02E-02	6.00E-01	2.83E-01
10	4.28E-02	1.20E-03	4.46E-01	5.37E-01
14	4.56E-02	9.99E-03	5.86E-01	5.61E-01
17	3.23E-02	8.38E-03	5.69E-01	7.79E-01

Ageing Duration	$\Delta\epsilon_2$	τ_2	α_2	γ_2	**Error**
0	3.17E+00	3.72E+08	1.11E+00	7.71E-01	7.46E-04
3	7.63E+00	1.40E-06	1.14E+00	9.00E-02	2.45E-01
7	7.74E-01	6.66E-08	1.22E+00	7.60E-01	5.85E-04
10	5.46E-01	6.68E-08	1.24E+00	5.79E-01	7.13E-04
14	3.56E+00	7.11E-07	1.02E+00	3.82E-01	7.21E-02
17	2.58E+00	2.00E-07	1.05E+00	6.35E-01	1.02E-02

4.6 Space Charge

To investigate the effect ageing has on charge movement in the bulk of the polymer, dc space charge (SC) measurements were completed. Measurements were taken using the PEA technique described in section 3.5. A minimum for three 100 μm LDPE samples were stressed at 40 kV mm^{-1} for 40 minutes and then the charge decay monitored for a further 30 minutes for each ageing duration. Measurements were taken with the applied field on (V_{on}) and off (V_{off}). A typical example of the results in the V_{off} condition with the sample short circuited are presented here. This allows charge in the bulk to be investigated without the additional presence of electrode charge created by the applied field.

Figure 4.27 presents the polarisation and decay of space charge for virgin LDPE. To aid presentation the legends for the SC profiles are included separately in figures 4.27(b) and 4.27(d) for polarisation and decay measurements respectively. In the

virgin material there is a very quick build up of homocharge injected from the high voltage (HV) electrode and migrates across the bulk of the polymer. A small quantity of negative charge is injected from the ground electrode but does not migrate far into the bulk. Over the 40 minute stressing duration a steady state in charge accumulation is quickly achieved. Similar profiles are often seen in the literature for LDPE [12, 83]. At the meeting point between positive and negative charge, recombination is thought to occur and used to explain the EL emission seen under dc fields [91].

The SC profiles during charge decay show the charge nearest the electrodes to decay slightly. The charge within the bulk decays very little during the 30 minutes duration decay was monitored for. After 30 minutes a large amount of the charge formed during polarisation remained. This suggests a quantity of deep trapping sites exist that stop the relaxation of trapped charge. An analysis of the rate of charge accumulation and decay allows a better interpretation of charge trapping energies and is shown in section 4.6.1.

Figure 4.28 shows the SC formation during electrical stressing of the samples UV aged in air (the virgin result is included for comparison). After 3 days of ageing there is clearly a greater quantity of charge accumulated within the polymer. The charge mostly remains near the electrodes with only a small packet of charge forming within the bulk. The samples aged 7 days show an even smaller quantity of charge in the bulk of the polymer, charge mostly accumulates at the electrodes. The quantity of charge trapped near the electrodes continues to grow with further ageing of 10, 14 and 17 days. As opposed to the steady state condition reached in the virgin sample, the aged samples continue to grow in charge density with electrical stressing duration. This is most noticeable in 14 and 17 days aged samples.

This behaviour can be explained by an increase in charge trapping sites. Oxidation products are thought to act as deep trapping sites and were shown to accumulate by FTIR spectroscopy [40]. After short ageing durations an increase in charge traps very near the electrode-polymer interface restricts the injection and migration of charge into the bulk of the polymer. Further ageing and the quantity of these charge traps increases and charge now continues to grow with electrical stressing but remains near the electrodes.

Figure 4.29 shows the decay of accumulated charge in the air aged samples after removal of the electric field. The sample aged for 3 days shows very little decay of the accumulated charge suggesting it is trapped in deep charge trapping sites.

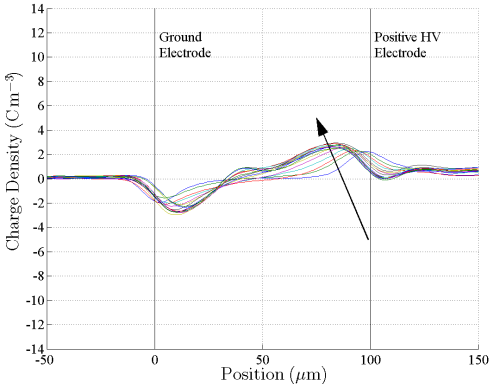

(a) Polarisation

(b) Legend for Polarisation Measurements

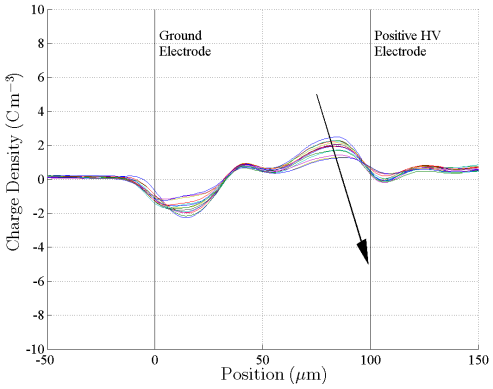

(c) Decay

(d) Legend for Decay Measurements

FIGURE 4.27: Space charge profiles using the pulsed electro acoustic technique for virgin LDPE stressed at 40 $kV_{dc}\,mm^{-1}$.

Further ageing and the accumulated charge decays to a greater extent, particularly in the 10 days aged sample. This suggests there may be an increase in lower energy trapping sites with further ageing.

The SC profiles were also collected for samples photo-irradiated in a nitrogen environment (figure 4.30). The charge accumulation is clearly very different to that of samples aged in an air environment. After both 3 and 7 days of ageing there is a large accumulation of charge within the bulk of the polymer compared with that near the electrodes. With further ageing the charge remains concentrated near the electrodes and a reduced accumulation of charge within the bulk is seen.

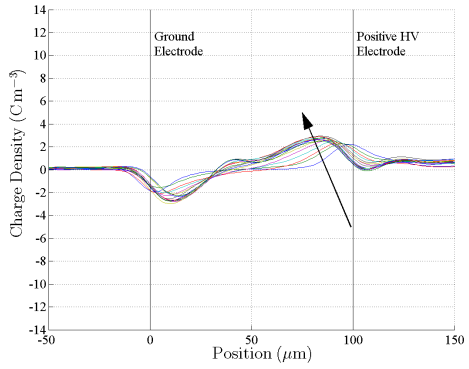

(a) Virgin sample

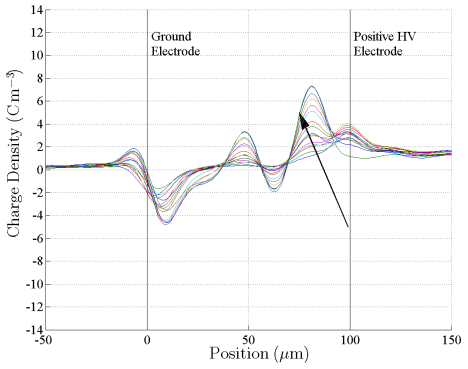

(b) Aged 3 days

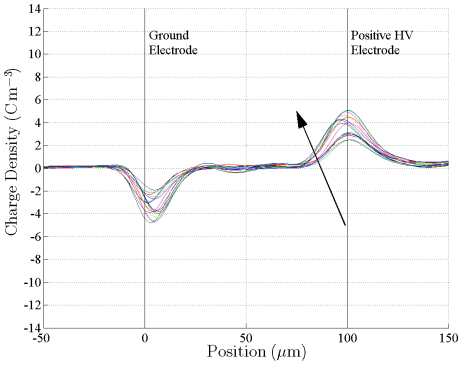

(c) Aged 7 days

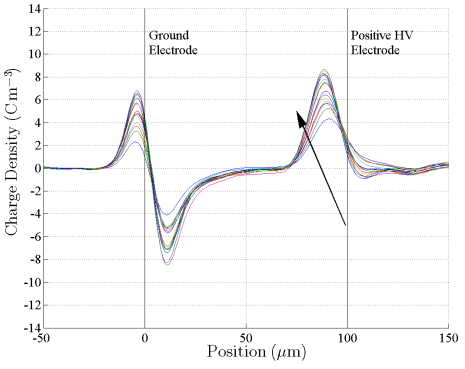

(d) Aged 10 days

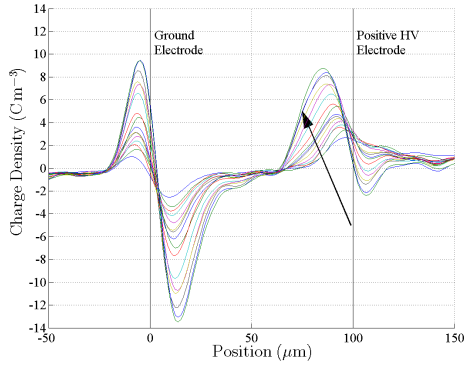

(e) Aged 14 days

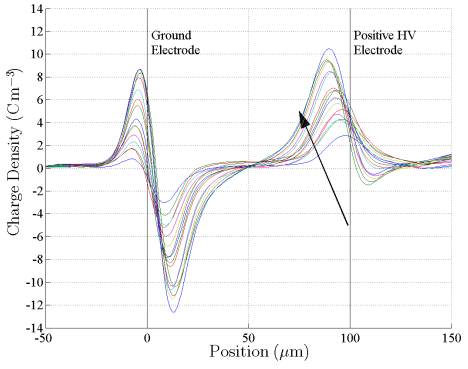

(f) Aged 17 days

FIGURE 4.28: Space charge volts off measurements during polarisation of samples UV aged in air

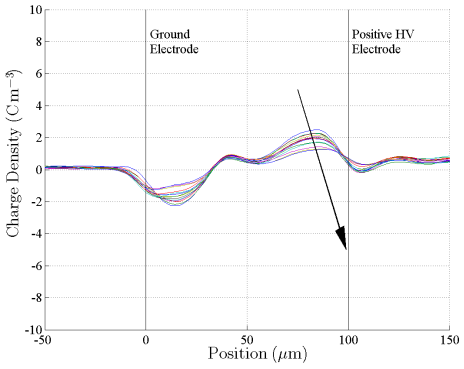

(a) Virgin sample

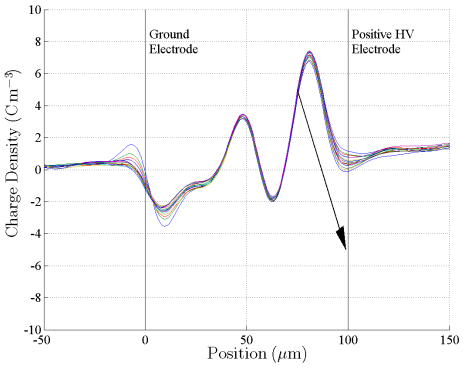

(b) Aged 3 days

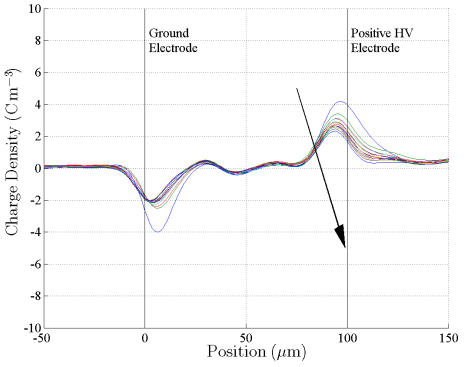

(c) Aged 7 days

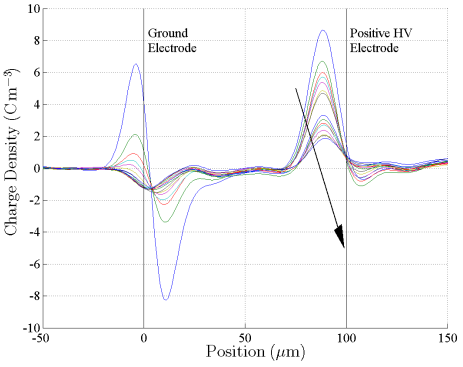

(d) Aged 10 days

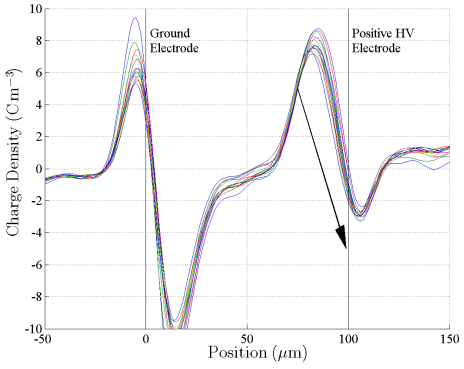

(e) Aged 14 days

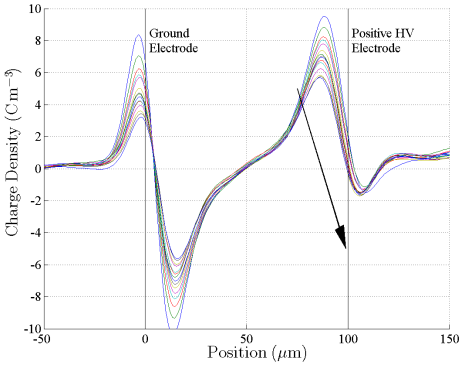

(f) Aged 17 days

FIGURE 4.29: Space charge decay measurements of samples UV aged in air

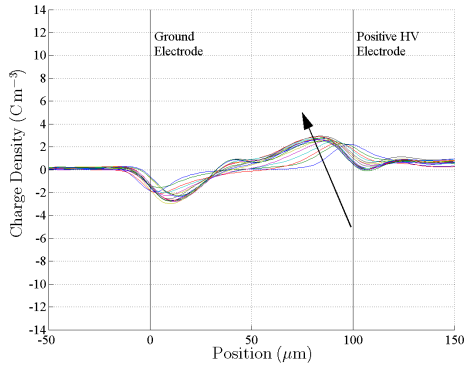

(a) Virgin sample

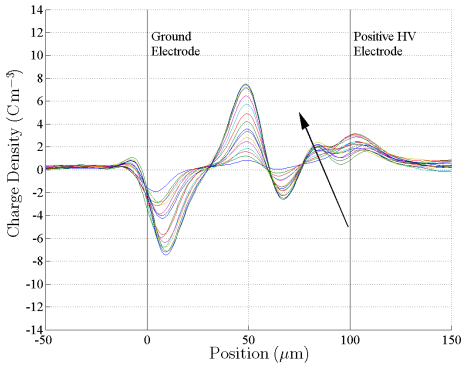

(b) Aged 3 days

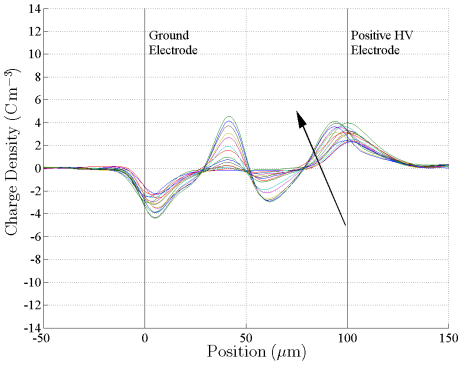

(c) Aged 7 days

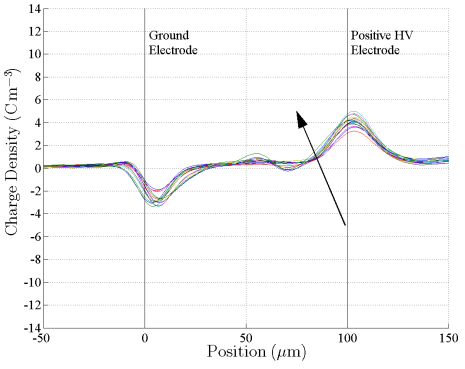

(d) Aged 10 days

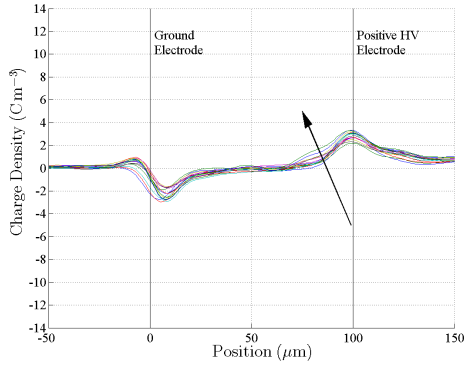

(e) Aged 14 days

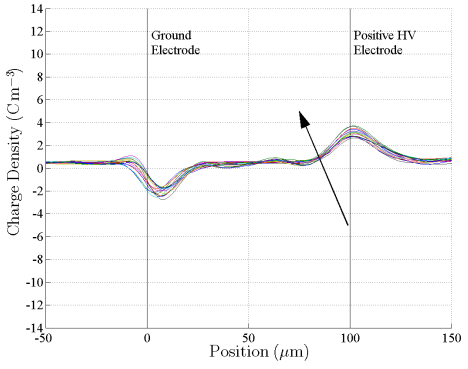

(f) Aged 17 days

FIGURE 4.30: Space charge volts off measurements during polarisation of samples UV aged in nitrogen

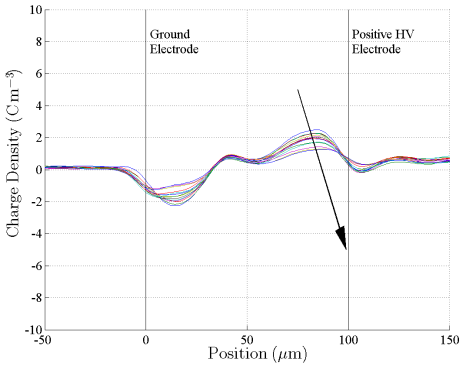

(a) Virgin sample

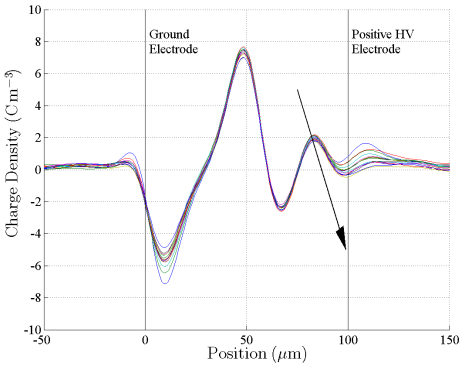

(b) Aged 3 days

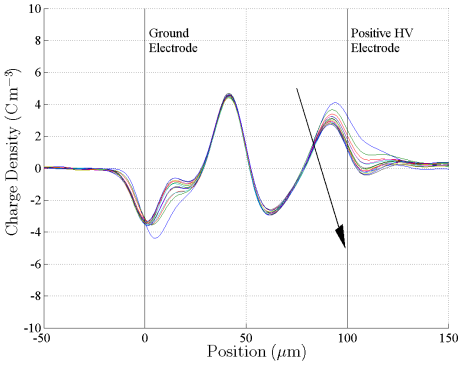

(c) Aged 7 days

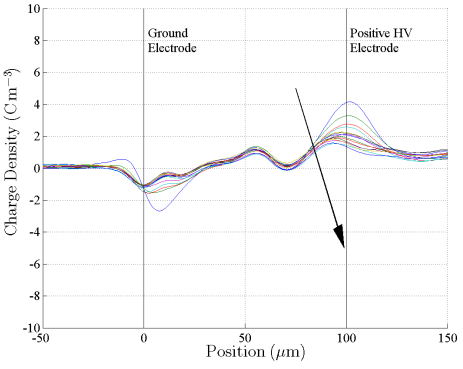

(d) Aged 10 days

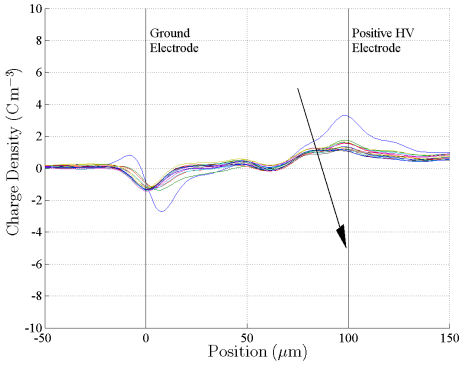

(e) Aged 14 days

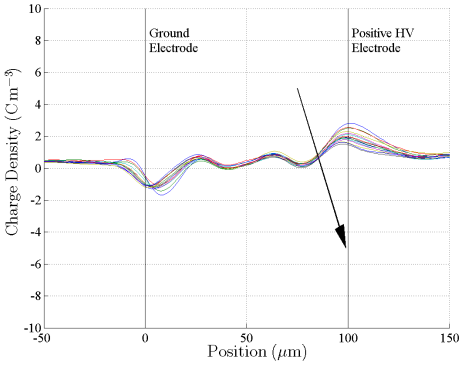

(f) Aged 17 days

FIGURE 4.31: Space charge decay measurements of samples UV aged in nitrogen

The decay of charge from the nitrogen aged samples is shown in figure 4.31. As with air aged samples after 3 days of ageing there is very little decay of charge. In more heavily aged samples there is initially a quick decay of charge and then a constant level is reached. The similar profile seen in air and nitrogen samples aged 3 days could be explained due to oxidation products within the bulk. Oxidation products have been shown by FTIR spectroscopy to occur in nitrogen samples even without the oxygen in the atmosphere. This is thought to occur due to oxygen not being able to be removed during the 10 minute vacuum extraction. Therefore this oxygen remaining within the bulk is likely to be present in both the air and nitrogen aged samples. This suggests that the initial oxidation products will form throughout the bulk of the polymer and explain the similar charge profiles seen in both materials. Another explanation is the process of chain-scission and cross-linking that are likely to occur as a result of photo-irradiation.

4.6.1 Total Charge

Investigating the rate of charge accumulation and decay can give an indication of the energy levels of charge trapping sites [43]. The total charge (total charge (Q)) in the bulk of the polymer at each time interval can be calculated using:

$$Q = \left(\int_0^d |\rho(x)| dx \right) A \tag{4.7}$$

Where $\rho(x)$ is the charge density, A is the area of the electrodes ($\pi \times 0.005^2$ mm^2) and d is the the thickness of the sample (100×10^{-6} m).

The results shown in figure 4.32 compare the charge build up and decay for samples aged in an air environment. In the virgin sample during polarisation the results clearly show a very quick (less than 5 minutes) build up in total charge. The total charge then reduces with continued electrical stressing. The SC profile would suggest this is due to the SC limited injection of charge at the electrodes and the recombination of opposite polarity charge in the polymer bulk. After ageing for 3 days the initial build up of charge is at a similar rate but no longer reaching a steady state. The total charge continues to grow for the full 40 minutes of electrical stressing. After ageing for 7 and 10 days, the sample returns to an initially quick build-up in charge before reaching a constant state, again suggesting some SC limited charge injection affect. With further ageing, a large quantity of charge accumulates within the polymer and continues to grow with stressing time.

The decay of accumulated charge also changes as a result of photo-oxidation. The virgin and 3 days aged sample showing very little decay of accumulated charge. This decay profile relates to high energy (deep) trapping sites and therefore, there is a relatively low probability of releasing trapped charge at room temperature [43]. The samples aged for 7 and 10 days show an initially very quick decay of charge. After 5 minutes of decay most of the charge has relaxed and a very slow decay rate continues. This is associated with the presence of shallow trapping sites that readily release trapped charge [25]. Heavily aged samples of 14 and 17 days show an initially quick charge decay but the rate reduces to a similar trend as the virgin and 3 days aged sample. This suggests a mixture of shallow and deep trapping sites and it is clear from the level of charge reached that a comparatively large quantity of charge trapping sites exist.

The charge accumulation and decay for samples UV aged in a nitrogen atmosphere are shown in figure 4.33. After ageing for 3 days, as with the samples aged in air, the total charge initially increases at a similar rate to the virgin sample. Rather than reaching a steady state this time it continues to increase with stressing duration but at a slower rate. As the ageing time of the samples increases the initially faster rate of charge growth disappears and a slower rate is seen for the entire stressing duration. The rate and quantity of charge accumulation reduces with ageing duration. In heavily aged samples of 14 and 17 days there is significantly reduced charge accumulation compared with the virgin sample.

Investigating the decay of charge there is little change in the rate of decay. In the aged samples most of the accumulated charge remains after field removal. This suggests most of the charge trapping sites produced are higher energy and do not readily release trapped charge.

From analysing both the total charge and SC profiles, it is clear that the effect of photo-irradiation has produced significant changes in the charge trapping properties of LDPE. In the case of the samples aged in air it is known that large quantities of oxidation products form and are expected to be concentrated near the sample surface. The change in total charge and restriction of charge near the electrodes could be due to an increased concentration of charge trapping sites near the electrodes. After short ageing times this creates a SC limited injection situation [41, 200]. With further ageing the concentration of oxidation products becomes so great that charge can easily build up further into the polymer. This reduces the effect of the charge concentration on the local electric field and a greater total charge can develop. The easier injection of charge into the polymer could be

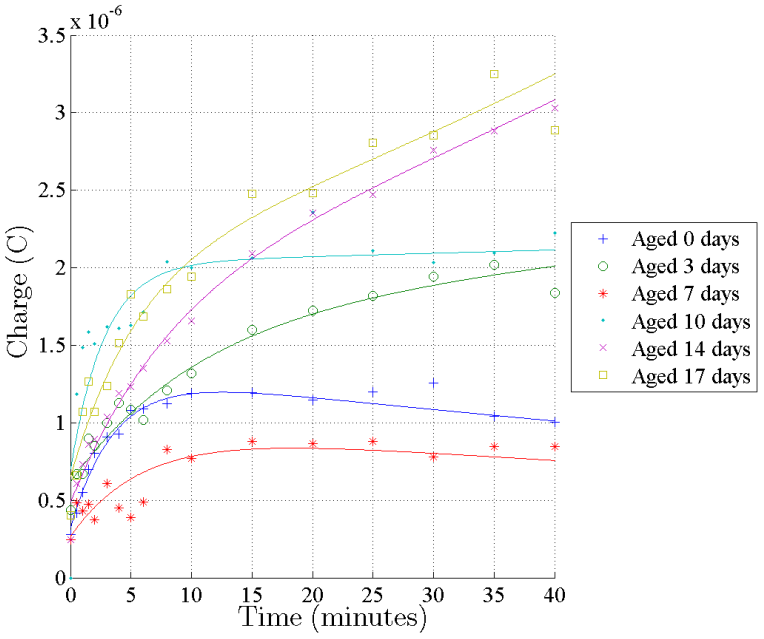

(a) Polarising

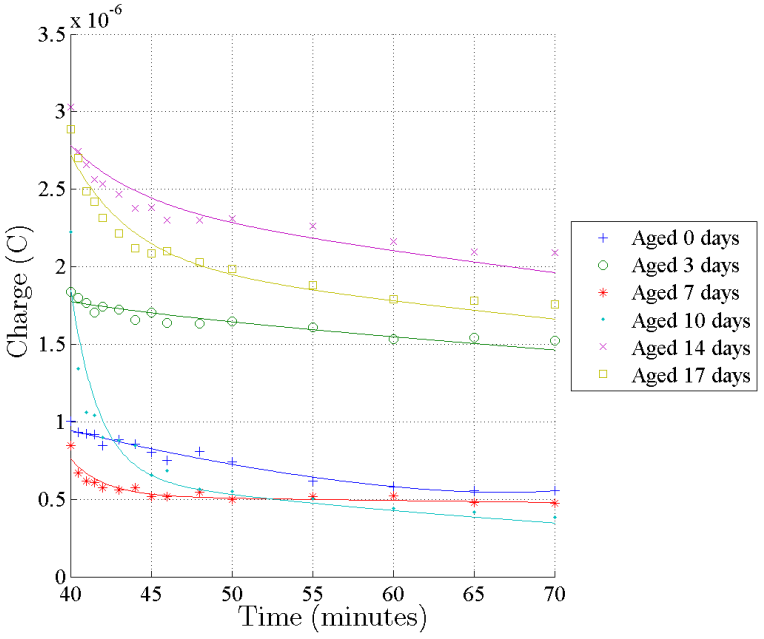

(b) Decay

FIGURE 4.32: Total charge in samples UV aged in air

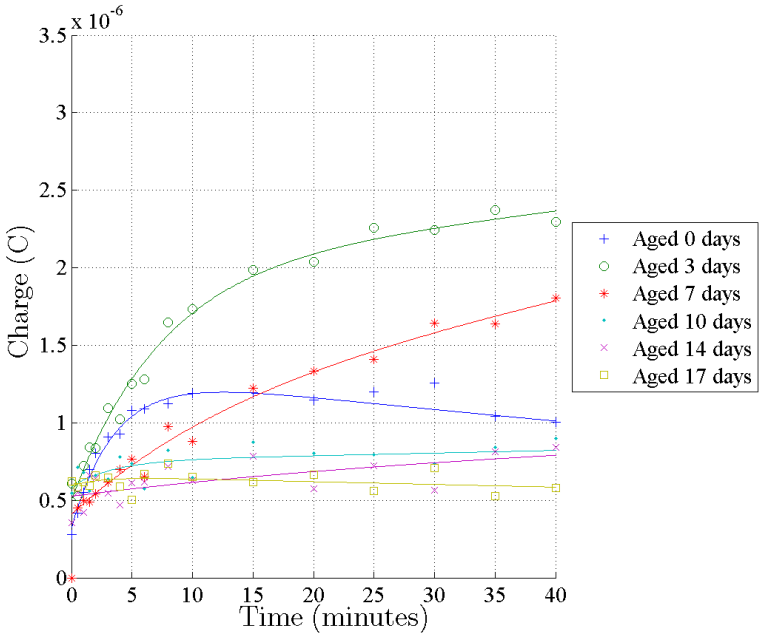

(a) Polarising

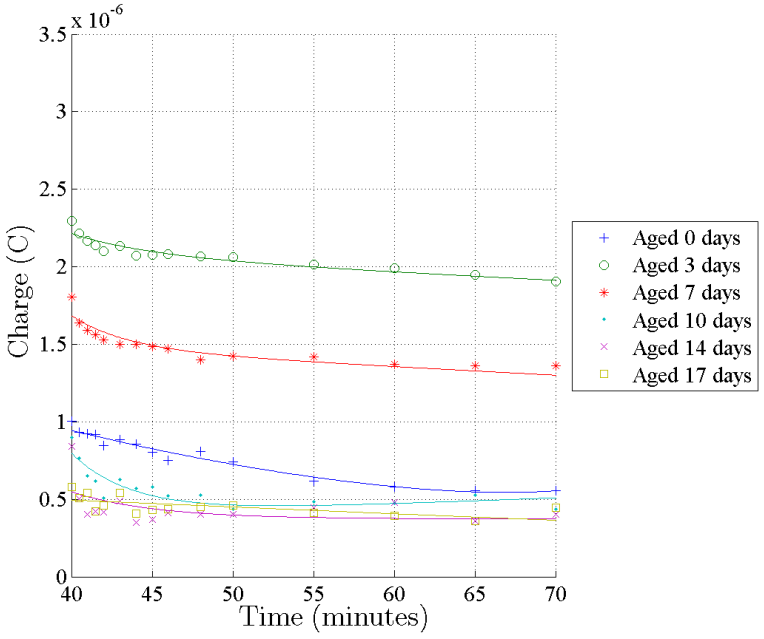

(b) Decay

FIGURE 4.33: Total charge in samples UV aged in nitrogen

due to the increased concentration of shallow trapping sites that seem to result from continued ageing.

The samples aged in a nitrogen environment show a different trend in SC profiles and total charge levels. The trend in results is similar initially to those aged in an air environment. This suggests that small concentrations of oxidation products shown by FTIR spectra may be responsible for the similar behaviour in charge movement. Alternatively, photo-irradiation will also cause other changes in the polarisation and charge decay properties of the polymer. These changes may relate to oxidation products, chain-scission, cross-linking reactions along with the consumption or release of any additives that may have been used during the polymer manufacturer. Due to large changes in charge movement within the bulk of the polymer it can be expected that large changes in charge movement at the electrode-polymer interface must also have occurred. This region is expected to significantly influence the charge injection, trapping and recombination leading to EL emission.

As a result of ageing, the SC measurements have shown significant changes in the accumulation of charge within the polymer. Samples aged for 3 days in air or nitrogen show similar trends with an increase in charge within the bulk of the polymer. Further ageing in air showed the total quantity of charge to increase and become concentrated near the electrodes. The samples aged in nitrogen show a significant reduction in the quantity of charge injected into the polymer. This clearly shows a significant change in the charge trapping properties of the polymer as a result of ageing. New charge trapping sites could be caused by a range of chemical changes as a result of the photo-irradiation. These include oxidation products, chain-scission, cross-linking and vinyl groups. The affect these have on the movement of charge in the polymer can therefore be expected to alter typical EL emission.

4.7 Electroluminescence

As discussed in section 2.5, EL under ac fields is thought to have the potential to investigate change in charge movement very near the electrode-polymer interface. The previous sections have detailed changes in oxidation products, cross-linking, dielectric properties and space charge, all expected to influence the charge movement at the interface. This section investigates changes in EL behaviour as a result of ageing with the aim of improving the understanding of the affect these changes have on EL phenomena.

As mentioned previously (section 3.6.5) all quantitative measurements are only taken on results delivering a good EL image with no bright spots. An example of a good image is shown in figure 4.34 and images for all ageing duration can be found in appendix C.

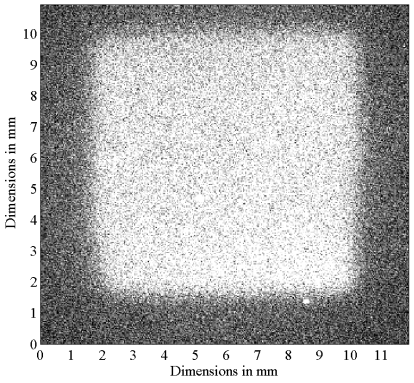

FIGURE 4.34: Electroluminescence image from a LDPE sample UV aged 3 days, stressed at 40 $kV_{rms}\,mm^{-1}$

4.7.1 Electroluminescence intensity

The results presented in figure 4.35 compare the EL intensity for samples UV aged in air as the applied field is increased. Measurements were collected using the same method as shown in section 3.7.1 for the virgin samples. The emission is accumulated on the CCD for 5 seconds and repeated 20 times for each field level, the mean and range are presented here. The aged samples show the same correlation of an increase in intensity with increases in the applied field. However, the intensity at each field level does change as a result of the ageing duration. After ageing for only 3 and 7 days there is a significant increase in intensity compared with the virgin samples. After 10 days of ageing the intensity is approximately equal to that of the virgin sample. Further ageing of 14 and 17 days and the EL intensity reduces below the virgin sample at all field levels. If the intensity at 60 $kV_{rms}\,mm^{-1}$ is considered then after 3 days the intensity has increased by more than 150 % above the background level of the virgin sample. After 7 days this increase has reduced to 120 % and only 10 % after 10 days compared with the virgin sample. Ageing for 14 and 17 days and the emission under a field of 60 $kV_{rms}\,mm^{-1}$ has reduced by 20 and 50 % respectively. This trend in EL intensity with ageing suggests that initially there is significantly increased charge recombination that reduces with further ageing.

The samples aged in a nitrogen environment have a reduced increase in oxidation products, thought to play a key role in charge trapping. Figure 4.36 shows the EL intensity measurements collected for samples UV aged in a nitrogen atmosphere. The EL intensity results show a completely different trend in behaviour with ageing time. The total EL intensity varies very little, with changes rarely greater than the range in measurement error of approximately 10 %. This lack of change with intensity suggests the oxidation products present in the air aged samples are the dominant factor effecting EL intensity.

4.7.2 Point on Wave Electroluminescence

To further investigate changes in EL as a result of ageing this section describes POW measurements to investigate changes in the phase difference as a result of ageing. As shown in the virgin results (figure 3.23) the peak of the EL is expected to lead the applied field by a phase difference of approximately 35^o. This phase difference is thought to be created due to the build up of trapped charge near the electrode-polymer interface, causing an enhancement of the local electric field. Changes in the quantity and location of charge should influence changes in the phase difference of the EL emission.

The measurements were collected over the same 40 to 90 $kV_{pk}\,mm^{-1}$ in 10 $kV\,mm^{-1}$ increments as detailed in the methodology (section 3.6.6). Due to the reduced intensity of heavily aged samples, measurements could only be compared with fields greater than 60 $kV_{pk}\,mm^{-1}$. The same filter method was used as for virgin samples to allow clear comparison between different samples. Figure 4.37 shows the POW EL for samples aged in air stressed at 70 $kV_{pk}\,mm^{-1}$. The results show the same shape in EL emission as for virgin samples and the same trend in peak intensity as seen in the previous section. The relative change in intensity is altered due to the noisier measurement and also increased background level, for this reason intensity measurements were completed separately (figure 4.35). There is clearly a shift in the phase angle of the peak EL emission as a result of UV ageing in air.

As with the virgin results changes in the phase difference are taken as the difference between the peak of the applied field and the peak of the EL for each half cycle. As with virgin materials, with a sinusoidal applied field the phase difference is always positive (the EL peak occurs before the applied field), but as ageing time increases the phase difference reduces. The phase difference is compared in figure 4.38 for the aged samples at field stresses of 60, 70, 80 and 90 $kV_{pk}mm^{-1}$. The

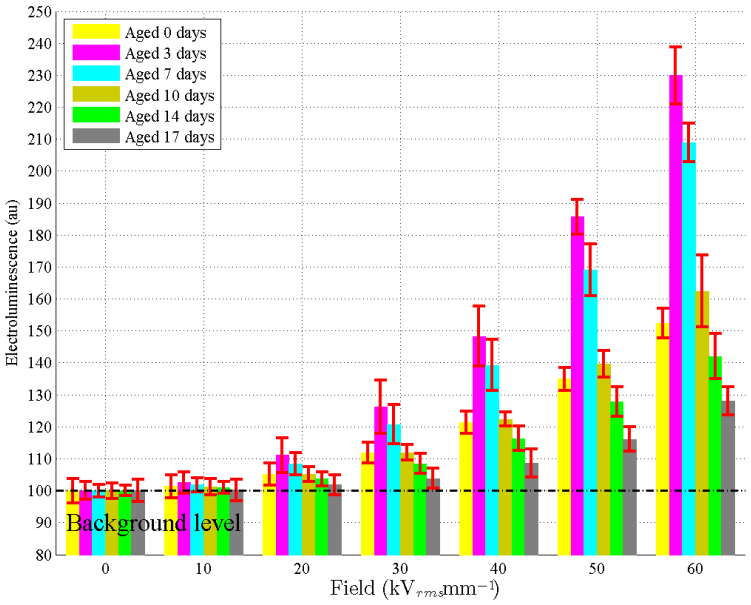

FIGURE 4.35: Electroluminescence intensity for samples UV aged in air

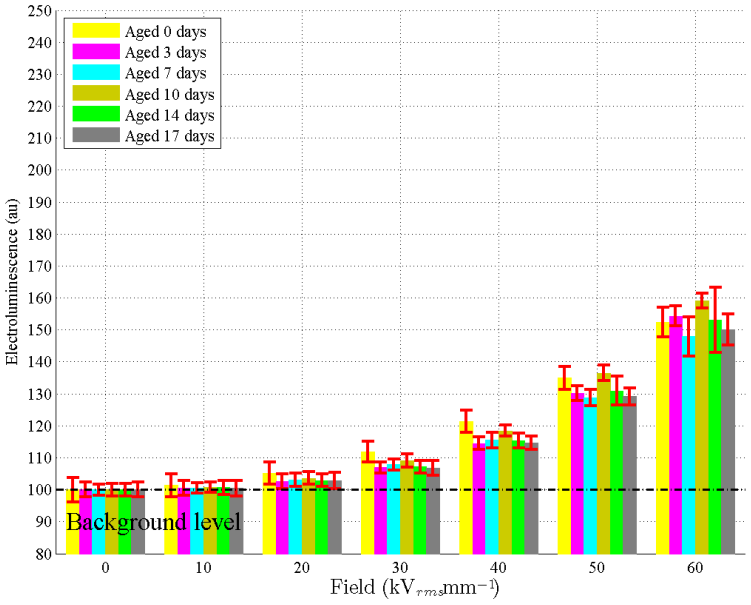

FIGURE 4.36: Electroluminescence intensity of samples UV aged in nitrogen

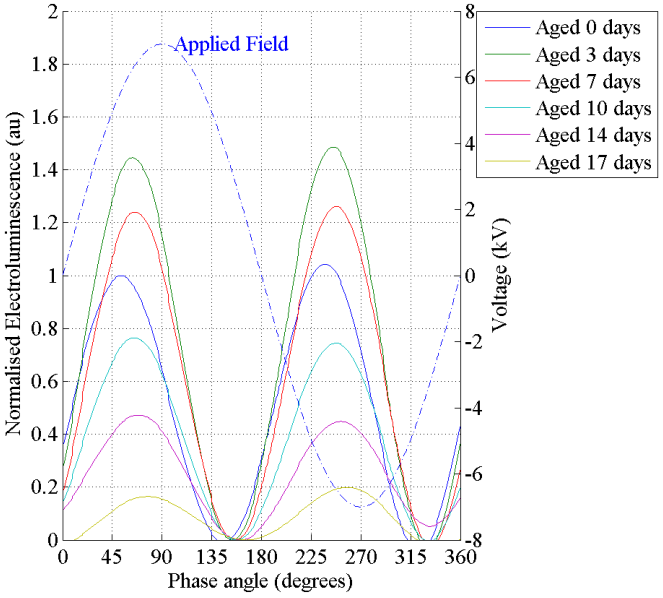

FIGURE 4.37: Point on wave electroluminescence at 70 $kV_{pk}\,mm^{-1}$ for samples UV aged in air

mean phase difference of 3 samples and error bars showing the range in measured value are presented.

From comparison with the virgin result it can be seen that there is a slight increase in the phase difference as the applied field is increased and this has often been reported in the literature (section 2.5.3). At the 60 $kV_{pk}\,mm^{-1}$ measurement there is clearly a reduction in the phase difference as the ageing duration increases, reducing by approximately 10 degrees over the 17 days. The phase difference reduces slightly after 3 days of ageing and then remains approximately constant from 7 to 17 days of ageing. If the relationship with field is considered it can be seen that the samples aged 3 and 7 days still maintain a slight increase in the phase difference with the applied field. However, further ageing and this phase shift does not occur and the 17 days aged sample shows the reverse relationship with the phase difference reducing at higher fields. This shift in the phase difference suggests that in aged samples the charge trapped near the electrode-polymer interface is having less influence on the local electric field, the possible reasons for this are detailed in chapter 5.

The POW EL data for samples aged in a nitrogen atmosphere are presented in figure 4.39. As before the samples were stressed under a 70 $kV_{pk}\,mm^{-1}$ field. The results support the reduced change in intensity seen previously, but still show significant changes in the phase angle of the peak EL emission. The larger range

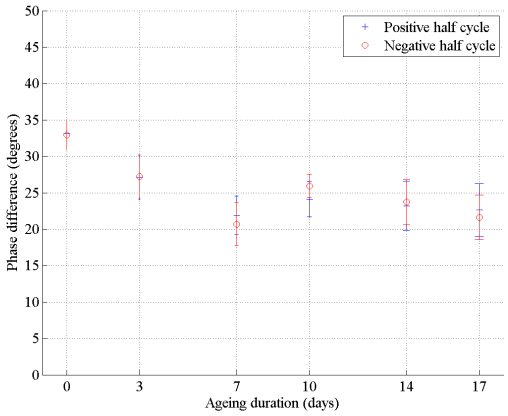

(a) 60 $kV_{pk}\,mm^{-1}$

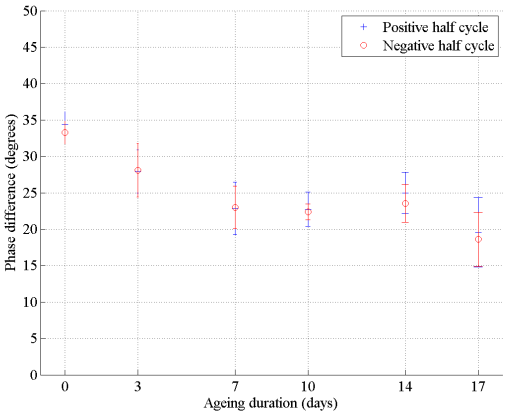

(b) 70 $kV_{pk}\,mm^{-1}$

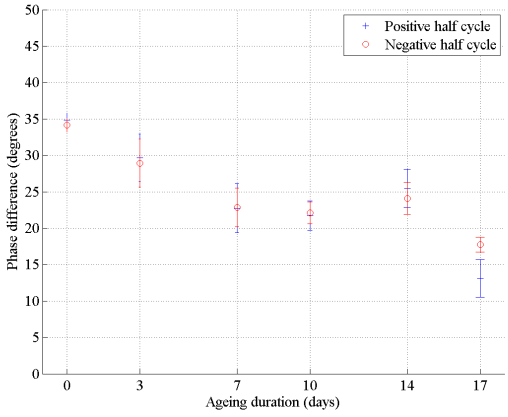

(c) 80 $kV_{pk}\,mm^{-1}$

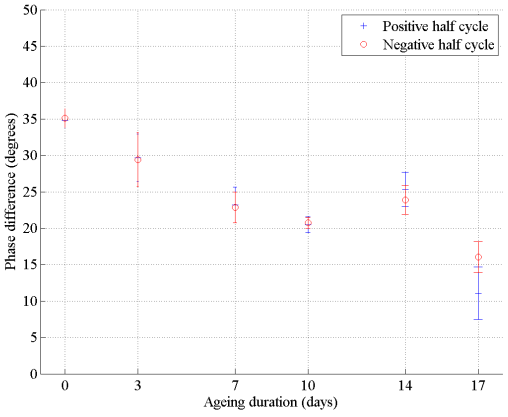

(d) 90 $kV_{pk}\,mm^{-1}$

FIGURE 4.38: Phase difference between peak electroluminescence and peak of applied field for samples UV aged in air

in peak intensities is thought to be due to the noiser POW measurements, rather than changes in the EL intensity.

The phase difference of 3 samples for each ageing condition is shown in figure 4.40, covering the field range of 60 to 90 $kV_{pk}\,mm^{-1}$. In the case of the nitrogen aged samples the change in phase difference is greater than that seen for samples aged in air, shifting by approximately 15^o. In the case of the nitrogen aged samples the shift is approximately the same for all ageing durations. The same behaviour with field seems to be apparent as with the samples aged in air. At the shorter ageing durations (3, 7 and 10 days) there is a small correlation between the phase

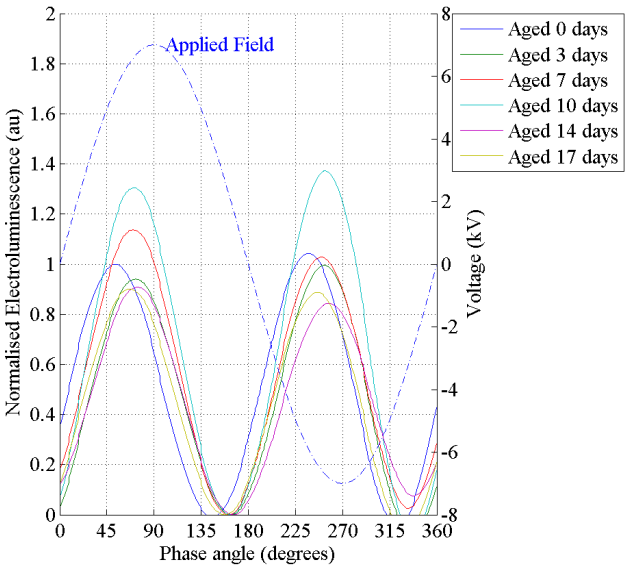

FIGURE 4.39: Point on wave electroluminescence at 70 $kV_{pk}\,mm^{-1}$ for samples UV aged in nitrogen

difference and the applied field. Ageing at 17 days shows a negative correlation but the shift is not as extreme as in the air aged samples.

The samples aged in a nitrogen atmosphere show very little change in intensity. However, they do show a significant change in the phase difference. This suggests the mechanisms controlling these behaviours are not directly linked. A change in intensity is closely related to the amount of charge recombination. The phase difference relates to the ability of charge to cross the electrode-polymer interface due to the energy barrier and therefore the local electric field.

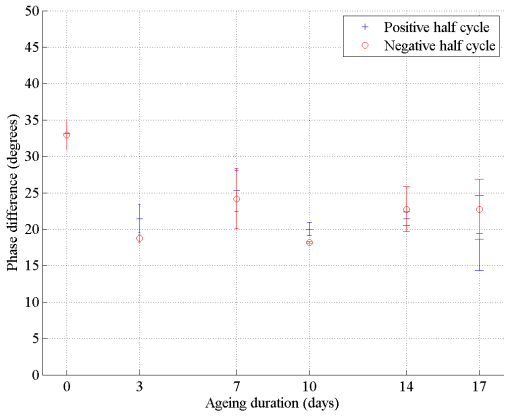

(a) 60 kV_{pk} mm^{-1}

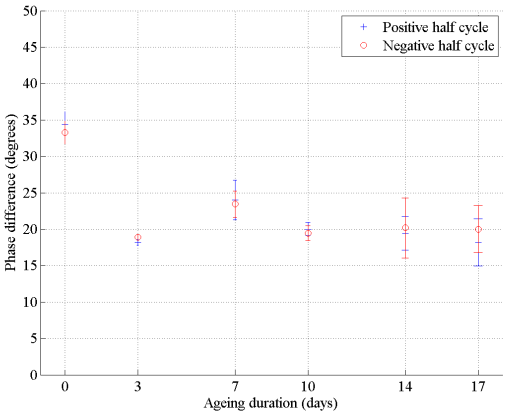

(b) 70 kV_{pk} mm^{-1}

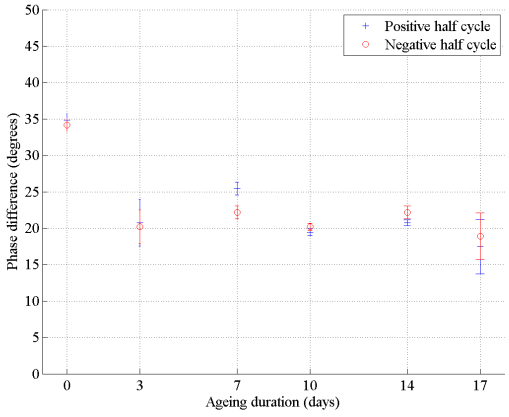

(c) 80 kV_{pk} mm^{-1}

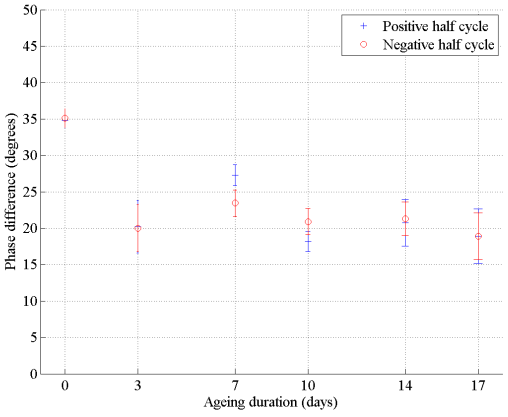

(d) 90 kV_{pk} mm^{-1}

FIGURE 4.40: Phase difference between peak electroluminescence and peak of applied field for samples UV aged in nitrogen

4.8 Summary of Results

This chapter has presented results showing changes in LDPE samples as a result of UV ageing in air and nitrogen environments. The changes were investigated in terms of optical and chemical properties initially to then interpret changes in charge trapping properties and movement.

UV-Vis spectroscopy results show very little change in the optical transparency of samples aged in air or nitrogen environements at the wavelengths of relevance to EL. Therefore any change in EL could be related to changes in charge movement as a result of ageing. The UV-Vis measurements did show an increased absorption

around the UV excitation wavelength (253.7 nm), particularly for samples aged in air. This increased absorption is thought to be due to the photo-oxidation reactions and may lead to the auto-acceleration of the photo-irradiation process.

Analysis of the IR spectra allowed changes in oxidation products to be identified. The results showed a significant increase in carbonyl and hydroxyl groups for samples aged in air and a slight increase for samples aged in nitrogen. The slight increase in nitrogen is thought to be due to oxygen that is not fully removed from the sample during degassing and also may explain the slight increase in UV absorption. The concentration of carbonyl groups followed a time squared increase and hydroxyl groups increase proportionally with ageing duration. The FTIR spectra and knowledge of the photo-oxidaiton processes suggests ketones, aldehydes and carboxylic acids are the most likely carbonyl products along with alcohols and carboxylic acids for hydroxyl groups. These carbonyl and hydroxyl groups have often been discussed in literature as chemical (deep) trapping sites and so a change in the movement of charge for samples aged in air and nitrogen is expected.

As well as photo-oxidation products, exposure of LDPE to UV radiation is expected to cause the photo-crosslinking of the polymer. Investigation into the cross-linking of the polymer aged in air showed a significant initial increase and then gradual reduction in the percentage of the sample cross-linked. Samples aged in a nitrogen environment showed a more gradual increase but with a maximum limit greater than those aged in air. This higher level is thought to be due to the lack of competition between photo-crosslinking and photo-oxidation reactions and the slower cross-linking rate to be due to the additional UV absorption of the quartz ageing vessel.

Analysis of the electrical strength of the polymer as a result of ageing in air shows a reduction in the breakdown strength with ageing duration. Analysing the results using the 2-parameter Weibull distribution showed an increase in the spread of the data (the β value) suggesting a change in the dominant failure mechanism [27]. The samples aged in a nitrogen environment show an increase in the dielectric strength as a result of UV ageing. This suggests the reduction in dielectric strength is due to the presence of oxidation products whereas the increased cross-linking of the nitrogen aged sample increases its breakdown strength.

Investigating changes in the dielectric relaxation of the polymer as a result of ageing has shown a range of changes. Comparing the $\epsilon^{'}$ of samples aged in air and nitrogen environments showed increases in both cases, but the increase being

greater for the samples aged in air. The increase occurred continuously with ageing but may have reached a maximum between 14 and 17 days of ageing. The $\tan\delta$ of the materials was also investigated with ageing duration. Increases in $\tan\delta$ represent an increase in energy loss during polarisation of the material. Samples aged in an air environment show an increasing growth in $\tan\delta$ with ageing duration, creating a significantly more lossy material after 17 days of ageing. The samples aged in a nitrogen environment also show a smaller increase over the 17 day ageing duration.

Space charge measurements completed using the PEA method allowed any changes in charge trapping properties to be identified as a result of ageing. In the case of the air and nitrogen aged samples the accumulation after 3 days of ageing seems very similar. Results show an increase in the quantity of charge in the bulk and very slow charge decay. This suggests that initially similar processes occur in both environments, such as the formation of oxidation products, though at too low a level to be detectable by FTIR. Further ageing and the accumulation of charge within the polymer differs significantly. In the air aged samples the charging rate reduces and the total charge accumulation increases but remains near to the electrodes. In the nitrogen aged samples less charge accumulates within the polymer and the rate of charge decay remains similar as ageing time increases. Analysis of the SC rate of charge decay in the air aged samples suggests initially a large quantity of higher energy trapping sites. As the ageing duration increases the rate of charge decay increases, suggesting an increase of lower energy trapping sites. In the nitrogen aged samples there was very little change in the rate of charge decay.

EL is thought to be very sensitive to changes in charge movement near the electrode-polymer interface and therefore the changes in charge trapping as a result of photo-oxidation and photo-crosslinking should have a significant effect. Samples aged in air for a few days showed an increase in intensity, further ageing and the EL intensity was reduced to much lower levels. The samples aged in a nitrogen environment showed negligible change in intensity as a result of UV ageing. Investigating the POW data as a result of UV ageing in air showed the gradual reduction in phase difference for 3 and 7 days ageing and then remaining roughly constant with further ageing. The samples aged in nitrogen showed a significant reduction after just 3 days of UV ageing that remained constant for the rest of the ageing durations. The samples aged in air had a change in phase degrees of approximately 10^o over the 17 days, the nitrogen samples showed a reduction of approximately 15^o. The very different behaviour seen in intensity measurements

but similar trends in phase difference for samples aged in air and nitrogen suggests two different underlying mechanisms. The EL intensity is assumed to relate closely with changes in the charge trapping sites and therefore availability for charge recombination. The phase difference will relate to the local electric field required for charge to overcome an injection barrier at the electrode-polymer interface.

All these results have shown EL to be significantly affected by the photo-oxidation and photo-irradiation processes. The following chapter will analyse and correlate the different results to explain changes in the charge movement. From this analysis a model that simulates EL behaviour has been further adapted to account for the affects of ageing.

Chapter 5

Discussion of Experimental Results and Simulation Studies of Electroluminescence

The previous chapter showed that the UV ageing of LDPE in both air and nitrogen environments resulted in changes in terms of both the intensity and the phase difference of the EL emission. This indicates its potential use as a tool to detect ageing processes within electrical insulation. This chapter analyses the results, using the changes in optical, chemical and electrical properties of the polymer to understand possible causes of the measured changes in EL. Using measurable data from these results the changes in the EL have been simulated using the bipolar charge recombination model proposed by Ariffin and Lewin [19].

Analysing the behaviour of EL with regard to different ageing environments shows the changes in intensity to be most affected by ageing in air. The phase difference however, shifts significantly after ageing in both air and nitrogen environments. Ageing in air revealed that the intensity initially increases significantly and then with further ageing the total intensity reduces to below that of the virgin sample. The samples aged in a nitrogen environment showed little change in intensity as a result of ageing.

A similar trend in EL intensity for the air aged samples has been shown in literature as a result of the UV ageing of PP [123]. Though the ageing duration of the PP was significantly shorter at less than 4 hours. The PP contained anti-oxidant and the consumption of this was used to explain the initial increase. Anti-oxidant was thought to originally have trapped injected charge. After its consumption

by oxidation reactions the charge was instead able to contribute towards the EL reactions [172]. The LDPE material used in this experiment is listed as additive free in the suppliers datasheet [129]. However, it is possible that antioxidant may have been required and remained from the production of the films. Since the presence and type of antioxidant is unknown it is difficult to investigate the IR spectra. As the ageing time increases there is no reduction in the IR at any wavenumber, as would be expected due to the consumption of an antioxidant [201]. Also, since the samples aged in a nitrogen environment do show a small increase in oxidation products the same consumption of any antioxidant would be expected. However, the EL for samples aged in nitrogen show no increase in intensity suggesting if any antioxidant is present it is not the explanation for the increased intensity. This suggests the differences in emission intensity relates to the formation or removal of charge trapping sites under the different ageing environments.

5.1 Oxidation Products

The exposure of LDPE to UV radiation results in the formation of typical oxidation products and cross-links. The chemical reactions leading to their formation were described previously (section 2.3). The most dominant reaction is dependent on the ageing environment and it is seen that oxidation products are greatest in air and cross-linking reactions greatest in nitrogen.

As expected, the IR spectra shows that the samples aged in an air environment have a much greater increase in oxidation products, such as carbonyl and hydroxyl groups, than those aged in nitrogen. The samples aged in nitrogen were not expected to show any increase in the concentration of oxidation products but a small increase was seen. This small increase may be due to some oxygen remaining in the bulk of the sample during degassing, particularly since there seemed to be little correlation with ageing duration. Any differences are likely to be due to slight differences in vacuum quality and ageing duration.

The UV-Vis spectra showed that virgin LDPE is more than 70% transparent at the excitation wavelength and so the entire bulk of the polymer is exposed to the UV radiation. However, the formation of oxidation products are expected to be limited by the diffusion of oxygen into the polymer [75]. Gulmine *et al.* [56] has suggested an exponential decay model for the carbonyl group concentation through LDPE as a result of UV ageing (300 nm irradiation). Experimental results to support the model suggest a 45% reduction in attenuated total reflectance (ATR) FTIR

absorbtion spectra due to carbonyl groups within the first 1 μm and a reduction of 85% within 10 μm. Some of the oxygen will already have been present within the samples, as is shown by the oxidation products for samples aged in nitrogen. This will initially produce oxidation products throughout the bulk of the polymer and supports the similar PEA SC profiles for samples aged in air or nitrogen environments for 3 days.

Although there is an increased absorption of UV radiation by the oxidation products the PL measurements showed a reduced fluorescence. This suggests a difference in the excitation and relaxation mechanisms. The relaxation after excitation by UV absorption may potentially be through non-radiative pathways as opposed to the radiative pathways resulting in fluorescence. This could explain the reduced EL intensity as a result of ageing for both air and nitrogen environments. However, EL emission is believed to relate more closely with the triplet ($T_{1,2,3}$) relaxation pathways of phosphorescence rather than fluorescence [21]. Laurent [99] has suggested a similar observation to explain increased EL in PP. An increase in luminescent centres is suggested to explain the increased EL, eventually the quantity increasing to the point where they quench the emission. To explain the differences between air and nitrogen samples the possible location of new recombination centres as a result of oxidation reactions has to be considered. The increased EL in samples aged in air could be as a result of new recombination centres near the sample surface. The lack of change for samples aged in nitrogen may be due to oxidation reactions that are more likely to take place within the polymer bulk. The reduction in EL intensity seen in air aged samples is then due to the increasing quantity of carbonyl groups such that they quench the emission due to increased non-radiative relaxations from excited states. This explanation alone though does not give any explanation for the phase shift of the EL intensity peak seen in the POW EL measurements.

The photo-irradiated samples also show an increase in $\tan\delta$ (the dielectric loss tangent) with ageing time, the greatest increase being for samples aged in air. The comparison presented in figure 5.1 compares the changes in carbonyl groups with changes in the $\tan\delta$ loss measurements. The time squared trend for carbonyl groups is included for reference. The trend for the nitrogen samples is set constant at the level of the virgin sample. There is clearly a correlation between $\tan\delta$ and the carbonyl concentration for samples aged in air, both increasing with a similar relationship. Similarly the samples aged in a nitrogen environment showed an increase in $\tan\delta$ at the ageing durations where an increase in carbonyl groups was also detected.

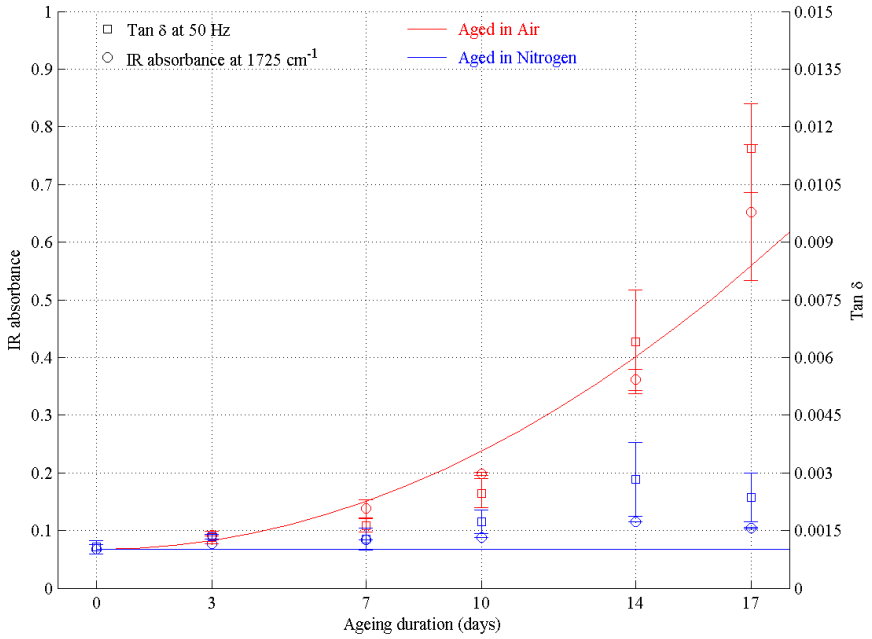

FIGURE 5.1: Comparison between IR absorption at 1725 cm^{-1} and tan δ with ageing duration

An explanation for the increase in tan δ with increased numbers of carbonyl groups relates to their polar nature. The addition of polar groups into the PE structure can introduce dipole moments and therefore increased charge movement [26]. Other reported research has also supported this suggestion, showing a correlation between oxidation products and tan δ [55, 74, 202, 203]. Various polymeric materials have had their carbonyl group concentration increased by different oxidation processes and all show an increase in tan δ measurements.

5.2 Wavelength of Electroluminescence

One aspect of the EL emission that could not be measured was the wavelength of the emission. Due to the very low emission levels from LDPE, the systems for measuring the wavelength at the TDHVL and the LAPLACE were not sensitive enough to measure the virgin material. The ability to investigate this could provide valuable information into the changes in the excitation centres responsible for the EL emission, particularly to clarify the initial increase seen for short ageing durations. A shift in the ratios between different wavelengths of the emission is expected if the addition of different energy trapping sites are responsible for the changes in measured EL.

A shift in the wavelength of the emission may cause an apparent change in the EL intensity due to the optical transparency of the detection system. An approximation of the wavelength shift needed is shown in figure 5.2. The approximation assumes the shape of the spectral emission remains the same and the entire spectrum shifts in one direction or the other, this is unlikely and there is more likely to be a change at specific wavelengths. The typical spectrum for LDPE at 60 $kV_{rms}\,mm^{-1}$ of Ariffin *et al.* [204] was used. The quantum efficiency of the CCD window [154], fused quartz lens [205] and window of the vacuum chamber [133] were all accounted for.

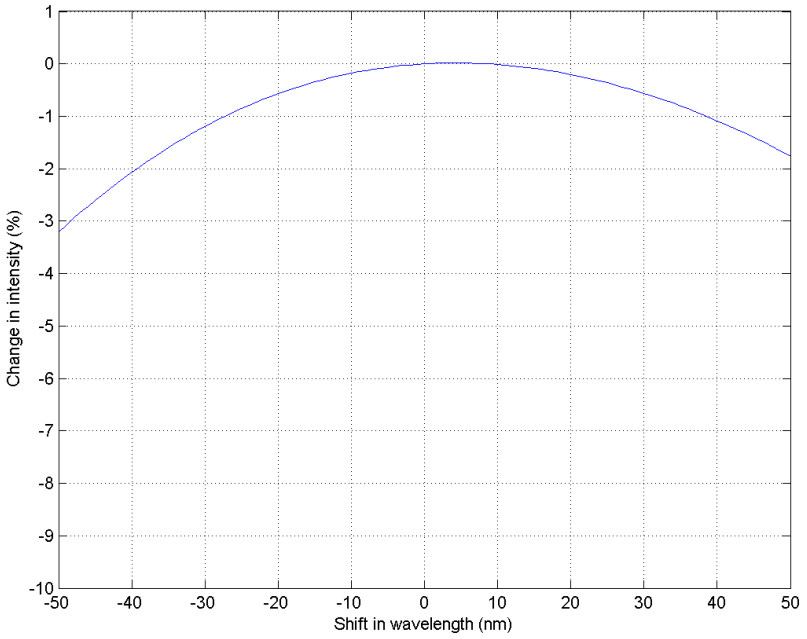

FIGURE 5.2: An approximation of the wavelength shift required to increase or reduce the electroluminescence intensity

The results suggest that any significant change in the wavelength would result in a reduction in measured EL intensity by the CCD. There is a very slight increase of less than 0.2% if the emission shifts 10 nm to longer wavelengths. However, even with a large 50 nm shift the intensity only drops between 2 and 3% whereas the measured change in intensity is always greater than 10% (figure 4.35). This approximation indicates that due to the relatively flat quantum efficiency of the optical system, a large change in wavelength is required. This suggests that although new recombination centres may change the wavelength of the emission, this change in wavelength cannot be the only explanation for the observed reduction in EL intensity.

5.3 Modelling Changes in Electroluminescence

The experimental results showed changes in the EL as a result of photo-irradiation in air and nitrogen environments. In order to interpret changes in the charge movement as a result of ageing, a model has been adapted to investigate the effect of changing physical parameters on EL emission.

Work has previously been reported on simulating EL emission in an effort to further understand the underlying mechanisms. An initial method by Alison *et al.* [111] simulated EL under an ac stress in epoxy resin from a pin-plane arrangement. The model assumed a fixed concentric space charge region near the injecting (pin) electrode. The EL emitted was assumed to be due to the injection, trapping and recombination of charge carriers within this region (bipolar charge recombination). Further developments to this model by Ariffin and Lewin [19] simulated EL due to a uniform field arrangement in PE based materials. Their model assumed a fixed SC region very near the injecting electrode in which a uniform distribution of charge is able to recombine. Very recent developments by Baudoin *et al.* [23] have accounted for the transport of charge into the polymer, resulting in a time varying SC region.

Although ac and dc EL are both thought to relate to bipolar charge recombination, the physical location of the recombination being the differing factor, models are unable to consistently simulate both. A model by Le Roy *et al.* [206] simulating the transport of charge has shown a good agreement with measured data for EL due to a dc field. The same model and parameters however, did not fit with the experimental data when subjected to an ac field. The shape and phase difference between the applied field and EL being found to be completely different. This is thought to be due to a lack of simulated charge build up in a space charge region near the injecting electrode. This accumulation of charge near the electrode-polymer interface produces a significant alteration in the local electric field seen in the other models that is responsible for the phase shift in the EL emission.

The two most recent models by Ariffin and Lewin [19] (model 1) and Baudoin *et al.* [23] (model 2) both simulate charge injection using the same approximation for injection current density by Hare *et al.* [207]. EL is also assumed to be a result of the recombination of trapped charge with an opposite polarity free charge carrier. The models do differ in their approximation of the space charge region. Model 1 simplifies the charge distribution as a uniform SC region (X) over a depth of 10 nm from the electrode-polymer interface (figure 5.3(a)). The SC region is assumed to

be constant for all durations, fields, waveforms and frequencies [19]. Model 2 uses an exponential distribution of charge trapping energies (figure 5.3(b)) and accounts for the transport of charge by defining the resultant charge mobility (μ) [23, 98], such that;

$$\mu = \frac{2vd}{E} \exp\left(-\frac{\Delta_f}{kT}\right) \sinh\left(\frac{eEd}{2kT}\right) \tag{5.1}$$

Where v is the attempt to jump frequency, d is the average distance between traps, E is the electric field, Δ_f is the upper filled level of traps, k is the Boltzmann constant (8.617×10^{-5} eV K^{-1}), T is the temperature, e is the elementary charge (1.602×10^{-19} C). This allows the penetration depth of injected charge to vary and therefore the SC region to change as a result of the applied waveform.

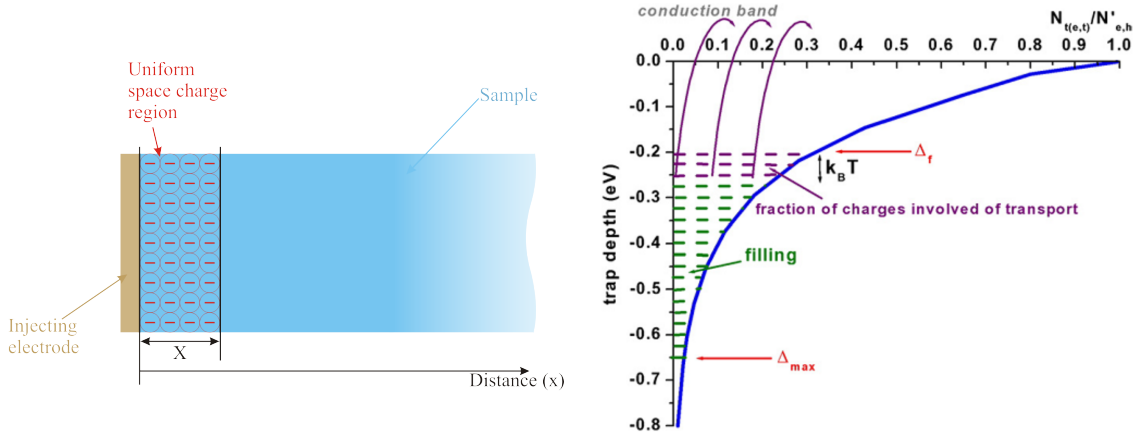

(a) Uniform space charge region (model 1)

(b) Exponential distribution of trapping energies (model 2) [23]

FIGURE 5.3: Differing charge distributions for model 1 and model 2

Analysis of the charge penetration depth in model 2 shows the presence of charge (with charge density greater than 1 C m^{-3}) up to 6 nm from the injecting electrode for a 50 Hz, 60 kV$_{pk}$ mm^{-1}, sinusoidal applied field [98]. This is smaller than the 10 nm uniform SC distribution assumed by model 1 but of a similar magnitude. Very recently it has also been suggested by model 2 that more than 95 % of the EL originates from charge recombination less than 1 nm from the injecting electrode [208]. The problem both of these models have is the exceedingly high charge density they predict to be present in these SC regions. Model 1 suggests peak charge densities in the order of 10^6 C m^{-3} and model 2 suggests levels of 10^5 C m^{-3} [23]. Measured levels of charge density using the PEA technique under

ac or dc have suggested peak charge densities near the electrodes in the order of 10^1 C m^{-3} [94, 209]. However, it must also be understood that SC measurement techniques, such as PEA, average over much larger regions than the EL is thought to originate from. The SC regions of the models are up to 3 orders of magnitude smaller than even high resolution PEA systems [210]. The high quantities of charge are required by the models to alter the local electric field at the injecting electrode thought to explain the phase differences seen in measured EL. However the charge levels are impossibly high such that significant material degradation would result.

Both models have shown a good fit with various experimentally collected data sets. Model 1 has been compared with measurements for various field strengths [19], differing frequencies [22], different waveforms and waveform symmetry [47]. Model 2 has shown good agreement with model 1 and measured data at increasing fields and different waveforms [23, 98] along with investigations at different dc offsets [208] and frequencies [211]. Neither model has looked at simulating change in EL due to different material properties, either as a result of ageing or the use of different materials.

Model 2 has a significant computational cost for the benefit of a more thorough simulation of the charge movement through the space charge region [98]. A comparison in simulated EL from both models with experimental measurements of EL are shown in figure 5.4. Due to the inability to translate the output from the EMCCD camera into photon quantity, both the models and measured data are normalised to the magnitude of their associated peak in the first half cycle. The simulated data from both models closely fits the shape and phase difference of the measured data. There is a deviation as the measured data reduces to zero, the models suggest EL does not fully reduce to zero during each cycle of the applied field. This cannot currently be confirmed experimentally due to the EL levels reducing below the noise level of the detection system.

Since both models produce a very good fit with experimental data either is suitable for use in this work. Due to the significant computation time of model 2 along with no improvement on the resultant simulation, model 1 was used. A simulation using model 2 takes more than 8 hours compared with only 2 minutes in model 1. The following sections will briefly describe the model and various developments allowing it to simulate EL as a result of ageing. The model was coded and executed using the numerical computing environment, MATLAB® and the relevant simulation code is included in appendix D.

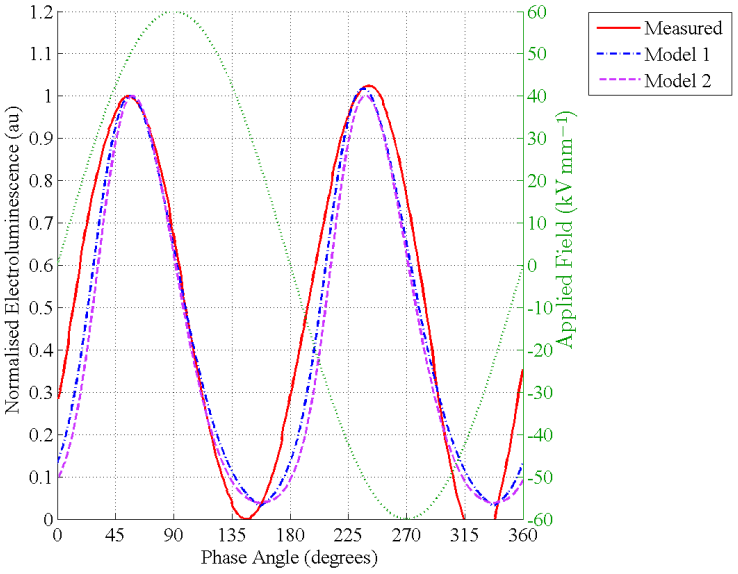

FIGURE 5.4: Model 1 and model 2 compared with measured electroluminescence

5.3.1 Description of Electroluminescence Model

The model used in this work develops upon that proposed by Ariffin [47]. This model has been fully described in literature and so only a summary of its principles shall be given here [19, 47, 204]. The simulation has been optimised for virgin LDPE and those values are shown in table 5.1 [47].

In the simulation EL is assumed to occur due to the recombination of opposite polarity charge carriers from a uniform SC region at both electrodes. Since the recombination coefficients are equal for electrons and holes the recombination of charge is assumed to be equal at both electrodes. To simplify the computation only the emission from electrode 1 is simulated (I_1). The total EL (I_{total}) is then calculated using

$$I_{total} = A\left(I_1 + BI_2\right) = AI_1 + ABI_1 \tag{5.2}$$

Where I_1 is the emission from the electrode nearest the detection system (the ring electrode in the experiment) and I_2 is the emission from the other electrode (the plane electrode). A is a constant to account for absorption due to the gold layer and optical arrangement and B is a constant to account for the light absorption due to the polymer bulk (UV-Vis spectroscopy showing it to be approximately 5 %).

Basic equations often used to describe the movement of charge within a solid as a function of time (t) and position (x) are, Poisson's equation;

$$\nabla \cdot E = \frac{\rho(x,t)}{\epsilon_0 \epsilon'} \tag{5.3}$$

and the continuity equation [212].

$$\nabla \cdot j = -\frac{\partial \rho(x,t)}{\partial t} \tag{5.4}$$

Where ρ is the net charge density, ϵ_0 and ϵ' are the vacuum and relative permittivities respectively (ϵ' is approximately 2.3 for virgin LDPE) and j is the current density. The transport of charge is not accounted for within this simulation and therefore (5.3) and (5.4) are used in the following section to describe the injection of charge into the space charge region.

Charge injection

As discussed in section 2.1.3 two approximations for current density are regularly discussed in the literature, the Richardson-Schottky (equation 2.10) and the Fowler-Nordheim (equation 2.11) injection. A numerical investigation by Hare *et al.* [207] showed a large field region where the current density is not accurately estimated by either approximation. Instead an approximation was proposed showing a reasonable fit with both injection theories over the range 30 to 330 kV mm^{-1}. POW EL is regularly measured throughout the range 40 to 100 kV mm^{-1} suggesting this approximation to be suitable for this application. The approximated injection current density for electrons and holes can be approximated using:

$$\begin{aligned} j_e(t) &= -\alpha_e \exp\left(\beta_e E_{0(t)}\right) \\ j_h(t) &= \alpha_h \exp\left(\beta_h E_{0(t)}\right) \end{aligned} \tag{5.5}$$

Where $\alpha_{e,h}$ and $\beta_{e,h}$ are the injection parameter constants for electrons and holes and E_0 is the applied electric field at the injecting electrode. $\alpha_{e,h}$ and $\beta_{e,h}$ are assumed to be the same for both electrons and holes ($\alpha_e = \alpha_h$, $\beta_e = \beta_h$). They have been optimised for virgin LDPE (values shown in table 5.1) and produced a good fit with measured EL from a range different applied waveforms [23, 47, 98, 204].

To calculate the electric field at the injecting electrode the effect of the space charge region has to be considered. The charge injected into the space charge region is assumed to be uniformly distributed. Poisson's equation (equation 5.3) can then be rewritten to determine the time dependent change in the electric field ($\Delta E(t)$). This is affected by the charge density and the space charge region (X), such that,

$$\Delta E(t) = \frac{\rho(t)}{\epsilon_0 \epsilon_r} X \tag{5.6}$$

The electric field at the electrode can now be defined, accounting for the affect of the space charge region, that is,

$$E_{_0}(t) = \frac{V(t)}{L} - \frac{\rho(t)}{\epsilon_0 \epsilon_r} \left(X - \frac{X^2}{2L} \right) \tag{5.7}$$

Where $V(t)$ is the applied voltage and L is the thickness of the sample. Differentiating this with respect to time gives.

$$\dot{E}_{_0}(t) = \frac{\dot{V}(t)}{L} - \frac{\dot{\rho}(t)}{\epsilon_0 \epsilon_r} (X - \frac{X^2}{2L}) \tag{5.8}$$

Since the charge density is uniform over the space charge region the continuity equation (equation 5.4) can be rewritten as.

$$\dot{\rho}(t) = \frac{j(t)}{X} \tag{5.9}$$

Substituting (5.9) into (5.8) allows the electric field at the injecting electrode to be calculated in terms of the size of the space charge region and the injection current density. Since X is very small compared to L this results in.

$$\dot{E}_0(t) = \frac{\dot{V}(t)}{L} - \frac{j(t)}{\epsilon_0 \epsilon_r} \tag{5.10}$$

Substituting the Hare *et al.* [207] approximation for $j_{_{e,h}}(t)$ (equation 5.5) into equation 5.10 produces a first-order differential equation for the local electric field at the electrode.

$$\dot{E}_0(t) = \frac{\dot{V}(t)}{L} - \frac{\alpha}{\epsilon_0 \epsilon_r} \exp(\beta E_0(t)) \tag{5.11}$$

This can be solved numerically using the Runge-Kutta method, a simple and fast computational method for estimating the solution to first-order differential equations. It operates by evaluating the derivative at 4 trial points per time step (Δt_{EL}); once at the initial point, twice at trial midpoints and once at a trial end point. The weighted average of these four trial points giving an estimation for the change over a single time step. The time step for the Runge-Kutta method (Δt_R) is $\frac{1}{2000f}$, where f is the applied field frequency ($\Delta t_R = 10$ μs at 50 Hz). The time step for the EL simulation (Δt_{EL}) is $\frac{1}{1000f}$.

Charge Recombination

Using the value of the injection current at the local electric field it is then possible to simulate the density of mobile electrons (ρ_{em}) and holes (ρ_{hm}) injected into the polymer per time step (time increment for simulating electroluminescence Δt_{EL}).

$$\begin{aligned} \rho_{em} &= j_e \frac{\Delta t_{EL}}{X} \\ \rho_{hm} &= j_h \frac{\Delta t_{EL}}{X} \end{aligned} \tag{5.12}$$

Where j_e and j_h are calculated using equation 5.5 shown previously.

Since the transport of charge out of the space charge region is not accounted for injected charge cannot remain mobile and so only 2 possibilities exist at the end of each time step. Charge either remains trapped within the space charge region or recombines with an opposite polarity trapped charge carrier. The charge recombination is therefore proportional to the density of mobile and trapped charge carriers, resulting in,

$$\begin{aligned} R_{em,ht} &= |M_{em,ht} \rho_{em} \rho_{ht}| \\ R_{hm,et} &= |M_{hm,et} \rho_{hm} \rho_{et}| \end{aligned} \tag{5.13}$$

Where $R_{em,ht}$ and $R_{hm,et}$ are the amount of charge recombinations between mobile electrons with trapped holes and mobile holes with trapped electrons respectively.

$M_{em,ht}$ and $M_{eh,et}$ are the respective recombination coefficients, ρ_{et} and ρ_{ht} are the number of trapped electrons and holes at the beginning of the time step.

The resultant EL from electrode 1 (I_1), during each time step is the sum of mobile electrons recombining with trapped holes and mobile holes recombining with trapped electrons, as shown by

$$I_1 = \frac{A\left(R_{em,ht} + R_{hm,et}\right)}{\Delta t_{EL}} \tag{5.14}$$

Where A is the photon detection coefficient of the measurement system including the gold electrode. In this work A is 1 since the units of measured EL are arbitrary and so the emission and simulation are normalised relative to the virgin measurement.

At the end of each time step the trapped charge density is recalculated for the following time step using:

$$\begin{aligned} \rho_{et_{\text{new}}} &= \rho_{et_{\text{old}}} + \rho_{em} - \left(q_e R_{em,ht} + q_h R_{hm,et}\right) \\ \rho_{ht_{\text{new}}} &= \rho_{ht_{\text{old}}} + \rho_{hm} - \left(q_h R_{hm,et} + q_e R_{em,ht}\right) \end{aligned} \tag{5.15}$$

Where q_h and q_e represent the charge of a hole and electron respectively ($\pm 1.6 \times 10^{-19}$ C).

The affect of different injection parameters and the field limits of the simulation were thoroughly investigated by Ariffin [47]. Optimised parameters for 100 μm LDPE stressed under a 50 Hz, sinusoidal field are shown in table 5.1.

TABLE 5.1: Parameters for simulating electroluminescence in virgin LDPE

Parameters	Description	Value	Units
$\alpha_{e,h}$	Charge injection constant	3×10^{-5}	$\mathrm{A\,m^{-2}}$
$\beta_{e,h}$	Charge injection constant	7×10^{-8}	$\mathrm{m\,V^{-1}}$
Δt_R	Time increment for Runge-Kutta method	10	μs
Δt_{EL}	Time increment for simulating EL	20	μs
ϵ_0	Permittivity of vacuum	8.85×10^{-12}	$\mathrm{F\,m^{-1}}$
ϵ'	Real relative permittivity	2.3	
ω	Angular frequency of applied voltage	100	$\pi\,\mathrm{rad\,s^{-1}}$
$M_{et,hm}$	Mobile electron - trapped hole coefficient	1.25×10^{-12}	$\mathrm{m^3\,C^{-2}}$
$M_{ht,em}$	Mobile hole - trapped electron coefficient	1.25×10^{-12}	$\mathrm{m^3\,C^{-2}}$
q_e	Charge of an electron	-1.6×10^{-19}	C
q_h	Charge of a hole	1.6×10^{-19}	C
A	Coefficient for absorption of gold and optics	1	
B	Coefficient for absorption of polymer bulk	0.95	
L	Thickness of polymeric sample	100	μm
X	Thickness of space charge region	10	nm

Steady state

The initial conditions of the EL model are assumed to have no trapped charge within the polymer ($\rho_{et} = \rho_{ht} = 0$). Therefore, initially there is no availability for charge recombination and so no EL during the first half cycle. During the second half cycle there will be charge recombination with charge remaining trapped at the end of the first half cycle, but due to the recombination coefficients not all charge will be able to recombine. With each subsequent cycle more charge will be injected than recombines until the situation where the quantity of charge injected during each half cycle is equal to the quantity of charge recombinations taking place, i.e. the steady state. This is not seen in measurement data because the steady state condition is expected to be reached very quickly, simulations suggest less than 10 seconds, a time resolution which is not possible experimentally.

The time taken to reach steady state will depend on the quantity of charge injected and trapped along with the charge recombination coefficients. Ageing is expected to alter the density or distribution of charge traps and will therefore affect the duration until a steady state is reached. In order to account for this, the simulation was allowed to run until a change in peak height of less than 0.1% occured for both the positive and negative half cycles. An example of the simulation until steady state is reached is shown in figure 5.5. The simulation under a lower field of 40 $\mathrm{kV_{pk}\,mm^{-1}}$ takes much longer to reach a steady state than when stressed at 80 $\mathrm{kV_{pk}\,mm^{-1}}$.

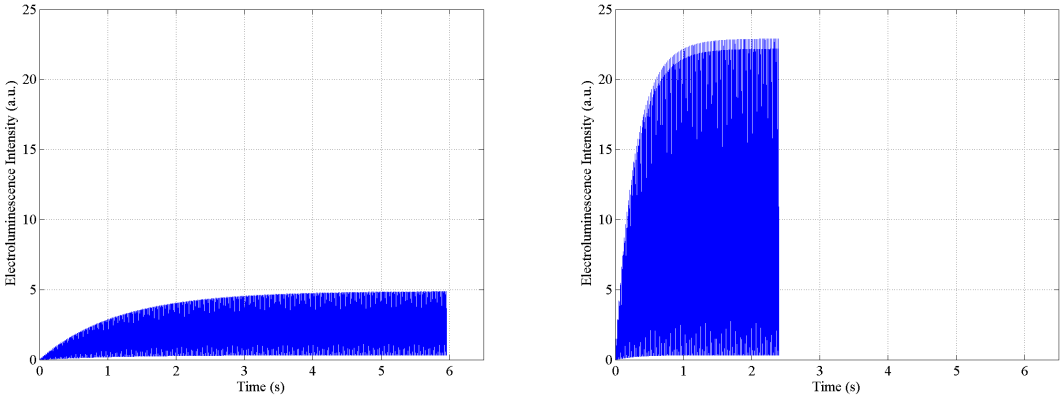

(a) Electrical field of 40 kV_{pk} mm^{-1}

(b) Electrical field of 80 kV_{pk} mm^{-1}

FIGURE 5.5: Simulated time to reach a steady state

5.3.2 Modelling Ageing

In simulating changes in EL as a result of ageing it is desirable to avoid the addition of arbitrary tuning parameters that have little physical meaning. Investigating the previously described model suggests that EL is controlled by changes in the density of charge available for recombination, that is,

$$\mathrm{EL}(t) \propto M_{e,h}\rho_{e,h}(t) \propto \frac{j_{e,h}(t)}{X} \tag{5.16}$$

Assuming the charge recombination coefficients remain unchanged with ageing duration, the EL can be assumed to relate purely to the injection current density ($j_{e,h}$) and SC region (X). These may not relate directly to measurable parameters but approximations can be made based on measurable changes as a result of ageing.

The ($j_{e,h}$) for the same applied field is controlled by $\alpha_{e,h}$, $\beta_{e,h}$, L and ϵ'. The thickness of the sample (L) remains constant with ageing duration. The following sections will simulate changes in these parameters with ageing using trends shown by the results reported in the previous Chapter.

5.3.3 Changes in the Space Charge Region

In previous work the SC region has always been assumed to exist over a fixed 10 nm depth into the polymer from the electrode [23, 204]. This is an unlikely situation since the depth of charge penetration could be expected to vary with

the applied field strength, applied waveform and frequency. However, this fixed SC region has been shown to accurately simulate the EL emission in a range of conditions [19, 22, 47].

As a result of photo-irradiation, results have shown increased oxidation products and cross-linking. Oxidation products are thought to act as charge trapping sites [213, 214]. This was confirmed by SC measurements showing photo-irradiation significantly alters the charge distribution within the bulk of the polymer. With the creation of new trapping sites due to this disorder, it is reasonable to assume changes in the trapping energies within the SC region will occur. The increased concentration of trapping sites near the surface will limit or increase the ability of charge to penetrate into the polymer. Investigations reported in the literature have shown an increased concentration of charge in the bulk after the formation of carbonyl groups near the surface [37, 215, 216]. This suggests that increased charge traps due to oxidation products may lead to enhanced charge injection.

Since this model simulates a uniform distribution of charge no account is made for the energy of a charge trap. In order to simulate changes in the charge trapping properties without the addition of other parameters the SC region can be varied. Changing the penetration depth of the SC region under the same charge injection conditions increases or reduces the charge density. To make assumptions about the way the density of charge trapping sites vary, the PEA profile nearest the HV electrode can be considered. To account for the resolution of the PEA system the total charge in 10 μm steps through the polymer are calculated and divided by the total charge within the polymer. This gives the percentage of total charge distributed in 10 μm steps through the polymer. Figure 5.6 shows how the percentage of total charge within 10 μm of the high voltage electrode changes with ageing duration. The results present the condition after 1 minute of electrical stressing under a 40 $kV_{dc}\,mm^{-1}$ field.

The results show that in virgin materials, after 1 minute, 20% of the charge is near the HV electrode. As the material is aged the percentage of the total charge increases for 3 and 7 days of ageing. After 10, 14 and 17 days of ageing the percentage of total charge has reduced below that of the virgin material. For more heavily aged samples a greater total quantity of charge was seen and so less must remain near the injecting electrode. Under the shorter stressing duration of an ac field this may be interpreted as an increased penetration depth of charge, simulated through an increased SC region.

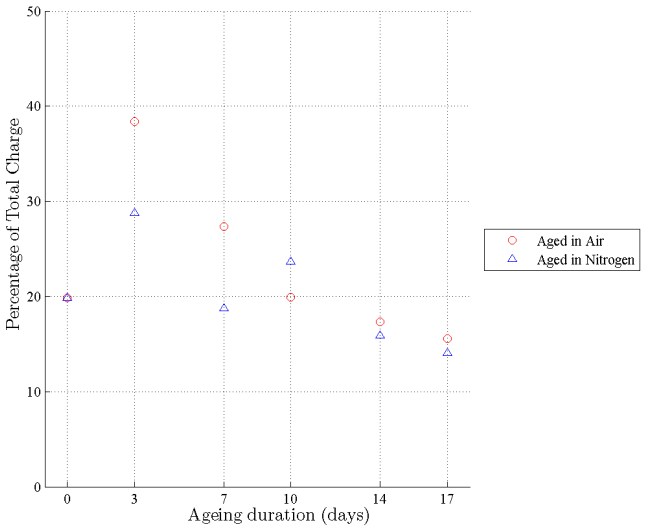

FIGURE 5.6: Percentage of total charge within 10 μm of the high voltage electrode after 1 minute of electrical stressing

For the nitrogen aged results the trend is less clear, these results suggest after 3 days of ageing there is also an increase in the percentage of charge near the injecting electrode. However, after 7, 14 and 17 days of ageing the percentage of total charge reduces. The 10 day aged sample appears out of sequence in these results.

The physical changes that can be used to explain the behaviour of the samples aged in air is due to the generation of oxidation products preferentially near the electrode-polymer interface [56]. If it is assumed that in the air aged samples there is initially an increased concentration of charge trapping sites at the electrode-polymer interface and if the same quantity of charge is assumed to be injected then more of this charge would be trapped in this region. As the ageing time increases, the concentration of charge trapping sites in this region continues to increase. With continued ageing it is unlikely the source of these charge trapping sites are able to move. Alternatively, the formation of new charge trapping sites may allow the same injected charge to be spread over a larger region. The same argument for nitrogen aged samples however is difficult to make. The initial increase could be explained due to oxidation products forming near the surface but due to the nitrogen environment they are not expected to form preferentially towards this region. The reduction in level could be due to the increase in oxidation products but the level shown by IR spectra in nitrogen aged samples is much lower than that of the air aged samples.

Figure 5.7(a) shows the variation in the percentage of charge from the virgin result. A trend line is applied to calculate the percentage change in the SC region, as shown in figure 5.7(b). The fit for the air samples is relatively good but it is difficult to get a good approximation for the nitrogen aged samples due to the unexplained change between 7 and 10 days of ageing.

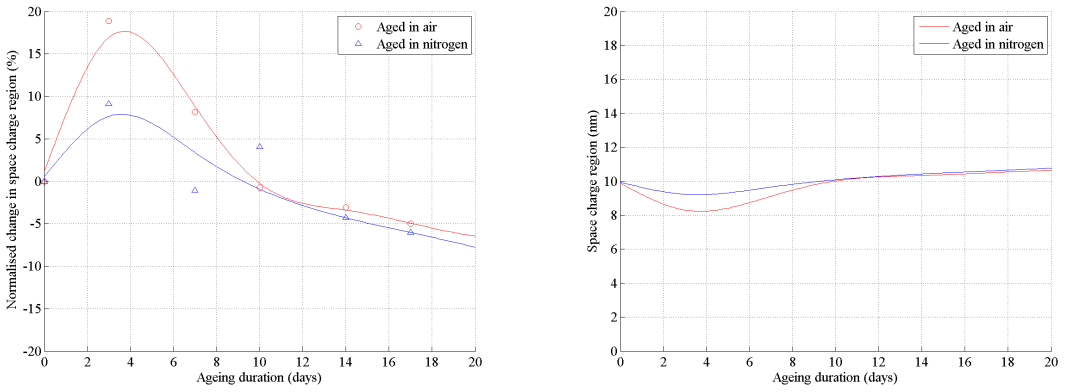

(a) Percentage change in space charge region

(b) Space charge region

FIGURE 5.7: Simulated variation in space charge region with ageing duration

Figure 5.8 compares the simulated changes in EL due to a varying space charge region with that of the measured EL as samples are aged. The simulation was completed to represent ageing durations from 0 to 18 days in 1 day steps and the EL as a result of a sinusoidal, 50 Hz, 60 $kV_{pk}\,mm^{-1}$ field. Comparisons are made in terms of the changes in intensity and phase difference, the phase difference being calculated as the average difference of both half cycles. The simulated intensity results are scaled to that of the measured virgin result.

The simulation shows the EL intensity to vary proportionally with the SC region. As shown previously (equation 5.16), X just acts as a scaling parameter for charge injected into the polymer. The change in intensity shows a similar trend with the samples aged in air suggesting a possible explanation for the increase in intensity. However the samples aged in a nitrogen atmosphere did not show an initial increase in intensity which simulating the change in SC region by the same method would predict. The simulated reduction in intensity after 10 days of ageing shows a close fit with the reduced EL for samples aged in both air and nitrogen. Ageing for more than 10 days also correlates with the significant increases in oxidation products seen in IR absorption spectra.

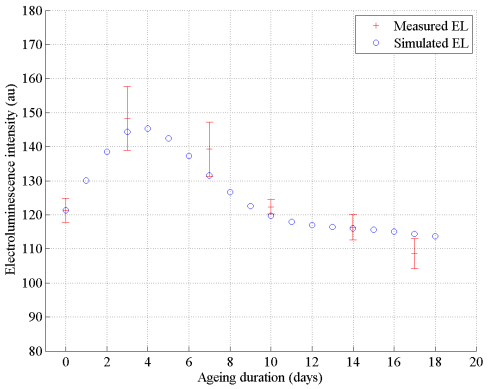

(a) EL intensity - Aged in air

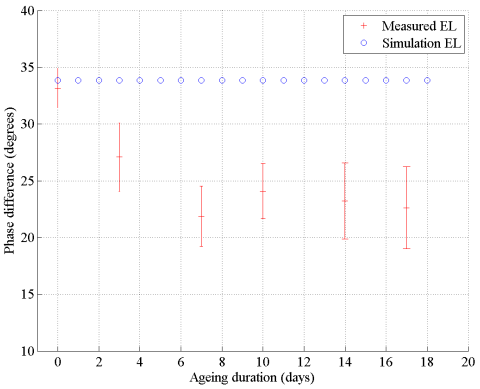

(b) EL phase angle - Aged in air

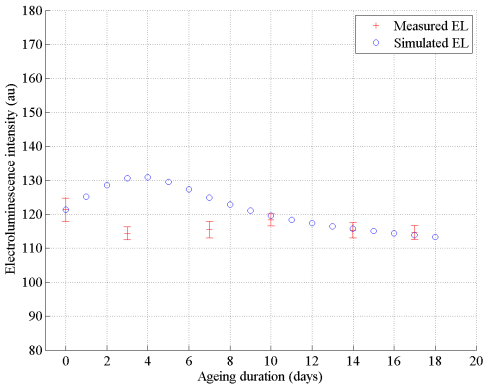

(c) EL intensity - Aged in nitrogen

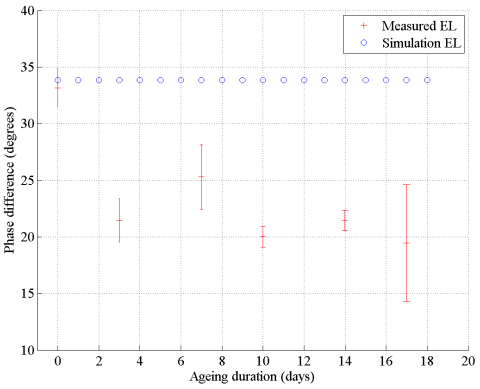

(d) EL phase angle - Aged in nitrogen

FIGURE 5.8: Simulated electroluminescence for a varying space charge region compared with measured data

The phase difference is accurately predicted by the model in the case of the virgin sample, however no significant change is seen as the SC region is varied. This is expected since the phase difference created by the model is due to the local electric field leading the applied field. This is predominately controlled by the injection current density since X is much smaller than the thickness of the sample (L) (equation 5.11). Changes as a result of ageing still leave X much smaller than L and so there is no measurable affect on the local electric field and therefore phase difference.

The assumptions made here on the movement of charge is that the formation of charge trapping sites has no effect on the charge injection barrier. The formation of new trapping sites in the region relating to EL would be expected to influence

the injection of charge into the polymer. Changes in the injection of charge across the electrode-polymer interface is controlled by the injection current density ($j_{e,h}$).

5.3.4 Changes in Current Density

As shown previously by equation 5.16 the injection current density ($j_{e,h}$) is the other parameter controlling the charge density and therefore the possibility of recombination leading to EL. Being a time dependent variable this is capable of explaining changes in both EL intensity and phase difference. The injection current density is affected by a range of parameters, some physical and some arbitrary. This section will discuss the possibilities these parameters change and the affect this has on simulating changes in EL as a result of ageing.

Increased Dielectric Loss

A relationship between the concentration of oxidation products and the $\tan\delta$ dielectric loss measurement was shown previously (figure 5.1). Increases in $\tan\delta$ typically identify an electrically lossy polymer due to either increases in dipole relaxation or increased movement of free charge through the polymer [38, 123]. If there is an increased conduction through the polymer but the same charge injection, then less charge will be available for recombination. However, carbonyl groups are thought to relate to deep trapping sites and therefore conduction (assuming hopping based) would result in large energy changes. The recombination from this hopping process could be expected to lead to a light emission by the same process as EL. Therefore any conduction process must be through low energy sites such that no measurable light emission is produced. It has been suggested that carbonyl groups may actually be responsible for both shallow and deep traps [46]. This then provides an explanation for increased conduction and charge mobility associated with oxidation products [85]. The increased quantity of shallow traps may then explain the non-light emitting charge movement while the deep traps explain the increased charge shown by PEA measurements. The rate of charge decay shown by PEA measurements also suggested an increasing concentration of lower energy trapping after longer ageing durations. This increase in conduction could also explain the reduced breakdown strength for samples aged in air through an increase in the probability of conduction pathways and subsequent thermal failure. The lack of a reduction in breakdown strength for samples aged in nitrogen is then explained due to the increased cross-linking and smaller concentration of oxidation products.

Measurements of dc conductivity in polyethylene oxide (PEO), a PE with the addition of oxygen based groups as part of the polymer backbone, shows values of 10^{-8} S m^{-1} [217, 218]. DC conductivity in unaged LDPE is typically of the order of 10^{-13} S m^{-1} [219, 220]. Investigations into LDPE have also shown significant increases in dc current density as a result of oxidation (1 to 2 orders of magnitude) [76, 221]. Both these sets of measurements support the idea of oxidation products enhancing the injection and conduction of charge through the polymer.

Since it is not possible to measure the conduction current simultaneously with EL measurements using the TDHVL experiment, an approximation for the change was made. Work by Tohyama *et al.* [222] has simultaneously measured the ac dissipation current (I_{dis}) and EL giving values of the order of 10^{-6} A [223, 224]. A quick approximation showed that to achieve a suitable reduction in the injection current density this needed to increase by an order of magnitude. Figure 5.9 shows the approximation of current, making the assumption that it follows a similar time squared increase as the carbonyl groups and $\tan\delta$ losses. The adjustment to the virgin current density (figure 5.9(b)) is calculated using

$$j(t) = j_0(t) - \frac{\Delta I_{dis}}{A} \tag{5.17}$$

Where $j_0(t)$ is the current density of the virgin material, ΔI_{dis} is the change in dissipation current compared to the virgin model and A is the area of the electrode used by Tohyama *et al.* [222] ($\pi 0.13^2$ m^2). The initial value of I_{dis} for virgin LDPE is accounted for in the optimisation of the α and β parameters. Since no phase information is known about the increased current a root mean square (rms) value was used.

Clearly the order of magnitude increase in current cannot purely relate to conduction processes. The measured dc current for LDPE is typically in the range of 10^{-12} - 10^{-9} A [219]. It is suggested instead that this is a contribution of loss processes removing charge from the ability to recombine. The total dissipation current can be considered to be a contribution of currents, that is

$$I_{dis} = I_c + I_{loss} + I_{rad} \tag{5.18}$$

Where I_c represents conduction processes, I_{rad} represents charge contributing to radiative recombination and I_{loss} represents charge lost through non-radiative recombination. Therefore I_{dis} increases due to a contribution from conduction pro-

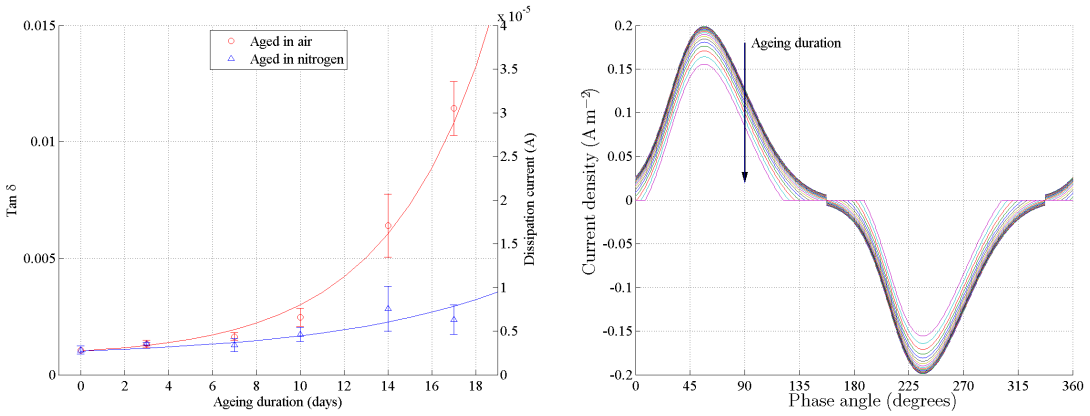

(a) Increase in conduction current with tan δ

(b) Simulated change in current density at injecting electrode for air aged samples

FIGURE 5.9: Correlation with change in rms conduction current and carbonyl groups

cesses and low energy trapping sites resulting in less charge available for recombination. This suggested increase in non-radiative recombination is also supported by the reduction in fluorescence emission as the concentration of oxidation products increased.

The results shown in figure 5.10 compare the EL intensity and phase difference for samples aged in air and nitrogen environments. The intensity is normalised to that of the virgin sample.

As expected the increased conduction current results in a reduced EL intensity as the ageing time is increased. It shows a very good fit with nitrogen aged samples where a very small increase in $\tan\delta$ was seen and very little change in EL. The samples aged in air show a reduction after 10 days of ageing with a similar shape to the simulation, but the simulation is offset. Since only the root mean square (rms) value for I_{dis} is subtracted there is no change in the phase of the injection current density. As such there is no change in the phase difference between the EL and applied field.

Real relative permittivity

The dielectric spectroscopy measurements shown in section 4.5 presented a relationship between the ageing duration and real relative permittivity ($\epsilon^{'}$). An increase in $\epsilon^{'}$, was seen for both air and nitrogen samples and relates to an increase in the polarisability of the material. Similar increases in $\epsilon^{'}$ have been reported in

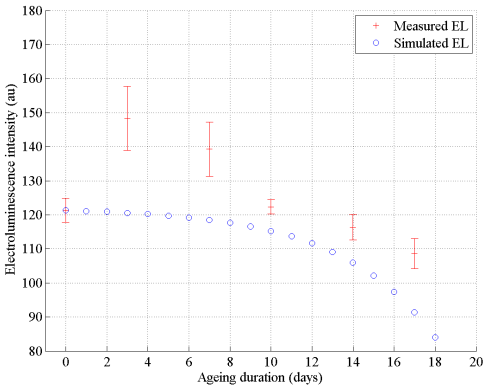

(a) EL intensity - Aged in air

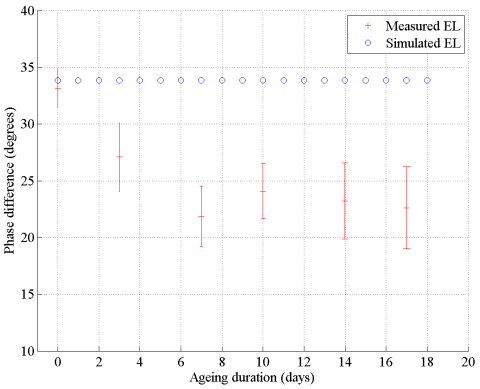

(b) EL phase angle - Aged in air

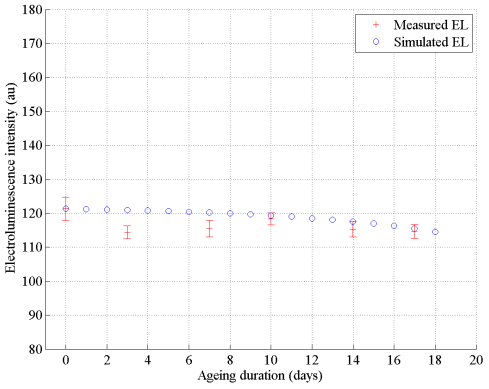

(c) EL intensity - Aged in nitrogen

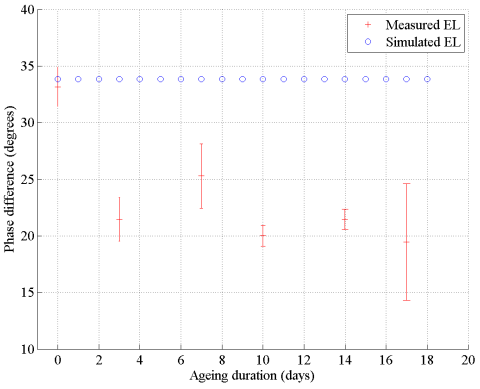

(d) EL phase angle - Aged in nitrogen

FIGURE 5.10: Simulated electrouminescence for an increasing dissipation current compared with measured data

the literature as a result of the formation of oxidation products in XLPE [225]. The value of $\epsilon^{'}$ for samples aged in air show an almost continuous increase with ageing duration whereas those samples aged in nitrogen showed an initial increase and then a constant level for continued ageing. Figure 5.11 shows a best fit for $\epsilon^{'}$ in the air and nitrogen aged samples with ageing time. The fit for nitrogen samples deviates from the measured results slightly (particularly at 14 days of ageing). The increases seen in nitrogen aged samples follow the concentration of oxidation products shown by IR spectra. The 14 day aged sample appeared to have a higher concentration, most likely due to a poorer extraction of oxygen prior to backfilling with nitrogen.

The $\epsilon^{'}$ is used to determine the electric field at the injecting electrode (equation 5.11) and as such the injecting current density. The comparison between simulated

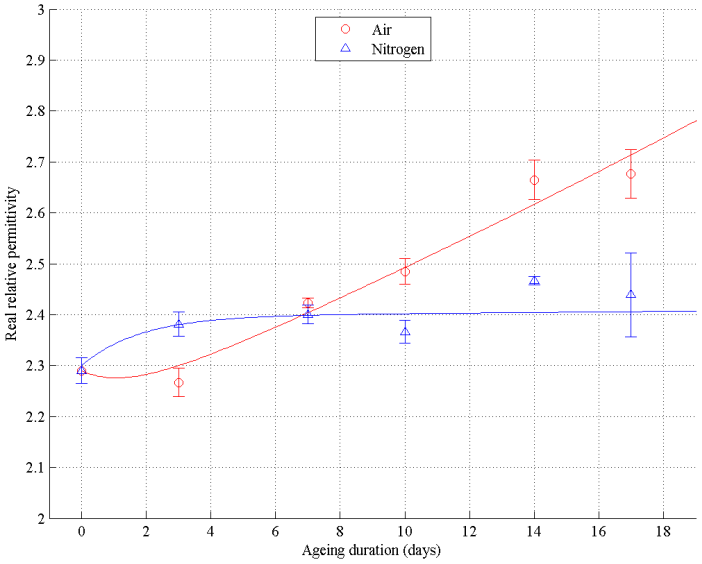

FIGURE 5.11: Best fit to measured changes in real relative permittivity for simulation

and measured EL as a result of changes in ϵ' are shown in figure 5.12, normalised to the virgin result. The results show an increase in ϵ' results in an increase in intensity along with a reduction in the phase difference. This occurs because it reduces the influence injected charge has on the local electric field. The increase in intensity does not follow with the measured change in intensity for either the air or nitrogen aged results. Changes in ϵ' does affect the simulated EL in terms of phase difference. The phase difference in the air sample continues to reduce as the ageing time increases and in the nitrogen samples a step change is seen. The change however is not of the same magnitude as the measured results.

Combined affect

The changes in ϵ' and increase in I_{dis} are both thought to relate to the increase in oxidation products creating a more polarisable material and the introduction of conduction pathways and increased possibility of non-radiative recombination. Therefore analysing the combined affect of these assumptions may be of interest. A comparison between measured and simulated data is shown in figure 5.13, normalised to the virgin result.

The results for air samples show an initial slight increase in intensity up to 10 days of ageing due to the increase in ϵ'. After 10 days the significant increase in oxidation products and $\tan\delta$ causes the increase in I_{dis} and therefore reduction in EL, closely matching the measured data. The samples aged in nitrogen showed

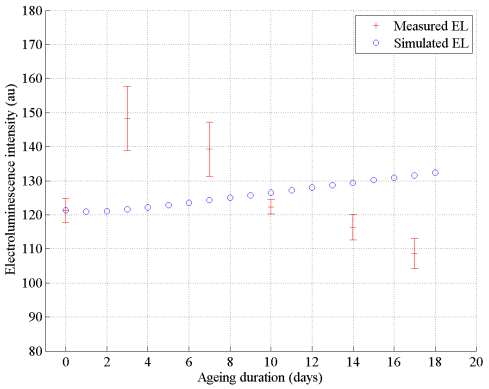

(a) EL intensity - Aged in air

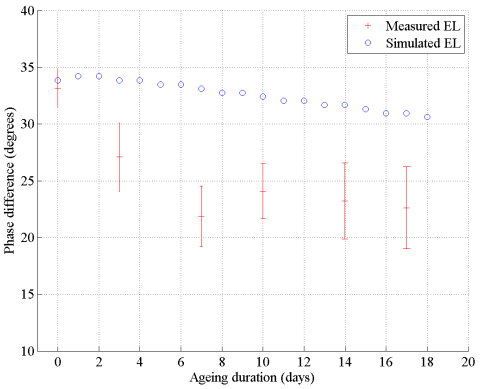

(b) EL phase angle - Aged in air

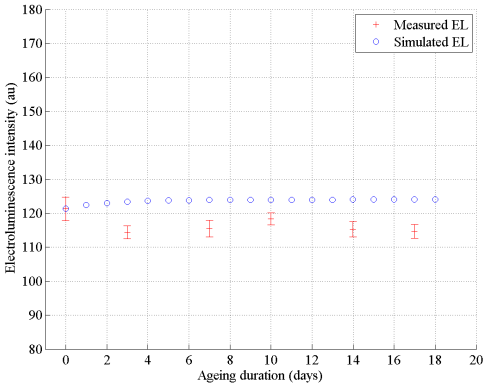

(c) EL intensity - Aged in nitrogen

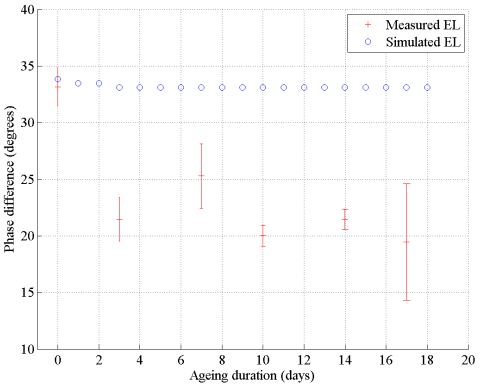

(d) EL phase angle - Aged in nitrogen

FIGURE 5.12: Simulated electrouminescence for an increase in real relative permittivity compared with measured data

little measured change in intensity which the simulation also agrees with though being marginally offset from the measured data due to the step increase in ϵ'.

Analysing the phase difference shows it to decrease continuously in the air aged simulation, following a similar trend to the measured results but with a much smaller magnitude of change. The samples aged in a nitrogen atmosphere show a step change in the phase difference which the simulation also shows but again on a much smaller scale. The simulated change in the phase difference of the samples aged in nitrogen is smaller than the air aged samples, different from the trend seen in the measured EL.

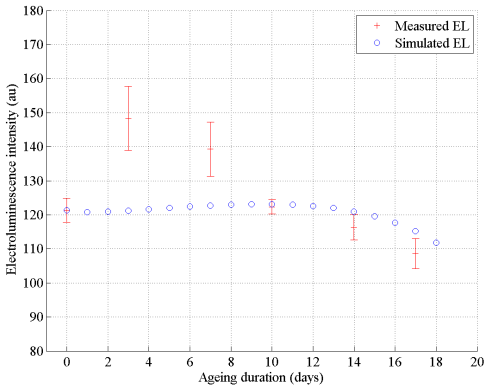

(a) EL intensity - Air aged samples

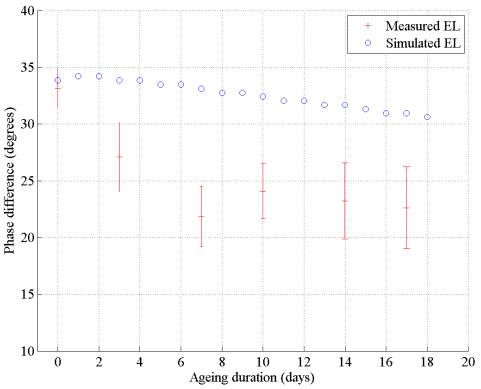

(b) EL phase angle - Air aged samples

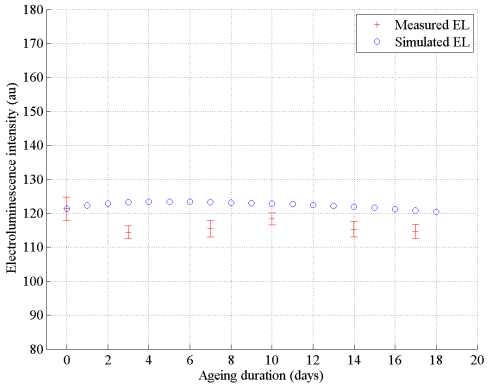

(c) EL intensity - Nitrogen aged samples

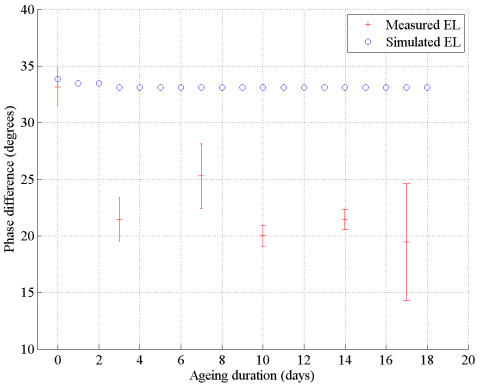

(d) EL phase angle - Nitrogen aged samples

FIGURE 5.13: Simulated electrouminescence for the combined changes in real relative permittivity and increasing dissipation current compared with measured data

5.3.5 Charge Injection Parameters

In order for the model to simulate a bigger shift in the phase difference a large change in the phase of the injection current is required. This would require either a much larger change in the $\epsilon^{'}$ or some phase knowledge of changes in the I_{dis}. The measurements completed for $\epsilon^{'}$ measure the bulk properties of the polymer whereas the ac EL is thought to occur very near the electrode-polymer interface. It is expected that the behaviour of charge in this very small region is significantly different to the bulk properties, particularly as a result of photo-irradiation. There is currently no way to accurately measure the electrical properties of the polymer over this very small region.

As a result of photo-irradiation the charge injection barrier can be expected to change due to changes in the disorder and hence charge trapping properties at the electrode-polymer interface. In the simulation the properties of the charge injection barrier are grouped in with the optimisation of the α and β parameters for the injection current density (equation 5.5). In this work these have been optimised for virgin LDPE. Simulating changes in these parameters as a result of ageing may provide a good fit with measured EL but provide no useful information to help understand the phenomena.

Since the large shift in phase difference is seen in both air and nitrogen materials it suggests a relationship with a very sudden change in surface properties as a result of ageing. These properties being particularly difficult to measure independently of the bulk properties of the polymer.

5.4 Summary

This chapter has discussed changes in oxidation products as a result of ageing and associated the increases in $\tan\delta$ and reductions in fluorescence with them. The increase in $\tan\delta$ following the same time squared increase in carbonyl groups for samples aged in air and the small fluctuations for samples aged in nitrogen. Simulating this behaviour to represent an increase in dissipation current showed a good correlation with the reduction in measured EL intensity for both samples aged in air and nitrogen. An increase in dissipation current explained by the increase in shallow trapping sites allowing an increase in low energy conduction or non-radiative recombination process that increases with the concentration in carbonyl groups.

Dielectric spectroscopy had also shown increases in $\epsilon^{'}$ as a result of ageing and including this change in simulations showed an increase in EL. The results showed a similar trend in the change of phase difference but still not at the same level as the 10 to 15^{o} phase shift seen in measured results. The increased contribution of polarisable dipoles producing changes in the bulk $\epsilon^{'}$ measurement are therefore thought to only have a small contribution on the EL

The model used has previously always assumed a 10 nm space charge region, though this cannot be confirmed experimentally. The PEA measurements suggest a possible change in the penetration depth of charge into the polymer after short stressing durations. Using the percentage of charge near the HV electrode in SC measurements to simulate percentage changes in the space charge region (X) with

ageing showed a good fit with EL intensity for the air aged samples. This suggests that the formation of new trapping sites could affect the penetration of charge into the polymer. The increased concentration of charge trapping sites very near the polymer surface leads to increased charge trapping in this region and therefore increased EL. The reduction in EL due to further increases in oxidation products is because their increased concentration allows for increased non-radiative relaxations and conduction.

Using these measured parameters to represent changes in the EL as a result of ageing requires the assumption that the surface states change in the same way as the bulk properties. This is almost certainly not going to be the case due to the greater disorder at the surface states. The simulations do show that changes in the movement of charge into the polymer as a result of ageing contributes to changes in EL intensity. This relates to the formation of new shallow and deep trapping sites as a result of photo-irradiation. To simulate changes in the phase difference arbitrary tuning parameters would be needed to control the movement of charge across the electrode-polymer interface. Since this does not provide useful information into understanding the EL phenomena this has not been considered in this work.

Chapter 6

Conclusions and Further Work

6.1 Conclusions

During service, polymeric insulation used in high voltage systems ages until eventually the end of its usable life is reached, typically resulting in catastrophic failure. Historically ageing was related to the enhanced electric fields created by the presence of impurities and protrusions within the polymeric system. Improvements in the quality of cable manufacturing has led investigations to look in more depth at the accumulation of charge within the insulating polymer. Investigating the accumulation of this charge as the material ages will allow a better understanding of the influence it has on any eventual degradation processes. This understanding can help improve polymeric material design, lifetime estimation and condition monitoring, all of great importance to the electrical industry.

EL is a low level light emitted from polymeric materials when subjected to an electric field. The emission is thought to occur due to the bipolar charge recombination theory involving the injection, trapping and recombination of opposite polarity charge carriers. Under ac fields very little charge accumulates within the polymer bulk and therefore EL is thought to originate from very near the electrode-polymer interface. Measurement of this phenomenon therefore offers the potential of investigating changes in charge movement in this region.

A lot of research has previously been done to understand the influence electrode arrangement, material and applied waveform has on EL emission. Investigations for different materials report a strong relationship between intensity and the chemical structure of the material. Materials with aromatic chemical groups

produce a stronger emission and this is thought to relate to their increased charge trapping properties.

A development to the EL experiment at the TDHVL improved its sensitivity through the use of an EMCCD camera. The EMCCD camera allowing low noise, high sensitivity images to be collected along with high speed measurements required for POW investigations. The use of a batch filter for post processing the raw data allowing the signal to be presented cleanly without the addition of any artificial phase shift in the POW result. A comparison with POW data on the same material at the TDHVL and the LAPLACE confirmed a phase difference between the applied field and the EL of a virgin LDPE sample of approximately 35^o.

LDPE films were aged using a UV source in both air and nitrogen environments. The ageing in nitrogen greatly reduced the influence of oxygen on the ageing process. Photo-irradiation in air showed increases in typical oxidation products, such as carbonyl and hydroxyl products measured through FTIR absorption spectroscopy. Ageing in nitrogen also showed a small increase in oxidation products, likely due to oxygen remaining after degassing of the polymer. In both environments significant quantities of cross-linking took place, the greatest when ageing in a nitrogen environment due to the reduced competition in reaction processes. The main difference thought to exist between the two environments is related to the location of any oxidation products produced. In an oxygen environment these are thought to be preferential towards the surface due to the abundance of oxygen, cross-linking therefore being the main component within the polymer bulk. In a nitrogen aged sample any oxygen after degassing is expected to be distributed throughout the polymer bulk.

As a result of ageing the dielectric strength of a polymer was expected to reduce. Investigations into changes as a result of photo-irradiation showed a reduction for samples aged in air whereas an increase was seen for samples aged in nitrogen. The increase relates to the cross-linking of the polymer, creating a more rigid structure and reducing the probability of failure. The reduction in dielectric strength of air aged samples is because easier charge injection and movement are created by the oxidation products.

Dielectric spectroscopy measurements showed significant changes in the sample as a result of ageing. The increase in oxidation products results in an increase in real relative permittivity and $\tan\delta$. The samples aged in an air environment follow the same trend in $\tan\delta$ with ageing duration as the IR absorption created

by carbonyl groups. Analysis of the imaginary permittivity using the HN model shows an increase in the dielectric loss and broadening of the relaxation peaks as oxidation products increase. The samples aged in a nitrogen environment show a smaller increase in imaginary permittivity and sharper relaxation peaks.

Measurements of changes in the SC formation as a result of ageing show significant changes in charge trapping properties. After 3 days of ageing similar changes in the SC profiles were seen for samples aged in air and nitrogen. The charge decay profiles suggest a large quantity of deep trapping sites throughout the sample, relating to photo-irradiation reactions and oxidation products. With further ageing in air the charge accumulates nearer the electrodes and the decay profile suggests more shallow trapping sites. Ageing in nitrogen reveals that the total amount of charge within the polymer bulk decreases and that there is little change in the charge decay rate.

In order to accurately compare EL from UV aged LDPE, its optical properties had to be checked. UV-Vis spectroscopy confirmed very little change in the absorption of light in the spectrum relevant to the EL emission. The EL intensity showed significant increases in intensity compared with a virgin sample after just 3 and 7 days of ageing in air. With further ageing the intensity reduced to below that of a virgin sample. The samples aged in nitrogen showed very little change in intensity as a result of ageing. The initial increase in intensity is due to the production of oxidation products very near the surface that enhance the availability of charge trapping sites. With further ageing the continued production of oxidation products result in an increased ability for charge to migrate into the polymer bulk or relax through non-radiative pathways.

Investigating changes in the phase difference between the peak of the EL and applied field show significant changes as a result of ageing. In samples aged in both air and nitrogen environments there was a significant shift after just 3 days of ageing. The virgin results showed a phase difference of approximately 35^o. The samples aged in air showed a gradual shift as ageing time increased to approximately 25^o. The samples aged in nitrogen reduced in phase difference to approximately 22^o after just 3 days of ageing and remained almost constant with further ageing. The phase difference between the applied field and the EL is thought to relate to the presence of charge at the electrode-polymer interface. The charge causing the local electric field to be altered such that it leads the applied field in order for charge to be injected across the interface into the polymer. To explain the changes seen with ageing this suggests the local energy levels at the

electrode-polymer interface change in order to have less affect on the local electric field. Since the phase shift occurs in both air and nitrogen aged samples this suggests it does not directly relate to the production of oxidation products.

To further understand the EL phenomena modelling was undertaken to explain both the change in phase difference and intensity as a result of ageing. The model simulated EL due to the recombination of charge injected into a uniform SC region. In previous work this model has always assumed a fixed SC region. As a result of ageing the density of charge trapping sites were expected to vary. This was simulated by assuming the same quantity of charge was injected into a SC region that varied with ageing duration. The change in percentage of total charge near the HV electrode shown by the PEA measurements was used to vary the SC region. The simulation showed a good agreement with the measured change in EL intensity for samples aged in air. The simulation did not agree with the results for samples aged in nitrogen for less than 10 days. Changing the SC region had no affect on the phase difference of the simulated EL due to it having very little affect on the determination of the local electric field in the model.

The presence of carbonyl groups were also thought to increase conduction and non-radiative relaxation processes. This was simulated by a reduction in the amount of charge injected into the SC region by following the time squared increase of the carbonyl related IR absorption and $\tan\delta$ measurements. The simulation showed a similar trend in reduction of intensity for the samples aged in both air and nitrogen. Since this method only assumed an increase in conduction and non-radiative relaxation there was no method to represent the increase in EL intensity or simulate the change in phase difference. In order to simulate changes in phase difference assumptions would need to be made about the affect of ageing on the charge injection barrier. Since in the model these are controlled by arbitrary α and β parameters there is little benefit in simulating changes.

This work has shown EL to be affected by the ageing of LDPE. The increase in intensity of samples aged in air is explained by an increase in charge trapping properties very near the electrode-polymer interface due to oxidation processes. As ageing continues the EL reduces which is explained by further increases in oxidation products. This further concentration of oxidation products increases the possibility of non-radiative relaxation from the excited energy state. These changes in EL intensity combined with the shift in phase difference as a result of ageing provide support for EL as a condition monitoring tool.

6.2 Further Work

This project has shown a relationship between EL emission and ageing in LDPE. Some recommendations for further directions of this project are given below.

This work has demonstrated that the presence of charge trapping sites very near the electrode-polymer interface have a significant affect on the EL behaviour. One area where this could be investigated further maybe in the use of nano-filled polymeric systems. The presence of a known additives within a polymeric system may affect the charge quantity near the electrode-polymer interface and EL investigations would identify this. It is difficult to control the distribution of micro- and nano-filler within the polymeric system. In a polymeric destined for use in high voltage dc transmission systems it is desirable to have minimum charge accumulation within the insulator due to the enhanced electrical stress this can cause. A comparison between the ac EL and dc PEA measurements may make it possible to identify the affect particular nano-fillers have on charge injection and migration.

Another area which is currently not measurable due to the sensitivity of equipment currently readily available relates to the build up in EL suggested by the modelling of EL behaviour. Assuming a polymeric system which is initially free of any trapped charge the model suggests it builds in intensity during stressing time. A steady state is reached at a point were the quantity of charge injected is equal to the quantity of charge recombining during each half cycle, resulting in a steady EL during each cycle. This could be measured in terms of intensity (during 1 cycle) or POW measurements, the later requiring the most sensitive of systems. If the EL was seen to increase as suggested by the model this would provide further support for the bipolar charge recombination theory as opposed to some other mechanisms (such as hot electron injection). A problem with this also relates to overcoming problems with overshooting at field switch on and the possible influence it may have on EL.

This work has only investigated the relationship between ageing by photo-irradiation of LDPE films. It would be of great interest to further this by investigating other materials with stronger emission characteristics (such as PET or PEN). Both PET and PEN have very different UV absorption characteristics, being fully absorbent to this 253.7 nm radiation. This would force all changes as a result of photo-irradation to be concentrated to the surface of the polymer, in terms of oxidation products and cross-linking. This may therefore have a very

different affect on the EL and may further explain some of the behaviour seen here.

In an effort to further the possibilities of using EL as a condition monitoring tool it would be useful to compare and characterise some in service aged materials. Samples aged due to service situations will age in a range of different ways in different positions and so a range of characterisation techniques are required. It is also particularly difficult to know exactly what stresses a particular sample has been exposed to so the changes are more difficult to relate. The ability to produce an ageing related trend would show support for the technique as a condition monitoring tool. Initially investigation of other ageing mechanisms may provide some characteristic data.

In this work it was not possible to measure changes in the wavelength of the EL as a result of photo-irradiation. This was not possible due to the high dark current and readout noise of the spectroscopy detection system available. Accurately measuring changes in the wavelength of the emission would make it possible to identify changes in the energy levels of trapping sites. This would likely be simpler with a polymer that naturally emitted a stronger EL emission.

References

[1] G. F. Moore, *Electric Cables Handbook*, Blackwell Science Ltd, Oxford, UK, 3rd edition, 1997.

[2] L. Dissado and J. Fothergill, *Electrical Degradation and Breakdown in Polymers*, Peter Peregrinus Ltd., London, UK, 1992.

[3] C. Dang, J. L. Parpal and J. P. Crine, 'Electrical aging of extruded dielectric cables: Review of existing theories and data', *IEEE Transactions on Dielectrics and Electrical Insulation*, vol. 3(2), pp. 237–247, 1996.

[4] J. Densley, 'Ageing mechanisms and diagnostics for power cables - an overview', *IEEE Electrical Insulation Magazine*, vol. 17(1), pp. 14 –22, 2001.

[5] C. Mayoux, 'Degradation of insulating materials under electrical stress', *IEEE Transactions on Dielectrics and Electrical Insulation*, vol. 7(5), pp. 590 – 601, 2000.

[6] T. Tanaka, 'Aging of polymeric and composite insulating materials. aspects of interfacial performance in aging', *IEEE Transactions on Dielectrics and Electrical Insulation*, vol. 9(5), pp. 704 – 716, 2002.

[7] Y. Cao, P. C. Irwin and K. Younsi, 'The future of nanodielectrics in the electrical power industry', *IEEE Transactions on Dielectrics and Electrical Insulation*, vol. 11(5), pp. 797–807, 2004.

[8] G. C. Montanari, D. Fabiani, F. Palmieri, D. Kaempfer, R. Thomann and R. Mulhaupt, 'Modification of electrical properties and performance of EVA and PP insulation through nanostructure by organophilic silicates', *IEEE Transactions on Dielectrics and Electrical Insulation*, vol. 11(5), pp. 754–762, 2004.

[9] J. Densley, R. Bartnikas and B. S. Bernstein, 'Multi-stress ageing of extruded insulation systems for transmission cables', *IEEE Electrical Insulation Magazine*, vol. 9(1), pp. 15–17, 1993.

[10] L. A. Dissado, G. Mazzanti and G. C. Montanari, 'The role of trapped space charges in the electrical aging of insulating materials', *IEEE Transactions on Dielectrics and Electrical Insulation*, vol. 4(5), pp. 496–506, 1997.

[11] Y. W. Zhang, J. Lewiner, C. Alquie and N. Hampton, 'Evidence of strong correlation between space-charge buildup and breakdown in cable insulation', *IEEE Transactions on Dielectrics and Electrical Insulation*, vol. 3(6), pp. 778–783, 1996.

[12] G. Chen, M. Fu, X. Z. Liu and L. S. Zhong, 'AC aging and space-charge characteristics in low-density polyethylene polymeric insulation', *Journal of Applied Physics*, vol. 97(8), 2005.

[13] Z. Xu, PhD thesis: *Space Charge Measurement and Analysis in Low Density Polyethylene Film*, Univeristy of Southampton, School of Electronics and Computer Science, 2009.

[14] R. J. Fleming, 'Space charge profile measurement techniques: Recent advances and future directions', *IEEE Transactions on Dielectrics and Electrical Insulation*, vol. 12(5), pp. 967–978, 2005.

[15] G. C. Montanari, C. Laurent, G. Teyssedre, A. Campus and U. H. Nilsson, 'From LDPE to XLPE: Investigating the change of electrical properties part I: Space charge, conduction and lifetime', *IEEE Transactions on Dielectrics and Electrical Insulation*, vol. 12(3), pp. 438–446, 2005.

[16] T. Mizutani, 'Space charge measurement techniques and space charge in polyethylene', *IEEE Transactions on Dielectrics and Electrical Insulation*, vol. 1(5), pp. 923–933, 1994.

[17] D. Mary, M. Albertini and C. Laurent, 'Understanding optical emissions from electrically stressed insulating polymers: Electroluminescence in poly(ethylene terephthalate) and poly(ethylene 2,6-naphthalate) films', *Journal of Physics D: Applied Physics*, vol. 30(2), pp. 171–184, 1997.

[18] A. M. Ariffin, P. L. Lewin and S. J. Dodd, 'Determining the occurrence of electroluminescence in polymeric materials with respect to the applied alternating electrical stress', In the proceedings of *IEEE International Conference on Solid Dielectrics*, pp. 703–706, 2007.

[19] A. M. Ariffin and P. L. Lewin, 'Phase-resolved measurement and modelling of electroluminescence phenomenon in polyethylene subjected to high electrical stress', In the proceedings of *International Conference on Condition Monitoring and Diagnosis*, pp. 264–267, 2008.

[20] G. Teyssedre, C. Laurent, G. C. Montanari, F. Palmieri, A. See, L. A. Dissado and J. C. Fothergill, 'Charge distribution and electroluminescence in cross-linked polyethylene under DC field', *Journal of Physics D: Applied Physics*, vol. 34(18), pp. 2830–2844, 2001.

[21] C. Laurent, F. Massines and C. Mayoux, 'Optical emission due to space charge effects in electrically stressed polymers', *IEEE Transactions on Dielectrics and Electrical Insulation*, vol. 4(5), pp. 585–603, 1997.

[22] A. M. Ariffin, N. M. Tajudin, S. Sulaiman, Y. H. M. Thayoob and P. L. Lewin, 'Comparing simulation results and experimental measurements of electroluminescence phenomenon in dielectric materials', In the proceedings of *IEEE International Symposium on Electrical Insulation*, pp. 1–5, 2010.

[23] F. Baudoin, D. H. Mills, P. L. Lewin, S. L. Roy, G. Teyssedre and C. Laurent, 'Modeling electroluminescence in insulating polymers under ac stress: effect of excitation waveform', *Journal of Physics D: Applied Physics*, vol. 44(16), 2011.

[24] G. Montanari and D. Fabiani, 'Evaluation of DC insulation performance based on space-charge measurements and accelerated life tests', *IEEE Transactions on Dielectrics and Electrical Insulation*, vol. 7(3), pp. 322 – 328, 2000.

[25] T. Zhou, G. Chen, R. Liao and Z. Xu, 'Charge trapping and detrapping in polymeric materials: Trapping parameters', *Journal of Applied Physics*, vol. 110(4), 2011.

[26] D. K. Das-Gupta, 'Polyethylene: Structure, morphology, molecular motion and dielectric behavior', *IEEE Electrical Insulation Magazine*, vol. 10(3), pp. 5 –15, 1994.

[27] T. Blythe and D. Bloor, *Electrical Properties of Polymers*, Cambridge Universtiy Press, Cambridge, UK, 2nd edition, 2005.

[28] A. M. Ariffin, P. L. Lewin and S. J. Dodd, 'Comparison of electroluminescence phenomenon in LDPE, PET and PEN under the application of high

electrical stress', In the proceedings of *IEEE International Conference on Electrical Insulation and Dielectric Phenomena*, pp. 260 – 263, 2006.

[29] A. M. Ariffin, P. L. Lewin and S. J. Dodd, 'Comparison of electroluminescence of different high voltage cable materials under identical experimental conditions', In the proceedings of *IEEE International Symposium on Electrical Insulation*, pp. 166 – 169, 2006.

[30] R. A. V. Raff and J. B. Allison, *Polyethylene*, Interscience Publishers, Inc., New York, USA, 1956.

[31] T. J. Lewis, 'Polyethylene under electrical stress', *IEEE Transactions on Dielectrics and Electrical Insulation*, vol. 9(5), pp. 717–729, 2002.

[32] C. Hall, *Polymer Materials - An Introduction for Technologists and Scientists*, Macmillan Education Ltd., Hong Kong, 2nd edition, 1989.

[33] M. Ohring, *Engineering Materials Science*, Academic Press, London, UK, 1995.

[34] S. N. Kolesov, 'The influence of morphology on the electric strength of polymer insulation', *IEEE Transactions on Electrical Insulation*, vol. 15 (5), pp. 382 –388, 1980.

[35] Materialscientist, 'Spherultie2.png', online: http://en.wikipedia.org/wiki/File:Spherulite2.PNG, *GNU Free Documentation License*, September, 2011.

[36] K. S. Suh, S. J. Hwang, J. S. Noh and T. Takada, 'Effects of constituents of XLPE on the formation of space-charge', *IEEE Transactions on Dielectrics and Electrical Insulation*, vol. 1(6), pp. 1077–1083, 1994.

[37] N. Hirai, R. Minami, T. Tanaka, Y. Ohki, M. Okashita and T. Maeno, 'Chemical group in crosslinking byproducts responsible for charge trapping in polyethylene', *IEEE Transactions on Dielectrics and Electrical Insulation*, vol. 10(2), pp. 320–330, 2003.

[38] S. H. Carr, R. F. Cozzens, D. K. Davies, P. Fischer, V. Y. Merritt, P. J. H., D. A. Seanor and G. M. Sessler, *Electrical Properties of Polymers*, Academic Press, London, UK, 1982.

[39] T. J. Lewis, 'Charge transport, charge injection and breakdown in polymeric insulators', *Journal of Physics D: Applied Physics*, vol. 23(12), pp. 1469–1478, 1990.

[40] G. Teyssedre, C. Laurent, A. Aslanides, N. Quirke, L. A. Dissado, G. C. Montanari, A. Campus and L. Martinotto, 'Deep trapping centers in crosslinked polyethylene investigated by molecular modeling and luminescence techniques', *IEEE Transactions on Dielectrics and Electrical Insulation*, vol. 8 (5), pp. 744–752, 2001.

[41] G. C. Montanari, G. Mazzanti, F. Palmieri, A. Motori, G. Perego and S. Serra, 'Space-charge trapping and conduction in LDPE, HDPE and XLPE', *Journal of Physics D: Applied Physics*, vol. 34(18), pp. 2902–2911, 2001.

[42] M. Meunier, N. Quirke and A. Aslanides, 'Molecular modeling of electron traps in polymer insulators: Chemical defects and impurities', *Journal of Chemical Physics*, vol. 115(6), pp. 2876–2881, 2001.

[43] G. Chen and Z. Xu, 'Charge trapping and detrapping in polymeric materials', *Journal of Applied Physics*, vol. 106, 2009.

[44] M. Meunier, N. Quirke and A. Aslanides, 'Characterisation of charge carrier traps in polymeric insulators', In the proceedings of *IEEE International Conference on Electrical Insulation and Dielectric Phenomena*, pp. 21 – 24, 2000.

[45] M. Meunier and N. Quirke, 'Molecular modeling of electron trapping in polymer insulators', *Journal of Chemical Physics*, vol. 113(1), pp. 369–376, 2000.

[46] A. Huzayyin, S. Boggs and R. Ramprasad, 'Quantum mechanical studies of carbonyl impurities in dielectric polyethylene', *IEEE Transactions on Dielectrics and Electrical Insulation*, vol. 17(3), pp. 920 –925, 2010.

[47] A. M. Ariffin, PhD thesis: *The Measurement and Modelling of Electroluminescence in High Voltage Polymeric Cable Insulation Materials*, University of Southampton, School of Electronics and Computer Science, 2008.

[48] D. Halliday, R. Resnick and J. Walker, *Fundamentals of Physics International Edition*, John Wiley & Sons, 7th edition, 2005.

[49] B. M. Fanconi, 'Chain scission and mechanical failure of polyethylene', *Journal of Applied Physics*, vol. 54(10), pp. 5577 –5582, 1983.

[50] B. Ränby and J. F. Rabek, *Photodegradation, photo-oxidation and photostabilization of polymers*, John Wiley & Sons, London, UK, 1975.

[51] E. L. Leguenza, R. Robert and J. A. Giacometti, 'Dielectric and viscoelastic properties of cross-linked polyethylene aged under multistressing conditions', *IEEE Transactions on Dielectrics and Electrical Insulation*, vol. 11 (3), pp. 406 – 417, 2004.

[52] G. C. Montanari, 'Bringing an insulation to failure: The role of space charge', *IEEE Transactions on Dielectrics and Electrical Insulation*, vol. 18 (2), pp. 339 –364, 2011.

[53] V. K. Agarwal, H. M. Banford, B. S. Bernstein, E. L. Brancato, R. A. Fouracre, G. C. Montanari, J. L. Parpal, J. N. Seguin, D. M. Ryder and J. Tanaka, 'The mysteries of multifactor ageing', *IEEE Electrical Insulation Magazine*, vol. 11(3), pp. 37 –43, 1995.

[54] J. R. White and A. Turnbull, 'Weathering of polymers: Mechanisms of degradation and stabilization, testing strategies and modelling', *Journal of Materials Science*, vol. 29, pp. 584–613, 1994.

[55] F. P. L. Mantia and R. Schifani, 'Natural weathering of low density polyethylene: Part 2 - dielectric properties', *Polymer Degradation and Stability*, vol. 10(1), pp. 67 – 78, 1985.

[56] J. V. Gulmine, P. R. Janissek, H. M. Heise and L. Akcelrud, 'Degradation profile of polyethylene after artificial accelerated weathering', *Polymer Degradation and Stability*, vol. 79(3), pp. 385 – 397, 2003.

[57] P. A. Roseen, T. Reitberger, S. M. Gubanski and U. W. Gedde, 'PD resistance of thermally aged polyethylene and carbonyl-containing model polymers', *IEEE Transactions on Dielectrics and Electrical Insulation*, vol. 6(2), pp. 191–201, 1999.

[58] E. Suljovrujic, Z. Kacarevic-Popovic, D. Kostoski and J. Dojcilovic, 'Effect of ageing on the dielectric relaxation of oriented and gamma irradiated LDPE', *Polymer Degradation and Stability*, vol. 71(3), pp. 367–373, 2001.

[59] D. Feldman, 'Polymer weathering: Photo-oxidation', *Journal of Polymers and the Environment*, vol. 10, pp. 163–173, 2002.

[60] E. L. Leguenza, P. C. N. Scarpa and D. K. Das-Gupta, 'Dielectric behavior of aged polyethylene under UV radiation', *IEEE Transactions on Dielectrics and Electrical Insulation*, vol. 9(4), pp. 507–513, 2002.

[61] A. Singh, 'Irradiation of polyethylene: Some aspects of crosslinking and oxidative degradation', *Radiation Physics and Chemistry*, vol. 56(4), pp. 375 – 380, 1999.

[62] E. A. B. Moura, A. V. Ortiz, H. Wiebeck, A. B. A. Paula, A. L. A. Silva and L. G. A. Silva, 'Effects of gamma radiation on commercial food packaging films–study of changes in UV/VIS spectra', *Radiation Physics and Chemistry*, vol. 71(1-2), pp. 201 – 204, 2004.

[63] J. F. Heacock, F. B. Mallory and F. P. Gay, 'Photodegradation of polyethylene film', *Journal of Polymer Science Part A1: Polymer Chemistry*, vol. 6 (10), pp. 2921–2934, 1968.

[64] D. Marsacq, P. Hourquebie, L. Olmedo and H. Janah, 'Effects of physical and chemical defects of polyethylene on space charge behaviour', In the proceedings of *IEEE International Conference on Electrical Insulation and Dielectric Phenomena*, pp. 672–675, 1995.

[65] J. F. Rabek, *Photodegradation of Polymers*, Springer, Berlin, 1996.

[66] I. Craig, J. White, A. Shyichuk and I. Syrotynska, 'Photo-induced scission and crosslinking in LDPE, LLDPE, and HDPE', *Polymer Engineering & Science*, vol. 45(4), pp. 579–587, 2005.

[67] K. Yang, G. J. Zhang, D. M. Tu and Z. Yan, 'Space charge and electroluminescence characteristics of thermally aged LDPE films', *Applied Surface Science*, vol. 255(5), pp. 2735–2739, 2008.

[68] A. J. Peacock, 'The chemistry of polyethylene', *Journal of Macromolecular Science, Part C: Polymer Reviews*, vol. 41(4), pp. 285–323, 2001.

[69] Q. Wu, B. Qu, Y. Xu and Q. Wu, 'Surface photo-oxidation and photostabilization of photocross-linked polyethylene', *Polymer Degradation and Stability*, vol. 68(1), pp. 97 – 102, 2000.

[70] J. Gulmine and L. Akcelrud, 'FTIR characterization of aged xlpe', *Polymer Testing*, vol. 25(7), pp. 932 – 942, 2006.

[71] J. R. White and A. V. Shyichuk, 'Macromolecular scission and crosslinking rate changes during polyolefin photo-oxidation', *Polymer Degradation and Stability*, vol. 92(7), pp. 1161–1168, 2007.

[72] J. Jonsson, B. Ranby, F. Massines, D. Mary and C. Laurent, 'Spectral features of the luminescence of PE subjected to various excitation sources', *IEEE Transactions on Dielectrics and Electrical Insulation*, vol. 3 (6), pp. 859–865, 1996.

[73] P. K. Roy, P. Surekha, C. Rajagopal, S. N. Chatterjee and V. Choudhary, 'Studies on the photo-oxidative degradation of LDPE films in the presence of oxidised polyethylene', *Polymer Degradation and Stability*, vol. 92(6), pp. 1151–1160, 2007.

[74] P. Hedvig, *Dielectric Spectroscopy of Polymers*, Adam Hilger, Bristol, UK, 1977.

[75] L. Küpper, J. V. Gulmine, P. R. Janissek and H. M. Heise, 'Attenuated total reflection infrared spectroscopy for micro-domain analysis of polyethylene samples after accelerated ageing within weathering chambers', *Vibrational Spectroscopy*, vol. 34(1), pp. 63–72, 2004.

[76] C. Banmongkol, T. Mori, T. Mizutani, M. Ishioka and I. Ishino, 'Effects of oxidation on electrical conduction and breakdown of low-density polyethylene films with different densities', *Japanese Journal of Applied Physics*, vol. 37, pp. 872–877, 1998.

[77] A. Rivaton, J. L. Gardette, B. Mailhot and S. Morlat-Therlas, 'Basic aspects of polymer degradation', In the proceedings of *Conference on Macromolecules and Materials Science*, pp. 129–146, 2005.

[78] G. R. Cotten and W. Sacks, 'Oxidative crosslinking of polyethylene by ultraviolet light', *Journal of Polymer Science Part A: General Papers*, vol. 1 (4), pp. 1345–1351, 1963.

[79] F. Gugumus, 'Thermooxidative degradation of polyolefins in the solid state 4: Heterogeneous oxidation kinetics', *Polymer Degradation and Stability*, vol. 53(2), pp. 161–187, 1996.

[80] L. Ragnarsson and A. Albertsson, 'Total luminescence intensity as a tool to classify degradable polyethylene films by early degradation detection and changes in activation energy', *Biomacromolecules*, vol. 4(4), pp. 900–907, 2003.

[81] S. H. Lee, J. Park, C. R. Lee and K. S. Suh, 'The effect of low-molecular-weight species on space charge and conduction in LDPE', *IEEE Transactions on Dielectrics and Electrical Insulation*, vol. 4(4), pp. 425–432, 1997.

[82] X. Wang, N. Yoshimura, D. Tu, Y. Tanaka and T. Takada, 'Distribution characteristics and formation mechanism of space charge in PE materials', In the proceedings of *International Symposium on Electrical Insulating Materials*, pp. 109–112, 1998.

[83] Y. Sekii, T. Ohbayashi, T. Uchimura, U. Mochizuki and T. Maeno, 'The effects of material properties and inclusions on the space charge profiles of LDPE and XLPE', In the proceedings of *IEEE International Conference on Electrical Insulation and Dielectric Phenomena*, pp. 635–639, 2002.

[84] B. B. Miburo, 'Simplified lewis structure drawing for nonscience majors', *Journal of Chemical Education*, vol. 75(3), pp. 317 – 319, 1998.

[85] T. Mizutani, T. Tsukahara and M. Ieda, 'The effects of oxidation on the electrical conduction of polyethylene', *Journal of Physics D: Applied Physics*, vol. 13(9), pp. 1673 – 1679, 1980.

[86] H. Kon, Y. Suzuoki, T. Mizutani and T. Suzuki, 'Study of space-charge behavior in polyethylene for cable insulation by laser-induced-pressure-pulse technique', In the proceedings of *International Conference on Properties and Applications of Dielectric Materials*, pp. 383–386, 1994.

[87] T. Mizutani, S. Ikeda and M. Ieda, 'Oxidation-enhanced TSC and TSSP of polyethylene', *Japanese Journal of Applied Physics*, vol. 25, pp. 22–26, 1986.

[88] M. Ieda and Y. Suzuoki, 'Space charge and solid insulating materials: In pursuit of space charge control by molecular design', *IEEE Electrical Insulation Magazine*, vol. 13(6), pp. 10–17, 1997.

[89] R. Nath and M. M. Perlman, 'Steady-state bulk trap-modulated hopping conduction in doped linear low-density polyethylene', *Journal of Applied Physics*, vol. 65(12), pp. 4854–4858, 1989.

[90] T. Mizuno, Y. Liu, W. Shionoya, K. Yasuoka and S. Ishii, 'Investigation of charge injection in gas-impregenated polyethylene by measurement of electroluminescence under AC voltage', *Japanese journal of applied physics*, vol. 36(2), pp. 754–760, 1997.

[91] S. Le Roy, H. Miyake, Y. Tanaka, T. Takada, G. Teyssedre and C. Laurent, 'Simultaneous measurement of electroluminescence and space charge distribution in low density polyethylene under a uniform DC field', *Journal of Physics D: Applied Physics*, vol. 38(1), pp. 89–94, 2005.

[92] N. Hozumi, G. Teyssedre, C. Laurent and K. Fukunaga, 'Behaviour of space charge correlated with electroluminescence in cross-linked polyethylene', *Journal of Physics D: Applied Physics*, vol. 37(9), pp. 1327–1333, 2004.

[93] G. Teyssedre, G. Tardieu, D. Mary and C. Laurent, 'AC and DC electroluminescence in insulating polymers and implication for electrical ageing', *Journal of Physics D: Applied Physics*, vol. 34(14), pp. 2220–2229, 2001.

[94] C. Laurent, G. Teyssedre and G. C. Montanari, 'Time-resolved space charge and electroluminescence measurements in polyethylene under AC stress', *IEEE Transactions on Dielectrics and Electrical Insulation*, vol. 11(4), pp. 554–560, 2004.

[95] A. Fujita, S. S. Bamji, A. Abou-Dakka and A. T. Bulinski, 'Electroluminescence and space charge distribution in XLPE subjected to AC fields at various frequencies', In the proceedings of *IEEE International Conference on Electrical Insulation and Dielectric Phenomena*, pp. 772–775, 2007.

[96] A. M. Ariffin, P. L. Lewin, D. H. Mills and S. J. Dodd, 'The effect of voltage waveform on phase-resolved electroluminescence measurements', In the proceedings of *IEEE International Conference on Electrical Insulation and Dielectric Phenomena*, pp. 603 – 606, 2008.

[97] D. Mary and D. Malec, 'Electroluminescence measurements to detect accumulated charge at the electrode-insulator interface', *IEEE Transactions on Dielectrics and Electrical Insulation*, vol. 8(5), pp. 771–775, 2001.

[98] F. Baudoin, D. H. Mills, P. L. Lewin, S. Le Roy, G. Teyssedre and C. Laurent, 'Contribution to the modelling of electroluminescence in high voltage polymeric materials', In the proceedings of *IEEE International Conference on Electrical Insulation and Dielectric Phenomena*, 2010.

[99] C. Laurent, 'Optical prebreakdown warnings in insulating polymers', *IEEE Electrical Insulation Magazine*, vol. 15(2), pp. 5–13, 1999.

[100] G. Teyssedre, L. Cisse, D. Mary and C. Laurent, 'Identification of the components of the electroluminescence spectrum of PE excited in uniform fields', *IEEE Transactions on Dielectrics and Electrical Insulation*, vol. 6 (1), pp. 11–19, 1999.

[101] G. Teyssedre, L. Cisse, C. Laurent, F. Massines and P. Tiemblo, 'Spectral analysis of optical emission due to isothermal charge recombination in poly-

olefins', *IEEE Transactions on Dielectrics and Electrical Insulation*, vol. 5 (4), pp. 527–535, 1998.

[102] N. Shimizu and C. Laurent, 'Electrical tree initiation', *IEEE Transactions on Dielectrics and Electrical Insulation*, vol. 5(5), pp. 651–659, 1998.

[103] F. Zong-Huai, T. Takahashi, J. Suzuki, H. Miyata, S. Iemura, T. Itoh, T. Nakiri and N. Shimizu, 'Relation between electroluminescence and degradation in XLPE', *IEEE Transactions on Dielectrics and Electrical Insulation*, vol. 8(1), pp. 91–96, 2001.

[104] N. Shimizu, T. Mito, S. Mizuno and Y. Muramoto, 'Tree initiation at electroluminescence starting voltage in XLPE', In the proceedings of *IEEE International Conference on Electrical Insulation and Dielectric Phenomena*, pp. 670–673, 2008.

[105] T. Mizuno, Y. S. Liu, W. Shionoya, K. Yasuoka, S. Ishii, H. Miyata and A. Yokoyama, 'Electroluminescence in insulating polymers in AC electric fields', *IEEE Transactions on Dielectrics and Electrical Insulation*, vol. 4 (4), pp. 433–438, 1997.

[106] C. Laurent and G. Teyssedre, 'Hot electron and partial-discharge induced ageing of polymers', In the proceedings of *International Symposium on Ionizing Radiation and Polymers*, pp. 442–447, 2003.

[107] W. W. Piper and F. E. Williams, 'Theory of electroluminescence', *Physics Review*, vol. 98(6), pp. 1809–1813, 1955.

[108] J. Jonsson, B. Ranby, D. Mary, C. Laurent and C. Mayoux, 'Electroluminescence from polyolefins subjected to a homogeneous AC field', *IEEE Transactions on Dielectrics and Electrical Insulation*, vol. 2(1), pp. 107–113, 1995.

[109] S. Le Roy, G. Teyssedre and C. Laurent, 'Charge transport and dissipative processes in insulating polymers: Experiments and model', *IEEE Transactions on Dielectrics and Electrical Insulation*, vol. 12(4), pp. 644–654, 2005.

[110] G. Teyssedre and C. Laurent, 'Evidence of hot electron-induced chemical degradation in electroluminescence spectra of polyethylene', *Journal of Applied Physics*, vol. 103(4), 2008.

[111] J. M. Alison, J. V. Champion, S. J. Dodd and G. C. Stevens, 'Dynamic bipolar charge recombination model for electroluminescence in polymer-based insulation during electrical tree initiation', *Journal of Physics D: Applied Physics*, vol. 28(8), pp. 1693–1701, 1995.

[112] P. L. Lewin, S. J. Dodd and A. M. Ariffin, 'Simulation of electroluminescence using a bipolar recombination model', In the proceedings of *IEEE International Conference on Solid Dielectrics*, pp. 15–18, 2007.

[113] C. Laurent, C. Mayoux and S. Noel, 'Mechanisms of electroluminescence during aging of polyethylene', *Journal of Applied Physics*, vol. 58(11), pp. 4346–4353, 1985.

[114] S. S. Bamji, 'Electroluminescence - a technique to detect the initiation of degradation in polymeric insulation', *IEEE Electrical Insulation Magazine*, vol. 15(3), pp. 9–14, 1999.

[115] K. I. Wong, P. L. Lewin and S. J. Dodd, 'Electroluminescence phenomena of low density polyethylene film under applied AC voltage', In the proceedings of *IEEE International Conference on Electrical Insulation and Dielectric Phenomena*, pp. 245–248, 2003.

[116] S. J. Dodd, P. L. Lewin and K. I. Wong, 'Phase resolved electroluminescence measurements in thin films of low density polyethylene using a charge coupled device camera', *IEEE Transactions on Dielectrics and Electrical Insulation*, vol. 13(1), pp. 168–180, 2006.

[117] S. S. Bamji, A. T. Bulinski and M. Abou-Dakka, 'Luminescence and space charge in polymeric dielectrics', *IEEE Transactions on Dielectrics and Electrical Insulation*, vol. 16(5), pp. 1376–1392, 2009.

[118] D. Mary, G. Teyssedre and C. Laurent, 'Electroluminescence in saturated polyesters: Temperature dependence and correlation with space charge measurements', In the proceedings of *IEEE International Conference on Electrical Insulation and Dielectric Phenomena*, pp. 201 – 204, 2003.

[119] K. I. Wong, PhD thesis: *Study of Early Electrical Aging of Polyethylene using Electroluminescence Technique*, University of Southampton, School of Electronics and Computer Science, 2003.

[120] A. M. Ariffin, P. L. Lewin and S. J. Dodd, 'The influence of absorbed gases on electroluminescence phenomenon in polymeric materials subjected to high

electrical stress', In the proceedings of *IEEE International Conference on Electrical Insulation and Dielectric Phenomena*, pp. 33–36, 2007.

[121] L. Cisse, G. Teyssedre, D. Mary and C. Laurent, 'Influence of frequency, electrode material and superimposed DC on AC electroluminescence in polymer films', *IEEE Transactions on Dielectrics and Electrical Insulation*, vol. 9(1), pp. 124–129, 2002.

[122] A. S. Alghamdi, D. H. Mills and P. L. Lewin, 'Influence of ageing on space charge and electroluminescence of epoxy resin', In the proceedings of *IEEE International Conference on Solid Dielectrics*, pp. 88 – 91, 2010.

[123] J. Jonsson, B. Ranby, C. Laurent and C. Mayoux, 'Influence of thermal and UV aging on electroluminescence of polypropylene films', *IEEE Transactions on Dielectrics and Electrical Insulation*, vol. 3(1), pp. 148 –152, 1996.

[124] D. Mary, G. Teyssedre and C. Laurent, 'UV-induced degradation of poly(ethylene naphthalate) films from the standpoint of electrical and luminescence properties', In the proceedings of *IEEE International Conference on Electrical Insulation and Dielectric Phenomena*, pp. 165 – 168, 2001.

[125] G. Teyssedre, D. Mary, J. L. Auge and C. Laurent, 'Dependence of electroluminescence intensity and spectral distribution on ageing time in polyethylene napthalate as modelled by space charge modified internal field', *Journal of Physics D: Applied Physics*, vol. 32, pp. 2296–2305, 1999.

[126] V. G. Barkhudaryan, 'Alterations of molecular characteristics of polyethylene under the influence of uv-radiation', *Polymer*, vol. 41(15), pp. 5787–5791, 2000.

[127] P. C. N. Scarpa and D. K. Das-Gupta, 'Dielectric spectroscopy of polyethylene with and without carbon black', In the proceedings of *IEEE International Symposium on Electrical Insulation*, pp. 149–152, 1998.

[128] L. K. Martin and C. Q. Yang, 'Infrared spectroscopy studies of the photooxidation of a polyethylene nonwoven fabric', *Journal of Polymers and the Environment*, vol. 2, pp. 153–160, 1994.

[129] P. Europa, 'Riblene FF20 - low density polyethylene technical data sheet', *provided by supplier*, 2010.

[130] P. Gijsman and J. Sampers, 'The influence of oxygen pressure and temperature on the UV-degradation chemistry of polyethylene', *Polymer Degradation and Stability*, vol. 58, pp. 55–59, 1997.

[131] F. Oldervoll and E. Ildstad, 'Space charge, oxidation and morphology changes in low density polyethylene during high voltage DC ageing', In the proceedings of *IEEE International Symposium on Electrical Insulation*, pp. 477–480, 2000.

[132] F. Khabbaz, A. Albertsson and S. Karlsson, 'Chemical and morphological changes of environmentally degradable polyethylene films exposed to thermo-oxidation', *Polymer Degradation and Stability*, vol. 63(1), pp. 127–138, 1999.

[133] H. B. Ltd., 'Technical data on clear fused quartz', online: http://www.h-baumbach.co.uk/, October, 2011.

[134] B. H. Stuart, *Infrared Spectroscopy: Fundamentals and Applications*, John Wiley & Sons, Ltd., London, UK, 2004.

[135] ASTM, 'Standard test method for dielectric breakdown voltage and dielectric strength of solid electrical insulating materials at commercial power frequencies ASTM D149-97a', standard no. *D149-97a*, 2004.

[136] M. Reading, PhD thesis: *An Investigation into the Structure and Properties of Polyethylene Oxide Nanocomposites*, University of Southampton, School of Electronics and Computer Science, 2010.

[137] I. L. Hosier, A. S. Vaughan and S. G. Swingler, 'The effects of measuring technique and sample preparation on the breakdown strength of polyethylene', *IEEE Transactions on Dielectrics and Electrical Insulation*, vol. 9(3), pp. 353–361, 2002.

[138] C. P. Martin, A. S. Vaughan and S. J. Sutton, 'On morphology, molecular composition and breakdown behaviour in semi-crystalline polymers', In the proceedings of *IEEE International Conference on Electrical Insulation and Dielectric Phenomena*, pp. 309 – 312, 2003.

[139] G. Chen and A. E. Davies, 'The influence of defects on the short-term breakdown characteristics and long-term dc performance of LDPE insulation', *IEEE Transactions on Dielectrics and Electrical Insulation*, vol. 7(3), pp. 401–407, 2000.

[140] C. D. Green, PhD thesis: *Polyethylene-Montmorillonite Nanocomposites*, University of Southampton, School of Electronics and Computer Science, 2008.

[141] I. L. Hosier, PhD thesis: *Morphology and Electrical Properties of Polyethylene*, University of Reading, Department of Physics, 1996.

[142] G. Gherbaz, PhD thesis: *Nanostructured Polymers: Morphology and Properties*, University of Southampton, School of Electronics and Computer Science, 2009.

[143] E. Schlosser and A. Schnhals, 'Recent development in dielectric relaxation spectroscopy of polymers', *Colloid & Polymer Science*, vol. 267, pp. 963–969, 1989.

[144] T. Liu, J. Fothergill, S. Dodd and U. Nilsson, 'Dielectric spectroscopy measurements on very low loss cross-linked polyethylene power cables', *Journal of Physics: Conference Series*, vol. 183(1), 2009.

[145] G. Chen, 'Interfaces and space charge in polymeric insulating materials', In the proceedings of *Materials Research Society Symposium*, 2005.

[146] T. Takada, Y. Tanaka, N. Adachi and X. Q., 'Comparison between the PEA method and the PWP method for space charge measurement in solid dielectrics', *IEEE Transactions on Dielectrics and Electrical Insulation*, vol. 5(6), pp. 944–951, 1998.

[147] G. Chen, T. Y. G. Tay, A. E. Davies, Y. Tanaka and T. Takada, 'Electrodes and charge injection in low-density polyethylene - using the pulsed electroacoustic technique', *IEEE Transactions on Dielectrics and Electrical Insulation*, vol. 8(6), pp. 867–873, 2001.

[148] G. Chen, Y. L. Chong and M. Fu, 'Calibration of the pulsed electroacoustic technique in the presence of trapped charge', *Measurement Science and Technology*, vol. 17(7), pp. 1974–1980, 2006.

[149] G. Chen and Z. Xu, 'Space charge dynamics in low density polyethylene under DC electric fields', *Journal of Physics: Conference Series*, vol. 142, 2008.

[150] T. Maeno, T. Futami, H. Kushibe, T. Takada and C. M. Cooke, 'Measurement of spatial charge distribution in thick dielectrics using the pulsed

electroacoustic method', *IEEE Transactions on Electrical Insulation*, vol. 23 (3), pp. 433–439, 1988.

[151] K. Bambery and R. Fleming, 'The temperature dependence of space charge accumulation in cross-linked polyethylene', *Journal of Thermal Analysis and Calorimetry*, vol. 50, pp. 19–31, 1997.

[152] S. Delpino, D. Fabiani, G. C. Montanari, C. Laurent, G. Teyssedre, P. H. F. Morshuis, R. Bodega and L. A. Dissado, 'Polymeric HVDC cable design and space charge accumulation. Part 2: Insulation interfaces', *IEEE Electrical Insulation Magazine*, vol. 24(1), pp. 14 –24, 2008.

[153] F. L. Pedrotti, L. M. Pedrotti and L. S. Pedrotti, *Introduction to Optics*, Pearson Prentice Hall, 3rd edition, 2007.

[154] P. Instruments, 'Datasheet for ProEM: 512B rev. M.2', *provided by manufactuer*, 2009.

[155] G. Teyssedre, J. L. Franceschi and C. Laurent, 'Cathodo- and electroluminescence spectra in insulating polymers: A parallel approach for inferring electrical ageing mechanisms', In the proceedings of *IEEE International Conference on Electrical Insulation and Dielectric Phenomena*, 2007.

[156] M. S. Robbins and B. J. Hadwen, 'The noise performance of electron multiplying charge-coupled devices', *IEEE Transactions on Electron Devices*, vol. 50(5), pp. 1227–1232, 2003.

[157] S. M. Tulloch and V. S. Dhillon, 'On the use of electron-multiplying CCDs for astronomical spectroscopy', *Monthly Notices of the Royal Astronomical Society*, vol. 411(1), pp. 211–225, 2011.

[158] P. Instruments, 'ProEM^{TM} EMCCD camera system user manual', *provided by manufacturer*, 2009.

[159] Q. Technologies, 'K550X sputter coater instruction manual', *provided by manufacturer*, 2007.

[160] P. Instruments, 'Datasheet for PI-MAX3: 1024i rev. M.1', *provided by manufacturer*, 2009.

[161] S. S. Bamji, A. T. Bulinski, L. Cisse and K. Tohyama, 'Effect of frequency on XLPE cable insulation at high electric field', In the proceedings of *IEEE International Conference on Electrical Insulation and Dielectric Phenomena*, pp. 169 –172, 2001.

[162] M. T. Inc., 'Datasheet for PIC16F627A/628A/648A', *provided by manufacturer*, 2007.

[163] R. Allen, 'Princeton Instruments, imaging applications specialist', *private communication*, 2009.

[164] G. Zhang, K. Yang, M. Dong, W. Zhao and Z. Yan, 'Surface electroluminescence phenomena correlated with trapping parameters of insulating polymers', *Applied Surface Science*, vol. 254, pp. 1450–1455, 2007.

[165] P. Elmer, 'Technical specifications for the LAMBDA 25/35/45 UV/Vis spectrophotometers', *provided by manufacture*, 2004.

[166] DC Scientific, 'Refractive index standards', online: http://dcglass.com/products-and-services/measurement-calibration-standards/refractive-index-standards, 2011.

[167] M. Daimon and A. Masumura, 'Measurement of the refractive index of distilled water from the near-infrared region to the ultraviolet region', *Applied Optics*, vol. 46(18), pp. 3811–3820, 2007.

[168] T. M. Aminabhavi, V. B. Patil, M. I. Aralaguppi, J. D. Ortego and K. C. Hansen, 'Density and refractive index of the binary mixtures of cyclohexane with dodecane, tridecane, tetradecane, and pentadecane at (298.15, 303.15, and 308.15) k', *Journal of Chemical & Engineering Data*, vol. 41 (3), pp. 526–528, 1996.

[169] F. M. Rugg, J. J. Smith and R. C. Bacon, 'Infrared spectrophotometric studies on polyethylene. II. oxidation', *Journal of Polymer Science*, vol. 13 (72), pp. 535 – 547, 1954.

[170] P. Roy, P. Surekha, C. Rajagopal and V. Choudhary, 'Effect of cobalt carboxylates on the photo-oxidative degradation of low-density polyethylene. part-i', *Polymer Degradation and Stability*, vol. 91(9), pp. 1980 – 1988, 2006.

[171] B. Valeur, *Molecular Fluorescence: Principles and Applications*, John Wiley & Sons, London, UK, 2002.

[172] G. Teyssedre, C. Laurent, G. C. Montanari, A. Campus and U. H. Nilsson, 'From LDPE to XLPE: Investigating the change of electrical properties. part II: Luminescence', *IEEE Transactions on Dielectrics and Electrical Insulation*, vol. 12(3), pp. 447–454, 2005.

[173] C. Laurent, F. Massines, C. Mayoux, D. Ryder, M. and C. Olliff, 'Comparison between photo- and electro-induced luminescence spectra of polyethylene', In the proceedings of *IEEE International Conference on Electrical Insulation and Dielectric Phenomena*, pp. 93–96, 1995.

[174] C. W. G. Charlston, D. M. Ryder, C. J. Olliff, C. Laurent, F. Massines, G. Teyssedre and P. Tiemblo, 'The use of luminescence spectroscopy to evaluate oxidation processes in polyolefin films', In the proceedings of *IEEE Internation Conference on Electrical Insulation and Dielectric Phenomena*, pp. 250–253, 1997.

[175] H. A. Khonakdar, S. H. Jafari, M. Taheri, U. Wagenknecht, D. Jehnichen and L. Hussler, 'Thermal and wide angle x-ray analysis of chemically and radiation-crosslinked low and high density polyethylenes', *Journal of Applied Polymer Science*, vol. 100(4), pp. 3264–3271, 2006.

[176] ASTM, 'Standard test methods for determination of gel content and swell ratio of crosslinked etyhlene plastics', standard no. *D2765-01*, 2006.

[177] K. Sirisinha and S. Chimdist, 'Comparison of techniques for determining crosslinking in silane-water crosslinked materials', *Polymer Testing*, vol. 25 (4), pp. 518–526, 2006.

[178] J. V. Gulmine and L. Akcelrud, 'Correlations between the processing variables and morphology of crosslinked polyethylene', *Journal of Applied Polymer Science*, vol. 94(1), pp. 222 – 230, 2004.

[179] M. Celina and G. A. George, 'Characterisation and degradation studies of peroxide and silane crosslinked polyethylene', *Polymer Degradation and Stability*, vol. 48(2), pp. 297–312, 1995.

[180] D. Gheysari and A. Behjat, 'Radiation crosslinking of LDPE and HDPE with 5 and 10 MeV electron beams', *European Polymer Journal*, vol. 37 (10), pp. 2011–2016, 2001.

[181] Q. Wu and B. Qu, 'Photoinitiating characteristics of benzophenone derivatives as new initiators in the photocrosslinking of polyethylene', *Polymer Engineering and Science*, vol. 41(7), pp. 1220–1226, 2001.

[182] D. Miličević, S. Trifunović, M. Popović, T. V. Milić and E. Suljovrujić, 'The influence of orientation on the radiation-induced crosslinking/oxidative behavior of different PEs', *Nuclear Instruments and Methods in Physics Research Section B*, vol. 260(2), pp. 603–612, 2007.

[183] B. Ränby, 'Photoinitiated modifications of polymers: Photocrosslinking, surface photografting and photolamination', *Materials Research Innovations*, vol. 2, pp. 64–71, 1998.

[184] L. Tang, M. Yan, C. Liu, P. Wang and B. Qu, 'Effect of UV-photocrosslinking on the nonisothermal crystallization kinetics of polyethylene', *Journal of Applied Polymer Science*, vol. 108(1), pp. 174–180, 2008.

[185] B. Qu and B. Ränby, 'Photocross-linking of low-density polyethylene. II. structure and morphology', *Journal of Applied Polymer Science*, vol. 48(4), pp. 711–719, 1993.

[186] Y. Kong and J. N. Hay, 'The enthalpy of fusion and degree of crystallinity of polymers as measured by dsc', *European Polymer Journal*, vol. 39(8), pp. 1721 – 1727, 2003.

[187] F. Khabbaz, A. Albertsson and S. Karlsson, 'Trapping of volatile low molecular weight photoproducts in inert and enhanced degradable LDPE', *Polymer Degradation and Stability*, vol. 61(2), pp. 329–342, 1998.

[188] H. Khonakdar, S. Jafari, U. Wagenknecht and D. Jehnichen, 'Effect of electron-irradiation on cross-link density and crystalline structure of low- and high-density polyethylene', *Radiation Physics and Chemistry*, vol. 75 (1), pp. 78 – 86, 2006.

[189] M. Sanchis, V. Blanes, M. Blanes, D. Garcia and R. Balart, 'Surface modification of low density polyethylene (LDPE) film by low pressure O2 plasma treatment', *European Polymer Journal*, vol. 42(7), pp. 1558–1568, 2006.

[190] M. Ieda, 'Dielectric breakdown process of polymers', *IEEE Transactions on Electrical Insulation*, vol. 15(3), pp. 206–224, 1980.

[191] T. Takahashi, H. Ohtsuka, H. Takehana and T. Niwa, 'Study on improvements to the dielectric breakdown strength of extruded dielectric cables', *IEEE Transactions on Power Apparatus and Systems*, vol. PAS-104(8), pp. 1945 –1950, 1985.

[192] Y. Ohki, N. Fuse, S. Hikosaka, Y. Takemura, M. Mizuno and K. Fukunaga, 'Complex permittivity spectra of several insulating polymers at electrical and THz frequencies', In the proceedings of *IEEE International Conference on Electrical Insulation and Dielectric Phenomena*, pp. 7 –10, 2009.

[193] D. Kostoski, J. Dojčilović, L. Novaković and E. Suljovrujić, 'Effects of charge trapping in gamma irradiated and accelerated aged low-density polyethylene', *Polymer Degradation and Stability*, vol. 91(9), pp. 2229–2232, 2006.

[194] F. Kremer, A. Schönhals, P. Lunkenheimer, A. Loidl, A. Huwe, S. A. Rózański, G. Floudas, J. Mijlovic, P. A. M. Steeman, J. V. Turnhout, R. Böhmer, G. Diezemann, R. Richert and T. Pakula, *Broadband Dielectric Spectroscopy*, Springer, 2003.

[195] D. N. Long, PhD thesis: *Impulse Ageing of Polymeric Materials*, University of Southampton, School of Electronics and Computer Science, Southampton, 2011.

[196] D. K. Das-Gupta, 'Dielectric and related molecular processes in polymers', *IEEE Transactions on Dielectrics and Electrical Insulation*, vol. 8(1), pp. 6–14, 2001.

[197] F. Kremer, 'Dielectric spectroscopy yesterday, today and tomorrow', *Journal of Non-Crystalline Solids*, vol. 305(1-3), pp. 1 – 9, 2002.

[198] Z. Zorn, 'Logarithmic moments of relaxation time distributions', *The Journal of Chemical Physics*, vol. 116(8), pp. 3204–3209, 2002.

[199] P. Sanzi, F. Monti, G. C. Montanari and D. K. Das-Guptaz, 'Polarization behaviour of cross-linked polyethylene (XLPE)', In the proceedings of *International Symposium on Electrets*, pp. 47–50, 1999.

[200] M. M. Perlman and A. Kumar, 'Injection-limited trap modulated hopping conduction in carbonyl doped polyethylene', *Journal of Applied Physics*, vol. 72(11), pp. 5265–5268, 1992.

[201] J. P. Crine, S. Pelissou, Y. McNicoll and H. St-Onge, 'A critical evaluation of analytical techniques for the characterization of extruded dielectric cables', *IEEE Transactions on Electrical Insulation*, vol. 26(1), pp. 131–139, 1991.

[202] E. Suljovrujic, 'Gel production, oxidative degradation and dielectric properties of isotactic polypropylene irradiated under various atmospheres', *Polymer Degradation and Stability*, vol. 94(4), pp. 521–526, 2009.

[203] E. Suljovrujic, 'Some aspects of structural electrophysics of irradiated oriented LLDPE', *Nuclear Instruments and Methods in Physics Research Section B: Beam Interactions with Materials and Atoms*, vol. 236(1-4), pp. 399–406, 2005.

[204] A. M. Ariffin, P. L. Lewin and S. J. Dodd, 'Electroluminescence measurements of low-density polyethylene (LDPE) films subjected to high electrical stresses in different gas environments', *IEEE Transactions on Dielectrics and Electrical Insulation*, vol. 18(1), pp. 130–139, 2011.

[205] *Thor Labs Catalogue*, volume 21, Thor Labs, 2011.

[206] S. Le Roy, G. Teyssedre, C. Laurent, G. C. Montanari and F. Palmieri, 'Description of charge transport in polyethylene using a fluid model with a constant mobility: fitting model and experiments', *Journal of Physics D: Applied Physics*, vol. 39(7), pp. 1427 – 1436, 2006.

[207] R. W. Hare, R. M. Hill and C. J. Budd, 'Modelling charge injection and motion in solid dielectrics under high electric field', *Journal of Physics D: Applied Physics*, vol. 26(7), pp. 1084–1093, 1993.

[208] F. Baudoin, D. H. Mills, P. L. Lewin, S. Le Roy, G. Teyssedre and C. Laurent, 'Modeling transient effects in AC electroluminescence of insulating polymers due to voltage offset or space charge', , Awaiting submission, 2011.

[209] J. Zhao, Z. Xu, G. Chen and P. L. Lewin, 'Space charge behavior in polyethylene under ac electric fields', In the proceedings of *IEEE International Conference on Electrical Insulation and Dielectric Phenomena*, pp. 105–108, 2011.

[210] T. Maeno and K. Fukunaga, 'High-resolution PEA charge distribution measurement system', *IEEE Transactions on Dielectrics and Electrical Insulation*, vol. 3(6), pp. 754–757, 1996.

[211] F. Baudoin, D. H. Mills, P. L. Lewin, S. Le Roy, G. Teyssedre and C. Laurent, 'Modelling electroluminescence in insulating polymers under sinusoidal stress: Effect of applied voltage, frequency and offset', In the proceedings of *IEEE International Conference on Electrical Insulation and Dielectric Phenomena*, 2011.

[212] P. Hammond and J. K. Sykulski, *Engineering Electromagnetism: Physical Processes and Computation*, Oxford University Press, Oxford, UK, 1994.

[213] T. Mizutani and M. Ieda, 'TSC from corona-charged high-density polyethylene and the effects of oxidation', *Journal of Physics D: Applied Physics*, vol. 11(2), pp. 185–191, 1978.

[214] G. Chen, L. S. Zhong, H. K. Xie, H. M. Banford and A. E. Davies, 'The influence of oxidation on space charge formation in gamma-irradiated low-density polyethylene', *Radiation Physics and Chemistry*, vol. 66(3), pp. 247–255, 2003.

[215] K. S. Suh, J. H. Koo, S. H. Lee, J. K. Park and T. Takada, 'Effects of sample preparation conditions and short chains on space charge formation in LDPE', *IEEE Transactions on Dielectrics and Electrical Insulation*, vol. 3 (2), pp. 153–160, 1996.

[216] Y. Suzuoki, T. Furuta, H. Yamada, S. O. Han, T. Mizutani, M. Ieda and N. Yoshifuji, 'Study of space charge in polyethylene by direct probing: Effects of oxidation', *IEEE Transactions on Electrical Insulation*, vol. 26 (6), pp. 1073–1079, 1991.

[217] H. Devendrappa, U. V. Subba Rao and M. V. N. Ambika Prasad, 'Study of dc conductivity and battery application of polyethylene oxide/polyaniline and its composites', *Journal of Power Sources*, vol. 155(2), pp. 368–374, 2006.

[218] R. Mishra and K. J. Rao, 'Electrical conductivity studies of poly(ethyleneoxide)-poly(vinylalcohol) blends', *Solid State Ionics*, vol. 106 (12), pp. 113–127, 1998.

[219] E. R. Neagu and J. N. Marat-Mendes, 'Space-charge-controlled conductivity in low-density polyethylene', *Applied Physics Letters*, vol. 82(12), pp. 1920–1922, 2003.

[220] M. Goshowaki, I. Endoh, K. Noguchi, U. Kawabe and Y. Sekii, 'Influence of antioxidants on electrical conduction in LDPE and XLPE', *Journal of Electrostatics*, vol. 65(9), pp. 551–554, 2007.

[221] S. Katakai and K. Yahagi, 'Effect of thermal ageing on breakdown strength of polyethylene', *Japanese Journal of Applied Physics*, vol. 24, pp. 441–445, 1985.

[222] K. Tohyama, S. S. Bamji and A. T. Bulinski, 'Simultaneous measurement of electroluminescence and dissipation current in cable insulation', In the proceedings of *International Conference on Properties and Applications of Dielectric Materials*, pp. 1051 – 1054, 2003.

[223] S. Imai, K. Tohyama, Y. Murakami and M. Nagao, 'Frequency dependence of electroluminescence and dissipation current waveform in LDPE film', In the proceedings of *IEEE International Conference on Electrical Insulation and Dielectric Phenomena*, 2008.

[224] M. Nagao, M. Kosaki, K. Tohyama and T. Tokoro, 'High-field dissipation current waveform in e-beam-irradiated XLPE film at high temperature', *IEEE Transactions on Dielectrics and Electrical Insulation*, vol. 3(3), pp. 375–379, 1996.

[225] M. Nedjar, 'Effect of thermal aging on the electrical properties of crosslinked polyethylene', *Journal of Applied Polymer Science*, vol. 111(4), pp. 1985–1990, 2009.

Appendices

Appendix A

ProEM Quantum Efficiency

Figure A.1 shows the quantum efficiency of the EMCCD camera used to detect EL [154].

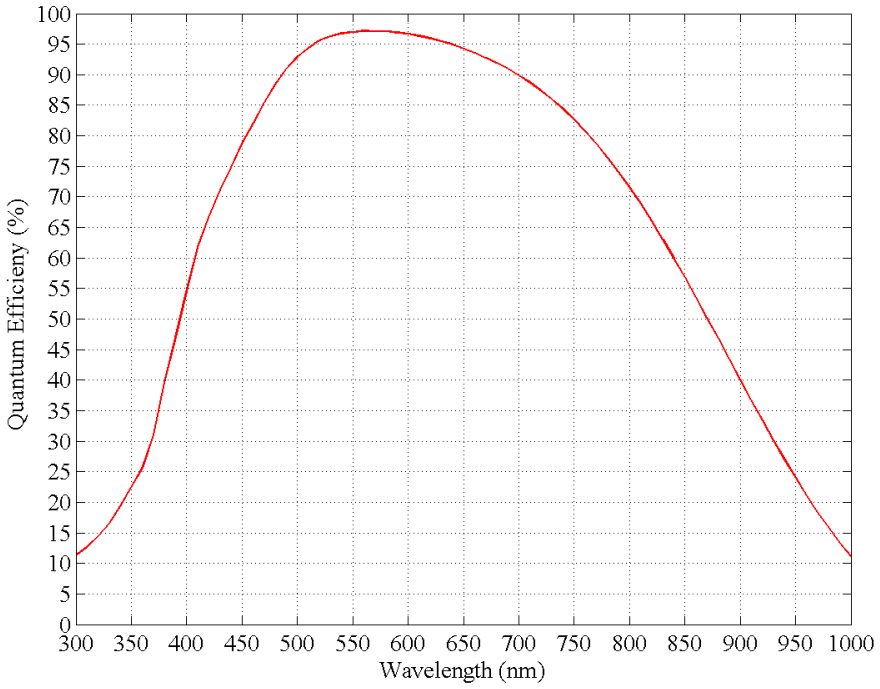

FIGURE A.1: Quantum efficiency of ProEM

Appendix B

Point on Wave Electroluminescence

B.1 Custom Built Trigger System

A custom built system was assembled to trigger the detection system for measuring EL. The system waited until the camera was ready to take an exposure and then until the zero crossing point of the applied field was reached. Each subsequent exposure was then taken as soon as the camera was ready, this process set out previously in figure 3.17. The circuit arrangement of the PIC chip is shown in figure B.1 and the code programmed onto it written in assembler shown below.

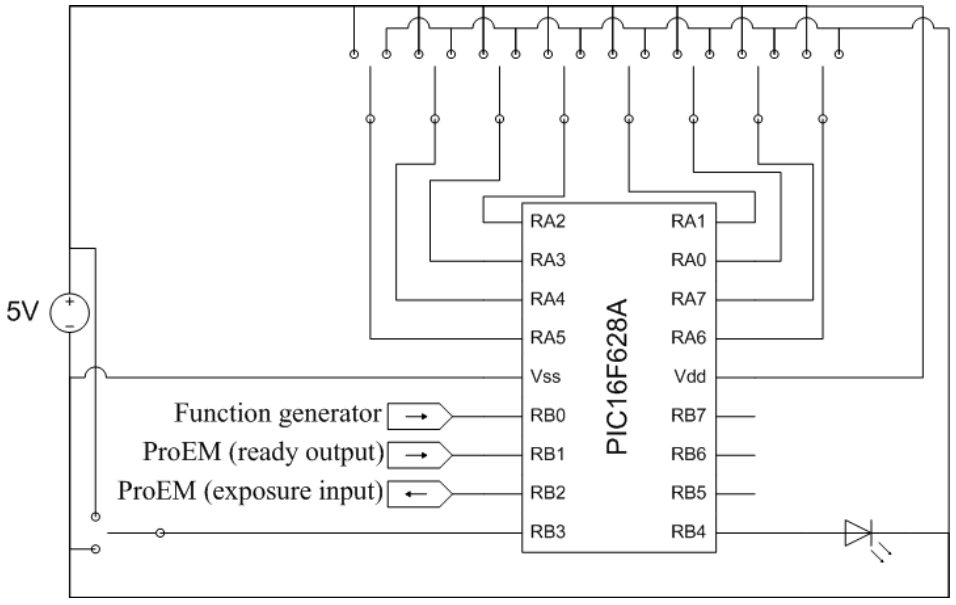

FIGURE B.1: Circuit diagram for the custom built trigger system

```
;Triggers the camera based on the zero crossing point of the ...
    applied voltage and the status of the camera
;General Registers
    STATUS = 03h      ;Status register
      RP0 = 5h        ;RP0 and RP1 used for setting memory banks
      RP1 = 6h

;Port and data flow control
    PORTA = 05h           ;User setting for number of exposures ...
     (input)
    PORTB = 06h
     RB)   = 0h       ;Ready signal from ProEM (input)
     FGEN = 1h        ;Function generator zero crossing point (input)
      RB2   = 2h       ;Trigger to ProEM (output)
      RB3   = 3h       ;Start measurement switch (input)
      RB4   = 4h       ;LED to show system is running (output)
    TRISA = 85h           ;TRIS used to control I/O of Port A and ...
     Port B
    TRISB = 86h
    CMCON = 1Fh           ;Controls analogue comparators in Port A

;Variables
    COUNT = 21h           ;COUNT and STORE used for delay circuit
    COUNT1 = 22h
    STORE = 23h
    STORE1 = 24h

;Initialise
  MOVLW 0x07            ;Turn comparitors on PORTA off
  MOVWF  CMCON           ;Set  ports for I/O
  BCF        STATUS,  RP1     ;Move to memory bank 1
  BSF        STATUS,  RP0
    MOVLW   0xEB
    MOVWF    TRISB          ;Set all portB to inputs except RB2
    MOVLW   0xff
    MOVWF    TRISA          ;Set all portA to inputs
  BCF        STATUS,  RP0     ;Move to memory bank 0
  BCF        STATUS,  RP1

  BCF        PORTB,   RB2     ;Initialise LED and trigger is off
  BCF        PORTB,   RB4

;Setup Exposure Counter
  CLRF   COUNT           ;Clear COUNT and STORE registers
  CLRF   COUNT1
```

```
43    CLRF    STORE
44    CLRF    STORE1
45
46      MOVLW    0x0A
47      MOVWF     STORE           ;Decimal value of 10 used for inner loop
48
49  ;Begin
50   INITIAL BCF      PORTB,  RB4  ;Turn LED off
51          BTFSS    PORTB,
       RB3        ;Checks if start switch by operator
52              GOTO     INITIAL               ;If not waits until has
53          MOVF     PORTA, 0              ;Reads PORTA and puts into ...
       STORE1 for outer delay
54          MOVWF    STORE1
55
56          MOVF     STORE,  0           ;Copy STORE to COUNT, COUNT ...
       reduces during loop
57        MOVWF  COUNT               ;so restores to original value
58          MOVF     STORE1, 0
59        MOVWF  COUNT1
60
61          BSF      PORTB,   RB4       ;Turn LED on - operating
62
63  ;Zero crossing point
64  ;Waits for low incase started mid way through a pulse
65   TRIGLOW BTFSC    PORTA, FGEN ;If trigger input is low then continues
66      GOTO
       TRIGLOW     ;Otherwise repeats check until trigger input is low
67      ;Debounce code to check system is actually low before continueing
68             BTFSC     PORTA, FGEN
69         GOTO      TRIGLOW
70         BTFSC     PORTA, FGEN
71         GOTO      TRIGLOW
72  ;Waits for zero crossing point
73   TRIGGER BTFSS    PORTA, FGEN ;Tests to see if value has gone high
74      GOTO     TRIGGER     ;Loops until goes high
75      ;Debounce code to check system remains high and isn't an ...
       aritificial measurement
76         BTFSS     PORTA, FGEN
77         GOTO      TRIGGER
78         BTFSS     PORTA, FGEN
79         GOTO      TRIGGER
80      BSF  PORTB, LED          ;Turns LED on
81
82      BTFSS    PORTB,
       RB0     ;Test to check ProEM is waiting for trigger
```

```
83              GOTO     TRIGLOW       ;If not waits for next ...
    synchronisation trigger so that there is a known delay
84                           ;between zero crossing and first exposure
85          BSF      PORTB,  RB2     ;Sets the trigger for the camera ...
    high if it is waiting for a trigger then
86                           ;continues with rest of counter
87          GOTO     READOUT         ;This moves it into the counter ...
    loop, shouldn't return here until after x
88                           ;exposures completed
89
90 ;Loop for between each set
91  PREREAD BTFSS    PORTB,
      RB0  ;Test to check system is waiting for trigger
92      GOTO     PREREAD            ;If not continues to loop
93      BSF      PORTB,  RB2        ;Turns trigger output on once ...
    ProEM is waiting for trigger
94
95  READOUT BTFSC    PORTB,
      RB0  ;Test if camera has received trigger and is now exposing
96              GOTO     READOUT          ;Loop if it hasn't
97      BCF      PORTB,   RB2        ;Turn trigger output off so new ...
    rising edge for next trigger
98
99      DECFSZ   COUNT           ;Reduce the inner counter value
100             GOTO     PREREAD     ;Exposes agein if not zero
101         MOVF
    STORE,  0       ;Move contents of STORE register to WORK register
102         MOVWF
    COUNT             ;Reset COUNT to original value for inner loop
103         DECFSZ
    COUNT1      ;Decrease COUNT1 register and see if zero
104             GOTO     PREREAD     ;Expose again if not zero
105         GOTO     INITIAL         ;Return to beginning to ...
    re-synchronize with applied field
106  end
```

B.2 Confirmation of POW trigger system

To confirm the timing accuracy and operation of the EL detection system an light emitting diode (LED) was used. The LED was connected to a PIC chip and monitored the zero crossing point output from the function generator. At the zero-crossing point the LED was turned on for approximately 1 ms, repeating on ever cycle of the ac field. The EL detection system then operated as if collecting EL measurements, except with the EM amplification at 1 (rather than 100) due to the stronger emission. The comparison shown in figure B.2 shows the measured light to increase at approximately same point as the turn on of the LED, both occurring marginally after the zero crossing point of the applied field. The time delay between the applied field and the LED can be put down to delays in the PIC chip and triggering system and therefore accounted for in the post processing of the EL POW measurements.

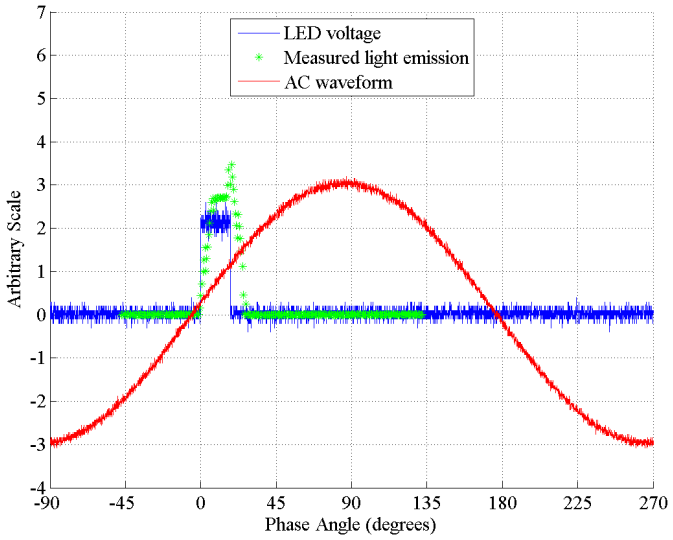

FIGURE B.2: LED emission to confirm timing accuracy of EL detection system

The code used on the PIC to control the LED is shown below.

```
; This code turns an LED on and off in sync with the applied field
; The default setting is to turn the LED on and off after 1 ms
; ---- CODE ----
;CONSTANTS
;General Variables
    STATUS = 03h     ;Status register
     RP0 = 5h        ;RP0 and RP1 used for setting memory banks
     RP1 = 6h
```

```
;Ports
    PORTA = 05h      ;Port A – Inputs
     FGEN = 0h       ;RA0 – Pulse from Fgenerator
    PORTB = 06h      ;Port B – Outputs
     LED = 2h        ;RB2 – LED control
;Port Control
    TRISA = 85h      ;TRIS used to control I/O setting Port A / B
    TRISB = 86h
    CMCON = 1Fh      ;Controls analogue comparators in Port A

;Variables
    STORE1 = 21h     ;Variables for storing delays
    STORE2 = 22h
    STORE3 = 23h
    COUNT1 = 24h     ;Temporay store as delay decreases
    COUNT2 = 25h
    COUNT3 = 26h
    A_MASK = 27h

;PROGRAM
;Setup PIC for operation
   MOVLW    0x07        ;Turn comparitors of PORTA off
   MOVWF     CMCON
   BCF       STATUS,  RP1 ;Move to memory bank 1
   BSF       STATUS,  RP0
    MOVLW   0x00
    MOVWF    TRISB       ;Set all Port B to outputs
    MOVLW   0xff
    MOVWF    TRISA       ;Set all Port A to inputs
   BCF       STATUS,  RP0 ;Move to memory bank 0
   BCF       STATUS,  RP1

   BCF       PORTB,   LED ;Ensures LED turned off

;Initially set delay registers giving total delay of 1.006 ms
   CLRF      STORE1      ;Set store 1
    MOVLW   0x52
    MOVWF    STORE1
   CLRF      STORE2      ;Set store 2
    MOVLW   0x04
    MOVWF    STORE2
   CLRF      STORE3      ;Set store 3
    MOVLW   0x01
    MOVWF    STORE3
;START OF REPEATING CODE
 BEGIN   BCF      PORTB,  LED  ;Turn LED off
```

```
55      MOVF      STORE1, 0       ;Copy files to temp store
56      MOVWF     COUNT1
57      MOVF      STORE2, 0
58      MOVWF     COUNT2
59      MOVF      STORE3, 0
60      MOVWF     COUNT3
61  ;Waits for low incase started mid way through a pulse
62   TRIGLOW BTFSC    PORTA,
        FGEN ;If trigger input is low then continues
63      GOTO
        TRIGLOW     ;Otherwise repeats check until trigger input is low
64      ;Debounce code to check system is actually low before continueing
65              BTFSC     PORTA,  FGEN
66          GOTO      TRIGLOW
67          BTFSC     PORTA,  FGEN
68          GOTO      TRIGLOW
69  ;Waits for zero crossing point
70   TRIGGER BTFSS    PORTA,  FGEN ;Tests to see if value has gone high
71      GOTO     TRIGGER     ;Loops until goes high
72      ;Debounce code to check system remains high and isn't an ...
        aritificial measurement
73          BTFSS     PORTA,  FGEN
74          GOTO      TRIGGER
75          BTFSS     PORTA,  FGEN
76          GOTO      TRIGGER
77     BSF   PORTB,  LED          ;Turns LED on
78
79  ;Wait for approximately 1 ms
80      DELAY1   DECFSZ
        COUNT1      ;Decreases file, skips next line if zero
81      GOTO     DELAY1
82      DELAY2   MOVF     STORE1, 0   ;Decreases next counter variable
83      MOVWF    COUNT1
84      DECFSZ   COUNT2
85      GOTO     DELAY1
86      DELAY3   MOVF     STORE2, 0   ;Decreases next counter variable
87      MOVWF    COUNT2
88      DECFSZ   COUNT3
89      GOTO     DELAY1
90
91  GOTO  BEGIN      ;Repeat for the next ac cycle
92  end
```

Appendix C

Electroluminescence Images

This section presents typical images of the EL from LDPE stressed under a sinusoidal, 50 Hz, 40 $kV_{rms}\,mm^{-1}$. The same grey scale is used throughout all images. Figure C.1 shows the emission from a virgin sample, figure C.2 shows the EL emission from samples after UV ageing in air and figure C.3 shows the EL from samples after UV ageing in nitrogen.

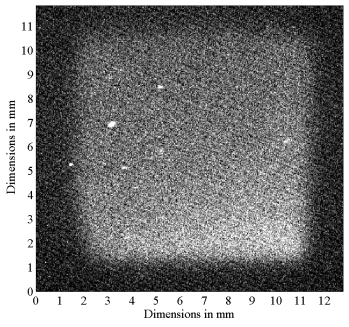

(a) Aged 0 days

FIGURE C.1: Electroluminescence images of virgin samples

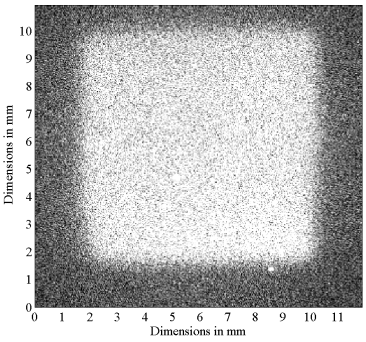

(a) Aged 3 days in air

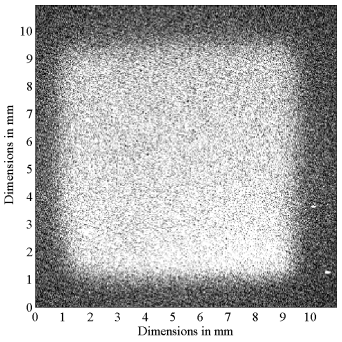

(b) Aged 7 days in air

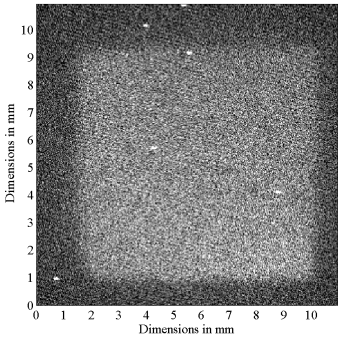

(c) Aged 10 days in air

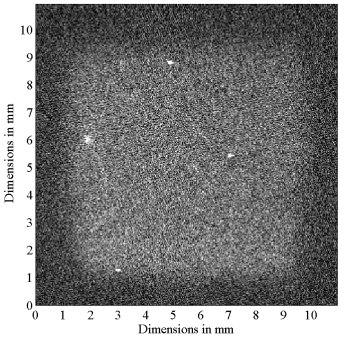

(d) Aged 14 days in air

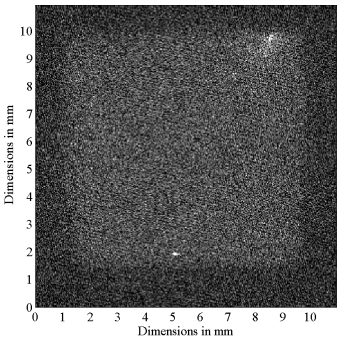

(e) Aged 17 days in air

FIGURE C.2: Electroluminescence images for samples aged in air

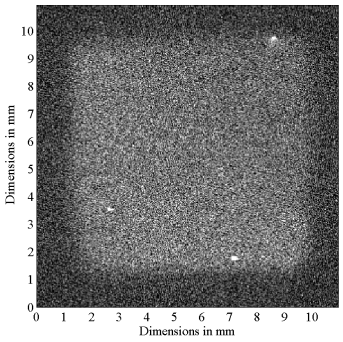

(a) Aged 3 days in nitrogen

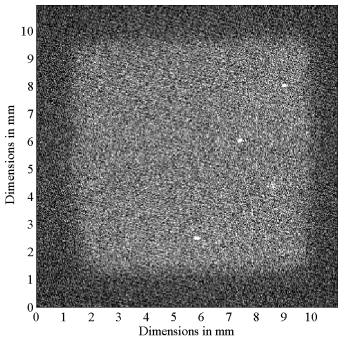

(b) Aged 7 days in nitrogen

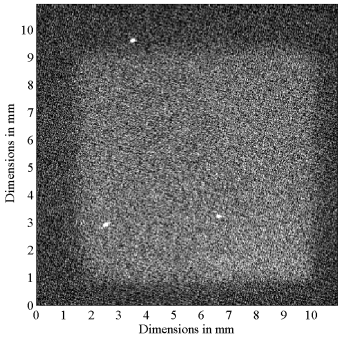

(c) Aged 10 days in nitrogen

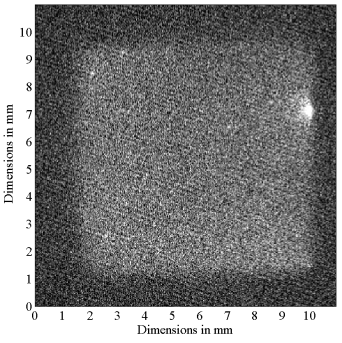

(d) Aged 14 days in nitrogen

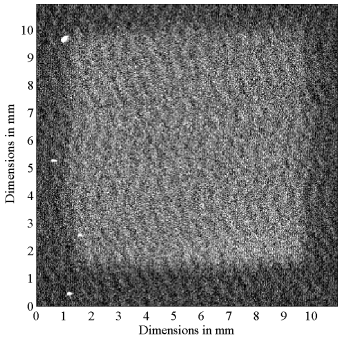

(e) Aged 17 days in nitrogen

FIGURE C.3: Electroluminescence images for samples aged in nitrogen

Appendix D

Electroluminescence Simulation Code

The following code is used to calculate the initial conditions for the simulation and the second block of code simulates the EL until a steady state is reached. The code was executed in the commercial software MATLAB®.

```
% This code collects the various parameters for ageing and then ...
    simulates
% the steady state electric field.

dbstop if error
%Initialise
    clear all %Clear memory
    close all %Close any open figures
%Simultation Control
    intAccuracy = 0.1; % \% Change between 2 peaks over 2 cycles
    intElectrodeArea = pi*0.0175^2; %Electrode area in meters^2
    strGas = 'N2'; %Ageing condition ('air','N2')
    vecAge = 0:1:18; %Values to take from Ic for simulating EL
%Figure control
    legLocation = 'EastOutside'; %Location of legend in plots
%Directories
    dirResults = '<Results Directory>'; %Folder for all results
    dirParams = '<Parameters Directory>'; %Contains directory for ...
    results
%Optimised parameters for LDPE
    e0 = 8.8542e-12; %Permittivity of free space e0 = 8.8542e-12
    er = 2.3; %Simulated
```

```
21      f = 50; %Frequency in Hz - FIXED FOR THIS SIMULATION
22          w=2*pi*f;
23      r = 8; %Number of ac cycles
24      a = 6e-3; %Value for alpha in a*e^(bt) equation
25      b = 7e-8; %Value for beta in a*e^(bt) equation
26      Meh = 1.25e12; %e,m-h,t recombination coefficient Meh=1.25e12;
27      Mhe = 1.25e12; %h,m-e,t recombination coefficient Mhe=1.25e12;
28      V = 5657; %4kVrms voltage for comparison with Temporal results
29          Vrms = 4; %Rms voltage in kV - used purely for comparison ...
        with experimental
30      L = 100 *1e-6; %Thickness of sample in um converted to meters.
31      X = 10 *1e-9; %Thickness of space charge region converted to ...
        meters
32      qe=-1.6e-19;     %charge for electron
33      qh=1.6e-19;      %charge for hole
34  %------VAPPDOTPERL CALCULATION------ Voltage applied per cycle
35          tmax=r*(1/f);        %number of cycles * period of 1 cycle
36          dt=pi/(1000*w);      %time increment
37          t=0:dt:tmax;         %time setting
38          N=length(t);         %total number of elements per run
39          VappdotperL = zeros(length(t),1); %--VARIABLE PREALLOCATION
40      for i=1:N            %total number of elements
41          VappdotperL(i)=(V*w/L)*cos(w*t(i));
42      end
43  %-----PARAMETERS FOR AGEING
44      load([dirParams <strParams> strGas '.mat'],'t', ['simParams_' ...
        strGas])
45      simParams = eval(['simParams_' strGas]); %Renames variable so ...
        rest of code will work correctly
46      simParams = simParams(ismember(t,vecAge)); %Simulates EL at ...
        the ages specified by vecAge
47                  %ismember identifies where the values of vecAge ...
        appear in t
48              clear('simParams*','t') %Tidying Variables
49      ElectricField = zeros((((N-1)/2)+1),length(vecAge)); ...
        %VARIABLE PREALLOCATION
50      Phase = ElectricField; %VARIABLE PREALLOCATION
51  %------SOLVING FOR ELECTRIC FIELD USING RUNGE-KUTTA METHOD------
52  for int = 1:length(vecAge)
53      e0er = e0*((1*simParams(int).Er)-0);
54      if true==true %Calculating changes electric field over 8 ...
        cycles of applied field
55      K1 = zeros(((N-1)/2),1);        %---VARIABLE PREALLOCATION
56      K2 = K1;        %---VARIABLE PREALLOCATION
57      K3 = K1;        %---VARIABLE PREALLOCATION
58      K4 = K1;        %---VARIABLE PREALLOCATION
```

```
59      E = zeros((((N-1)/2)+1),1);         %---VARIABLE PREALLOCATION
60      T = zeros((((N-1)/2)+1),1);         %---VARIABLE PREALLOCATION
61      E(1)=0; T(1)=0; j=1;     %initial conditions
62      h=2*dt;                  %value of h for iteration
63      for i=1:(N-1)/2;         %number of elements for iteration
64          ...
      K1(i)=h*(VappdotperL(j)-sign(E(i))*(a/e0er)*exp(sign(E(i))*b*E(i)));
65          Einc1=E(i)+(K1(i)/2);
66          ...
      K2(i)=h*(VappdotperL(j+1)-sign(E(i))*(a/e0er)*exp(sign(E(i))*b*Einc1));
67          Einc2=E(i)+(K2(i)/2);
68          ...
      K3(i)=h*(VappdotperL(j+1)-sign(E(i))*(a/e0er)*exp(sign(E(i))*b*Einc2));
69          Einc3=E(i)+K3(i);
70          ...
      K4(i)=h*(VappdotperL(j+2)-sign(E(i))*(a/e0er)*exp(sign(E(i))*b*Einc3));
71          E(i+1)=E(i)+(1/6)*(K1(i)+2*K2(i)+2*K3(i)+K4(i));
72          T(i+1)=T(i)+h;
73          j=j+2;
74      end
75      Phase(:,int) = T *(360/(1/f)); %Dont think need phase for ...
      every result but avoids confusion when looking at later on
76      ElectricField(:,int) = E;
77      clear('K1','K2','K3','K4','E','h') %Tidying Variables
78      end
79  end
80  clear('VappdotperL') %Free up memory
81      %------PLOTTING ELECTRIC FIELD AGAINST TIME------
82          strLegend = cell(1,length(vecAge)); %VARIABLE PREALLOCATION
83      figure('Name','Electric field vs time')
84      hold all
85      for int = 1:length(vecAge)
86          plot(Phase(:,int),ElectricField(:,int))
87          strLegend{int} = ['Aged ' num2str(vecAge(int)) ' days-' ...
      strGas];
88      end
89      hold off
90          xlabel('Phase Angle (degrees)')
91          ylabel('Electric Field (V/m)')
92          grid on
93          legend(strLegend,'Location',legLocation)
94              saveas(gcf, [dirResults 'EFieldvsTime-' strGas ...
      '.fig']) %Save the electric field vs time
95              saveas(gcf, [dirResults 'EFieldvsTime-' strGas ...
      '.png']) %Save the electric field vs time
96  %------DIVIDING PLOT INTO FOUR SECTIONS, AND------
```

```
%------CONVERTING SECTIONS INTO MATRIX FORM-------
    tt=(2*1/f)/dt;          %number of elements for VappdotperL = ...
    period of 2 cycles / time increment
    Ee = zeros(4,floor(tt/2));          %---VARIABLE PREALLOCATION
    E4 = zeros(size(Ee,2),numel(simParams)); %VARIABLE PREALLOCATION
    for int = 1:length(vecAge)
    for j=1:4           %number of sections
        for i=1:(tt/2)    %number of elements per section, ...
    converts tt to an integer
            d=fix(i+((j-1)*tt/2)); %fix round towards zero
            Ee(j,i)=ElectricField(d,int);
        end
    end
    E4(:,int)=Ee(4,:)';         %taking the fourth row values
    end
%------PLOTTING ELECTRIC FIELD OF THE FOURTH SECTION------
    dnew=2*dt;          %increment time for fourth section
    tnew=(2*1/f)-dnew;      %maximum time for fourth section ...
    assuming 2 cycles of applied field
    Phase_Steady = (0:dnew:tnew)*(360/(1/f)); %Steady state phase
%Save and clear up some variables
    save([dirResults 'SimulatedIc-' strGas ...
    '.mat'],'Phase','ElectricField','vecIc','vecAge') %Save results
clear('Phase','ElectricField')
pack %Reload variables to try and increase efficiency of memory ...
    useage
    %Plot Figure
    figure('Name','Electric field of fourth section')
    hold all
        for int=1:length(vecAge)
            plot(Phase_Steady,E4(:,int))
        end
    hold off
        xlabel('Phase Angle (degrees)')
        ylabel('Electric Field (V/m)')
        grid on
        legend(strLegend,'Location',legLocation)
    saveas(gcf, [dirResults 'EFieldFourthSection-' strGas ...
    '.fig']) %Save the field of fourth section graph
    saveas(gcf, [dirResults 'EFieldFourthSection-' strGas ...
    '.png']) %Save the field of fourth section graph
%------CURRENT DENSITY CALCULATION USING VALUES OF------
%--------ELECTRIC FIELD FROM THE FOURTH SECTION---------
  J4Orig  = sign(E4)*a.*exp(sign(E4)*b.*E4); %Calculates original ...
    current density assuming no conduction
  vecJc2 = zeros(1,length(vecAge));
```

```
135     for int = 1:length(vecAge)
136         vecJc2(int) = vecIc(int) / intElectrodeArea; %Alternative ...
        where the conduction current is assumed to be in phase with ...
        the applied field
137     end
138         temp_Jc2 = vecJc2(1);
139         for int = 1:length(vecAge)
140             vecJc2(int) = vecJc2(int) - temp_Jc2; %Scaling to ...
        virgin result
141         end
142     J4 = zeros(length(J4Orig),length(vecAge)); %VARIABLE ...
        PREALLOCATION
143     J4sign = sign(J4Orig); %Gets sign so can subtract RMS
144     J4Abs = abs(J4Orig); %Gets the absolute value
145     for int = 1:length(vecAge)
146         J4Aged = J4Abs(:,int) - vecJc2(int);
147             NegCurrent = J4Aged < 0; %Remove any negative current ...
        since not possible
148             J4Aged(NegCurrent) = 0;
149         J4(:,int) = J4Aged .* J4sign(:,int);
150     end
151 %------PLOTTING CURRENT DENSITY AGAINST TIME------
152     figure('Name','Current density ageinst time')
153     hold all
154     for int = 1:length(vecAge)
155         plot(Phase_Steady,J4(:,int))
156     end
157     hold off
158         xlabel('Phase Angle (degrees)')
159         ylabel('Current Density (A/m^2)')
160         grid on
161         legend(strLegend,'Location',legLocation)
162             saveas(gcf, [dirResults 'JvsTime-' strGas '.fig']) ...
        %Save the current density vs time
163             saveas(gcf, [dirResults 'JvsTime-' strGas '.png']) ...
        %Save the current density vs time
164 %-----CALCULATING ELECTROLUMINESCENCE INTENSITY -----
165 %------ UNTIL A STEADY STATE IS REACHED ------
166     tend=4-dnew; %tend = 4seconds - iteration
167     t_Elength=size(E4,1); %Used for VARIABLE PREALLOCATION
168         IFinal = zeros(t_Elength,length(vecAge)); %VARIABLE ...
        PREALLOCATION
169         Time2SteadyState = zeros(1,length(vecAge)); %VARIABLE ...
        PREALLOCATION (rev:1164)
170     for int = 1:length(vecAge) %Simulate EL
171         %Trapped charge is set to 0 between each simulation
```

```
172         TrappedCharge.pet1 = 0; TrappedCharge.pht1 = 0; %No ...
    trapped holes or electrons at ground electrode
173         TrappedCharge.pet2 = 0; TrappedCharge.pht2 = 0; %No ...
    trapped holes or electrons at HV electrode
174
175         [I,noCycles, TrappedCharge] = ...
    fctSteadyStateEL(E4(:,int),... %Electric field at ...
    electrode-polymer interface
176                     J4(:,int),... %Current density at injecting ...
    electrode
177                     dnew,... %Time step
178                     stcParams(int).X,... %Space charge region
179                     Meh, Mhe,... %Charge of an electron / hole
180                     TrappedCharge,... %Trapped charge from ...
    previous cycle
181                     intAccuracy); %Accuracy of simulation between ...
    two half cycles
182         IFinal(:,int) = I(:,noCycles-1);
183         Time2SteadyState(int) = noCycles * 2/f;
184         for j=1:noCycles-1
185             EL(int).ISteady(((j-1)*t_Elength)+1:(j*t_Elength)) = ...
    I(:,j)'; %Produces a continuous row for the...
186                     %EL data until a steady state is reached
187         end
188         EL(int).TSteady = ...
    single(0:dnew:((length(EL(int).ISteady)*dnew)-dnew));
189         clear('I') %Free up memory since don't need entire data ...
    set anymore
190     end
191 %------PLOTTING ELECTROLUMINESCENCE INTENSITY AGAINST TIME------
192     for int = 1:length(vecAge)
193     figure('Name','EL until steady state-')
194         plot(EL(int).TSteady,EL(int).ISteady)
195     title([strGas '-Ic=' num2str(simParams(int).Ic) ',Er=' ...
    num2str(vecEr(int))])
196     xlabel('Time (s)')
197     ylabel('EL Intensity (a.u.)')
198        saveas(gcf, [dirResults 'EL2SteadyState-' ...
    num2str(vecAge(int)) '-' strGas '.fig']) %Save the EL vs time ...
    graph
199        saveas(gcf, [dirResults 'EL2SteadyState-' ...
    num2str(vecAge(int)) '-' strGas '.png']) %Save the EL vs time ...
    graph
200     end
201 %------------ PLOT ELECTROLUMINESCENCE INTENSITY OVER FINAL CYCLE ------
202  figure('Name','EL over the final cycle')
```

```
 hold all
    strLegend = cell(1,length(vecAge)); %VARIABLE PREALLOCATION
    for int = 1:length(vecAge)
        plot(Phase_Steady,IFinal(:,int))
        strLegend{int} = ['Ageing Time = ' num2str(vecAge(int)) ...
    'days-' strGas];
    end
hold off
xlabel('Phase Angle (degrees)')
ylabel('Electroluminescence (au)')
xlim([0 360])
grid on
legend(strLegend,'Location',legLocation)
clear strLegend
    saveas(gcf,[dirResults 'EL-SteadyState-' strGas '.fig'])
    saveas(gcf,[dirResults 'EL-SteadyState-' strGas '.png'])
% SAVE RESULTS
    save([dirResults 'Results-' strGas ...
    '.mat'],'IFinal','IPeakPos','IPeakNeg','IPhasePos','IPhaseNeg','Phase_Steady',
    'vecIc','vecEr','Time2SteadyState','EL') %Saves results
```

```
function [I,j, TrappedCharge] = fctSteadyStateEL(E4, J4, dnew, X, ...
    Meh, Mhe, qe, qh, TrappedCharge,intAccuracy)
%FCTSTEADYSTATEEL Simulates EL until a steady state is reached
% INPUTS
    %E2 = electric field
    %J2 = Injection current density
    %dnew = Simulation time step
    %X = space charge region
    %Meh = Recombination coefficient
    %Mhe = Recombination coefficient
    %qe = Charge of an electron
    %qh = Charge of a hole
    %TrappedCharge = Initial condition for charge
    %intAccuracy = Accuracy to simulate two (% change between ...
    peaks over 2 cycles of the applied field.
% OUTPUTS
    %I = Emission intensity from 1 side of the sample
    %j = Number of cycles simulated
    %TrappedCharge = Steady state charge condition
%HOW
    %Calculates the EL intensity during the electric field.
    %Calculates the difference between the 2 peaks.
```

```
21      %When the difference between the 2 peaks remains unchanged ...
        over 2 cycles then the steady state EL value is returned.
22  %Fixes accuracy value if not passed from calling function
23  if exist('intAccuracy','var')
24  else
25      intAccuracy = 0.1; %Percentage change in difference between peaks
26  end
27  intPerCycle = length(E4); %Number of points per 2 cycles
28  intCycles = 2000; %number of electric field cycles to initially ...
        preallocate for - (preallocation for speed)
29  boComplete = false; %Boolean to exit while loop
30      E4sign = sign(E4); %Identifies the positive and negative ...
        parts of the...
31          %electric field at the ground (ring) electrode
32      t_E4Neg1 = E4sign <=0;
33      t_E4Pos1 = E4sign > 0;
34
35      negE4sign = sign(-E4); %Positive and negative parts of ...
        electric field at HV electrode
36      t_E4Neg2 = negE4sign <=0;
37      t_E4Pos2 = negE4sign > 0;
38
39      %Calculate the condition for the mobile electrons and trapped ...
        holes
40          pem1 = J4*(dnew/X).*t_E4Neg1; %phm = 0 for negative - ...
        Electrode 1;
41          pem2 = -J4*(dnew/X).*t_E4Neg2; %phm = 0 for negative - ...
        Electrode 2;
42          phm1 = J4*(dnew/X).*t_E4Pos1; %pem = 0 for positive - ...
        Electrode 1
43          phm2 = -J4*(dnew/X).*t_E4Pos2; %pem = 0 for positive - ...
        Electrode 1
44
45      pet1= zeros(size(pem1,1),intCycles/2); %VARIABLE PREALLOCATION
46      pet2 = zeros(size(pem2,1),intCycles/2); %VARIABLE PREALLOCATION
47      pht1 = pet1; %VARIABLE PREALLOCATION
48      pht2 = pet2; %VARIABLE PREALLOCATION
49      Rmobe1=pet1; %VARIABLE PREALLOCATION
50      Rmobe2=pet2; %VARIABLE PREALLOCATION
51      Rmobh1=pet1; %VARIABLE PREALLOCATION
52      Rmobh2=pet2; %VARIABLE PREALLOCATION
53      I1 = pet1; %VARIABLE PREALLOCATION
54      I2 = pet2; %VARIABLE PREALLOCATION
55      I = I1+I2; %VARIABLE PREALLOCATION
56          t_diffPrevious=0;
57          t_PosCur = 0; %Current positive half cycle peak
```

```
58          t_NegCur = 0; %Current negative half cycle peak
59          t_PosPre = 0; %Previous positive half cycle peak
60          t_NegPre = 0; %Previous negative half cycle peak
61
62      pet1(1) = TrappedCharge.pet1; pht1(1) = TrappedCharge.pht1; ...
        %Loads from previous simulation
63      pet2(1) = TrappedCharge.pet2; pht2(1) = TrappedCharge.pht2; ...
        %Loads from previous simulation
64      i=1; %Beginning of iterative loop
65      j=1; %First set of 2 cycles
66
67      while boComplete == false %Iterative loop to calculate the EL ...
        intensity
68            %Calculate recombination of electrons and holes for ...
        electrode 1
69            Rmobe1(i,j)=abs(Meh*pem1(i)*pht1(i,j));  %mobile ...
        electron -> trapped hole recombination - Electrode 1
70            Rmobe2(i,j)=abs(Meh*pem2(i)*pht2(i,j)); %mobile ...
        electron -> trapped hole recombination - Electrode 2
71            Rmobh1(i,j)=abs(Mhe*phm1(i)*pet1(i,j));  %mobile hole ...
        -> trapped electron recombination - Electrode 1
72            Rmobh2(i,j)=abs(Mhe*phm2(i)*pet2(i,j));  %mobile hole ...
        -> trapped electron recombination - Electrode 2
73          % Calculate the EL emission
74                I1(i,j) = 1e-25 * (Rmobe1(i,j)+Rmobh1(i,j))/dnew; ...
        %Added in so can determine steady state - Electrode 1
75                I2(i,j) = 0.8e-25*(Rmobe2(i,j)+Rmobh2(i,j))/dnew; ...
        %Added in so can determine steady state - Electrode 2
76                       %0.8 since some light is absorbed by the ...
        material and the gold.
77                I(i,j) = I1(i,j)+I2(i,j); %Total intensity from ...
        both electrodes
78
79            %Identify if cycles have been equal and if have can ...
        end, if not will start calculating for
80            %next cycles.
81            %Rev:1153 - Steady state is now determined by a minimum ...
        change in both the positive and
82            %negative half cycle peaks.
83
84            if i == intPerCycle %When at end of electric field ...
        simulation move onto next column
85                if rem(j,1) == 0 %Tests every 2 cycles of the ...
        applied field (1 iterations of j) - Rev:1153
86                      t_PosCur = max(I(1:intPerCycle/4,j)); %Max in ...
        1st half of 1st half cycle
```

```
87                  t_NegCur = ...
    max(I((intPerCycle/4)+1:intPerCycle/2,j)); %Max in 2nd half of ...
    1st half cycle
88              t_diffPos = t_PosCur - t_PosPre; %Difference ...
    between peaks of positive half cycles
89              t_diffNeg = t_NegCur - t_NegPre; %Difference ...
    between peaks of negative half cycles
90              if and(abs(t_diffPos) < (intAccuracy/100),...
91                    abs(t_diffNeg <  (intAccuracy/100))) %Stops ...
    once there is...
92                          %barely any change in difference ...
    between peaks, therefore suggestin a...
93                          %steady state has been reached.
94                      %Set values for Trapped Charge so can use ...
    them in next part of simulation
95                      TrappedCharge.pet1 = ...
    pet1(i,j)+pem1(i)-qe*Rmobe1(i,j)+qh*Rmobh1(i,j); %Trapped ...
    electron density; - Electrode 1
96                      TrappedCharge.pet2 = ...
    pet2(i,j)+pem2(i)-qe*Rmobe2(i,j)+qh*Rmobh2(i,j); %Trapped ...
    electron density; - Electrode 2
97                      TrappedCharge.pht1 = ...
    pht1(i,j)+phm1(i)-qh*Rmobh1(i,j)+qe*Rmobe1(i,j); %Trapped hole ...
    density - Electrode 1
98                      TrappedCharge.pht2 = ...
    pht2(i,j)+phm2(i)-qh*Rmobh2(i,j)+qe*Rmobe2(i,j); %Trapped hole ...
    density - Electrode 2
99                   boComplete = true; %Ends iterative loop
100             end
101             t_PosPre = t_PosCur; %Set previous values
102             t_NegPre = t_NegCur;
103             %t_diffPrevious = t_diffCurrent; %If hasn't ...
    exited then will...
104                         %set previous = current and iterate
105         end
106         %Since has reached end of data for electric field ...
    will iterate j and continue in next
107                 %column
108         pet1(1,j+1) = ...
    pet1(i,j)+pem1(i)-qe*Rmobe1(i,j)+qh*Rmobh1(i,j); %Trapped ...
    electron density; - Electrode 1
109         pet2(1,j+1) = ...
    pet2(i,j)+pem2(i)-qe*Rmobe2(i,j)+qh*Rmobh2(i,j); %Trapped ...
    electron density; - Electrode 2
```

```
110             pht1(1,j+1) = ...
    pht1(i,j)+phm1(i)-qh*Rmobh1(i,j)+qe*Rmobe1(i,j); %Trapped hole ...
    density - Electrode 1
111             pht2(1,j+1) = ...
    pht2(i,j)+phm2(i)-qh*Rmobh2(i,j)+qe*Rmobe2(i,j); %Trapped hole ...
    density - Electrode 2
112             i=1;
113             j=j+1;
114         else
115             pet1(i+1,j) = ...
    pet1(i,j)+pem1(i)-qe*Rmobe1(i,j)+qh*Rmobh1(i,j); %Trapped ...
    electron density; - Electrode 1
116             pet2(i+1,j) = ...
    pet2(i,j)+pem2(i)-qe*Rmobe2(i,j)+qh*Rmobh2(i,j); %Trapped ...
    electron density; - Electrode 2
117             pht1(i+1,j) = ...
    pht1(i,j)+phm1(i)-qh*Rmobh1(i,j)+qe*Rmobe1(i,j); %Trapped hole ...
    density - Electrode 1
118             pht2(i+1,j) = ...
    pht2(i,j)+phm2(i)-qh*Rmobh2(i,j)+qe*Rmobe2(i,j); %Trapped hole ...
    density - Electrode 2
119             i=i+1; %Iterate i
120         end
121
122         if j ≥ 2000 %control to avoid endless loops %Increased ...
    to improve results which were getting stopped by upper limit
123             break
124         end
125
126         ii=j;
127     end
```